

Hydrogels for DNA isolation from blood

Dissertation

zur Erlangung des Grades

Doktor der Naturwissenschaften

im Promotionsfach Chemie

am Fachbereich Chemie, Pharmazie und Geowissenschaften
der Johannes Gutenberg-Universität Mainz

vorgelegt von

Piotr Maciej Jakubowicz
geboren in Warschau

Mainz, im September 2013

Dekan:	.....
1. Berichterstatter:	.....
2. Berichterstatter:	.....
Tag der mündlichen Prüfung:	.....

for my parents

Abstract

This dissertation describes the synthesis of surface attached hydrogel biomaterials, characterization of their properties, evaluation of structuring concepts and the investigation of these materials in the isolation of DNA from human whole blood.
Photosensitive hydrogel precursor materials on the basis of hydroxyethylmethacrylate (HEMA) were synthesized by free radical polymerization. In order to obtain surface bound hydrogel films, the precursors were deposited on a suitable substrate and subsequently irradatiated with UV - light to accomplish the formation of crosslinks in the film and create surface attachment. The composition of the polymerization precursor materials was determined by comprehensive NMR and GPC studies, revealing the copolymerization behaviour of the used monomers - HEMA derivatives and the photocrosslinker MABP - and their respective distribution in the hydrogel precursors. The degree of crosslinking of the hydrogels was characterized with UV/vis spectroscopy. Stress-strain measurements were conducted in order to investigate the mechanical properties of the biomaterials. Moreover, the swelling process and biomolecule adsorption properties of the hydrogels were investigated with SPR/OW spectroscopy. For this, the deposition and binding of the hydrogels on gold or SiO_2 surfaces was facilitated with photocrosslinkable adhesion promotors. The produced hydrogels were mechanically rigid and stable under the conditions of PCR and blood lysis. Furthermore, strategies towards the increase of hydrogel surface structure and porosity with porosigens, 2D laser interference lithography and photocleavable blockcopolymers were investigated.
At last, a combinatorial strategy was used for the determination of the usefulness of hydrogels for the isolation from DNA from blood. A series of functionalized hydrogel precursors were synthesized, transferred to the surface inside a PCR tube and subsequently screened in regard to DNA adsorption properties with Taqman quantitative PCR. This approach yielded a promising candidate for a functional PCR tube coating that would allow the entire DNA isolation procedure being carried out in a single reaction container. Thereforce, the practical application of such macromolecular architectures can be envisioned to improve industrial DNA diagnostic processes.

Contents

1 Introduction

1.1 From Aristotle to DNA

$\gamma\epsilon\nu\epsilon\tau\iota\kappa o\varsigma$

– *genetikos*, ancient greek for *origin*

Man has long been aware of the phenomenon of heredity in nature, as can be discovered in early discussions of the ancient philosophers of Hippocrates and Aristotle [1]. But it was not before the *experiments on plant hybridization* by Gregor Mendel [2] and Charles Darwin's *theory of evolution by natural selection* [3] one hundred and fifty years ago that science made it's first steps in developing an understanding of these processes in nature. It took mankind one hundred more years to pass from biological theories into detailed chemical knowledge about the origin of biological traits and hereditary behaviour: the isolation of deoxyribonucleic acid (DNA) as genetic material in 1944 by Avery, MacLeod and McCarty [4], the coverage of the structure of DNA by James Watson and Francis Crick in 1953 [5], and the "cracking" of the genetic code in 1967 by Marshall Nirenberg, Har Gobind Khorana, Sydney Brenner and Francis Crick [6, 7] laid the fundamental groundwork for the understanding of the *molecule of life*.

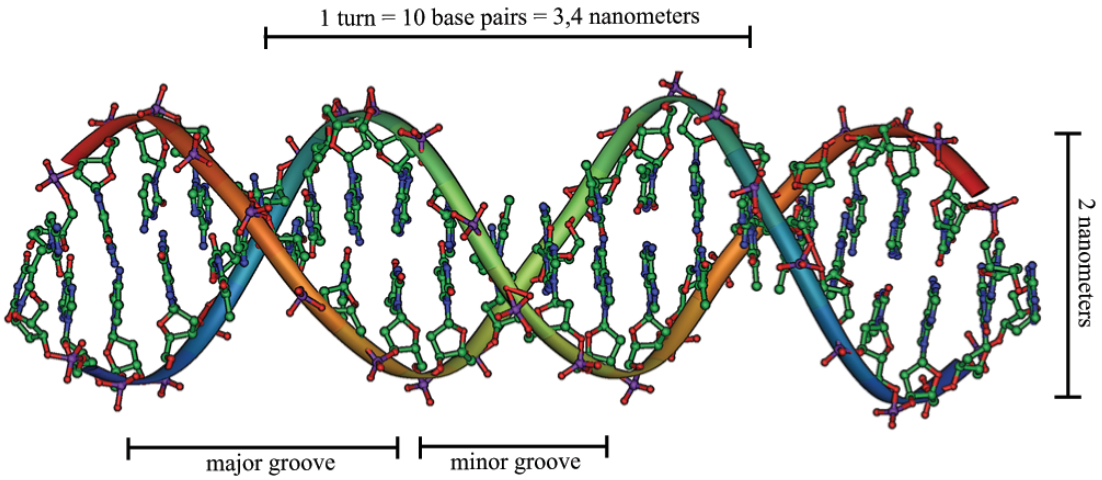

Fig. 1.1 Fragment of a DNA molecule showing the double helix structure and geometric size parameters. About one hundred trillion (a thousand, thousand million) cells make up our human bodies. Every one of them is organized into tissues, such as bone, skin, muscle, and thrombocyte - and almost every type of cell contains all of the organism's genetic information stored in the form deoxyribonucleic acid (DNA). The average length of DNA molecules in uncoiled form is about 5 cm. The genetic information is stored in a code of sequences of four complementary nucleobases - adenosine, guanine, thymine and cytosine - that are stored in the inside of the DNA double strand [8].

Within DNA, a molecule of great structural complexity and size (Fig. 1.1), is stored the very information that serves as fundamental biochemical instruction manual: genes are a sequence of codes that form the blueprint for the production of proteins. They have direct control over the entire biochemistry of the human organism, including important processes such as the cell's life cycle, metabolism, reproduction and repair mechanisms. Information is codified in a sequence of chemical building blocks, namely the corresponding nucleotides of the purines adenine, guanine, thymine and cytosine. Not only does the genetic code define all intrinsic functions and properties of living organisms on this planet - mortality, fertility or adaptation to natural environments - but it also triggers a certain amount of malfunctions like cancer and genetical deceases [8].

The promises and hopes projected into potential discoveries on DNA research sparked new scientific disciplines like bioinformatics, pharmacogenomics, proteomics, transcriptonomics and others. Endeavours such as the Human Genome Project successfully completed the sequencing of 99% of the human genome - the chemical sequence of the three billion nucleotide base pairs, an estimated 50,000 to 100,000 genes - with an accuracy of 99.99%. Its most extraordinary promise: A revolution in medicine, giving the chance to rid the world of many if not all the major diseases [9]. Diseases that take many a life and cost hundreds of millions of dollars each year. Given these circumstances it is no surprise that huge efforts are directed into understanding, isolating and controlling DNA with the ultimate hope of gaining the power to improve our form of existence according to our wishes.

1.2 Isolating DNA

DNA is not only a promising playing field for researchers. It has already found its way into day to day applications in the biomedical community, be it in the field of forensics [10] or in clinical use e.g the screening of hereditary deceases [11], human immunodeficiency virus (HIV) [12], and parentage tests [13]. DNA, however, is not easily accessible: it can only be found in the nucleus of a cell where it lies wrapped in a complex structure of proteins. As such, it is not trivial to get hold of this molecule even in small quantities [8].

The state of the art procedures [14, 15, 16] to obtain DNA from human whole blood involve a complicated multi-step protocol. Moreover, sophisticated automation processes are required in order for the DNA isolation being affordable for a larger quantity of samples. This protocol can be divided into three distinct chemical steps (see Fig. 1.2). At the current state of technology, a single reaction container is not sufficient to isolate

DNA in quantities that are deemed to be sufficient for further analysis. As a consequence, multiple containers have to be used in DNA isolation and analysis procedures.
The market demand for isolating DNA from human and animal whole blood is rising year by year and currently makes up an approximate volume of 130 million preparations per annum. This corresponds roughly to a financial value of 147 million US$ [17, 18] - enough to spark initiatives that seek to improve the effectivity of DNA isolations in academic research and the industrial sector. Two key areas are of particular interest: the progression of the automation process and the creation of enhanced biomaterials [19]. Fig. 1.2 illustrates a possible improvement that can be obtained with the use of a chemical modification of the reaction container on the base of a functional polymer coating that would lead to optimized conditions for DNA isolation.

1.3 Why hydrogels?

Hydrogels - water-swollen, crosslinked polymer materials, as depicted in figure 1.3(a) - have received significant attention because of their exceptional promise in fields such as drug delivery [20], wound healing and tissue engineering [21], actuators [22], separation [23], industrial coatings [24], binding studies [25] and numerous other biomedical applications [26, 27, 28].

Hydrogels can be made from virtually any water-soluble polymer, encompassing a wide range of chemical compositions and physical properties. Moreover, hydrogels can be produced with many different synthetic procedures and formulated in a variety of physical forms, including slabs, microparticles, nanoparticles, coatings, and films [29]. As such, these polymers show great promise as functional coatings for analytes solved in hydrophilic solvents.

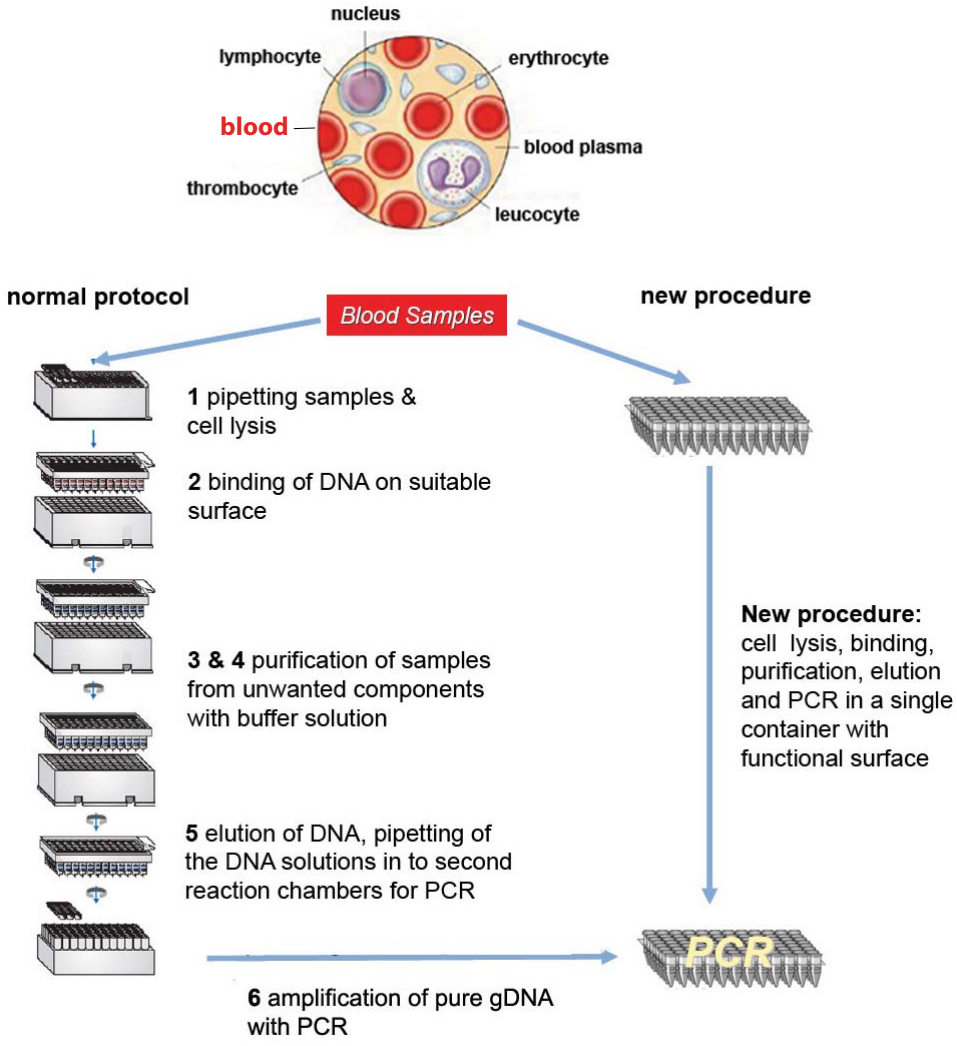

Fig. 1.2 Schematic overview of the DNA isolation procedure from blood: Only cells with a nucleus contain DNA and are relevant for the analysis. However, no separation of unrequired blood components such as red blood cells from human blood is necessary prior to the isolation procedure [14]. **(1)** the blood sample is directly pipetted into the reaction holders and digested under chaotropic conditions, namely elevated temperatures and specific salt concentrations. This is followed by **(2)** binding of DNA fragments to a suitable surface and **(3&4)** the purification in another set of containers. The purified and digested lysates are then applied to a 96-well purification tray containing a glass fiber membrane. The membrane is then **(5)** washed and high quality DNA is eluted in a two-step elution buffer system and concentrated for the **(6)** amplification with PCR. Each of the steps, lysis, washing and PCR is currently performed in a separate optimized sample holder. A transfer of the entire procedure into a single container would not only save money, but also reduce possible errors and improve the accuracy of the entire procedure.

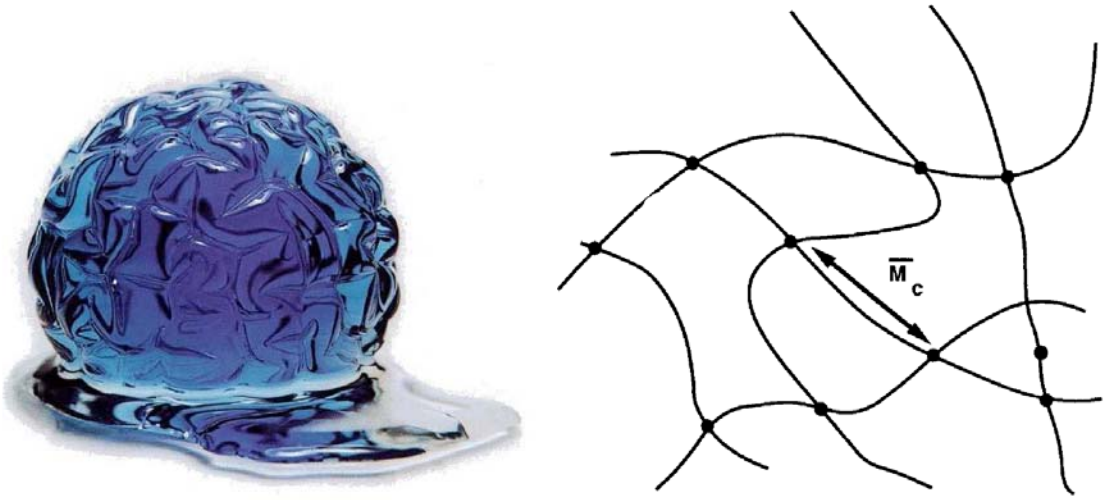

(a) Tanaka's famous hydrogel (b) ideal hydrogel network

Fig. 1.3 **left:** Example of a highly swollen polyelectrolyte hydrogel as created by Tanaka et al [34]. **right:** Illustration of M_c parameter in a hydrogel network as depicted by Peppas et al. [35].

The functionalization of hydrogels can be accomplished either by adding comonomers to the polymerization step or by the use of polymer analogous reactions that involve almost all high yield organic reactions. The latter strategy involves active ester chemistry, *click* chemistry, polymerization anhydrides, epoxides, aldehydes and ketones, including Michael-type and Friedel-Crafts reactions as well as methylations [30, 31, 32]. This can be exploited to modify the gel with a variety of molecules including biomolecules for biosensor applications and affinity binding [33].

The network structure of hydrogels can contain covalent bonds produced by the reaction of one or more comonomers and physical crosslinks resulting from entanglements. It can also contain association bonds such as hydrogen bonds or strong Van der Waals interactions between chains [36]. A last possibility would be the existence of crystallites that bring together two or more macromolecular chains [37].

The parameter that describes the basic structure of the hydrogel is the molecular weight between cross-links M_c. As shown in figure 1.3(b), it defines the average molecular size between two consecutive junctions regardless of the nature of those junctions. Additional parameters of importance is the specific volume of the polymer (polymer volume fraction) and the cross-linking density. The investigation of the network structure is difficult and can be carried out either by the use of theoretical models or by indirect experimental techniques. Theoretical simulations look into the formation of the network structure and the heterogeneities of the network with kinetic models that take into account the mass balances of the species [38] and statistic Monte Carlo Models [39]. These numeric simulations are run on simulation packages - such as the molecular dynamics simulation package ESPResSo developed in the MPIP [40] - that make use of highly parallelized computing infrastructure with the goal of calculating an approximation of the hydrogel swelling behaviour. However, no theory can predict exact behaviour due to the highly non-ideal thermodynamic behaviour of polymer networks in electrolyte solutions. The most accurate theory of hydrogel swelling characteristics is the Flory Rhener Theory and its variations [41, 42].
A practical method to determine the network parameter is discussed in chapter 4 and involves measurements of the mechanical properties and swelling behaviour of the gel [43, 44].

The diffusion through the hydrogel network is influenced by the structure and pore size of the gel. The latter is determined by the crosslinking, polymer composition, water content, size and nature of the solutes. The interaction among solutes, gel polymers, and solvents has an important effect on the diffusion. Diffusion is thereby best described by Ficks equation or by Maxwells equations which correlate the solutes flux with its chemical potential gradient in the system [26].
The crosslinking and swelling processes have a strong impact on the surface properties of the gel. Hydrogels exhibit a complex surface structure with single polymer chains ex-

tending from the surface into the solution and a gradual change at the interface between hydrogel and solution [45]. This effectively makes the extended polymer chains behave like polymer brushes and greatly influences adhesive and adsorptive interactions [46] e.g. the surface adsorption of DNA and other biomolecules.

1.4 Objective and scope of the thesis

The aim of this thesis is the synthesis and characterization of a functional hydrogel and its exploitation as a matrix for the isolation of gDNA from blood.

The hydrogel should function as a highly adsorptive film coating that would allow all steps of the isolation gDNA from human whole blood - cell lysis, adsorption, purification and PCR amplification - to be carried out in a single reaction container. To achieve this goal, a single sample vial with the functional coating should absorb enough DNA to perform a PCR reaction - typically, that would be an amount of about 5 to 10 ng of DNA. Furthermore, the adsorption process is required to work under *field conditions*: large amounts of impurities are present in the blood lysis mixture in the form of salts, proteins and lipids. These impurities might lead to coagulation processes and thus reduce the overall efficiency of the replication and adsorption processes of DNA. The material is required to be tolerant in regard to the conditions of the entire DNA isolation procedure and should adsorb gDNA in a reversible manner. At last, the designed hydrogel material should not disrupt the PCR and exhibit sufficient mechanical and thermal stability.
In addition to the design of a DNA adsorbing material that matches the particular requirements of the application and the exploration of a strategy for its synthesis, a structural and functional characterization of the hydrogel should occur in regard to mechanical and swelling properties.

While every chapter in this thesis contains an experimental section revealing experimental details, chapter 2 introduces the methods used for the synthesis of materials produced in this thesis. It also features a brief explanation of the analytic techniques that are used for the characterization of materials and the investigation of material properties.

Chapter 3 discusses the choice of hydrogel backbone polymer and synthetic strategy towards a hydrogel film with a high degree of flexibility in regard to deposition and functionalization. The core concept is to make use of a *photocrosslinkable hydrogel precursor* that can be transformed into a hydrogel network by irradiating the material with UV - light. The ease of deposition of such precursor materials on a substrate of choice and the controlled crosslinking procedure gives a versatile route to obtain reproducible hydrogel samples. In addition, the concept allows to tailor the crosslinking density and material properties of the gel. The utilization of a benzophenone derivative as photocrosslinking agent is evaluated and the free radical polymerization based synthesis and the properties of the hydrogel precursors are investigated by GPC and NMR studies.

Chapter 4 investigates and optimizes a) the film formation of the unmodified hydrogels from photocrosslinkable precursor materials and b) their attachment to a suitable substrate. The choice of polymer backbone material is explained and the film deposition process is optimized in regard to optical film quality, film height and crosslinking time. Furthermore, the gels are characterized in regard to their swelling and mechanical properties: the equilibrium swelling state and mechanical strength of the basic hydrogel matrix film are investigated concerning the parameters irradiation time and functional monomer content. At last, the adsorptive properties of the gel are subjected to a proof of principle test with a model system based on biotin-streptavidin, demonstrating the selective adsorptive potential of pHEMA based hydrogel biomaterials.

Chapter 5 investigates a possible route towards the chemical nanostructuring of the hydrogel surface with the use of photochemistry and blockcopolymers. For this, a strategy involving the synthesis of a photocleavable amphiphilic hydrogel precursor from two chemically different blockcopolymers and a photocleavable junction point is investigated.

Chapter 6 describes the combinatorial approach in finding a suitable functionalization of the hydrogel in regard to the isolation of gDNA from human whole blood. With the use of high-throughput quantitative PCR (QPCR), a series of hydrogel materials and lysis buffers is screened for exceptional performance in the isolation of gDNA from blood. That way, a suitable functionalization of the base hydrogel material to enhance the efficiency of gDNA isolation can be identified.

Thus, this thesis consists of work on the design and synthesis of hydrogel building blocks, their functionalization, characterization and fabrication into hydrogel films, the determination of their properties and nanostructuring, and the application of hydrogels in the isolation of gDNA from human whole blood.

2 Methods

This chapter introduces the general methods and techniques used for the synthesis and characterization of the materials produced in this thesis and the investigation of their properties.

2.1 Ultraviolet/visible (UV/vis) spectroscopy

UV/vis spectroscopy uses the absorption of light with wavelength from the ultra violet (UV) to the near infrared (IR) range e.g. for the determination of sample concentrations. During this process a target molecule is excited by light and undergoes an electronic transition. The sample of interest is placed into a light beam with tunable wavelength λ. The intensity of light passing through the sample (I) is recorded and compared to the intensity of the incident light beam (I_0). The ratio of $\frac{I}{I_0}$ is called the transmittance. Usually, the absorbance (A) of the solution is plotted in dependence of the excitation wavelength λ_{ex}. The absorption maximum - and thus the excitation wavelength - is related to the energy necessary to excite an electron from the HOMO to the LUMO. The absorbance is related to the concentration of the excited species and the quantum yield of the absorption process. According to the Lambert-Beer's law (equation 2.1), the absorbance of a solution is directly proportional to the concentration c of the absorbing

species. This is the case as long the concentration is kept low and the transmission path length d is kept constant. The molar extinction coefficient ϵ can often be taken from references. For exact measurements a concentration dependent calibration curve should be recorded to perform exact concentration determinations.

$$A = -\log(\frac{I}{I_0}) = \epsilon * c * d \tag{2.1}$$

UV/vis spectra in solution were recorded at room temperature on a Perkin-Elmer Lambda 100 spectrophotometer. The molar absorptivity ϵ is given in the unit $m^2 * mol^{-1}$, which is consistent with the SI standard. In order to eliminate aggregation phenomena in solution, spectra of samples of different concentrations were compared to give the properties for the monomeric species in solution, which is usually at a concentration of 10^{-6} to 10^{-7} mol. If not mentioned otherwise, chloroform (spectroscopic grade) was used as solvent and the measurement was performed at room temperature.

Film UV/vis spectra were recorded on the same instrument. The material of interest was solved in a good solvent and cast into a film of specific thickness. The substrate is use was a thin optical quality quartz glass manufactured by Hereaus.

2.2 Fourier transform infrared (FT-IR) spectroscopy

The infrared spectra were recorded with a Fourier Transformation IR Spectrometer (FTIR), Type 730, manufactured by the company Nicolet. The substances were measured in powder form with aid of an ATR unit. The data processing was done with the use of the program Nicolet OMIC E.S.P. 5.1.

2.3 Optical microscopy

Detailed optical images of the samples were recorded with an optical microscope using magnifications from 5x to 100x. The microscope used in this work was an Axioscope Zeiss, which could be operated in bright field, dark field, or differential interference contrast (DIC) mode. Images were recorded either with an Axiocam Zeiss color (1300x1030 pixels) or with a micro eye UI 1540SE CMOS (1280x1024 pixels) camera. Calibration of the images was conducted measuring μm sized gratings of known spacing. Image processing was conducted by Adobe Photoshop CS3.

2.4 Scanning electron microscopy (SEM)

Scanning electron microscopy (SEM) is a standard technique to characterize nanostructured materials microscopically. In comparison to visible light the smaller wavelength of accelerated electrons provides the possibility to resolve structures down to the nanometer range. The maximum resolution of two individual points with a distance d is given by the Abbe criterion, with N_A being the numerical aperture.

$$d = \frac{\lambda}{2N_A} \tag{2.2}$$

The contrast in SEM is given by the intensity of electrons at the detector while the focused electron beam is scanning over the sample surface. Thus is obtained a 2D resolved picture which displays the x,y-position dependent electron intensity at the detector. In low-voltage (LV) SEM electron beams with an acceleration voltage < 5 kV are used [47, 48, 49]. The electron beam interacts with the sample surface in several ways. The different electrons that are generated by the primary electron beam (PE) and detected

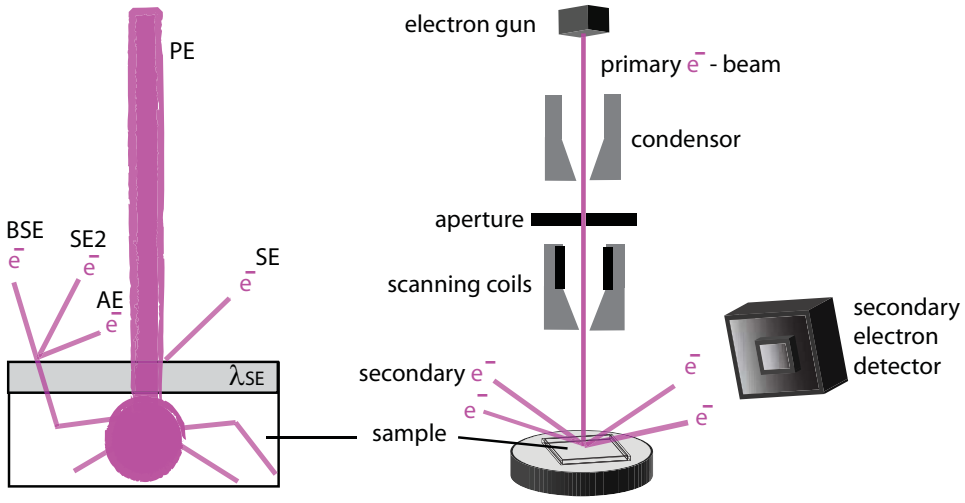

Fig. 2.1 **right:** Schematic of a scanning electron microscope (SEM). **left:** A primary electron beam (PE) hits the sample surface. Secondary electrons (SE), backscattered electrons (BSE), and Auger electrons (AE) are generated by interaction with the sample. Cathode luminescence (KL) and X-rays (X) are also present. The secondary electrons probe only a very thin layer of the sample (λ_{SE}).

by the secondary electron detector are depicted in figure Fig. 2.1.

Secondary electrons (SE) have low energies (< 50 eV). Therefore they can only leave the sample surface within a very thin film ($\lambda_{SE} = 1 - 10$ nm), which results in a high resolution, both laterally and in depth. Detection of SE gives topographic pictures of the sample surface. Backscattered electrons (BSE) have much higher energies and are measured with a different detector. BSE contain information about the samples material composition, since the scattering length (and thus intensity at the detector) is a function of the atomic number. However, the resolution is inferior as compared to SE.

SEM images were recorded on a LEO Gemini 1530 with an In-Lens SE detection system. Native, non-sputtered samples were used in all cases. The acceleration voltage ranged from $0,4$ kV to 5 kV.

2.5 Atomic force microscopy (AFM)

Atomic force microscopy (AFM) was used to investigate the surface structure on a small scale of 1 μm^2. In this microscope a cantilever - the critical element - with a tip at its end is used to scan the sample surface [50, 51, 52]. The sample is moved by a piezoelectric element in the xy-plane and in the z-direction [53].
The tip commonly consists of silicon nitride. In close proximity to a sample, surface forces described by Hook's law act on the cantilever. These forces can be van der Waals forces, capillary forces, electrostatic forces, magnetic forces, et cetera [54].
A laser beam is focused on the back of the cantilever. From there the laser beam is reflected towards a photodetector. The movement of the cantilever changes the position of the laser beam reflection. With the help of the photodetector, this change is converted into an electrical signal. In order to keep the cantilever deflection constant an electronic feedback control is used to adjust the z-position (height) of the sample. Finally the height information of the sample plotted in the xy-plane and results in a topographic picture of the sample surface.

Typically, AFM images are recorded in contact mode, where the tip is in physical contact with the sample surface. An alternative is the non-contact mode, also called tapping mode, which operates at a given tip-sample separation under oscillation of the cantilever at its resonance frequency. The AFM image in tapping mode maps the force of the oscillating contacts of the tip with the surface of the sample. For this the cantilever is kept at a constant distance above the sample which allows the recording of both the

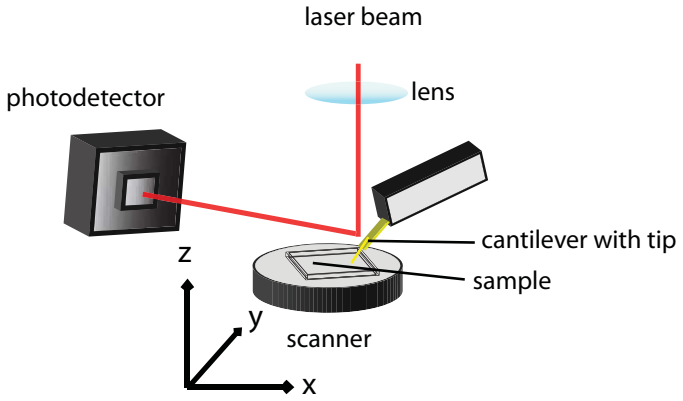

Fig. 2.2 Basic components of an AFM setup. The laser beam hits the tip of the cantilever from above and is then deflected towards the photodetector. The sample is mounted on a scanner which can be moved in x,y and z direction with the help of piezo crystals.

amplitude and the phase image. The height image displays the topography, whereas the phase image provides information about the mechanical properties of the sample. Furthermore, the tapping makes it possible to measure a surface under liquid medium such as water.

AFM images were recorded in tapping mode with a commercially available AFM (Dimension 3100 CL). Micro cantilevers manufactured by Olympus (160μm length, 50μm width, 4.6μm thickness) with an integrated tip and a nominal spring constant of 42 N/m were used. The tip was scanned at rates about 0.7 Hz in a total scan area of 1 μm^2.

2.6 Contact angle measurements

The shape of the liquid droplet on a solid surface is determined by the thermodynamic equilibrium [54]. Young's equation is the basis for a quantitative description of such wetting phenomena:

$$\gamma_L \cos\theta = \gamma_S - \gamma_{SL} \tag{2.3}$$

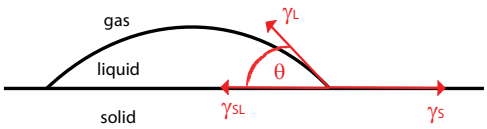

Fig. 2.3 Rim of a liquid drop with a contact angle θ on a solid surface. If the interfacial tension of the bare solid surface is higher than that of the solid-liquid interface ($\gamma_S > \gamma_{SL}$), the right hand side of Young's equation is positive. Then $\cos\theta$ has to be positive and the contact angle is smaller than 90°– the liquid partially wets the solid.

The contact angle θ is defined as the angle between the three phases of a solid surface, a liquid and a vapor phase. It is specific for every system and contains information about surface properties such as roughness and hydrophobicity. If a drop of a liquid is placed on a solid surface there are two possibilities: the liquid spreads on the surface completely ($\theta = 0°$) or a finite contact angle is established. Contact angle measurements are usually done in a environment with constant air humidity.

2.7 Stress-strain measurements

The bulk properties of a polymer are of high value when it comes to the application of the material. The mechanical properties, for example, dictate how the polymer actually behaves on a macroscopic scale. Stress-strain curves are an important measure of a material's mechanical properties. The measurement involves the observation of the behaviour of a polymer as one applies tension stress to it. The material is elongated (strain) to the point where it pulls apart [55].

Figure 4.17(a) shows generic stress-strain measurement curves. The force σ is plotted

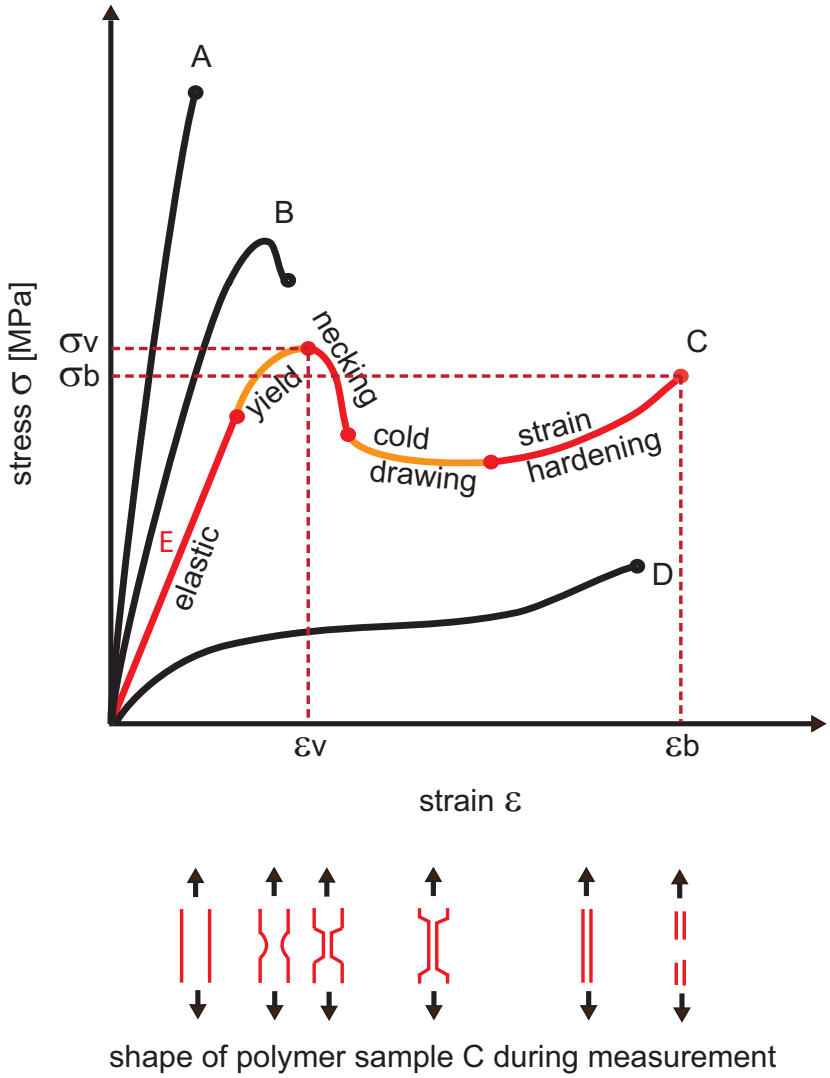

Fig. 2.4 Typical curve for stress strain measurement of polymer materials: (A) hard material with brittle fracture e.g. glassy polymer, (B) hard and strong material with limited plasticity, (C) hard and tough material with cold drawing e.g. typical semi crystaline polymer (D) soft and tough e.g rubber-like material (elastomer).
Important parameters and behaviour are depicted in curve (C): the elastic modulus E, yield stress σ_v, yield strain ϵ_v, stress at breaking point σ_b and breaking point draw ratio ϵ_b. During the *necking* a decrease of cross sectional area along the length of the sample can be observed. *Cold drawing* describes the extension of the neck region - polymer chains unravel and are aligned parallel to the force. The result is the so called *strain hardening*, in which the stress rises until fracture takes place.
The state of the polymer bone sample (C) in the various stages of the stress-strain measurements in depicted beneath the graph.

against the draw ratio ϵ of the material. In the beginning of the experiment the strength σ grows in linear fashion. This is the *elastic* region in which region Hooke's law is obeyed. The deformation is completely reversible and elasticity can be derived from an entropic mechanism. In practise the elastic region is unlikely to be perfect straight, and the elastic module E is taken as a tangent from the first part of the curve.
Once strain is about 1% to 2% deviation from normal linear behaviour is expected. This characteristic point is the moment in which the material irreversibly succumbs to the external force: the yield point. In polymers σ_v is identified as the local maximum on the stress-strain curve. If such a point is not present it is defined as the stress at which the stress-strain curve becomes markedly non-linear: typically, a strain of 1%. The draw axis intercept at the position of the maximum defines the yield strain ϵ_v. At a certain elongation the material breaks, and the force curve drops sharply to zero. By taking the force axis value of this point the tensile strength can be σ_b estimated, while the draw ratio at breaking point λ_b can be read out from the x axis.

$$E = \frac{d\sigma}{d\epsilon} = \frac{d\sigma}{\frac{\Delta l}{l_0}} = \frac{dF/A}{\frac{l-l_0}{l_0}} \tag{2.4}$$

$$\lambda = \epsilon + 1 \tag{2.5}$$

2.8 Surface plasmon resonance (SPR) and optical waveguide (OW) spectroscopy

This section gives a general overview over the SPR/OW spectroscopy method. The actual measurement procedure, materials and fitting details for SPR and OW experiments

are described in chapter 4.12.3.

2.8.1 On surface plasmons

Introduction

Plasmons are collective charge density oscillations in a bulk metal that can be described as propagating longitudinal waves. Normally, plasmons can not couple directly with light. However, there exist certain resonance conditions at the interface between a metal and a dielectric that allow the coupling between the oscillation mode of the electron wave and light. When the x-component of the wave vector of the incident light matches the x-component of the vector of the plasmon wave the excitation condition of a propagating electron density wave at the interface between metal and dielectric is met [56]. When an surface plasmon is excited, an electric field in the z-direction is enhanced that provides a remarkably high sensitivity for interfacial characterizations [57].

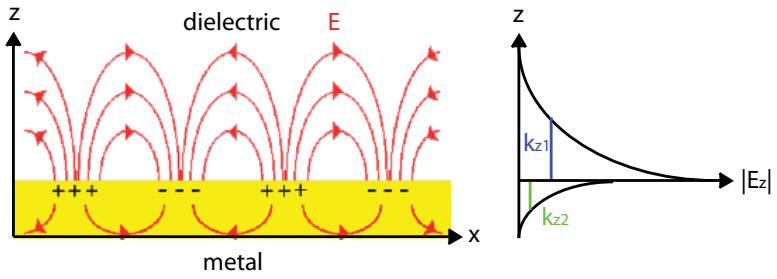

Fig. 2.5 Schematics of the electromagnetic field of surface plasmons propagating along the interface between a metal and dielectric. k_{z1} is the decay length into the dielectric and k_{z2} is the decay length (skin depth) into the metal.

As shown in Fig. 2.5, the plasmon's field strength is very high at the interface and decays exponentially into both metal and dielectric media. The field strength is subject to an absorption effect that is described by a constant that depends on the used materials, the excitation wavelength and the arrangement of the setup. In example, in the frequently

employed Kretschmann setup [57] with 50 nm of gold evaporated on a LaSFN9 glass slide substrate and water as a dielectric medium, the dampening constant is approximately 230 nm^{-1}. The experimental setup is discussed in more detail in section 2.8.3.

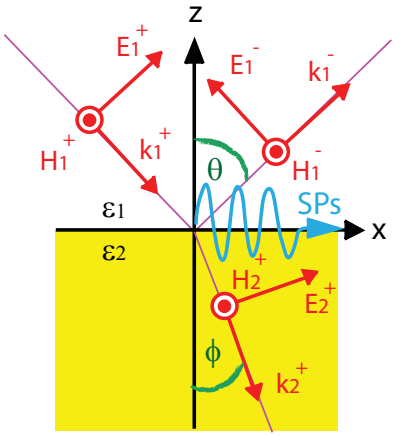

Fig. 2.6 Schematic visualization of the wavevectors and associated fields for coupling of light with surface plasmons. The picture shows an interface in the xy plane between two mediums m_1 ($z \geq 0$) and m_2 ($z \leq 0$). As surface plasmons are longitudinal waves the only possibility of excitation is the use of p-polarized light (TM mode) that has the electric field parallel to the incident plane. The resulting electromagnetic wave propagates along the x-direction and decays exponentially into medium m_1. E and H are the electric and magnetic components of light, ϵ is the dielectric constant of the medium, and ϕ is the incident angle of the light.

The concept of surface plasmons can be described by transmission, reflection and absorption of light at the interfaces of a multi layered surface. The incident photon propagation can be described using the wave vector $\vec{k}$. The z axis is perpendicular to the interface surface and xz is the propagation plane of the wave. The magnetic component of light $\vec{H}$ is irrelevant to the problem when assuming a non magnetic material and can thus be left out. Likewise, since p-polarized light has no electric field in y direction, the y component of the electric field of the electromagnetic wave can be ignored as well. The electric field of the travelling photon can be thus described as

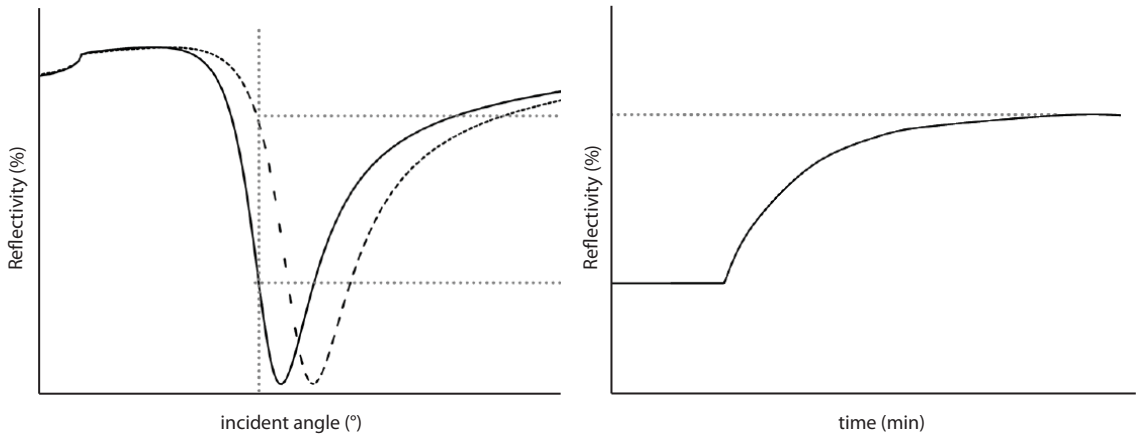

(a) generic SPR curve (b) kinetic SPR measurement

Fig. 2.7 Schematic depiction of a SPR measurement curve in **(a)** angular mode and **(b)** kinetic mode. During an adsorption or swelling process the reflection minimum shifts to higher angles (from solid to dashed line). When observed at a fixed angle Θ, this change of reflected intensity can be used to characterize the kinetics of the observed process.

$$E = E_0 \exp\left(i\omega t - i\vec{k}\vec{r}\right) = \frac{1}{\omega\epsilon\epsilon_0}\vec{k} \times \vec{E} \tag{2.6}$$

with i being the imaginary unit, ω the angular frequency, t the time and $\vec{r}$ the position of the wave vector, $\vec{E}$ the electric field of the travelling wave, and ϵ and ϵ_0 the dielectric constants and the permittivity of vacuum.

The amplitude of the wave vector can be described as a function of the refractive index n, the angular frequency ω and the speed of light in vacuum c.

$$|\vec{k}| = k = \sqrt{k_x^2 + k_y^2 + k_z^2} = n\frac{2\pi}{\lambda} = n\frac{\omega}{c} \tag{2.7}$$

Excitation of surface plasmons

In the case of a photon refracting on the interface of two optically different media Snell's law describes the relationship between refracting angle of transmission and refractive index:

$$n_1 \sin\theta = n_2 \sin\psi \tag{2.8}$$

Combining equations 2.8 and 2.7 gives

$$k_{x1} = k_{x2} = k_x \tag{2.9}$$

Furthermore, using equations 2.8 and 2.9 yields an expression for the z component of the wave vector $\vec{k}$ perpendicular to the interface

$$k_{z2}^2 = n_1^2(\frac{\omega}{c})^2(\frac{n_2^2}{n_1^2} - \sin^2\alpha) \tag{2.10}$$

In the case of $\sin\alpha > \frac{n_2}{n_1}$, the incident light is totally reflected at the bottom of a prism. The right part of equation 2.10 is purely imaginary, resulting in an evanescent field that can be described with the following equation:

$$E = \exp(-k_{z2}z)\exp(i\omega t - i\vec{k_x}x) \tag{2.11}$$

The decay of the electric field into medium 2 is defined by the first exponential term with

the k_{z2} decay length. However, the evanescent field is not a plasmon yet, as additional conditions for the excitation process have to be met.

The dispersion relation

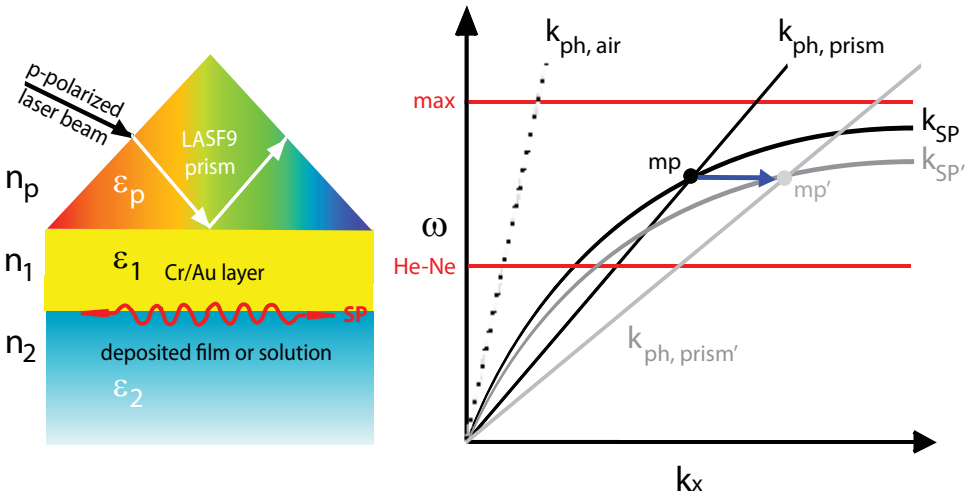

Fig. 2.8 **left**: Overview of the experimental setup in Kretschmann configuration with n being the refractive index and ϵ the dielectric constant of the respective materials. **right**: Dispersion relation for the x-component of free photons in a dielectric (dashed line, $k_{ph,air}$) and the x-component free photons in a prism/LASFN9 layer (solid line, $k_{ph,air}$). It can be seen that normal incident light can not couple directly with surface plasmons, as the measurement values ω and k_x are required to correlate through the dispersion relation in order excite an surface plasmon. k_{SP} and $k_{ph,SP'}$ are the dispersion curves of surface plasmons before and after adsorption of an additional layer, with mp and mp' being the momentum matching points for of the plasmons with the incident light.

$$Re(k_x) = \frac{\omega}{c}\sqrt{\frac{\epsilon_1(w) * \epsilon_2(w)}{\epsilon_1(w) + \epsilon_2(w)}} \tag{2.12}$$

The dispersion relation describes which combinations of two experimentally adjustable parameters - ω and k_x - will lead to the excitation of a surface plasmon. It is defined in

equation 2.12 and graphically shown in figure Fig. 2.8.

As seen on the graph, the correlation goes asymptotically to a maximum angular frequency ω_{max}. This implies that frequencies higher (or wavelengths lower) than that value will not permit for the excitation of a plasmon. The diagonal solid lines describe the dispersion relation between ω and the maximum feasible value for k_x for the incident light. The slope of this lines depends on the refractive index n_1 of the LaSFN9 materials (prism and substrate). Adsorption of molecules on the gold surface or any change in the refractive index in the field of the plasmon changes the wave vector of the plasmon, and thus influences the resonance angle θ.

However, if medium 1 (with refractive index n_1, as defined in Fig. 2.8) is a low refractive material such as air, it still appears impossible to excite a plasmon. This can be explained by the dispersion relation of the incident light. This linear relation, the so-called *light line*, is defined by

$$\omega = c * k_{x,ph}\sqrt{\epsilon_1} = c * k_{x,ph} * n \tag{2.13}$$

with θ being the incidient angle of the propagating light and $k_{x,ph}$ being the x component of the wave vector $k_{x,ph}$ of the free photon (eq. 2.14).

$$k_{x,ph} = \sin(\theta) * k_x \tag{2.14}$$

The dispersion relation of a free photon k_{ph} is propagating in a dielectric medium 2 is always smaller than the wave vector k_{SP} of a surface plasmon propagating along the interface between the metal medium 1 and the dielectric due to the negative dielectric

constant ϵ_1:

$$k_{x,ph} = \frac{\omega}{c} < \frac{\omega}{c}\sqrt{\frac{\epsilon_1 * \epsilon_2}{\epsilon_1 + \epsilon_2}} = k_{SP} \tag{2.15}$$

As such, it is not possible to make any coupling if medium 1 is air. It is, however, possible for higher refractive index materials like glass. For this reason it is necessary to couple the incident light into the system with a prism.

The propagation properties of the plasmon are dependent on the dielectric constants ϵ_i (and thus refractive indices n_i) of all media around the metal film and their respective layer thicknesses d_i. Altering these parameters will change the angle of incident light θ at which the plasmon can be excited.

2.8.2 On optical waveguide modes

Dielectric waveguides have been widely used to confine and guide light. If the coating is thick - around the wavelength of light - and is positioned in between two layers with a lower refractive index that the coating light can be confined by total internal reflection (TIR). In such a case non-radiative modes, so called optical waveguide modes, can be observed [58]. Both p- and s-polarized light - that is a light source in TM and TE mode - can excite these modes. In the measurement configuration used in this theses guided light is coupled out through the prism. Figure 2.9(b) shows these modes by recording the reflectivity as a function of incident angle.

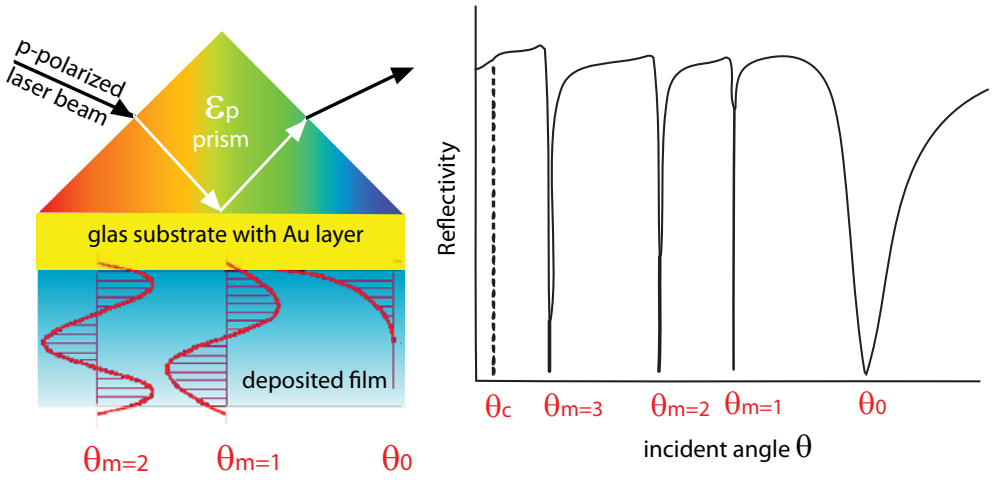

(a) Generic curve

(b) Measurement curves

Fig. 2.9 Schematic depiction of (a) an ATR waveguide configuration and (b) the corresponding scan curve for TM mode. The modes θ_m are indexed in regard to the number of nodes of their field distribution in their waveguide structure. θ_c is the critical angle.

2.8.3 Measurement setup

As mentioned before, no coupling of a surface plasmon is observed when light is directly incident on a flat metal film. This is happening due to the lack of a matching condition between the dispersion relation of surface plasmons and light propagating in air. To overcome this problem, two well known optical systems developed by Otto [59] and Kretschmann [57] can be used to match the dispersion conditions. Both methods are using attenuated total reflection (ATR) to excite surface plasmons. However, the Kretschmann configuration is less problematic, since the Otto configuration makes it difficult to to control the distance between the prism and the metal, and is therefore used in the OW experiments.

Essentially, the reflected light intensity is probed with a photodiode. Fig. 2.10 shows the typical experimental setup. In this Kretschmann configuration, plasmons are excited

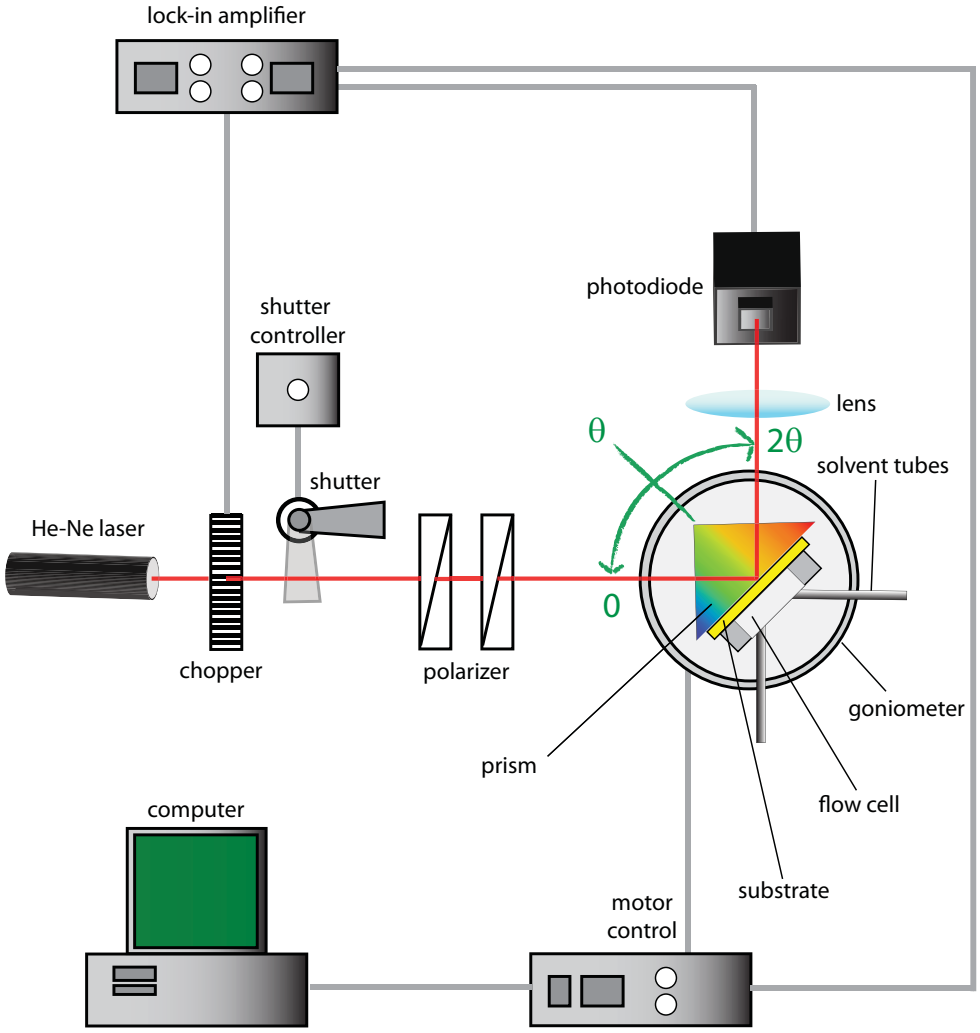

Fig. 2.10 SPR/OW spectroscopy setup in Kretschmann configuration.

via prism coupling. At most incidence angles, the laser light is reflected off the metal-prism interface, either by simple reflection or total internal reflection (TIR). At the angles where the momentum of the incoming light matches the plasmon requirements, destructive interference between the incoming and the back-coupled light leads to a minimum in the recording of the reflectivity. The recording of reflectivity as a function of the incident angle has been depicted in figure 2.7(a).

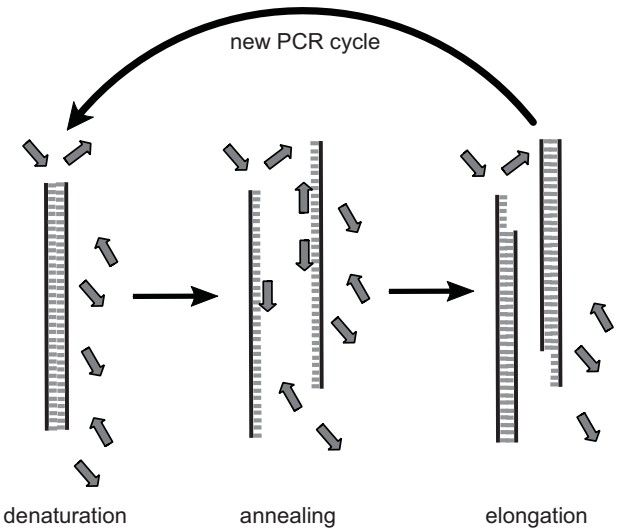

Fig. 2.11 Schematic description of a PCR cycle: the first step is the denaturation of template DNA molecules at 94 ℃. This is followed by the separation of DNA double strand to single strand molecules. In the annealing step, which takes place at 55 ℃, the primers are hybridized to the DNA single strands. The final step of the cycle is the elongation of the DNA: the amount of DNA is doubled through DNA polymerase enzyme activity.

2.9 Quantitative polymerase chain reaction (QPCR) and DNA detection

The polymerase chain reaction (PCR) is a technique in molecular biology that amplifies a single or a few copies of a piece of DNA across several orders of magnitude. That way thousands to millions of copies of a particular DNA sequence are generated. The most modern method of quantification of nucleic acids is the real time detection (RTD-) PCR, which uses markers to keep track of the kinetics of the reaction cycles. However, use of dye molecules for intercalation in double stranded DNA molecules has its drawbacks when it comes to the specifity regarding correct products and reaction artifacts [60, 61].

Early approaches used radio active nucleotide markers to attack this problem [62], which came with a higher workload due to the necessity to take and analyse aliquots. Nowadays,

the common strategy involves fluorescence resonance energy transfer (FRET) [63]. Numerous methods have been established: The molecular beacons method [64], hybridization probes method [65] and the Taqman method [66]. The latter method is the best known and is thus used in this study. It does not measure absolute amounts of nucleic acids but tracks the kinetics of the PCR reaction.

The Taqman method

The Taqman method is depicted in figure 2.12(b). Here, the reporter and quencher fluorophores are located on the same oligonucleotide. Once the nucleotide is no longer intact due to polymerase activity, the reporter is released into solution and emits in a specified wavelength. A CCD detector is then used to detect the rise of fluorescence signal over time.

The quantification of PCR product is not done in absolute but relative values. The values are based on a comparison of fluorescence signal over time. However, it is important to look into the characteristics of the PCR in order to maximize the efficiency of the detection. In the first phase of amplifications of a PCR the amount of template DNA is limited: the probability that a template molecule meets a primer and a polymeraze enzyme at the same time is suboptimal. In later stages of the QPCR the amount of DNA fragments grows exponentially. In the end phase, disturbing influences like a shortage of primers and nucleotides, temperature dependent denaturation of enzymes/nucleotides or the appearance of pyrophophates inhibit the reaction. As such, the middle phase of the amplification of the PCR is most interesting for the quantification process.

In order to assess the DNA amplification process a benchmark value is introduced: The point where the fluorescence signal can be clearly distinguished from the background noise is defined as the *cycle threshold* (C_T) value. This value is taken as a reference

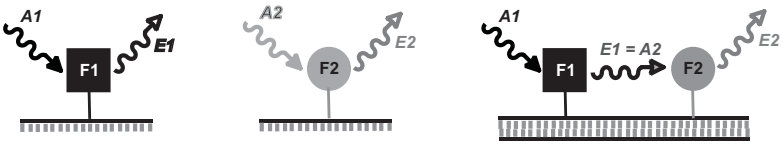

(a) FRET Primer for PCR

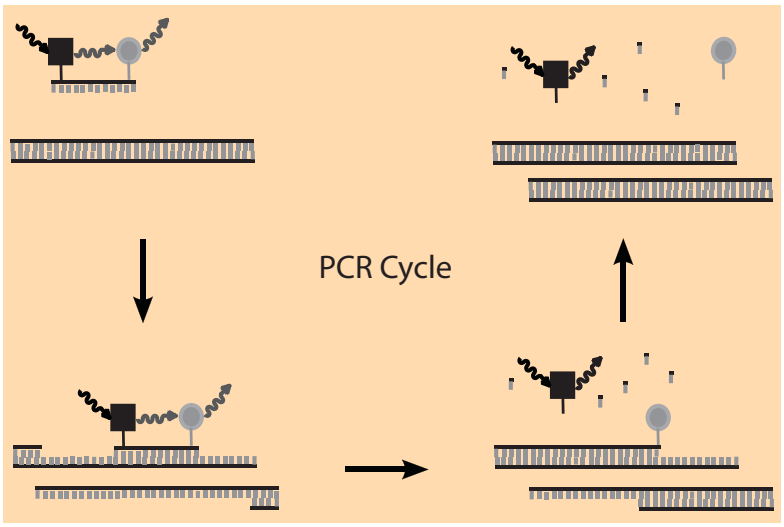

(b) Taqman RTD-PCR

Fig. 2.12 Schematic overview of the Taqman PCR method. **(a)** A donator fluorescence dye F1 with characteristic excitiation and emission spectra is exited by a specific wavelength A1 and emits light of a wavelength E1. If a acceptor fluorochrome F2 with an excitation spectrum matching the emission spectrum of the donor is brought within proximity of the donor energy is tranferred from the donor to the acceptor. **(b)** Taqman molecular beacons start to give fluorescence signal once the oligonucleotide is dismantled by the polymerase and are no longer in the proximity of the acceptor molecule.

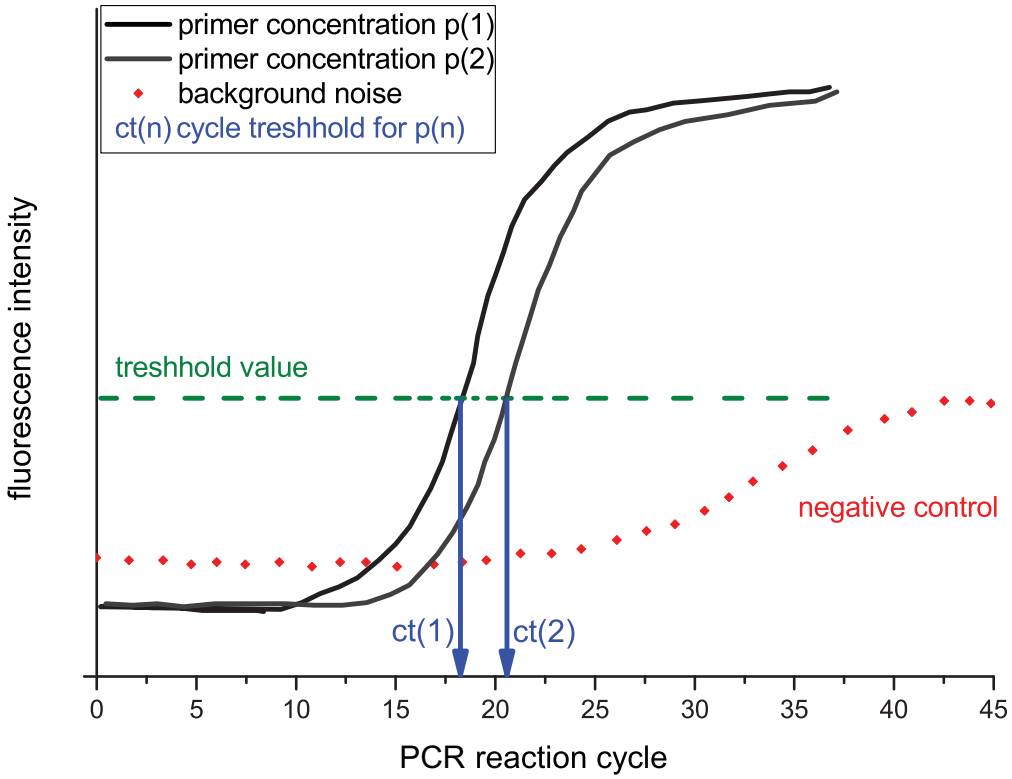

Fig. 2.13 Fluorescence curves for two Taqman PCR amplifications with different amounts of template DNA.

point at which the growth of DNA is still in the exponential region while not being affected by any of the aforementioned inhibiting factors (Fig. 2.13).

In order to calculate the amount of DNA in a sample, multiple PCR amplifications are run with a different amount of template DNA. The resulting standard curve is depicted in figure Fig. 2.14. While the resulting plot can the be used to estimate the original DNA amount in the sample from the C_T value, it is common to calculate these values with a program (Fig. 2.15).

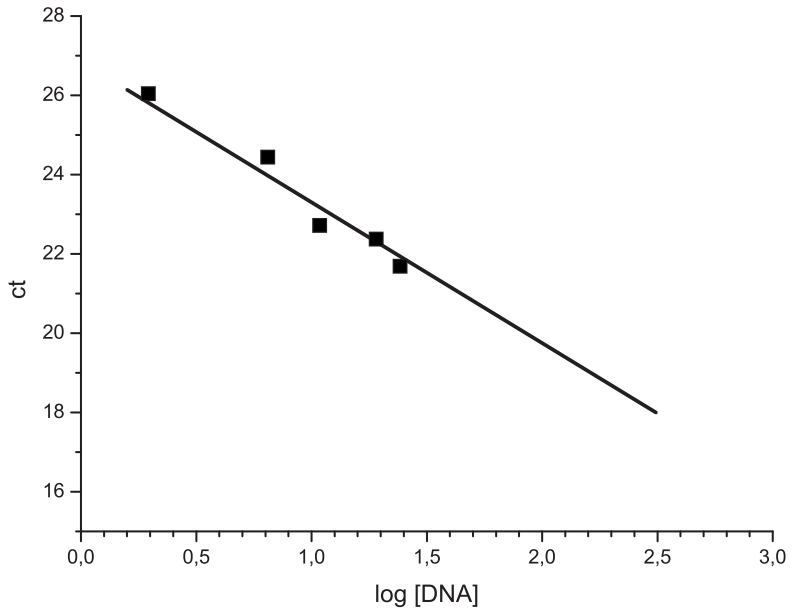

Fig. 2.14 Plotting the C_T values against DNA template concentrations allows to estimate the DNA amount in a sample.

2.10 Chemical analysis

2.10.1 Field desorption (FD) mass spectrometry

FD mass spectra were obtained on a VG Instruments ZAB 2-SE-FPD spectrometer.

2.10.2 Nuclear magnetic resonance (NMR) spectroscopy

^{1}H-NMR, ^{13}C-NMR, C-H correlation experiments were recorded in the listed deuterated solvents on a Bruker DPX 250, Bruker AMX 300, Bruker DRX 500 or a Bruker DRX 700 spectrometer. The deuterated solvent was used as an internal standard. In complicated cases, spectra were simulated using ACDLabs NMR prediction software to compare the results.

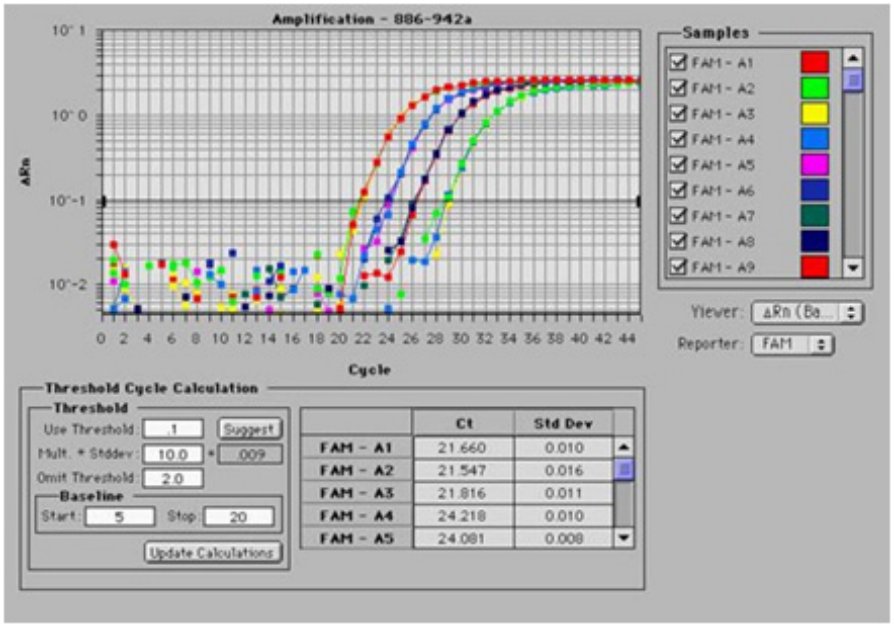

Fig. 2.15 Program for the evaluation of PCR data that is used to calculate the amounts of DNA in the samples.

2.10.3 Differential scanning calorimetry (DSC) and thermogravimetric analysis (TGA)

For TGA, a Mettler TG 50 thermogravimetric analyzer was used to determine the decomposition temperature. DSC was measured on a Mettler DSC 30 with heating and cooling rates of 10 °C/min. The measured temperature interval ranged from −150 °C until thermal decomposition of the material.

2.10.4 Gel permeation chromatography (GPC)

GPC measurements were conducted in DMF at a temperature of 60 °C relative to a PMMA standard on a PSS GRAM column from the company PSS. The concentration of the samples was 2 g/L and the flowing speed was 1 ml/min. The signal was detected by a refractive index (RI) detector and a UV detector. The data was evaluated by the

program WinGPC Unity (PSS).

2.11 General methods and materials

2.11.1 Chemicals and solvents

All used chemicals and solvents were obtained from the companies ABCR, Acros, Aldrich, Fluka, Lancaster, Merck and Strem. Monomers were recrystalized from solvent according to literature or purified by destillation under vacuum. All other chemicals - unless mentioned otherwise - were used as obtained.

2.11.2 Chromatography

Preparative column chromatography was performed on silica gel from Merck with a grain size of 0,063 to 0,200 mm (silica gel) or 0,04 to 0,063 mm (flash silica gel, Geduran Si 60). For analytical thin layer chromatography (TLC) silica gel coated substrates (60 F254 from Merck) were used.

Compounds were detected by fluorescence quenching at 254 nm, self-fluorescence at 366 nm or staining in an iodine vapor chamber. For eluents, analytically pure solvents (p.a. or technical grade) were distilled prior to the use. The compositions of the eluents are given together with the retention value R_f.

For repeated chromatographic separation of large batches it was chosen to use very short silica columns (low amount of silica gel) and operate with a solvent gradient during the entire separation procedure. After loading the column with the crude material, a specific volume of solvent was added on the column and sucked dry using a vacuum. The latter

step was repeated in a short time frame with a slightly higher solvent polarity until the product could be isolated from the solvent fractions.

2.11.3 Protective gas techniques

A Schlenk line was used for work with chemicals sensitive to water or oxygen.

3 Synthesis of photocrosslinkable pHEMA based hydrogel precursors

3.1 Introduction

This chapter describes the synthesis and the characterization of photocrosslinkable hydrogel precursors that are based on pHEMA. A general preparation method to obtain the pHEMA based polymer is developed and optimized in regard to polymerization conditions. Furthermore, the copolymerization behaviour of the monomers examined.

3.1.1 Choice of polymer material

Since their development by Wichterle and Lim in 1960 [67], poly(2-hydroxyethyl methacrylate) (pHEMA) and related hydrogels have been widely used for a variety of biological and medical applications [68] e.g. contact lenses. Their structure permits a water content similar to that in living tissues while being inert to biological degradation processes and permeable to metabolites. Furthermore, it is not absorbed by the body, withstands heat sterilization without damage and can be prepared in a variety of shapes and forms [69, 70, 71, 72, 73].

HEMA homopolymers are generally regarded as a hydrophilic but water-insoluble material [74, 75]: linear pHEMA with a degree of polymerization (DP) < 40 is completely water-soluble at 20 ℃ and pH $6,5$, whereas the homopolymers with DP > 40 are only able to swell in water [76]. The introduction of additional functional groups into the HEMA polymer makes it possible to tweak physical properties like water solubility [77] and swelling [78], thermal resistance [79], mechanical stabilities [80] and most importantly, biological characteristics like the adsorption of biomolecules [81]. For instance, HEMA based copolymers adsorb less protein albumin with increasing content of carboxylic groups due to the negatively charged surfaces, which was related to their increased biocompatibility [82]. Methacrylic acid (MAA) easily copolymerizes and provides polymer chains with carboxylic side groups, which are highly hydrophilic and thus able to form hydrogen bonds with corresponding groups. Small amounts of methacrylic acid comonomer contribute to a higher degree of swelling and reduce the 'skin effect' by supporting the formation of channels [72].

3.1.2 Fabrication of hydrogel films on surfaces

Many concepts have been developed to coat hydrogels on surfaces: spin coating of an photocrosslinkable polymer precursor material followed by crosslinking and surface attachment by UV-light [84, 85, 86], brushes grafted *in situ* from the surface by free radical polymerization [87, 88] and controlled radical polymerization techniques [89, 90, 91], functionalized polymers grafted to a modified substrate [92, 93], physical methods like plasma polymerization [94] and grafting by electron beam [95]. The first concept is used in this thesis for reasons explained below.

When it comes to the adjustment of a hydrogel to the specific requirements of an application, the concept of UV - light induced photocrosslinking of deposited polymer precursors gives a large degree of versatility in obtaining a hydrogel surface coating. This choice

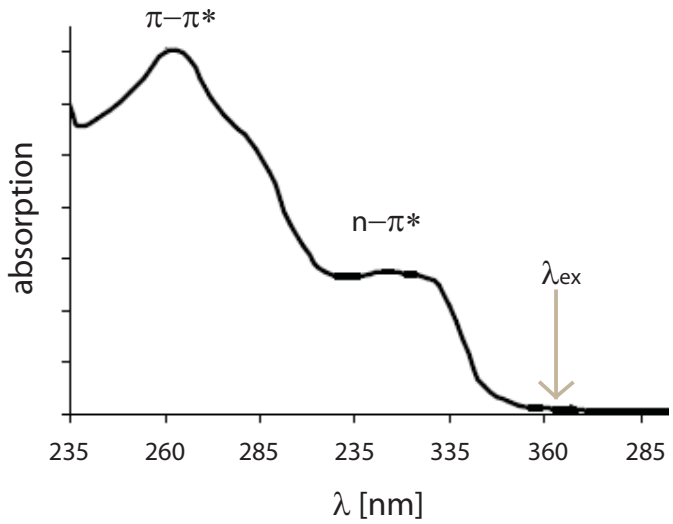

Fig. 3.1 UV/vis absorption spectrum and spectroscopic transitions of benzophenone, as measured in $CHCl_3$ with a concentration of 10^{-5} mol/L. The used excitation wavelength λ_{ex} is 365 nm. The absorption maxima can be shifted up to 20 nm depending on the solvent [83].

of strategy makes the functionalization of the hydrogel simple but elegant. Functional groups can be attached to a polymerizable group and included as functional monomers in the polymerization procedure. Or they can be added to the hydrogel precursor polymer chains via the route of post polymerization reactions. A last possibility is the coupling of functional molecules to the crosslinked hydrogel with the use of active groups like active esters [33] or peptide coupling reagents [96, 97].

3.2 Synthesis of the polymerizable photocrosslinkable group

Photocrosslinking is a technique widely used in the coating industry [98]. As such, there exist a variety of different photocrosslinking systems that have been extensively studied in the recent years: photosensitive ammonium dichromate, for instance, was used to crosslink pHEMA films containing hydrocortisone succinate by UV radiation [99]. Co-

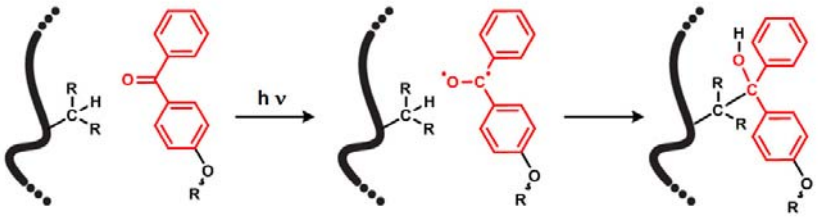

Fig. 3.2 Covalent crosslinking of aliphatic polymer strands can be done by exposing the polymer bound benzophenone groups to UV - light irradiation. The benzophenone molecule is excited and transitions into a diradical species that is responsible for the C-H insertion reaction.

valent binding to aliphatic polymer films was carried out by attaching the photosensitive reagent 4-azidobenzoimidate [100] and 4-azido pyridine derivatives [101] to HEMA polymer. Another interesting example was the photoinduced formation of the hydrogel network by selective [2+2] cycloadditon reactions of dimethylmaleinimideacrylamide groups attached to the polymer backbone [102].

For this work, a benzophenone derivative has been chosen as the UV-crosslinking group. It was already used for the crosslinking of pNIPAAm based hydrogels [85, 103] and belongs to one of the most important classes of photoexcitable molecules. It allows to perform crosslinking reactions at lower energies up to a wavelength of 400 nm, greatly reducing the amount of photodegradation to the polymer.
Fig. 3.1 shows the UV/vis absorption spectrum of benzophenone. The broad conjugation of the π - electron system shifts the $n - \pi^*$ transition of the carbonyl group to 330 nm, resulting in the formation of a biradical triplet excited state. This radical - as shown in Fig. 3.2 - then abstracts a hydrogen atom from neighbouring aliphatic C-H groups to form new C-C bonds [83, 104, 105].

The crosslinking of the polymer with benzophenone groups after polymerization allows a thorough characterization of the material. Once the formation of an insoluble hydrogel

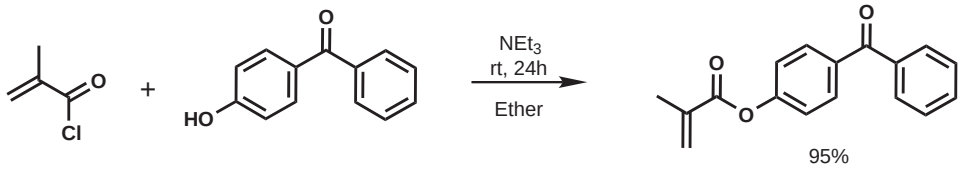

Fig. 3.3 Synthesis scheme of the photocrosslinkable monomer MABP.

network is complete, sample preparation and measurement might not be possible. An additional advantage is the fact that not only aliphatic polymers but every C-H-containing molecule can react photochemically with benzophenone, as reported for polyelectrolyte layers [106], chemically inert polystyrene (pS) or perylene carbon coatings [107]. Precisely this attribute makes benzophenone an ideal candidate when it comes to the surface attachment of hydrogel films to e.g. polypropylene (PP) substrates (see chapter 6). Also, benzophenone derivatives can be applied as adhesion promotor on glass and gold surfaces [85, 86], as done in chapter 4.2 for hydrogel film characterization experiments.
Fig. 3.3 shows the synthesis of the benzophenone monomer: 4-benzoylphenyl methacrylate (MABP) has been synthesized by reacting 4-hydroxybenzophenone with chloromethacrylic acid according to literature [104]. After copolymerization with a comonomer it allows to crosslink the polymer strands by UV-irradiation [85].

3.3 Synthesis of hydrogel precursors

The synthesis of a generic hydrogel precursor is demonstrated in Fig. 3.4. HEMA is taking the role as polymer backbone monomer, while MABP and a possible third functional co-monomer component are used in smaller amounts. The copolymers are synthesized by free radical copolymerization with the initiation being facilitated by thermal decomposition of azobisisobutyronitrile (AIBN). After reacting for one day at 65 °C, the copolymer is purified by threefold precipitation in cold diethylether and subsequent drying under

high vacuum at 25 ℃.

Table 3.1 Examples of polymerizations under variable reaction conditions with a HEMA / MABP ratio of 99:1. Partially crosslinked and crosslinked polymers are marked in the comments column.

solvent	monomer	M/I ratio	Mn	Mw	PDI	yield	comment
	w% solv.		g/mol	g/mol		%	
MeOH	8	200	23000	63500	2,8	68	high PDI
MeOH	12	200	18000	59000	3,3	77	high PDI
MeOH	22	500	45000	131000	2,9	81	part.crossl.
MeOH	35	1000	57000	321000	5,6	71	part.crossl.
MeOH	25	500	32000	81000	2,5	56	part.crossl.
MeOH	20		45000	121000	2,7		part.crossl.
DMF	10	100	36000	87000	2,4	92	good
DMF	11	200	42000	95000	2,3	90	good
DMF	25	200					crossl.
DMF	10	1000	101000	262300	2,6	96	good
THF	23	300					crossl.
THF	10	200	23500	77000	3,3	72	high PDI
EtOH	12	500	37200	103400	2,8	34	part.crossl.
EtOH H_2O 2:1	12	500	23000	78000	3,4	65	crossl.
dioxane	12	200	29000	81000	2,8	75	good
dioxane	20	200					crossl.

Because of the nature of free radical polymerization [108] and the used photocrosslinking concept (see chapter 4), precise control of the polymer chain length and molecular weight distribution is not possible and not of primary concern for the synthesis of the hydrogel precursors. As long as the photocrosslinking can be carried out in a manner that binds most chains to each other in covalent fashion, the hydrogel is going to be mechanically cohesive and not loose much material during the first swelling process [109].

While the synthetic method is principally not so much different from an already thoroughly investigated analogue system that uses NIPAAm as polymer backbone [109, 33], the usage of HEMA brings in a couple of problems which can be tracked to the occurrence of side reactions taking place during the polymerization. As such, uncontrolled crosslinking processes take place prior to the deposition procedure, greatly disturbing

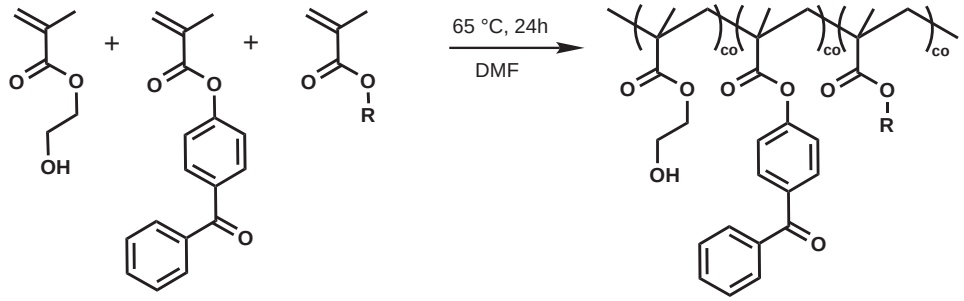

Fig. 3.4 Synthesis of hydrogel precursors by free radical polymerization in DMF. Note that it is the intention to produce not crosslinked and thus soluble polymer material.

the purification and handling of the hydrogel precursors. Consequently, the film deposition process can not be carried out at all. This makes the optimization of the reaction conditions in regard to the reduction of unwanted crosslinking a matter of great importance. It is pursued by analysing the hydrogel precursors obtained through different polymerization conditions.

Table 3.1 shows a compilation of several reaction parameters in which HEMA has a monomer mol fraction of 99%. The solvents methanol, ethanol, ethanol - water mixtures, tetrahydrofurane, dioxane and dimethylformamide are used to test the polymerization conditions. While the polymerization was running in all of these five solvents, methanol and dimethylformamide showed the best results in respect of product quality and ease of purification.

Polymerizations carried out in MeOH that either target a molecular weight beyond 70000 Dalton or are run with higher monomer concentrations than 12 wt% result in completely crosslinked or partially crosslinked polymers. Unfortunately, partially or completely crosslinked polymers are useless in regard of film deposition and have to be discarded. One way to get reproducible reaction results in MeOH - albeit at a lower yield - is to reduce the concentration of the reaction solution and to increase the initiator amount from 0.1 mol percent to 2 mol percent of the total monomer concentration.

The resulting polymers have with a very short chain length of about 150 units. These polymers are likely to contain many polymer chains that have no crosslinking group and thus can not be used to build a stable hydrogel network.
Compared to methanol as reaction medium, dimethylformamide (DMF) allows higher molecular weights and gives access to polymers with better polydispersity (PDI) values and product yields. Still, the monomer concentration remains a critical factor when it comes to the occurrence of unwanted crosslinking. The overall concentration of the monomers may not exceed 12 wt% of the total reaction mixture in order to obtain a reproducible PDI $(2,2-3,0)$ and prevent the formation of a hydrogel through chemical crosslinking processes. In addition, only the use of such low monomer concentrations allows the incorporation of protic monomers such as methacrylic acid (MAA) into the polymerization without experiencing unwanted crosslinking reactions.

The undesired chemical crosslinking and formation of hydrogels can be attributed to more than one process. A first explanation would be the normal side reactions of chain termination and branching that can found in a free radical polymerization [110]. Furthermore, it is known that a reversible disproportionation of monomethacrylates to dimethacrylates is taking place at the used reaction temperatures. Ultimately, this formation of corresponding glycols enlarges the amount of chemical crosslinkers in the reaction mixture [111]. In addition, the participation of CH_2-CH_2-OH groups during radical polymerization contributes to branching, as previously reported for polymerization of HEMA [74] and similar monomers [112, 113]. It is important to minimize such reactions because already a small amount of inter polymer strand crosslinks can greatly affect the properties of a polymer. Such side reactions are not an issue with the application of various water-soluble and water swellable polymers on HEMA basis that have been synthesized and studied by many research groups. However, these trans-esterification reactions pose a problem when it comes to purification and deposition of the synthesized photocross-

linkable hydrogel precursors. The solution to avoid this problem is the usage of DMF as reaction solvent and keeping the overall monomer weight percentage in the reaction mixture below 12 %.

Solubility

The synthesized copolymers were soluble in methanol, ethanol, dimethyl formamide, dimethyl acetamide, dimethyl sulfoxide, tetrahydrofuran and insoluble in n-hexane, water, acetone and chloro-group containing solvents such as dichloromethane and chloroform. This gives access to a wide range of solvents for the film deposition procedure.

3.3.1 Characterization by ^{1}H-NMR

Fig. 3.5 shows the ^{1}H-NMR spectra of the HEMA monomer and polymer in d-MeOH. The two singlets at 5,5 ppm and 6,3 ppm can be allocated to the unreacted olefinic hydrogen atoms of the monomer and are not existent in the polymer. This qualifies the usage of these signals as a monomer specific indicator for the conversion of the polymerization reaction. The triplets at 3,7 ppm and 4,2 ppm in the monomer spectrum represent the four hydrogen atoms in the hydroxyethyl side chain. These signals get broader during the transition from monomer to oligomer to polymer species. The same can be observed with the singlet at 2 ppm that is coming from the methyl group in the methacrylate moiety: it becomes broader and gets shifted to higher field due to the disappearance of the C-C double bond. Likewise, several signal bands can be found around 1 ppm and 2 ppm in the polymer spectrum. These broad bands are coming from CH_2 and CH_3 groups located at the polymer backbone.

The ^{1}H-NMR spectrum of the pHEMA-co-pMABP copolymer (Fig. 3.6) shows a signal

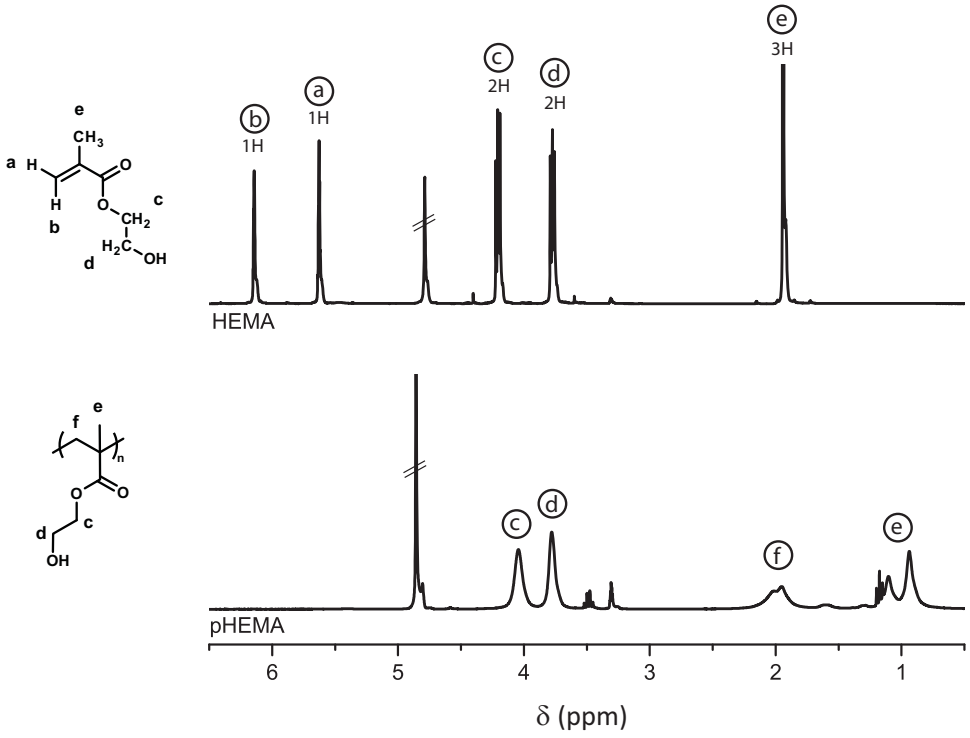

Fig. 3.5 250 MHz ^{1}H-NMR spectrums of HEMA and pHEMA as recorded in d-MEOH.

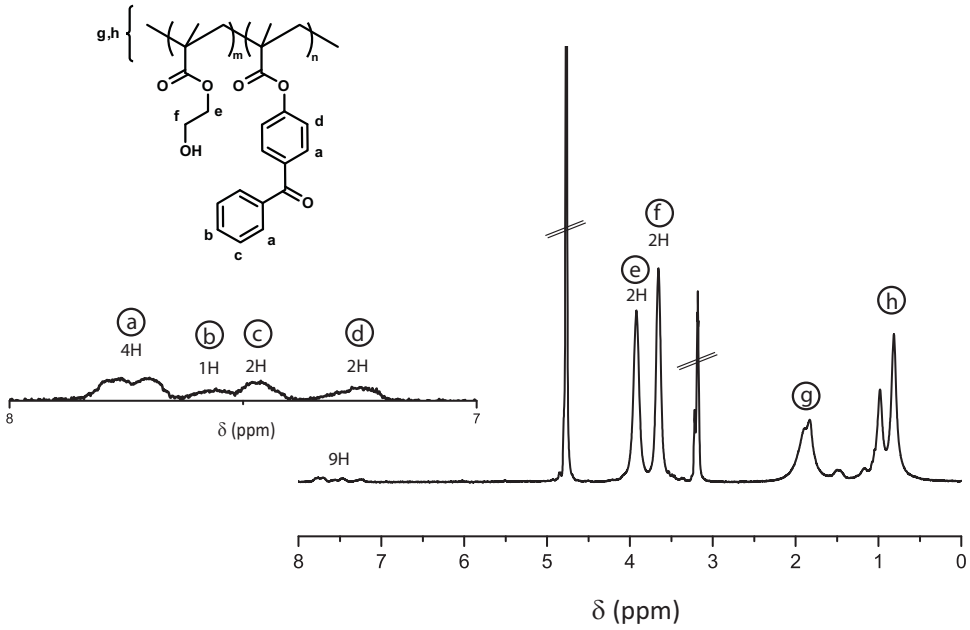

Fig. 3.6 250 MHz ^{1}H-NMR spectrum of pHEMA-co-pMABP in d-MEOH. The copolymer has a benzophenone content of 1%.

group in the aromatic region which corresponds to the nine protons on the aromatic ring of the benzophenone groups. The broadness of the signals can be explained by the fact that the benzophenone ring is covalently bonded to the polymer backbone and is thus reduced in its freedom of movement. The doublet signal at 7,8 ppm can be allocated to the protons at the 2 and 6 positions of the aromatic rings, while the single aromatic proton at 4 position shows in a signal at 7,6 ppm. The four hydrogen atoms at the 3 and 5 positions of the aromatic are split into two groups - the two hydrogen atoms near the backbone appear at higher field at 7,25 ppm while the two protons belonging to the terminal aromatic ring can be found at 7,45 ppm.

The broad signals at 4,0 and 3,7 ppm can be attributed to the hydroxyethyl side chains of the HEMA groups in the polymer. It is possible to make use of these two signal groups to calculate the amount of photocrosslinking groups inside the hydrogel precursors. The average number of photocrosslinking groups in all polymer chains is one ninth of the integral of the aromatic signal group, while the average number of HEMA groups per polymer chain is one fourth of the integral of the signal groups of the hydroxyethyl side chain. This gives the possibility to calculate the average relative amount of crosslinker groups in the hydrogel precursor N_{xrel} from the respective integrals a,b,c,d,e and f in the polymer spectrum in Fig. 3.6 with the following equation:

$$N_{xrel} = \frac{\frac{1}{9}\int(a+b+c+d)d\delta}{\frac{1}{9}\int(a+b+c+d)d\delta + \frac{1}{4}\int(e+f)d\delta} \tag{3.1}$$

3.4 Polymerization kinetics of HEMA and MABP

The copolymerization behaviour of MABP with NIPAAm has already been subject to qualitative discussion in the thesis of Patrick Beines [109]. The Q/e-values of NIPAAm

were compared to the Q/e-values of methacrylic acid phenyl ester - the latter being assumed to represent a close approximation of the MABP monomer. The author came to the conclusion that it would be likely for MABP ($r > 2$) to copolymerize with itself rather than with NIPAAm. NIPAAm ($r < 0.4$) would prefer to polymerize to MABP. As a consequence, it is expected that MABP would show a distribution gradient when polymerizing with the acrylic NIPAAm monomer. Given the fact that MABP is only used in very small amounts, the polymerization might result in a highly inhomogeneous composition of photocrosslinking groups in the polymer and could have an effect on the network formation. However, there is no quantitative data backing up this statement and no studies of the polymerization kinetics of HEMA and MABP are known in literature. As such the copolymerization of HEMA with MABP has been examined thoroughly with ^{1}H-NMR spectroscopy.

3.4.1 Basic procedure

The separate appearance of the hydrogen atoms on the alkene group in both HEMA and MABP in the ^{1}H-NMR spectrum gives the possibility to monitor each monomer conversion separately in the polymerization reaction. However, this can be only done by using a molecule that serves as internal standard for the kinetic measurements. Neither should such a reference molecule be affected by the polymerization reaction, nor may it not influence the kinetics of the polymerization in any major way. The easiest way to do this would be the addition of an inert compound that does not overlap with the important signal groups that are monitored with the ^{1}H-NMR spectroscopy measurements. Anisole, with its five aromatic protons, proves to be a good candidate in this regard.

The ^{1}H-NMR spectrum of the polymerization mixture before the beginning of the polymerization is shown in Fig. 3.7. The spectrum is recorded in deuterated DMF. The

integral of the signal group at 7,3 ppm is two thirds of the integral of the signal at 6,9 ppm. It can be attributed to the aromatic protons at 2 and 4 position of the anisole ring. The signal at 6,9 ppm belongs to the hydrogen atoms at 1,3 and 5 position of the aromatic ring. These anisole signals are taken as a reference regarding the ongoing polymerization process.

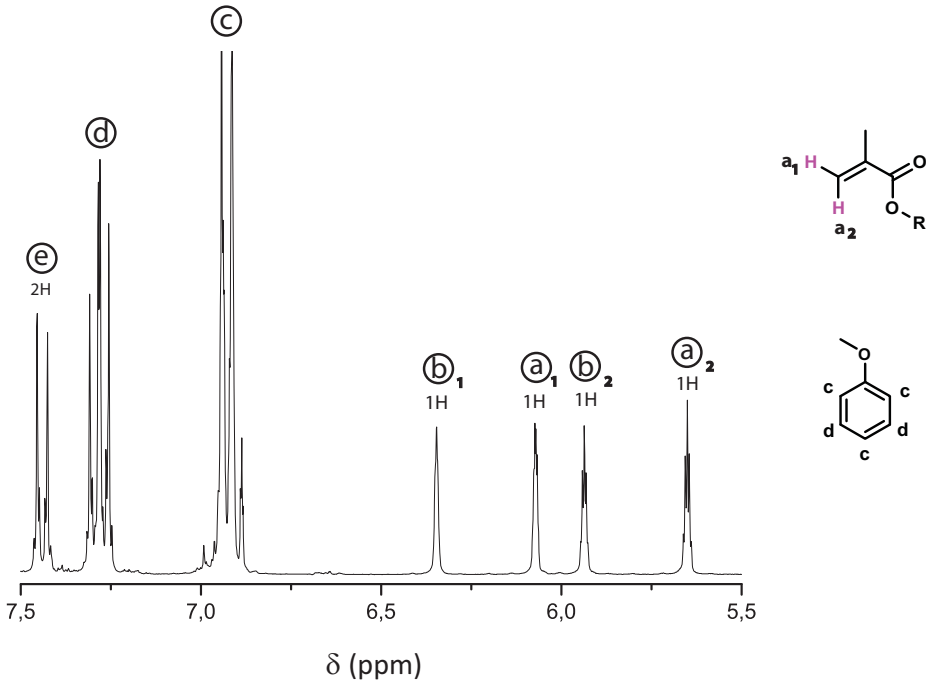

Fig. 3.7 ^{1}H-NMR spectrum in d-DMF with equimolar amounts of HEMA and MABP. The reference bands c and d come from hydrogen atoms bound to the aromatic ring of anisole. The signal group e comes from the aromatic hydrogen atoms of the benzophenone ring.

The doublet signal group at 7,45 ppm belongs to the two aromatic hydrogel atoms on the benzophenone ring that can be found next to the methacrylic ester oxygen atom. Since these protons are not involved in any way in the polymerization reaction, the signal is not supposed to change over time, and thus can be used as a standard for estimating the amount of MABP in the polymer solution. The singlets at 6,35 ppm (b_1) and 5,90 ppm (b_2) belong to the olefinic protons of the methacrylic moiety of MABP, while the two singlets at 6,20 ppm (a_1) and 5,65 ppm (a_2) belong to the hydrogen atoms

on the carbon double bond of HEMA. The hydrogen atom at Z – position of the olefinic double bond is shifted to lower field due to the proximity of the methacrylic ester oxygen atom. The integrals of the olefinic signals decrease proportionally to the conversion of the polymerization.

The conversion of HEMA at a specific time t can be calculated using equation 3.2. The average integral of both alkene hydrogen proton signals a_1 and a_2 is related to it's average value before the start of the reaction. The conversion of the monomer MABP is calculated by the same equation using the integrals of the singlets b.

$$conv(t) = \frac{\int a_1(t_0) + a_2(t_0)d\delta - \int a_1(t) + a_2(t)d\delta}{\int a_1(t_0) + a_2(t_0)d\delta} \tag{3.2}$$

The polymerizations were carried out in DMF at 65 °C with an initiator amount of 0.1 mol% of the total monomer concentration. The amount of anisole used is 5 mol% of the total monomer amount. This is done so that the reference material amount is as small as possible in order to minimize its effect on the reaction and to have a small error in regard of the measurement of the reference material signal by ^{1}H-NMR spectroscopy.

3.4.2 Investigation of polymerization conversion of an equimolar monomer mixture

A first impression on the copolymerization behaviour of HEMA and MABP can be gained by monitoring the conversion of the polymerization of an equimolar mixture of HEMA and MAPB. Starting from the unreacted mixture, aliquots are taken in regular time intervals after the beginning of the reaction until the polymerization has reached a high conversion.

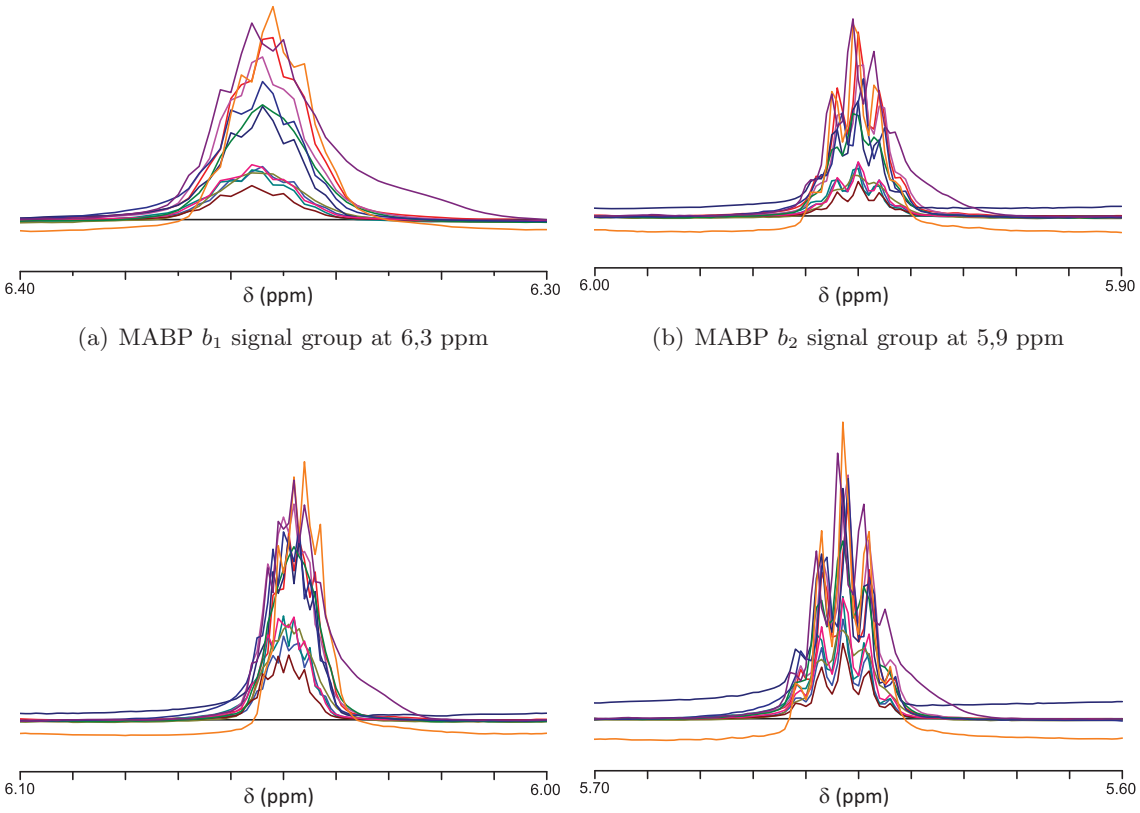

(a) MABP b_1 signal group at 6,3 ppm

(b) MABP b_2 signal group at 5,9 ppm

(c) HEMA a_1 signal group at 6,2 ppm

(d) HEMA a_2 signal group at 5,6 ppm

Fig. 3.8 300 MHz ^{1}H-NMR measurements showing the decrease of the olefinic hydrogen atom signals of the double bond in the methacrylic moiety of the comonomers during the polymerization.

Figure 3.9(a) shows the plot of the conversion of the polymerization reaction in respect of both monomers against time. The resulting conversion curve shows a typical shape of the free radical polymerization [108]: while the initial polymerization rate is very fast, it slows down quickly within the first hours of the reaction and reaches a plateau region at around 80% of conversion.

Figure 3.9(b) describes the relative amount of monomers in the polymer over time. In the beginning of the reaction, MABP shows a slightly higher rate of polymerization, giving the polymer an initial composition of 60% MABP and 40% HEMA. With the reaction proceeding into further stages, the amount of HEMA molecules becomes higher than the amount of MABP molecules. This statistical imbalance compensates the difference in monomer reactivity and results in a change towards a higher inclusion rate of HEMA at high conversions. In equimolar polymerization, the higher activity of MABP at the start of the reaction creates a gradient in the distribution of crosslinking groups in the polymer chain, resulting in a lower density of crosslinking groups at the towards the end of the polymers.

3.4.3 Measurement and calculation of monomer reactivity values

In order to investigate the polymerization behaviour in greater detail and calculate the reactivity ratios of the monomers in the reaction it is necessary to conduct multiple copolymerizations with variable feed parameters. The reactions are run in DMF with anisole as reference substance and an initiator concentration at 0.1 mol% of the total monomer amount. In order to minimize the error of the ^{1}H-NMR measurements and stay as close as possible to the theoretical assumptions of the kinetic equations discussed below, the conversion of the experiments is kept around 9,5%. After the reactions have been quenched the remaining monomers MABP (M_1) and HEMA (M_2) are quantified

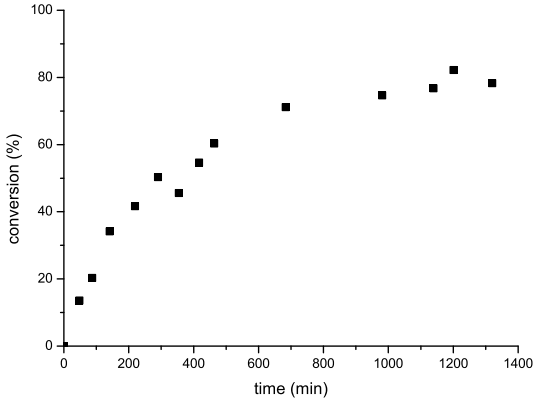

(a) Conversion – time

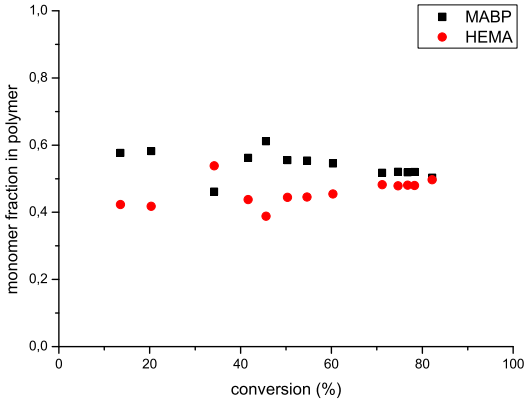

(b) Polymer composition

Fig. 3.9 Plots of kinetic experiment data from a polymerizations with a HEMA/MABP ratio of 1:1 and anisole as reference substance. The data was recorded in d-DMF with a 300 MHz ^{1}H-NMR spectrometer.

by ^{1}H-NMR spectroscopy by the use of equation 3.2.

The monomer fraction in the feed is defined as $f_1 = \frac{[M_1]}{[M_1]+[M_2]}$. The composition of the polymer regarding a specific monomer M_1 at time t can be described through the the amount of reacted monomer M_1 relative to the total amount of polymerized monomer: $F_1 = \frac{d[M_1]}{d[M_1]+d[M_2]}$ [110].

Under the two assumptions - the reactivity of the growing polymer chain is only affected by the nature of its reactive end group and is independent from chain length - there are four possible growth steps for a radical polymerization reaction [110, 114]. The copolymerization parameters are defined as the quotient of the growth constant of homopolymerization and the growth constant of heteropolymerization [115]: $r = \frac{k_{homo}}{k_{hetero}}$ is a measure for the probability of a addition to a given active species. If the r-values are both 1, there is no preference for either monomer species, and a statistical polymer is created. In the case that $r_1 = r_2 = 0$, the copolymerization goes in a perfectly alternating polymer. Block- or Homopolymers are created in the case of $r_1, r_2 >> 0$ [108].

Mayo-Lewis

Under the the conditions of the steady state assumption $k_{21}[M_2][M_1] = k_{21}[M_2][M_1]$ and the terminal model [110] the decrease of the monomer concentration $[M_1]$ and $[M_2]$ in the starting mixture the copolymer equation [108] can be written in the form of Mayo-Lewis [116]:

$$r_1 = f(r_2) = r_2 m_i + b_i = r_2 \frac{dM_1}{dM_2}(\frac{M_2}{M_1})^2 + \frac{M_2}{M_1}(\frac{dM_1}{dM_2} - 1) \tag{3.3}$$

The slope and axis intercept of equation 3.3 are known due to the chosen monomer

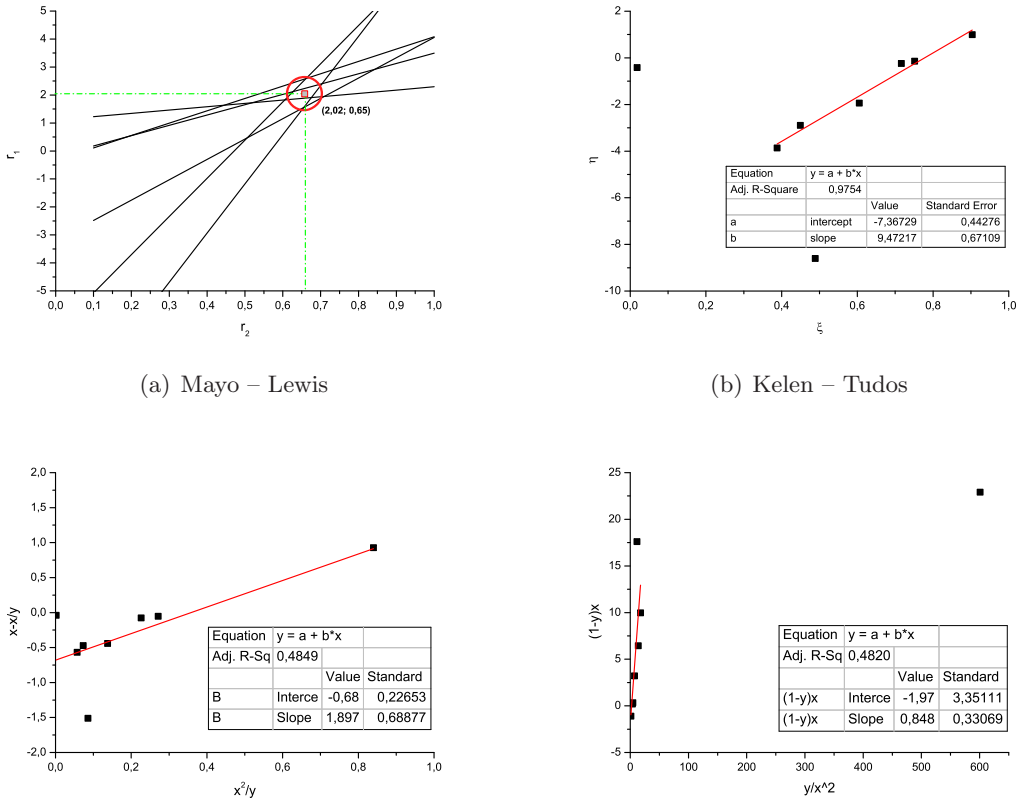

(a) Mayo – Lewis

(b) Kelen – Tudos

(c) Fineman – Ross with eq.(3.4)

(d) Fineman – Ross with eq.(3.5)

Fig. 3.10 Estimation of the r_1 and r_2 values from the kinetic ^{1}H-NMR measurements with three different methods: Mayo - Lewis (a), Kelen - Tudos (b) and Fineman - Ross (c&d).

ratios and measured copolymer compositions. Thus it is possible to draw a straight line $r_1 = f(r_2)$ for every copolymerization mixture. In theory, the coordinates of the crossing point of all lines are the copolymerization parameters r_1 and r_2 . In practise, the middle point of the smallest circle which crosses or touches every line is taken for a good estimation of those values.

Fineman-Ross

The r-value estimation after Fineman-Ross [117] uses a linearized form of the copolymer equation, in which $y = \frac{d[M_1]}{d[M_2]}$ is the instantaneous polymer composition, while $x = \frac{[M_1]}{[M_2]}$ is the instantaneous monomer composition:

$$x - \frac{x}{y} = r_1 \frac{x^2}{y} - r_2 \tag{3.4}$$

When plotting $x - \frac{x}{y}$ against $\frac{x^2}{y}$, the values for r_1 and r_2 can be read out of the slope and axis intercept respectively. Note that the slope is much better determined than the intercept. As such, the plot according to the second equation 3.5 is more useful to determine the r_2 parameter:

$$\frac{1-y}{x} = r_2 \frac{y}{x^2} - r_1 \tag{3.5}$$

Kelen-Tudos

The Kelen-Tudos method [118] is based on the eq. 3.6, where η (eq. 3.7) and ξ (eq. 3.8) are functions of the monomer mole fraction in the copolymer and in the feed respectively, and α is an appropriately chosen arbitrary parameter to obtain a uniform spread of the data regarding ξ in the interval of 0 and 1.

$$\eta = r_1 \xi - r_2 \frac{1-\xi}{\alpha} \tag{3.6}$$

$$\eta = \frac{\frac{M_1}{M_2}\frac{dM_2}{dM_1}(\frac{dM_1}{dM_2} - 1)}{\alpha + (\frac{M_1}{M_2})^2\frac{dM_2}{dM_1}} \tag{3.7}$$

$$\xi = \frac{(\frac{M_1}{M_2})^2\frac{dM_2}{dM_1}}{\alpha + (\frac{M_1}{M_2})^2\frac{dM_2}{dM_1}} \tag{3.8}$$

$$\alpha = \sqrt[n]{\prod_{1\leq i\leq n}(\frac{M_1}{M_2})^2\frac{dM_2}{dM_1}} \tag{3.9}$$

In order to obtain the values for r_1 and r_2, η is plottet against ξ. The obtained straight line is extrapolated to $\xi = 0$ and $\xi = 1$, which returns the values $-r_2/\alpha$ und r_1 as axis intersects respectively.

Table 3.2 r–values by Fineman-Ross

	slope	intercept	equation
r1	1,9	1,97	(3.4)
r2	0,85	0,68	(3.5)

3.4.4 Discussion of reactivity values

Table 3.3 Calculated r–values

Method	r1	r2
Mayo - Lewis	2,02	0,65
Fineman - Ross	1,9	0,85
Kelen - Tudos	2,1	0,6613

The average value of r_1 (2,0) is larger than 1 and that of r_2 (0.70) less than 1. This suggests the presence of a higher amount of MABP units in the copolymer than in the feed. The product of r_1 and r_2 - 1,4 - is slightly larger than 1, which indicates the

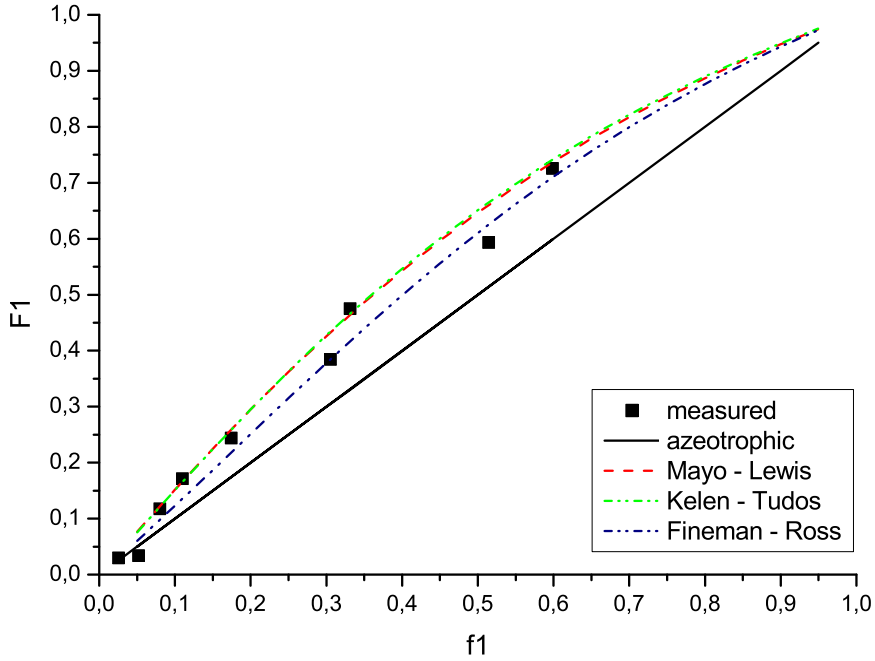

Fig. 3.11 Molar fraction of benzophenone in feed (f1) and polymer (F1), as measured with ^{1}H-NMR spectroscopy and calculated with the use of the copolymer equation (eq. 3.10).

formation of a random copolymer with longer sequence of MABP units in the copolymer [108].

Fig. 3.11 shows the results of the copolymerization with various monomer ratio in a feed - polymer diagram in an an early stage of the reaction. The r–values obtained by the Mayo - Lewis, Fineman - Ross and Kelen - Tudos methods are inserted into the copolymer equation (eq. 3.10) and result in curves that cover the distribution of measurements quite well.

$$F_1 = 1 - F_2 = \frac{r_1 f_1^2 + f_1 f_2}{r_1 f_1^2 + 2 f_1 f_2 + r_2 f_2^2} \tag{3.10}$$

As already found in the previous kinetic measurements in chapter 3.4.2 – and reflected by the estimated r–values – the amount of benzophenone in the feed and the polymer show a tendency towards a higher incorporation rate of benzophenone into the polymer in all feed compositions.

With the exception of the rough theoretical estimation of the copolymerization behaviour of benzophenone with the NIPAAm monomer [109], glycidyl methacrylate (GMA) [119] and the methyl methacrylate (MMA) [120], there are very little references regarding the r–values of benzophenone in the literature. In each case the r_1 values are greater than 1 and r_2 values are lesser than 1, which indicates that the amount of MABP in the copolymer is always greater than its corresponding ratio in the feed when reacting with similar methacrylic or acrylic monomers. Methacrylates like MMA show very similar copolymerization behaviour with benzophenone, as can be seen by the comparing the r–values determined of Vijayanand et al. ($r_1 = 2,121; r_2 = 0,634$) [120].

Given the fact that the initiaton with AIBN does not happen simultaneously but over a longer period of time [108], the number of benzophenone in polymer chains initiated at a later stage of the reaction might come with less benzophenone units, or could possibly even be made of pure HEMA monomers. However, the used HEMA/MABP monomer ratio in the reaction mixture is 99 : 1. Hence it is expected that the statistical influence is dominating the polymerization. Assuming a M_n of 130000 it is expected to find around ten photocrosslinker units in a copolymer chain.

3.4.5 Calculation of Q–e values from measurement data

The Q/e–scheme allows the prediction of the monomer reactivity ratios for comonomer pairs that have not yet been copolymerized. It is a useful correlation developed by Alfrey and Price [121], who proposed that the rate constant for a radical-monomer reaction,

e.g. for the reaction of M_1 radical with M_2 monomer, can be written as

$$k_{12} = \frac{P_1}{Q_2} \exp\left(-e_1(e_1 - e_2)\right) \tag{3.11}$$

P_1 represents the intrinsic reactivity of M_1 radical, Q_2 represents the intrinsic reactivity of M_2 monomer, e_1 represents the polarity of M_1 radical, and e_2 represents the polarity of M_2 monomer. By assuming that the same e value applies to both a monomer M and it's corresponding radical M•, one can write expressions for the rate constants k_{11}, k_{22} and k_{21} analogous to equation (3.11). These two equations can be appropriately combined to correlate monomer-radical reactivity with the parameters Q_1, Q_2, e_1, and e_2 and yield the monomer reactivity ratios in the form

$$r_1 = \frac{Q_1}{Q_2} \exp\left(-e_1(e_1 - e_2)\right) \tag{3.12}$$

$$r_2 = \frac{Q_2}{Q_1} \exp\left(-e_2(e_2 - e_1)\right) \tag{3.13}$$

The basis of the Q–e scheme (eqs. 3.11 to 3.13) is the theoretically unsatisfactory suggestion that the alternating tendency in polymerization is observed due to ground-state electrostatic interactions between permanent charges in the monomer and radical [122]. The Q–e scheme is best considered as an empirical approach to placing monomer reactivity on a quantitative basis. Monomer reactivity is separated into the parameter Q, which describes the resonance factor (and to a slight extent the steric factor) present in the monomer, and the parameter e, which describes the effect connected to its polarity.

Converting equation (3.13) to Q_1 and inserting it into equation (3.12) results in

$$e_1 = e_2 \pm \sqrt{-\ln r_1 r_2} \tag{3.14}$$

$$Q_1 = \frac{Q_2}{r_2} \exp\left(-e_2(e_2 - e_1)\right) \tag{3.15}$$

The Q–e values for copolymerization of HEMA in DMF can be found in literature [123, 124], while the r–values have been estimated from the copolymerization experiments listed in Table 3.3: the average r_1 value is 2,0, reflecting the preference of MABP to react more with its own species than with HEMA, while the r_2 value of 0,72 for HEMA represents a weak tendency towards the reaction with MABP.

First, the e_1 (polarity) value for monomer M_1 (MABP) was calculated for HEMA as reaction partner using eq. (3.14); r_1 and r_2 had been previously determined, and the value e_2 for the comonomer (HEMA) is from the literature. Next the reactivity value Q_1 for monomer M_1 (MABP) was calculated for HEMA by substituting the previously determined values of e_l and r_1, as well as the Q_2 and e_2 values for HEMA into eq.(3.14): Q_1 is calculated to be 0,84.

Unfortunately, it is mathematically not possible to calculate the Q–e values for MABP with HEMA monomer pair, since the equations above returns complex numbers as a result. Another monomer pair should have been chosen for the estimation of the r - parameters.

3.5 Conclusion

Basic photocrosslinkable hydrogel precursors were synthesized by free radical polymerization: HEMA was chosen as the monomer to form the majority of the polymer backbone,

while the content of the photocrosslinking comonomer MABP was adjusted to 1%. The reaction conditions have been optimized in order to minimize unwanted crosslinking reaction prior to photocrosslinking. The best synthetic results for the synthesis of the hydrogel precursor were obtained by using DMF as a solvent, a reaction time of 24 hours and a temperature of 65 °C. The copolymers obtained under these conditions had a PDI of about 2,5 and a M_w of about 250000. When spin coated with DMF as solvent, good films with excellent optical quality could be obtained.

The investigation of the polymerization kinetics and copolymerization behaviour of MABP with HEMA in DMF with ^{1}H-NMR spectroscopy measurements and further analysis with Mayo - Lewis, Fineman - Ross and Kelen - Tudos methods reveals the r values to be 2,0 and 0,7. This indicates a slight preference of inclusion of crosslinker into the polymer. However, due to the used monomer ratio of 99% HEMA to 1% MABP molecules in the reaction mixture, this preferential inclusion of MABP into the polymer can be neglected. The calculation of Q/e - values was not possible for the HEMA/MABP monomer pair because the corresponding r–values returned a complex number.

At the end, a reproducible method for the synthesis of photocrosslinkable hydrogel precursors has been established.

3.6 Experimental

3.6.1 General procedure for free radical polymerization

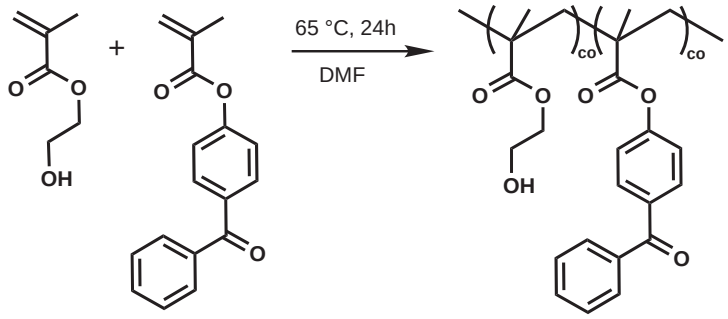

10 g freshly distilled HEMA, 0,202 g MABP (0,076 mol) and 0,003 g AIBN (1,9 10^{-5} mol) are solved in 70 ml dimethylformamide and degased for 30 minutes with argon. The reaction flask is sealed, covered with aluminium foil (to minimize light induced crosslinking) and immersed into an oil bath at 65 ℃. The reaction mixture is stirred for 24 hours. The polymerization is stopped by exposing the reaction mixture to air and immersing the reaction tube in liquid nitrogen. The reaction mixture is diluted with dimethylformamide, precipitated in 1,5 liters cold diethylether and dried under vacuum. The polymer is purified by repeated solvation in DMF, precipitation in diethylether and drying under vacuum.

^{1}H-NMR (250 MHz, d-MEOH): $\delta/ppm = 4,15$ (band, 2H, -CH_2); 3,80 (band, 2H, CH_2); 2,00 (band, 2H, CH_2); $1,50 - 1,00$ (band, 3H, CH_3).

3.6.2 4-Methacryloyloxybenzophenone

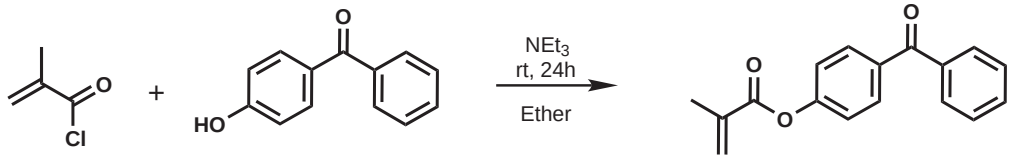

To a solution of 4-hydroxybenzophenone (5 g, 0,025 mol) in 25 ml dry ether are added 3,9 ml triethylamine (2,85 g, 0,0275 mol) . Dropwise addition of 2,4 ml methacrylic-acidchloride (2,6 g, 0,025 mol) is started after cooling the solution to 0 ℃. After the addition is completed, the reaction mixture is allowed to stir at room temperature for one day.

For purification the precipitated triethylammonium chloride is removed by filtration. The organic layer is extracted three times with 30 ml 0,1 molar HCl and three times 50 ml with destilled water. After this, the organic phase is concentrated under reduced pressure. The product is precipitated overnight in the refrigerator.

Yield: 6,3 g 95%

^{1}H-NMR (250 MHz, d-MEOH): $\delta/ppm = 2,00$ (s, 3H, -CH_3); 5,93 (s, 1H, CH=C); 6,31 (s, 1H, CH2= C);7,32-7,86$(m, 9H, C - H_{arom})$.

FT-IR (ATR, powder): n/cm^{-1} = 3049 w, 2979 w, 2927 w, 1730 s, 1651 s, 1595 s, 1497 w, 1446 m, 1409 w, 1318 m, 1301 m, 1278 m, 1199 s, 1161 s, 1148 s, 1126 s, 1012 m, 937 s, 922 s, 886 s, 805 m, 788 m, 733 s, 696 s, 677 s, 641 s.

4 Fabrication and characterization of hydrogel films

4.1 Introduction

This chapter describes the synthesis and the application of adhesion promotors to a substrate surface and the fabrication and surface attachment of hydrogel samples from photocrosslinkable precursor materials. Moreover, the characterization of hydrogel behaviour in regard to swelling, mechanical properties, thermal degradation, network parameters, diffusion and adsorption of biomolecules is described. In addition, the mesostructuring of the materials with with porosigens and 2D laser interference lithography is evaluated.

4.2 Preparation of hydrogel films

For most biological applications and many analytical methods it is necessary to immobilize the functional hydrogel material to a substrate. Because hydrogels are of hydrophilic nature and therefore easily separated from any surface, a covalent attachment to the substrate is much more stable than physisorption [125].

Since hydrogel precursors already have a photocrosslinkable moiety in the form of benzo-

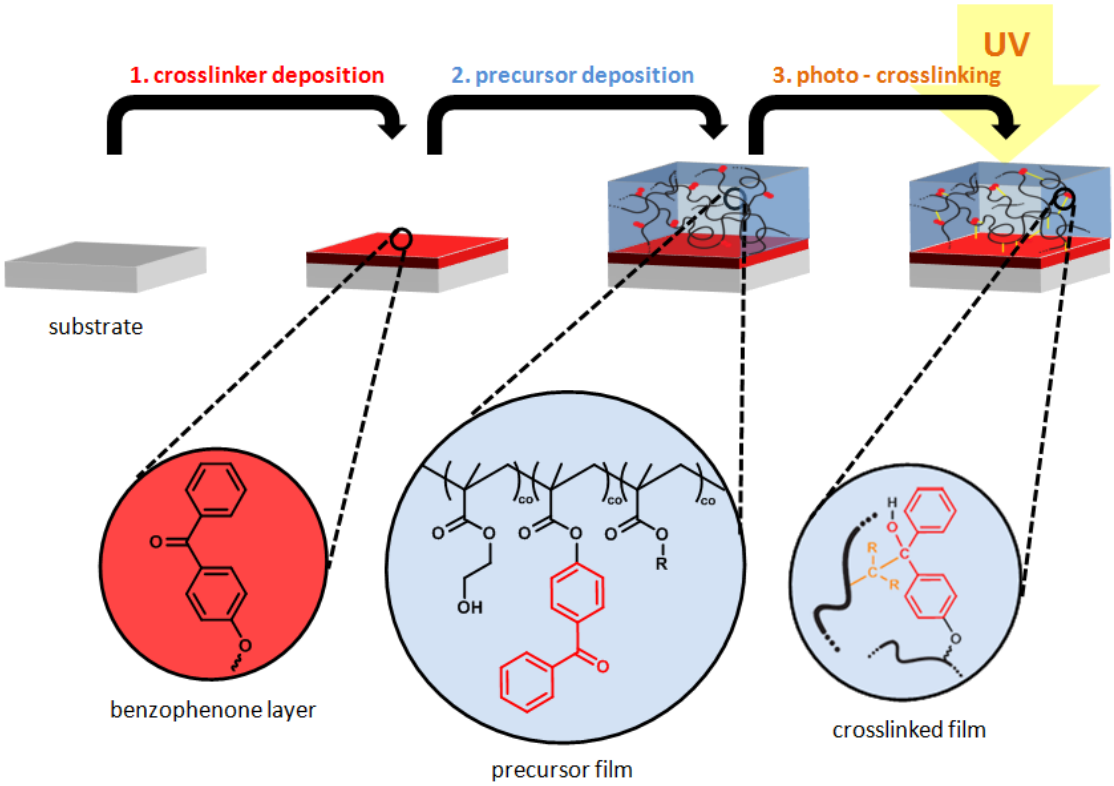

Fig. 4.1 Preparation of a surface attached hydrogel film. **(1)** Deposition of the adhesion promotor on the substrate surface. **(2)** Spin coating of the precursor materials. **(3)** Crosslinking of the benzophenone groups in the deposited film and on the substrate.

phenone group, it is very practical to use a derivative of the same molecule as adhesion promotor.

Fig. 4.1 shows the overall film fabrication concept: In a first step, the target substrate is functionalized with a layer of adhesion promotors which transform it into a surface capable of covalently binding to organic matter through photocrosslinking. This is followed by the film deposition of hydrogel precursors with an appropriate method. The film is then dried under high vacuum. This is necessary because leftovers of organic solvent molecules in the film could make the photocrosslinking groups react with the solvent rather than with the hydrogel precursors. Due to the nature of the photoinduced C-H insertion reaction of benzophenone it is not necessary to facilitate the attachment between the hydrogel and aliphatic polymer substrate with an adhesion promotor: benzophenone surface groups are capable of crosslinking into the surface groups of the polymer.

As a result, the UV light irradiation of a substrate functionalized with benzophenone and benzophenone containing polymer film creates crosslinks within the film and on the film - substrate interface, resulting in a surface bound polymer network.

4.2.1 Synthesis and application of adhesion promotors

SPR and OW spectroscopy measurements of the adsorption of molecules on the hydrogel surface and the hydrogel swelling behaviour need to be performed on a gold surface. Since the concept of photopatterning of gold surfaces with the use of self assembled monolayers (SAMs) of thiols or disulfides is already well known [126], a benzophenone-thiol derivative was chosen as the surface binding strategy.

The covalent binding of a hydrogel film to SiO_2 surfaces (e.g. glass, silicium wavers) can be facilitated by chemically modifying the surface of the substrate with the use of a benzophenone silane derivative. Both benzophenone monochlorsilane [86] and benzophenone triethoxysilane [127] derivatives have been used in literature. Of those two molecules,

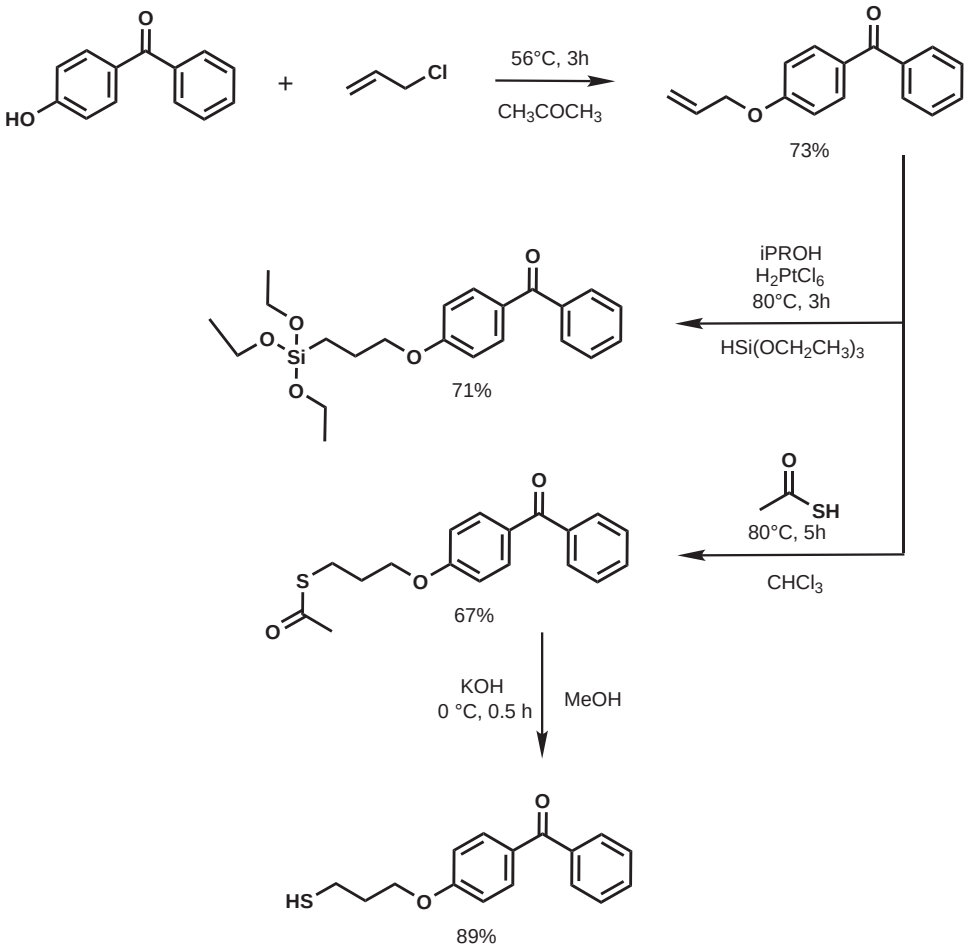

Fig. 4.2 Synthesis scheme of benzophenone based adhesion promotors for SiO_2 and gold substrate surfaces.

the latter has been chosen as adhesion promotor due to easier handling under ambient laboratory conditions, lower reactivity and better stability when it comes to storage. In addition, they can be purified by column chromatography using passivated silica gel e.g with hexamethlydisilazane (HMDS) or tetramethoxysilane (TMOS). The silane based photocrosslinkable adhesion promotor is also useful when it comes to the attachment of benzophenone groups to activated oxide surfaces e.g. plasma treated polymer surfaces and glass surfaces treated with *piranha solution*.

Thiol derivative for gold and silver surfaces

The synthesis scheme of the adhesion promotors is shown in Fig. 4.2. In a first step, 4-allyloxybenzophenone is synthesized in a nucleophilic substitution reaction from 4-hydroxybenzophenone [104]. Ethanethioic S-acid is then added to the double bond, resulting in S-3-(4-Benzoylphenoxy)propylethanthioate (PEBP) [85]. The latter molecule can be further transformed under basic conditions to the benzophenonethiol derivative. In this thesis, gold bound SAMs of PEBP were produced by incubating freshly sputtered gold substrates in an ethanolic solution of the benzophenone thiol.

Prior to the deposition of the hydrogel, the substrates were incubated overnight in a solution of the respective adhesion promotor. After the formation of the benzophenone layers, the substrates were cleaned with organic solvents. Contact angle measurements of water can easily illustrate the extent of surface modification: figure 4.3(a) shows the spreading of a water droplet on a freshly sputtered gold surface. Compared to the unmodified gold surface, the substrate with the benzophenone thiol SAM (figure 4.3(b)) has a significantly larger contact angle. The average contact angle of a clean glass substrate is 23 degrees, while the silanized substrate gives an average contact angle up to 65 degrees. This change can only be explained with a hydrophobic layer of benzophenone molecules forming the first layer of contact.
Hydrogel films deposited and crosslinked to the modified substrates showed a good resistance to mechanical interaction e.g. qualitative tests involving the scratching the crosslinked film with a spatula. In addition, the film stability was tested under aqueous conditions with SPR spectroscopy and proved to be stable in both in acidic ($pH > 3$) and basic ($pH < 9$, e.g. PBS buffer solution) milieu.

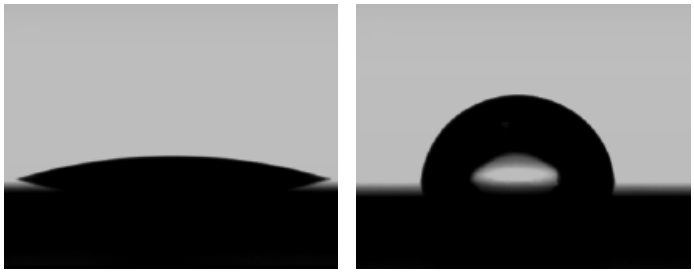

(a) gold surface (b) gold surface with SAM

Fig. 4.3 Contact angle measurements of water droplets on substrates used for the immobilization of hydrogel films in SPR/OW spectroscopy measurements. Both surfaces are freshly produced with sputtering/incubation techniques.

Ethoxysilane derivative for glass, silizium or plasma-activated polymer surfaces

To obtain the benzophenone silane derivative triethoxysilane is added in a hydrosilylation reaction with hexachloroplatinic acid as a catalyst to 4-allyloxybenzophenone [127]. Because of the convenient removal under high vacuum, triethoxysilane can be used in excess in this reaction. The catalyst is removed by column chromatography. The benzophenone triethoxysilane derivative can be stored conveniently in dry ethanolic solution in order to avoid self-condensation and enhance durability.

In order to achieve a more thorough binding of the substrate surface to the silane it is helpful to generate a more reactive SiO_2 surface. This is achieved by breaking the Si_2O bonds on the substrate surface through exposure to a strong acid like piranha solution [125]. The substrates are then incubated in a pre-hydrolysed solution of photoreactive silanes. In addition, consecutive heating speeds up silane-silane and silane-surface condensation reactions. The quality and extent of surface modification can easily be proven by contact angle measurements, as shown in figure 4.3(a).

4.2.2 Spin coating of hydrogel precursors

Spin coating is a fast and widely used method for preparing thin (10 nm) or thick (10 μm) polymer films on planar surfaces [128]. It involves the deposition of a polymer solution on a spinning subtrate. The quick evaporation of the solvent eventually leads to the formation of a uniform film. The thickness of the polymer films can be defined by the solvent, the concentration polymer in the solvent and the turning speed of the substrate.

Good solvents for pHEMA based hydrogel precursors are methanol, ethanol, 2-methoxy ethanol, DMF and DMSO [129]. While ethanol and methanol are the most suitable common solvents due to their biocompatibility and high volatility, it is DMF that gives the best results for the copolymer in terms of polymer solubility and control of material deposition.

Any substrate can be chosen for spin coating as long as the hydrogel precursor solution can adhese to it. Glass, chromium/gold covered glass, silicium, polypropylene and even oxygen-plasma activated polymer surfaces like PS or PP can be used.

Figure 4.4(a) shows the spin coating parameters for pHEMA-co-MABP precursors with a molecular weight M_n of roughly 80K Dalton and a polydispersity (PDI) of $2,5$. DMF proved to be an excellent solvent for the deposition of pHEMA based hydrogel precursors on gold, glass and quartz substrates. Very good control can be achieved for film thicknesses in the range of 20 nm to 15 μm. The produced films exhibit superb transparency, surface smoothness and homogeneity: Profiler measurements in one axis indicate no more than 5 nm height oscillation over a tracking length of 400 μm. Films cast from MeOH in the micrometer range proved to have a higher surface roughness and slight loss of transparency. These problems can be omitted by using $1:2$ mixtures of DMF and MeOH.

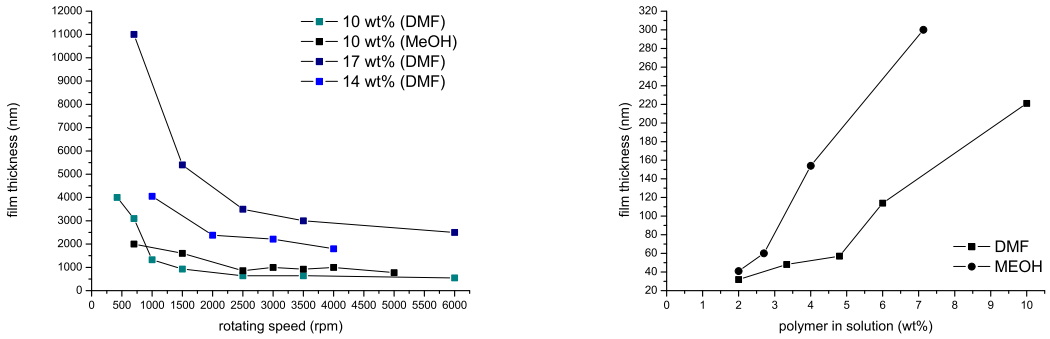

(a) rotation speed

(b) polymer concentration

Fig. 4.4 Film thickness of a hydrogel precursor film with the HEMA/MABP composition 99:1 in dependence on the spin coating parameters rotation speed and polymer weight percentage in solution.

4.2.3 Photocrosslinking of films

The spin coated hydrogel precursors films are crosslinked with UV light for a given period of time. It is to note that while the irradiation dose is set in specific time intervals of UV light exposure, the instrument has been adjusted to work with an internal energy sensor. In doing so, eventual fluctuations of the light source would be taken into account. On average, 6,28 J/cm^2 ($\lambda_{ex} = 365$ nm) are irradiated on the sample within a timeframe of 60 minutes.

4.3 Investigation of film crosslinking by UV/vis spectroscopy

UV/vis measurements have proven to be a good way to investigate the photocrosslinking behaviour of benzophenone (BP) in the hydrogel. Of special interest are the kinetics of the crosslinking reaction. They can be monitored by irradiating a sample of defined thickness in certain time intervals and subsequently measuring the remaining benzophenone

absorption in the UV/vis spectrometer.

The exposure of the benzophenone crosslinking groups towards light of a wavelength of 254 nm leads to a complete crosslinking of the sample within seconds. As the chosen crosslinking wavelength of 365 nm is not in the respective absorption maximum of the benzophenone group, the overall crosslinking process is slowed down considerably. This allows a controlled adjustment of the crosslinking density of the polymer sample in a time frame of 3 hours. Moreover, the photodegradation of the polymer is lessened due to the larger crosslinking wavelength and its corresponding lower energy dose. Figures 4.5(a) to 4.5(d) show the measured UV/vis spectra of four pHEMA films containing MABP with a MABP/HEMA ratio of 1:100 and film thicknesses of 0,2 μm, 0,9 μm, 1,6 μm and 25 μm. While the measurement of the thickest film reaches the limits of the spectrometer in use, all the measurements are still in the linear part of the molar absorption coefficient of MABP.

To compare the kinetic measurements of films of various thicknesses, the absorption maxima of the graphs at 265 nm have been normed with function $\Psi_{corr}(t)$ (equation 4.1). Its application is illustrated in Fig. 4.6: Only the difference between the photonic current density $\Psi(t)$ measured with the uncrosslinked sample after an irradiation time t and photonic current density $\Psi(t_{max})$ of the completely crosslinked samples gives a measure for the amount of total BP groups remaining in the hydrogel.

$$\Psi_{corr}(t) = \frac{\Psi(t) - \Psi(t_{max})}{\Psi(t_0) - \Psi(t_{max})} \tag{4.1}$$

The impact of the norming function on the measurement of the various pHEMA-co-pMABP films with UV/vis is shown in Fig. 4.7. The four samples exhibit slightly different decay behaviours: While all of them show an exponential decrease of the measured

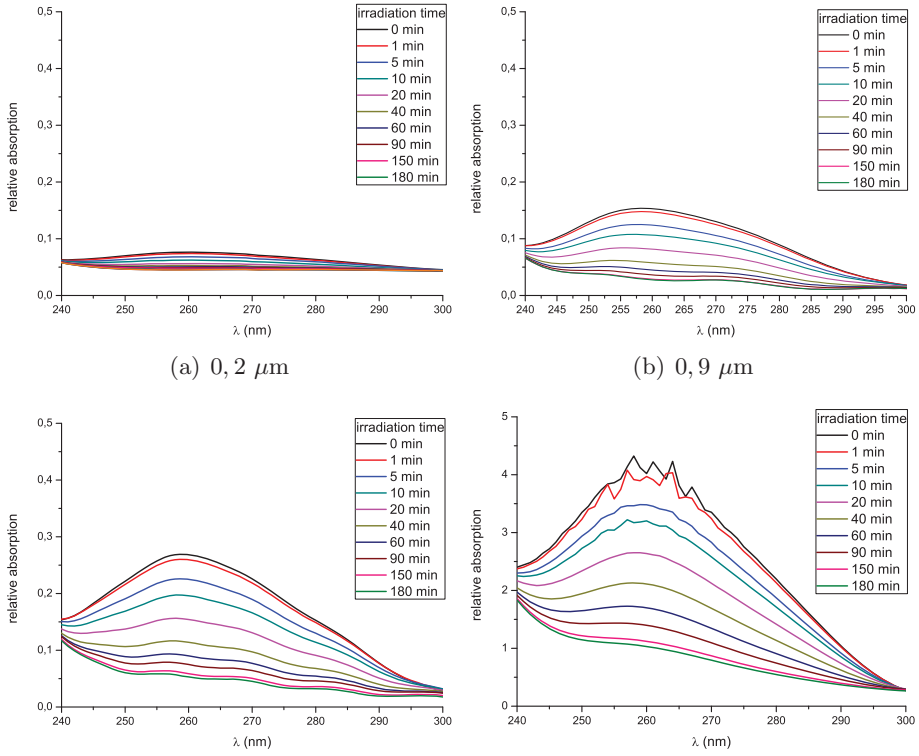

(a) $0,2\ \mu$m (b) $0,9\ \mu$m

(c) $1,6\ \mu$m (d) $25\ \mu$m

Fig. 4.5 UV/vis spectra of pHEMA-co-pMABP films of different thickness during the crosslinking process. The MABP/HEMA ratio in the hydrogels is 1:100.

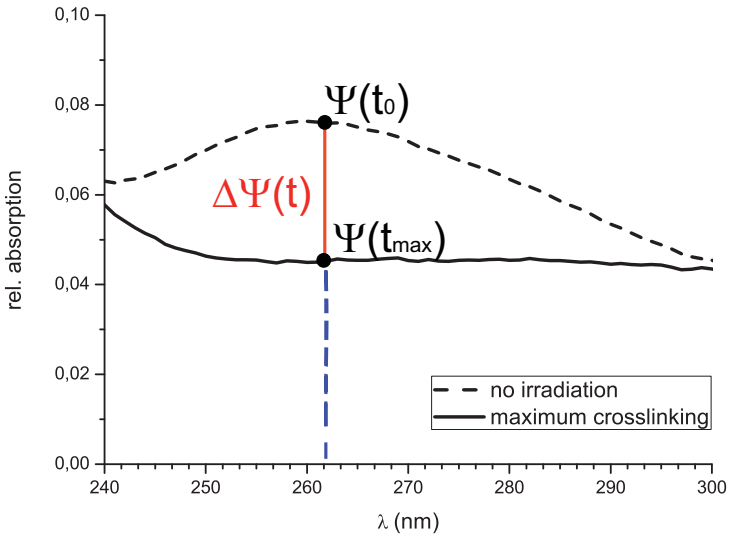

Fig. 4.6 Illustration of the correction function Ψ_{corr} (equation 4.1) that takes into account the base signal formed by the pHEMA hydrogel. t_{max} is the time when all benzophenone groups are degraded by photocrosslinking reactions.

signal, the benzophenone groups in the film with a thickness of 200 nm have completely reacted after 100 minutes, while the thicker films show a complete crosslinking around 200 and 300 minutes. The half life times of the BP groups in the thicker films are much more close: 50% of the original BP groups are crosslinked after approximately 25 minutes.

The light beam of the UV/vis spectrometer has a measurement area of the 0,36 cm^2 ($\pm$ 0,5 mm error per side). If we assume a random box distribution of the BP groups in the hydrogel film and take into account the linear behaviour of the molar absorption coefficient of MABP in the concentration range, it is possible to use ψ_{corr} to make an approximate calculation of the average number of groups in a hydrogel film volume, as discussed later in section 4.8.

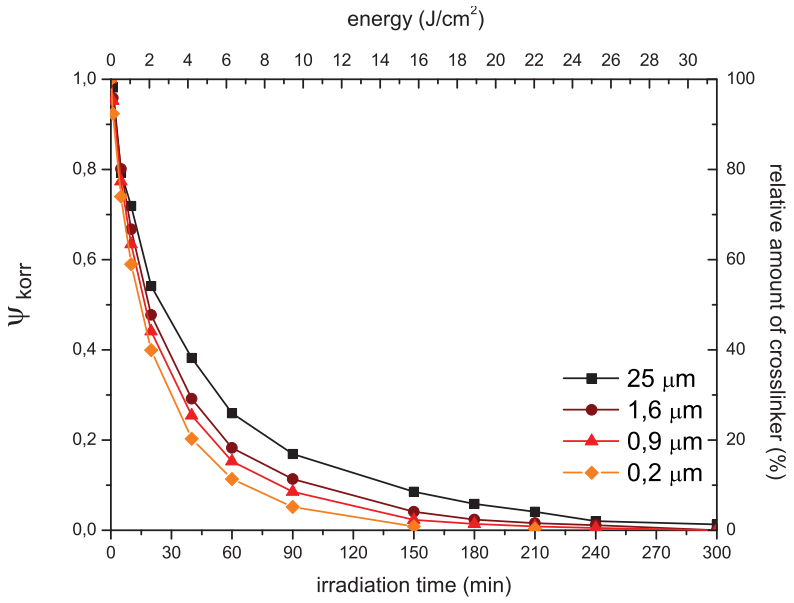

Fig. 4.7 Photocrosslinking behaviour of benzophenone units in the polymer film, as measured by UV/vis spectroscopy. The background signal has been removed with the correction function Ψ_{corr}. The irradiation wavelength λ_{ex} is 365 nm.

4.4 Characterization of swelling behaviour of hydrogel films with SPR/OW spectroscopy

The measurement setup and procedure of the hydrogel swelling measurement as done for SPR and OW spectroscopy is described in sections 2.8.3 and 4.12.3 respectively. In general, the measurement of the LaSFN9 substrate parameters with SPR is followed by the spin coating of the substrate with hydrogel material. Then, the hydrogel film is measured with OW spectroscopy in dry and swollen state.

Swelling behaviour of hydrogel films

There exist strong intermolecular and polymer-polymer interactions in glassy hydrogel samples. For example, hydrogen bonds and hydrophobic interactions [130] make the swelling process of gels a rather complicated phenomenon. It involves three successive steps [130, 131, 132, 133]: (1) the diffusion of water molecules into polymer network, (2) the relaxation of the hydrated polymer chains, and (3) the expansion of the polymer network into the surrounding aqueous solution. Different but interdependent definitions of the degree of swelling of a hydrogel are used in literature. In equation 4.2, the weight swelling degree q_w is calculated from the weight increase upon water uptake. It is calculated by dividing the weight of the swollen gel m by the weight of the dry hydrogel m_0. The volumetric swelling degree q_v is estimated by measuring swelling induced changes of the hydrogel sample size in dependence of a specific sample shape [44, 134, 135].
Surface plasmon resonance (SPR) and optical waveguide (OW) spectroscopy are useful techniques to investigate the swelling behaviour of hydrogel films through the measurement of the refractive index and height of a hydrogel film height [136, 137, 138, 85]. The determination of the uniaxial swelling degree q_s of a hydrogel film is done by dividing the swollen film thickness d through the dry film thickness d_0 after rinsing and drying.

$$q_s = \frac{d}{d_0} \qquad q_v = \frac{V}{V_0} \qquad q_w = \frac{m}{m_0} \tag{4.2}$$

The measurement variables obtained by SPR/OW spectroscopy are the film height d and refractive index n. Since optical methods are not the only means to determine film swelling, it is helpful to understand the relationship between uniaxial swelling, volumetric swelling, and weight swelling as shown in equation 4.3 and equation 4.2. Here, q_v and

q_w are the volumetric and weight swelling, δ_p and δ_{solv} are the density of the polymer and the respective solvent, and m and m_0 are the mass of the film in swollen and in dry state.

$$q_v = \frac{V}{V_0} = (\frac{d}{d_0} * A_{film}) = q_s^3 = \frac{(q_w - 1) * \delta_p}{\delta_{solv.}} = \frac{(m - m_0) * \delta_p}{m_0 * \delta_{solv.}} \tag{4.3}$$

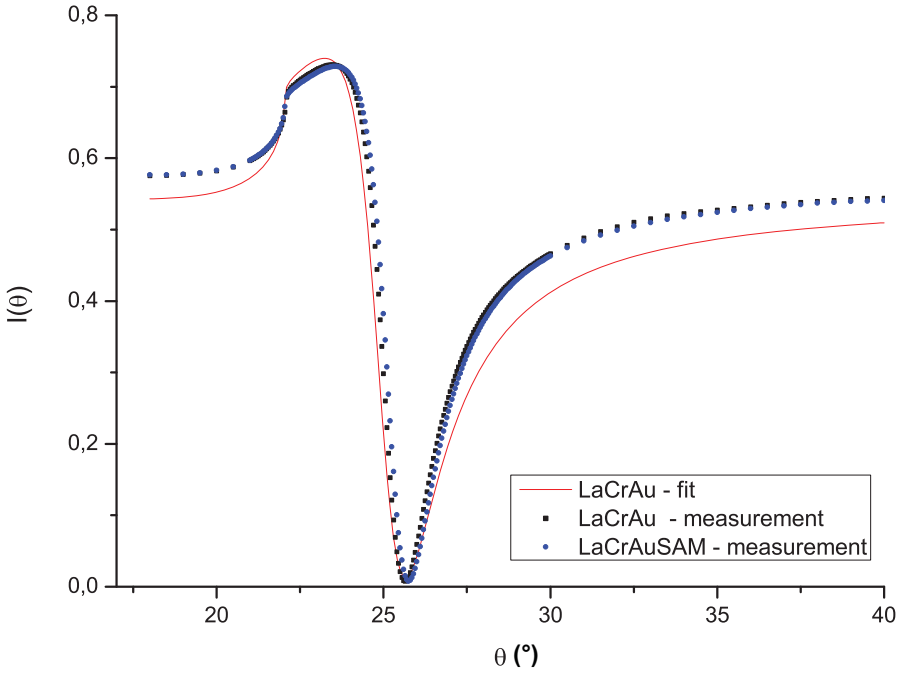

Fig. 4.8 Typical SPR measurement of a LaSFN9 glass slide with a chrome/gold bilayer for the determination of the film thickness. The measurement parameters obtained with the fitting program WinSpall are listed in Table 4.1.

Determination of substrate parameters by SPR spectroscopy

As the combined gold, chrome and benzophenone SAM layers on the LaSFN9 substrate do not exceed 50 nm it is impossible to estimate the substrate parameters with OW spectroscopy. Due to the nature of surface plasmon sensitivity it is possible to measure films up to a height 300 nm. This makes SPR spectroscopy the method of choice for the

determination of the substrate parameters.

Prior to any swelling experiments the LaSFN9 substrate is measured by SPR spectroscopy in order to determine the respective thickness and refractive index parameters of the deposited gold and chrome layers. A typical measurement curve is shown in Fig. 4.8. The plot of the fit calculations matches both critical points of the surface plasmon measurement curve, the minimum at 26° reflectivity and the turning point area around 22,5° reflectivity. The parameters for the specific film layers that are used in the iterative fitting procedure are displayed in table Table 4.1. They represent the typical range values for substrates that are used in the fitting procedure in the experiments with SPR/OW spectroscopy.

Table 4.1 Subtrate parameters of the various layers of the LaSFN9 substrate, as derived from SPR measurements: d is the film layer height, ϵ' and ϵ'' are the real and imaginary part of the dielectric constant.

Layer	d [nm]	ϵ'	ϵ''
LaSFN9	0	3,407	0
Cr	1,8	-4	16,8
Au	37,92	-12,4	1,6
BP-Thiol	1,96	0,9334	0
Air	0	1	0
air	0	1,774	0
water	0	1,000	0

Measuring the equilibrium swelling degree with OW spectroscopy

OW measurements generally need two waveguides to form a defined system. In the case of the fabricated pHEMA materials, the minimum film thickness to be able to observe two waveguides in the swollen state is determined to be 1 μm.

During the swelling process of the hydrogel film any difference in the thickness and the

refractive index can be observed by a change a) in the angular position of the surface plasmon and b) the number and position of the optical waveguide modes.

The most common method to extract the thickness and the refractive index from the SPR/OW spectroscopy data is to assume a homogeneous hydrogel film composed of one layer ("one box model") and to adjust the thickness and refractive index to the measured data (see chapter 2.8 for a theoretical introduction). Photocrosslinked hydrogel films with higher degrees of swelling, like the NIPAAm based gels with carboxylic groups studied by Patrick Beines and Robert Roskamp [109, 33] or dextran based gels investigated by Annette Brunsen [139] often do not fullfil this assumption. They require more complex fitting methods like the Wentzel-Kramers-Brillouin approximation [140, 141]. The swelling degree of the aforementioned gels is around 10 - and thus one magnitude higher than the swelling degree of pHEMA based hydrogels.
Additionally, another important factor that affects the homogeneity of a hydrogel film in regard to the measured z-axis comes into play: the high quality of the deposition process of pHEMA based hydrogel precursors. Films that were deposited from methanolic solution exhibit lower optical quality that both translates into the quality of wave guide modes and problems with the fitting of the recorded SPR spectra. In contrast to this, films that have been spin coated from DMF solution can be fitted very well with the use of the one box model. Even when containing small amount of comonomer - e.g. MAA - the hydrogel films exhibit an excellent homogeneity and very good optical quality in both the swollen and dry state. This can be explained with the fact that pHEMA based materials have a much lower tendency of swelling in comparison to hydrogels made from more hydrophilic monomers like NiPAAm or dextrane based materials. Similar deposition effects were also observed by xxxxxxxx xxx xxx xxxx with NiPAAm films spin coated from methanolic and chloroform solutions in the Knoll group.

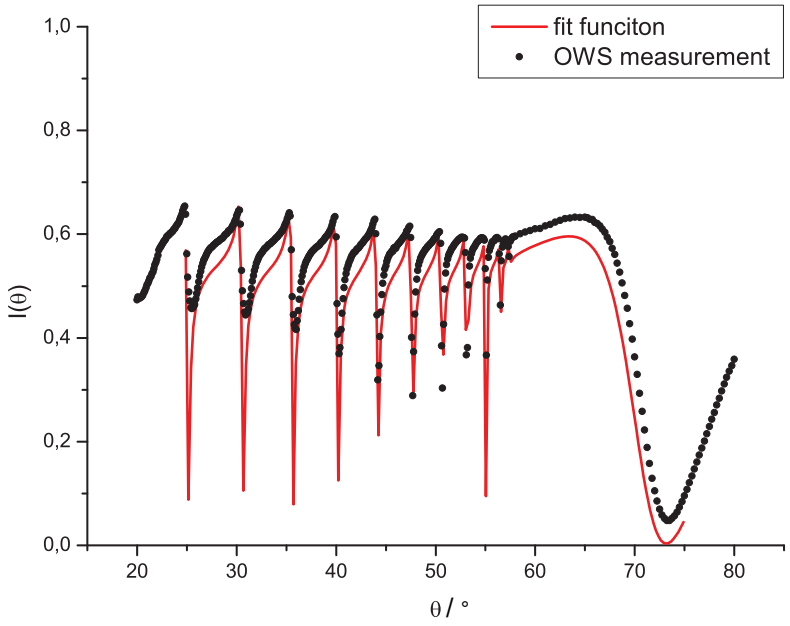

(a) dry film

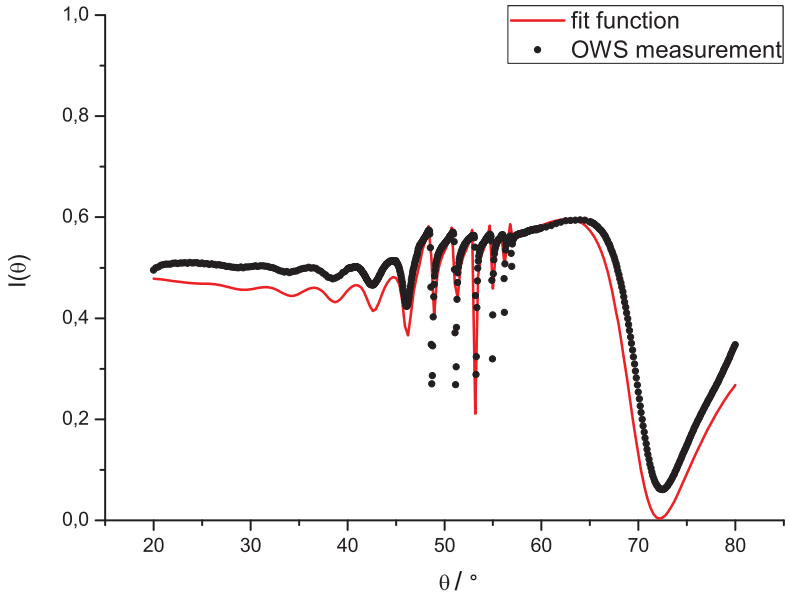

(b) film at equilibrium swelling

Fig. 4.9 Spectra of OW spectroscopy measurements of a dry and swollen pHEMA-co-pMABP (100:1) film after irradiation with UV light (λ = 365 nm) for one hour. The film thickness in the dry state is 3445 nm and swells to 3600 nm after soaking for 20 hours with Milli-Q water.

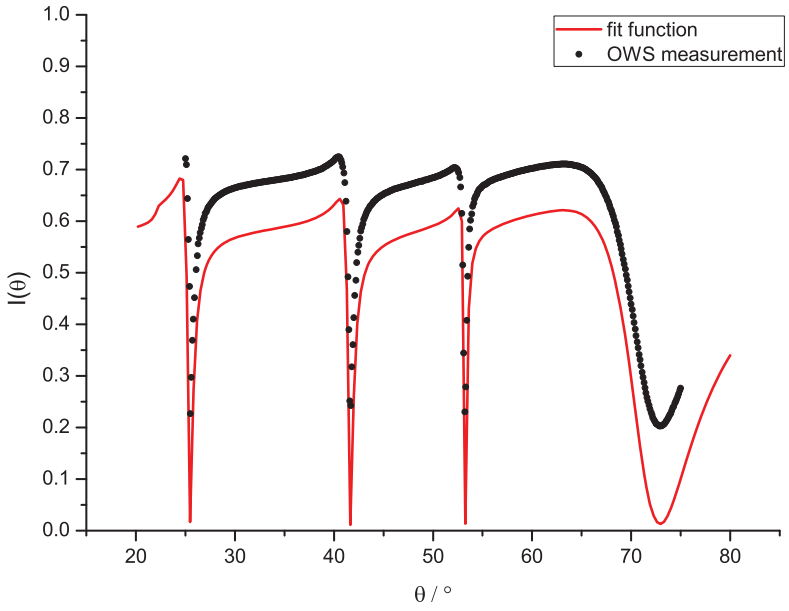

(a) dry film

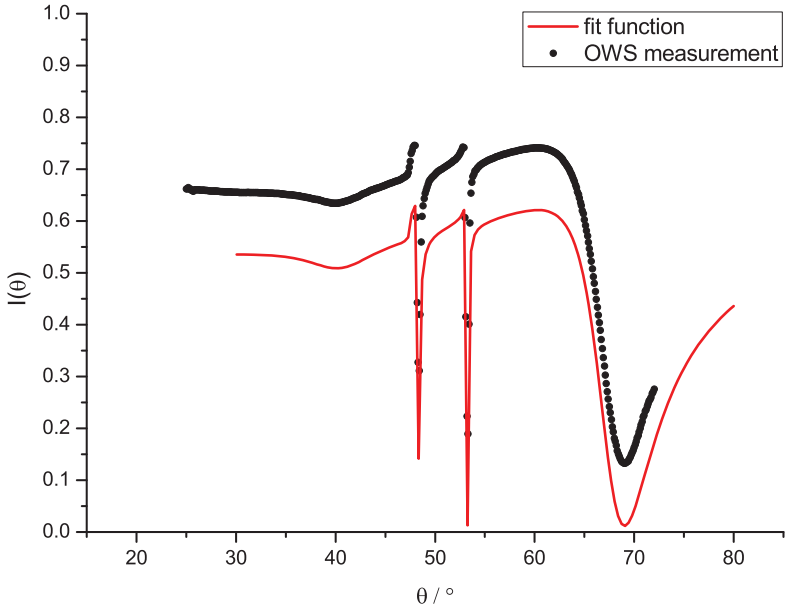

(b) film at equilibrium swelling

Fig. 4.10 Spectra of OW spectroscopy measurements of a dry and swollen pHEMA-co-pMABP-pMAA (100:1:10) film after irradiation with UV light ($\lambda = 365$ nm) for 15 minutes. The film thickness in the dry state is 945 nm and swells to 1215 nm after soaking for 20 hours with Milli-Q water.

Figures 4.9(a), 4.9(b), 4.10(a) and 4.10(b) show the OW measurement spectra of two pHEMA based hydrogel films in dry and swollen state. The films have been deposited to have a thickness of 3,42 μm and 0,94 μm respectively. The thicker film is made from pHEMA-co-pMABP hydrogel, while the thinner film consists of pHEMA-co-pMABP-co-pMAA polymer. While both films have a benzophenone content of 1% and were crosslinked at a wavelength of 365 nm, different irradiation times were used for each sample. The thicker hydrogel film was crosslinked for one hour, while the thinner film was crosslinked for 15 minutes.

At first, both films were measured in the dry state with OW spectroscopy (figures 4.9(a) and 4.9(b)). After exposing the films to water for 20 h no further change in reflectivity can be observed. This final state in the swelling process - the state of equilibrium swelling - is displayed in figures 4.9(b) and 4.10(b).

Both measurements show a very good coverage between experimental data and the fitting results using the one box model with the waveguides and the surface plasmon. This indicates that the hydrogel film has a very uniform density in both dry and swollen state. The film homogeneity in the dry state is a consequence of high quality of the spin coating of PHEMA materials with DMF. Samples deposited from other solvents such as ethanol do not show such well formed wave guides - either they can not be described with the one-box model, or they come with a high signal loss caused by inhomogeneities inside the film and on the film surface. It seems very likely that the low uniaxial swelling degree q_s of the films in the state of equilibrium swelling does not cause any sufficient gradients in film density that could have been measured by OW spectroscopy. This is reflected in the very similar fitting parameters of unmodified pHEMA-co-pMABP films that show almost no swelling.

Table 4.2 Fitting values for the OW spectroscopy measurements of two pHEMA films in dry and swollen state. The materials were polymerized using different monomer compositions. The substrate parameters for LaSFN9, Cr, and Au layers are listed in Table 4.1. Crosslinking times and monomer equivalents are listed below.

pHEMA	BP	MAA	t_x [min]		state	d [nm]	ϵ'	ϵ"
100	1	0	60		dry	3429	2,105	0
			60	swollen	20h	3602	2,0856	0
100	1	15	15		dry	945	2,105	0
			15	swollen	20h	1215	2,0316	0

Dependence of q_s on crosslinking degree

Because the pHEMA-co-pMABP hydrogel film is planned to be modified with functional comonomers and exposed to a change in the parameters temperature, crosslinking time and composition, it is interesting to investigate the magnitude of the response of the materials to changes in these parameters. The influence of MAA content and crosslinking time on the equilibrium swelling degree are investigated with the use of OW spectroscopy.

For this, pHEMA-co-pMABP-co-pMAA copolymers have been synthesized with the procedure mentioned in chapter 3.6.2. The amounts of the comonomers were set relatively to 100 equivalents (eq.) of HEMA: benzophenone was used in 1 eq., while the MAA content was set to 5, 10 and 20 equivalents. The produced materials are summarized in Table 4.3. The hydrogel samples for the OWS measurements were manufactured according to the protocol in the experimental section.

As shown in figure 4.11(a), an exponential decrease in uniaxial swelling degree q_s can be observed by increasing the crosslinking time from 15 to 60 minutes. The largest decrease in q_s can be observed in the first minutes of crosslinking. This reflects the results of the

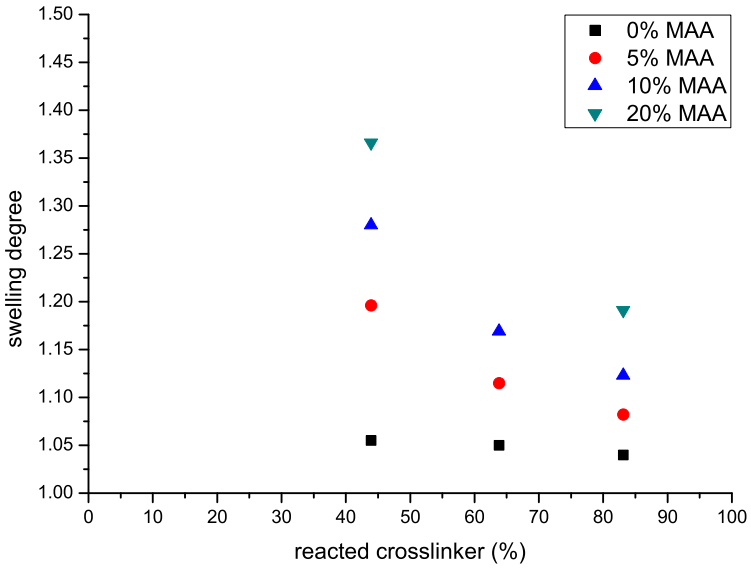

(a) Influence of crosslinking time on swelling at pH 7

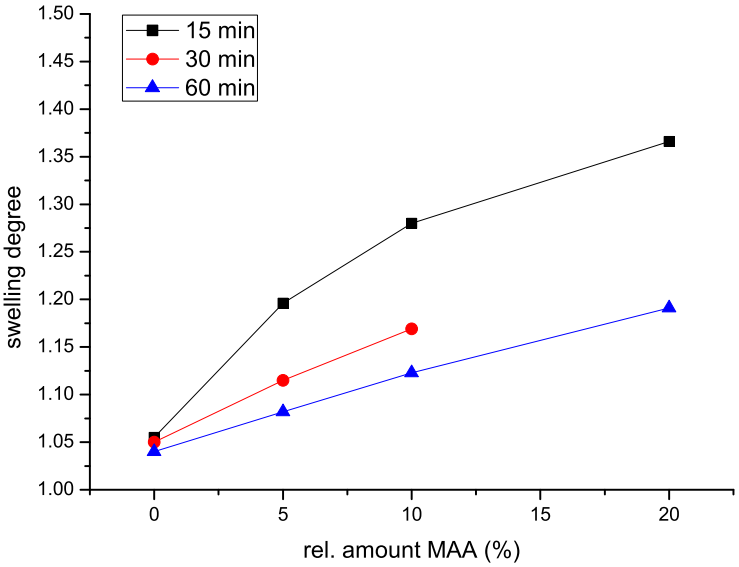

(b) Influence of MAA content on swelling at pH 7

Fig. 4.11 Dependence of the swelling degree of pHEMA-co-pMABP-co-pMAA hydrogels (1% BP content) in water on the parameters a) reacted crosslinking groups and b) relative MAA content as measured by OW spectroscopy.

Table 4.3 Relative monomer content of HEMA, MABP and MAA monomer units in the hydrogels used in the swelling experiments. While the ratio of HEMA and BP could be verified by ^{1}H-NMR spectroscopy, it is assumed that the incorporation of MAA is complete at high conversions.

HEMA	MABP	MAA	Mn	Mw	PDI
100	1	0	101000	273000	2,7
100	1	5	59000	143000	2,4
100	1	10	81000	218000	2,7
100	1	15	76000	220000	2,9

exponential crosslinking behaviour of the hydrogel precursors as investigated by UV/vis spectroscopy in chapter 4.3: While almost 45% of the benzophenone groups in the film have reacted upon UV irradiation, 60% of maximum photocrosslinking density is reached after 30 minutes, and up to 80% are reached after 60 minutes.

Figure 4.11(b) shows the influence of the MAA content on q_s. While samples at 50% crosslinking display a logarithmic relationship between q_s and the MAA content, higher crosslinking triggers a more linear dependence. At lower crosslinking densities, the forces linked to the interactions between negatively charged carboxy groups are dominating the retraction forces connected to the photoinduced covalent bonding. Higher crosslinking makes the polymer network more rigid, thus weakening the impact of negatively charged COO^- groups that are the source of increased electrostatic repulsive interactions inside the hydrogel.

4.5 Adsorption studies with streptavidin, IgG and blood plasma on biotinated films

The interaction of biotin and streptavidin (SA) is widely known to be one of the strongest noncovalent interactions and is thus taken advantage of in scientific laboratories [142]:

it is not only very useful for in vivo applications [143], but has been used in SPR experiments before [144, 145]. The usage of pHEMA-co-pMABP based materials as adsorptive material for DNA is of primary interest of this work. As such, it is decided to use a large biomolecule pair such as biotin - streptavidin as a known model system for basic proof of concept experiments. In previous experiments, the produced hydrogels have been sufficiently studied regarding the swelling properties and proven to be stable in a wide range of solvent conditions and crosslinking times. In this section, pHEMA based hydrogels are modified with biotin anchor groups for the usage in proof of principle experiments. The aim is to investigate the specific and unspecific adsorption properties of pHEMA based hydrogels to large molecules i.e. streptavidin.

4.5.1 Synthesis and characterization of biotinated hydrogel films

pHEMA materials are known to react reasonably well with peptide coupling reagents, thus opening the route for the addition of D-biotin to the HEMA based polymer backbone of the hydrogel precursors [146]. The post polymerization modification of the polymers is chosen instead of the synthesis of a biotinated HEMA monomer in order to make it easier to compare modified and unmodified pHEMA materials. Also, biotinated methacrylic acid is very hard to purify due to very bad solubility in many solvents.
Fig. 4.12 shows the addition of biotin to the precursor with the use of the peptide coupling agents DIC [147]. For this, D-biotin was first activated by DIC, and then added to a solution of precursor material in DMF.
One difficulty in making the partial conversion of the hydroxyl groups on the polymer backbone is the bad solubility of D-biotin in many organic solvents and water, which reduces the number of usable solvents to DMF. This also applies to the purification of the hydrogels, which is done by diffusing the residual components of the coupling reaction out of the DMF reation mixture.

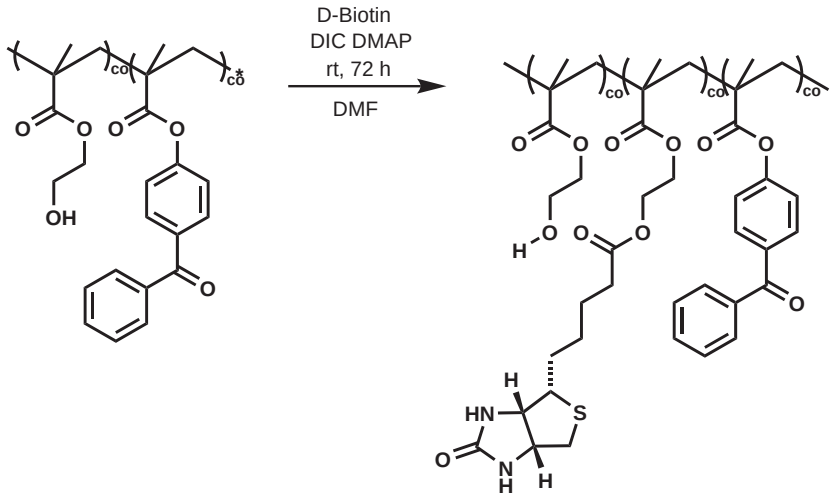

Fig. 4.12 Addition of (D)-biotin to pHEMA-co-pMABP hydrogel precursor with peptide coupling agents.

The ^{1}H-NMR analysis of the biotinated hydrogel precursor is displayed in Fig. 4.13: For ease of interpretation, the pure educts, the mixture between educts prior to the reaction and the purified product spectrum are shown. A first indication of the formation of biotinated polymer is the appearance of broader biotin signals in the product spectrum. An explanation for this effect would be the reduced freedom of movement that comes with the covalent binding of the biotin molecules to the polmyer backbone.

The ^{1}H-NMR spectrum of the hydrogel precursor has been extensively discussed in chapter 3.3.1. The spectrum of D-biotin has a doublet peak (a) at 6,4 ppm that can be attributed to the nitrogen bound hydrogen atoms on the biotin ring. Another characteristic signal group (b) appears at $4,4$ ppm and is connected to the single hydrogen atoms of the carbon atoms next to the aforementioned amine groups. The hydrogen atom closer to the propyl bridge has a smaller chemical shift. As the signal does not overlap with other atoms of the HEMA polymer it can be used as a reference signal for the biotination of the polymer.

The comparison of the educt and product spectra gives a weak proof for the formation of the product: the change in the chemical shift of the terminal CH_2 group (c) that

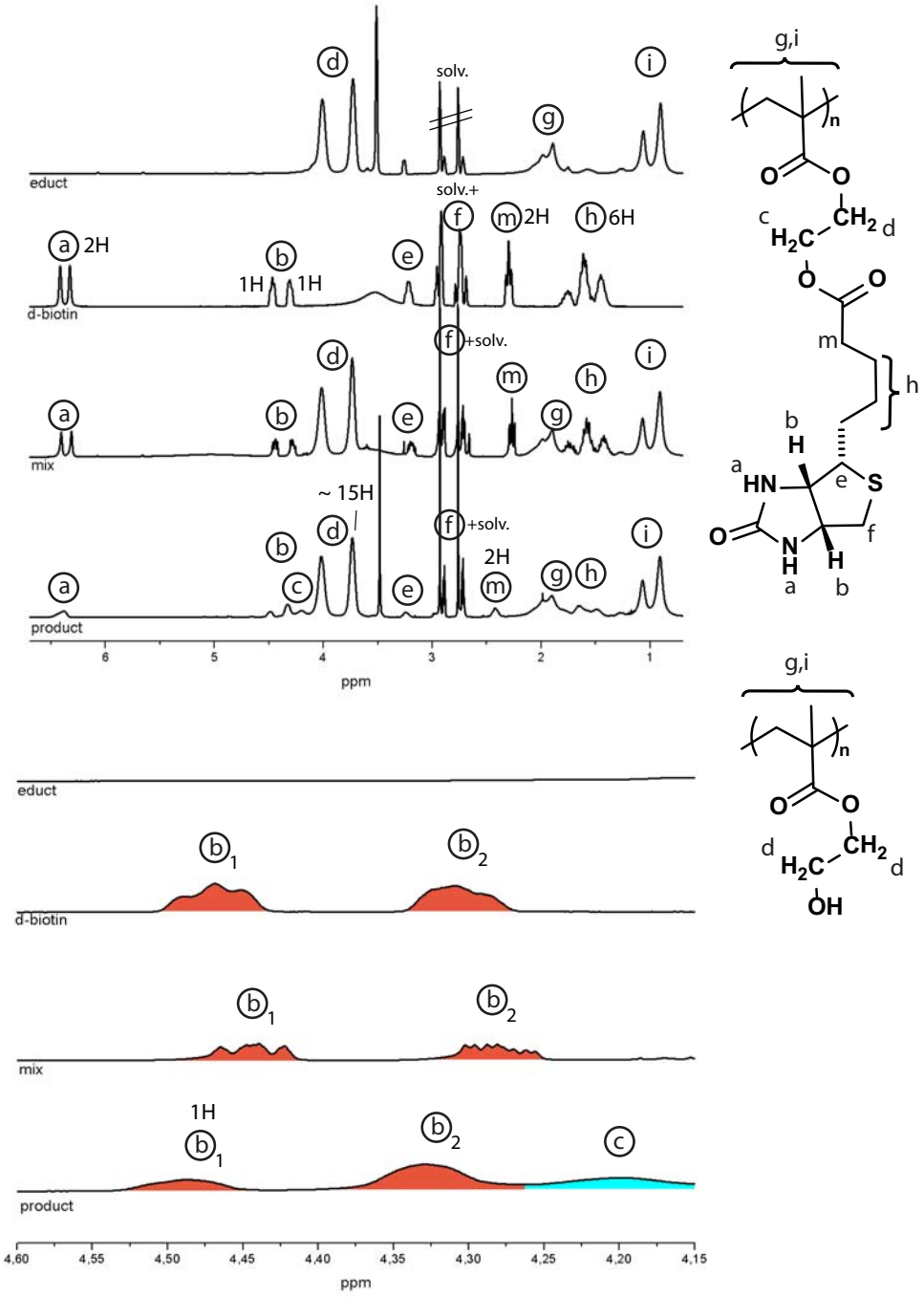

Fig. 4.13 300 MHz ^{1}H-NMR spectrum of purified biotinated pHEMA-co-pMABP hydrogel precursor in d-DMF and its comparison to educt/mixture spectra.

is located next to the HEMA hydroxyle group can only be explained through covalent attachment of the carboxylic group of the biotin molecule to the hydroxyle group of HEMA. In comparison to its position in the HEMA molecule, the CH_2 group at (c) position is exposed to the higher electron withdrawing effect of the ester group and thus shows around 4.2 ppm in the spectrum. Regrettably, this characteristic signal can not be quantified due to the overlapping signals with the HEMA CH_2 (d) bands.
Apart from signal group (b) there is only one signal that does not overlap with the d-DMF signals around 2,8 ppm or signal groups (d) and (g). As such, only the signal bands of the CH_2 group (m) at 2,3 ppm and the hydrogen atom at 4,5 ppm from signal group (b) can be integrated. The ratio of these signals is 2:1, as expected in theory.
However, it is possible to make an approximation of the relative amount of biotin groups bound to the HEMA polymer. This can be done by comparing the biotin signals (b) and (m) with a part of the (d) signal that comes from the HEMA CH_2 group near the polymer backbone. The (d)/(m) or (d)/(b_1) ratio is roughly $\frac{15}{2}$, which would correspond to an approximate polymer composition of 100 eq. HEMA, 1 eq. BP and 13 eq. biotinated HEMA.

4.5.2 Kinetic adsorption measurements with SPR

A qualitative proof of the improved adsorptive properties of modified gels in regard to large molecules can be given by monitoring the adsorption process with kinetic SPR measurements. The principle of the real time measurement technique is described in chapter 2.8. It makes use of the recording of the linear part of the surface plasmon at a fixed angle. The films - roughly 90 nm thick - are allowed to reach equilibrium swelling prior to the exposure of biological agents.
In order to study specific binding interactions, both biotinated hydrogel films and unmodified control samples are exposed to a solution of streptavidin (SA). The films that

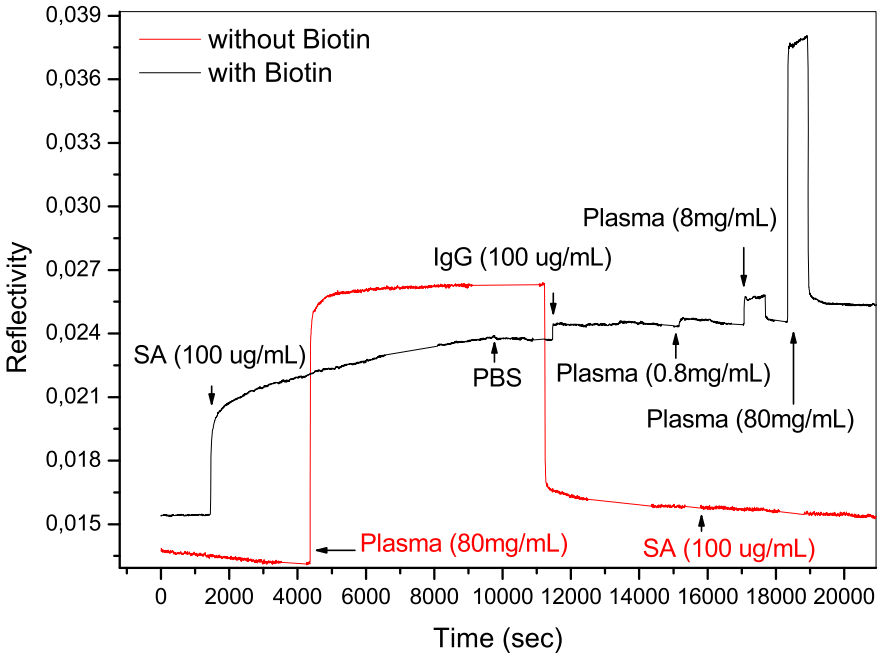

Fig. 4.14 Time evolution of the SPR minimum of a hydrogel film during the exposure to streptavidin (SA), IgG and blood plasma. The black curve is the measurement of biotinated hydrogel and the red curve is the unmodified control sample. The experiment shows that SA bound into the gel with biotin moieties. No such behaviour could be observed with the control sample. Both samples show very low unspecific and reversible binding to blood plasma.

are used as control samples consist of the same hydrogel that is subject to the modification with biotin. It is expected that the biotinated film will bind SA, while the unmodified sample will not. The permanent binding of SA to the film should be reflected in a permanent change of the recorded SPR signal intensity. Adsorption processes that are either weak or temporary will show as a weak signal that is not sustained during a rinsing process of the sample.
A second test in regard to specific binding can then be made with the injection of a solution of immunoglobulin G (IgG). This molecule binds permanently to the surface bound SA groups, resulting in a further signal change. At last, a blood plasma solution can be used to check whether the hydrogel films exhibit any unspecific binding interactions with the mixture of proteins, antibodies, antigens and hormons that can be found in blood plasma.

The experiment displayed in Fig. 4.14 shows a SPR real time recording of adsorption kinetics. The investigation is conducted for a pHEMA-co-pMAPB film with biotin groups (black curve) and for a control sample without biotin (red curve).
The injection of the streptavidin (SA) solution to the biotinated sample gives a sharp rise in reflectivity after 1500 seconds. This is followed by an exponential signal growth to a saturation point. A possible explanation for this behaviour would be the enrichment of SA in the measurement volume of the surface plasmon after the initial binding. Consequently, these adsorption processes would trigger the surveyed changes to the refractive index of the film. Contrary to the biotinated film the unmodified sample does not show a rise in reflectivity during exposure to SA solution. This is a hint that the SA molecules do not adsorb at the pHEMA-co-pMABP hydrogel surface - presumably because no biotin anchor position exist. The stability of the SA adsorption is tested with a rinsing of the cell with PBS solution after 8000 seconds. The stability of the reflectivity during the rinsing procedure indicates a stable binding between the biotinated film and SA.

When injecting a 100 $\mu g/ml$ solution of IgG after 12000 seconds to the biotinated sample (black curve) only a small rise of reflectivity can be observed. This suggests that a rather small amount of IgG groups has been captured by the surface bound streptavidin. One reason for this might be the small pore size of the hydrogel that prevents further diffusion of IgG into the film. The fact that the refractive index is being higher than 1,4 is an indicator that the high gel fraction of the hydrogels prevents any diffusion of large biomolecules molecules into the inside of the film. This is supported by the data gathered by OWS measurements in chapter 4.4 that show a high gel fraction of water-swollen pHEMA-co-pMABP hydrogels.
An additional explanation for a rather low adsorption of IgG could be a too high density of biotin moieties on the hydrogel surface: Each SA molecule can bind with more than one of it's four biotin recognizing binding sites to the film, leaving less possibilities for IgG to dock to the film bound SA.
All in all, a qualitative proof of SA binding to biotinated hydrogels can be shown. However, a quantitative statement can not be made with this set of data.

In addition to the adsorption experiments with SA and IgG, the biotinated and unmodified films are examined in regard to blood plasma adsorption. In both cases, the change of reflectivity regarding blood plasma injection is the same for both samples. This can be seen with a blood plasma solution of 80 mg/mL at 4200 seconds on the control sample curve (red curve) and at 18500 seconds in the graph of the biotinated hydrogel (black curve). Furthermore, the change in reflectivity - as observed at the injection of blood plasma solutions with a concentration of 0,8 mg/mL, 8,0 mg/mL and 80 mg/mL - is proportional to the amount of the biomaterial in solution.
At last, it can be shown that the unspecific adsorption of blood plasma on the film samples give a much weaker signal response than the specific binding observed from an SA solution of thousand-fold lower concentration. This is an additional hint towards the binding of SA to the hydrogel film.

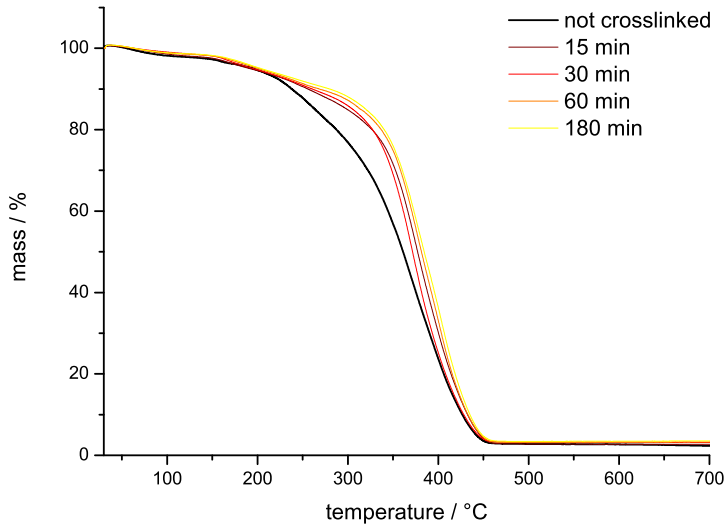

Fig. 4.15 Thermogravimetric analysis of pHEMA-co-pMABP polymers with different crosslinking times.

4.6 Characterization of bulk material with TGA and DSC

The influence of the extent of photocrosslinking on the thermal stability of pHEMA-co-pMABP based materials was investigated with thermogravimetric analysis (TGA). Typical weight loss curves of the copolymers at a heating rate 10 ℃ per minute under nitrogen atmosphere are shown in Fig. 4.15. It can be observed that the thermal stability increases with crosslinking time. The uncrosslinked copolymer has the strongest material loss with rising temperatures while the fully crosslinked sample having the strongest resistance towards thermal degradation. However, all curves with crosslinked material show strong similarities, while the measurement for the uncrosslinked sample is standing out. This can be explained with the results of the experiments conducted on the crosslinking behaviour of hydrogel precursors in chapter 4.3. It could be shown that even at a exposure to UV light for just 15 minutes around 50% of the maximum crosslinking density is reached.

Table 4.4 Results of DSC measurements of bulk polymer samples.

t_x [min]	0	15	30	60
T_g [°C]	101,91	102,75	103,27	103,76

Table 4.4 shows the dependence of the glass transition temperature T_g as obtained by dynamic scanning calorimetry (DSC) of the bulk pHEMA-co-pMABP materials. As expected, the T_g is growing with the amount of crosslinking inside the copolymer.

4.7 Stress-strain measurements on dry and swollen films

The evaluation of the mechanical properties of hydrogels is important to assess their suitability for a particular application. Here, the mechanical properties of the materials in dry and swollen state are of interest. The first one is useful for reasons of processibility, the second can be used to determine the parameters of mesh size and crosslinking density.

The theoretical background and method of stress-strain measurement is introduced in chapter 2.7. To examine the mechanic properties of the pHEMA films with the use of stress-strain measurements, films with thickness of 200 μm are deposited from a DMF solution into teflon holders. The solvent is evaporated under vacuum, leaving a film with good uniformity regarding thickness.
The films are subjected to photocrosslinking (λ_x = 365 nm) wavelength for a duration of 15, 30, 60 and 360 minutes. The samples which are crosslinked for 60 and 180 minutes show a much higher brittleness than the materials with shorter crosslinking times. This does not come as a surprise, as the stress-strain measurements are recorded at room temperature - below the estimated T_g values of the dry films. Three bone shaped samples with an average thickness of $212^{+}_{-}2$ μm are cut out for each crosslinking time

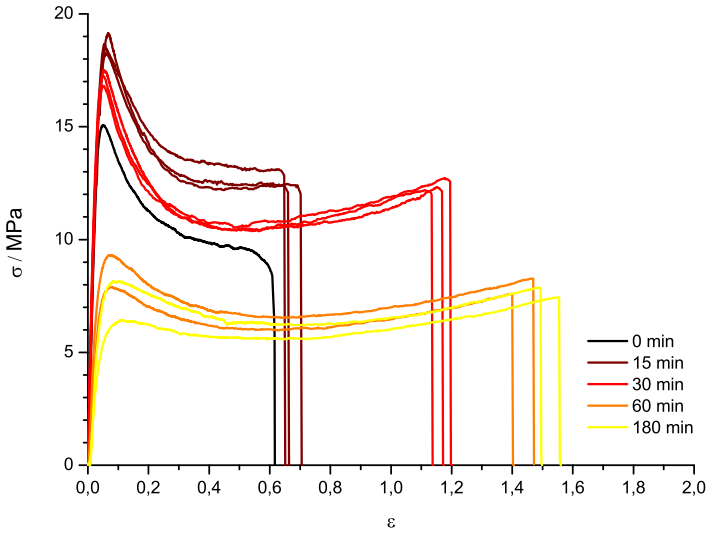

Fig. 4.16 Tensile strength experiments of pHEMA-co-MABP copolymer in dry state. The stress-strain curves show measurements for materials with different crosslinking densities.

and subsequently used for tensile strength experiments.

To record the stress-strain data, stretching speed was set to 1 mm/min while the drawing force was 10 N. For measurements in the wet state, the bone shaped films were allowed to swell for 72 hours in aqueous medium before measurement. The handling and tensile strength experiments with wet samples proved to be much more difficult. The increased stickyness of the hydrogel bones made it difficult to fix the materials in the measurement machine. The swollen samples were much easier to damage. Another unsolved problem proved to be the lack of a measure to prevent the gel bones from drying during the stress-strain measurement.

As expected, swollen samples showed significantly different stress strain behaviour due to the decreased number of chains per volume and the influence of water as plasticizer. However, the hydrogels did not show a consistent set of data: the necking of the material could not be seen in the plots, and deviation from linear behaviour could be observed.

As such it was decided only to use data obtained by measuring the dry materials.

Fig. 4.16 shows the tensile strength measurements of dry pHEMA-co-pMABP films for different irradiation times. The reproducibility of the measurements is very good, as shown in the overlapping of measurement curves for one specific irradiation time. While curves of different crosslinking times show similarities in the curve shape, they differ in several aspects.

As can be seen in fig. 4.18(a), the yield stress σ_v and breaking strength/fracture stress σ_b show a maximum around 15 to 20 minutes crosslinking time. Likewise, the samples of 15 with 30 minutes crosslinking show the strongest yielding and strain hardening behaviour. Once a certain tensile strenght is reached, the partly uncrosslinked polymers exhibit a greater potential for chain displacement. Also, the lower density of crosslinks translates into early rupture and lower network stability. The yield strain ϵ_v and breaking point draw ratio ϵ_b (Fig. 4.18(b)) exhibit a maximum at crosslinking times of 60 and 180 minutes. This can be explained with a maximum in crosslinking density and the corresponding stronger polymer network. The breaking point for uncrosslinked and lightly crosslinked samples shows rather *flowing* characteristics whereas the samples with higher degrees of crosslinking exhibit a sharp rupture. This reflects very well the higher relatively brittleness that comes with higher crosslinked samples.

In figure 4.17(a), the elastic module E of the dry films is plotted against the crosslinking time. It decreases from 530 MPa to 270 MPa with increasing amount of crosslinks. However, the measured data has to be handled very carefully, as shown in 4.17(b). The polymer samples exhibit a strong deviation from the expected linear stress-strain behaviour at low sample elongations. This issue can be tracked back to the brittleness of the materials [134] and makes it impossible to estimate the E module for samples with high crosslinking. In comparison to pHEMA materials produced in one step reaction

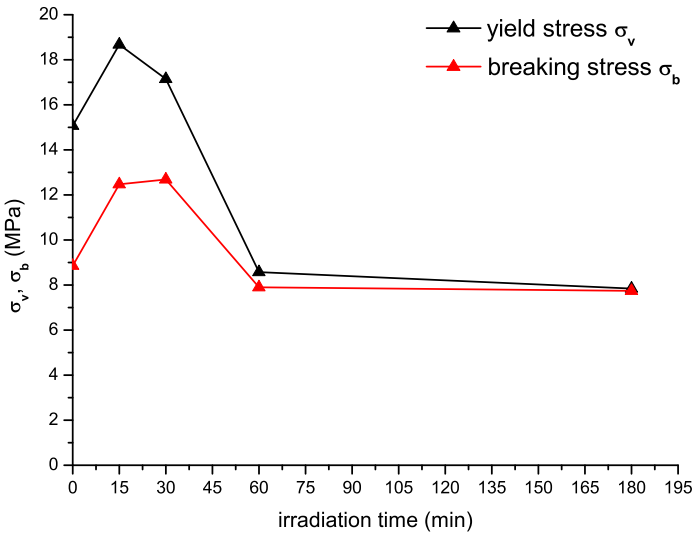

(a) Yield stress and breaking stress

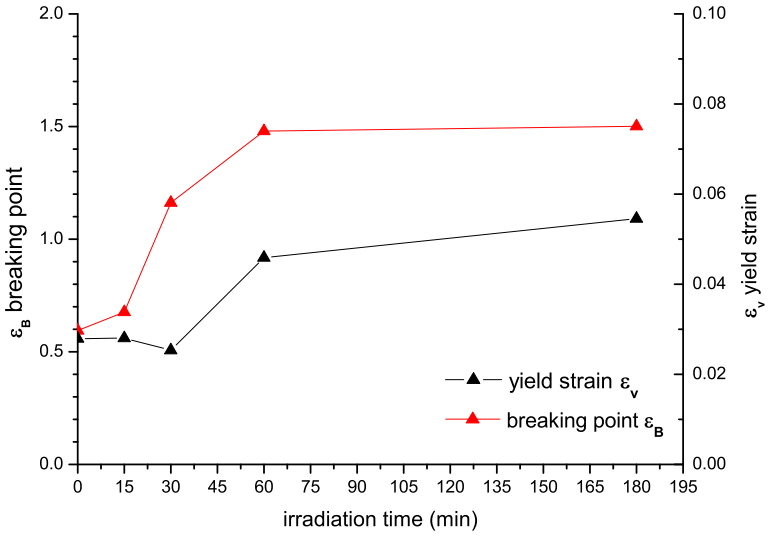

(b) Yield strain and breaking point draw ratio

Fig. 4.17 Stress strain parameters yield strain, breaking stress, yield strain and breaking point draw ratio of dry pHEMA hydrogel films in dependence of cross-linking time.

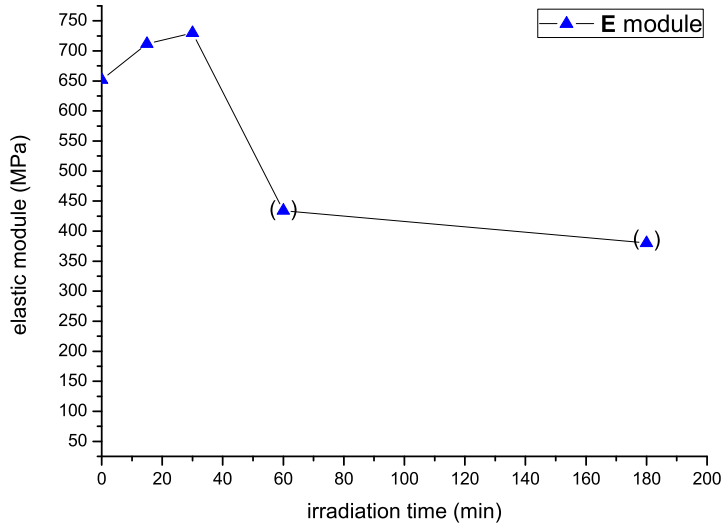

(a) Elastic module

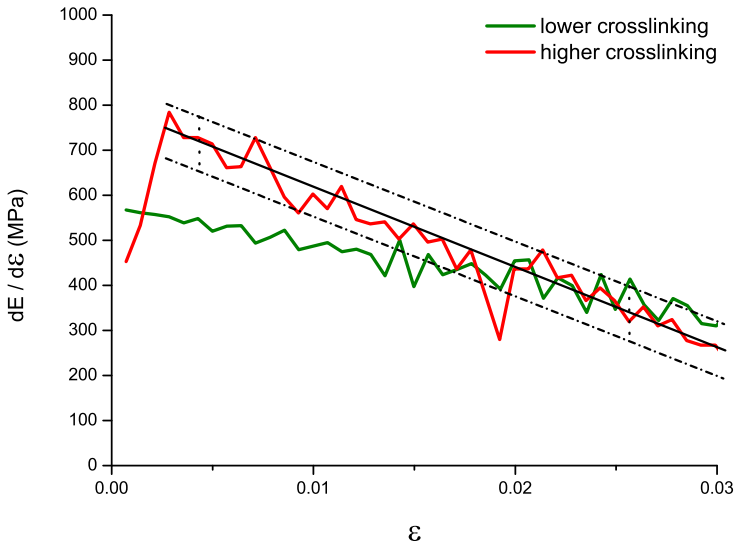

(b) Deviation from linear behaviour during measurement of E

Fig. 4.18 E module of dry pHEMA hydrogel films in dependence of crosslinking time.

in solution by other research groups, the films produced by the photocrosslinking of hydrogel precursors are much denser and of higher mechanical strength than the materials synthesized by other methods [148].

4.8 Theoretical crosslink density

The crosslinking density ν_ϵ - the number of elastically effective crosslinks per polymer volume - and the number average molar mass between crosslinks M_c can be estimated [134, 149, 150] by measurements of the mechanical behaviour in swollen state and the equilibrium swelling ratio. Unfortunatly, the static mechanical measurements of the pHEMA-co-pMABP hydrogels did not produce reliable data in the swollen state with the measurement setup in use, forcing to remain with theoretical values only.

The maximum theoretical crosslinking density ν_t - the number of effective crosslinks in a polymer network per unit volume - could be calculated by extending equation 4.4, where C_x is the concentration of crosslinked benzophenone units with the functionality f_x [134]:

$$\nu_t = \frac{f_x}{2} * C_x = \frac{3}{2} * C_x \tag{4.4}$$

In the example of photocrosslinkable pHEMA hydrogels, the functionalty f_x is equal to three. The olefinic monomer moiety of MABP is copolymerized into the backbone, the photoactive group makes up the third functional crosslinking point. The amount of crosslinks is dependent on the relative amount of crosslinked benzophenone units $x(t)$, which on the other hand can be estimated by the measurements involving the kinetics

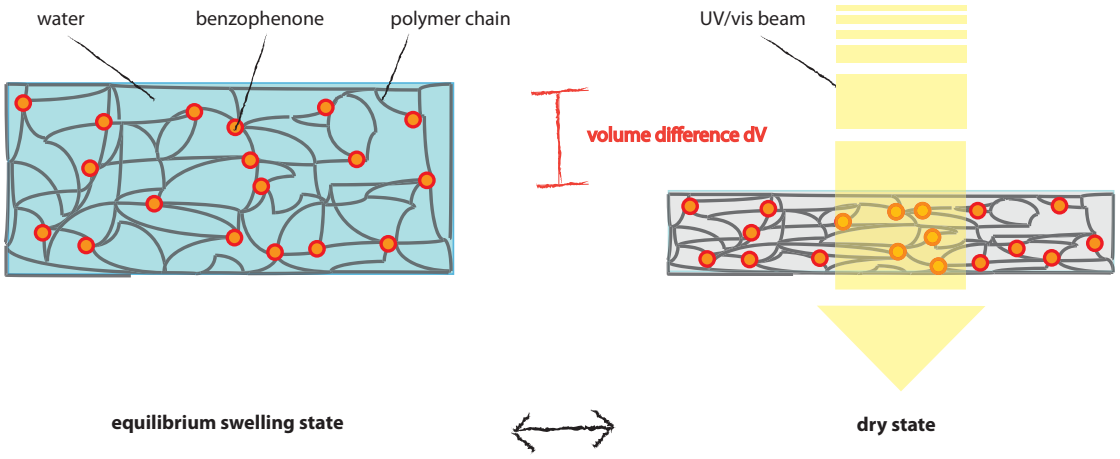

Fig. 4.19 Two dimensional scheme of the relation between the number of benzophenone groups per volume in a swollen and dry hydrogel film.

of UV irradiation, as previously discussed in chapter 4.3. An important correction is the incorporation of the swelling degree into the equation, which takes into account the increase of the overall volume of the polymer from the dry to the swollen state. The polymer gel fraction ϕ_p is connected to the hydrogel swelling in equilibrium through the following equation [151]: $\phi_p^{\frac{1}{3}} = (1/q_v)^{\frac{1}{3}} = (1/q_s) = \frac{s_0}{s}$. However, as the measured polymer films are fixed on a substrate, only one axis of expansion is of importance in a first approximation. Hence, the theoretical crosslink density is assumed to decrease with the factor of $1/q_s$ instead of $1/q_v$:

$$\nu_t(t_x, q_s) = \frac{3}{2} * C_x * x(t_x) * \frac{1}{q_s} \tag{4.5}$$

The UV/vis signal of the uncrosslinked benzophenone groups in the polymer is linear proportional to the concentration of benzophenone units C_x in the measured polymer volume. The beam area A_p of the UV/vis apparatus and the sample's film thickness d_p

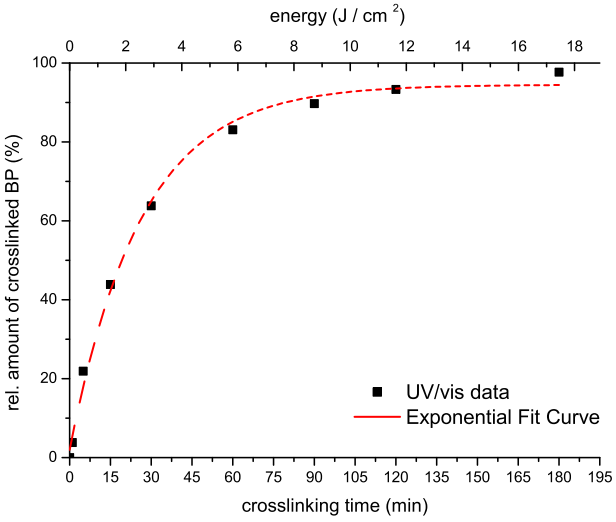

Fig. 4.20 The change of the intensity of the absorption maxima (at 254 nm) with irridiation time t_x gives an estimation for the relative amount of crosslinked benzophenone for a film with the thickness of 1,6 μm, as used in the OW spectroscopy swelling experiments. The decay function can be fitted with $I \cong exp(-0,038 * t_x)$, indicating exponential decay behaviour.

are known, while the molar absorption coefficient of BP in pHEMA films ψ_x is estimated by the use of UV/vis spectroscopy to be around 72 L/mol. Thus, it is possible to make a rough calculation to obtain the concentration of benzophenone units in the polymer volume C_x. This can be done with the assumption that the influence of the polymer matrix on the measurement can be neglected with equation 4.6:

$$C_x(t_0) = \frac{\psi_x}{A_p * d_p} = \frac{\psi_x}{V_p} \tag{4.6}$$

A second way to calculate the number of crosslinking groups in the dry polymer per volume is by using the relative amount of crosslinker groups in the polymer r_x and the polymer density δ_p. The parameter r_x can be quantified with reasonable precision by ^{1}H-NMR spectroscopy. The polymer density δ_p of data was estimated during the produc-

Table 4.5 Summary of network parameters depending on crosslinking time t_x

t_x	[min]	15	30	60
q_s		1,004	1,003	1,003
x(t_x)	[%]	37	58	83
$C_x(uv)$	[10^{-5} mol / m^3]	0,0787	0,1234	0,1766
$\nu_t(uv)$	[10^{-5} mol / m^3]	1,18	1,85	2,65

tion of the thick films for the stress-strain measurements, where a polymer solution of known weight percentage was dried into a film and its polymer volume was subsequently measured.

$$C_x(t_0) = \frac{n_x}{V_p} = \frac{r_x * \delta_p * V_p}{M_x} \tag{4.7}$$

In order to calculate the theoretical crosslinking density, the number of crosslinking groups per polymer volume $C_x(t_x)$ that have reacted after an irradiation time t_x has to be known. Fortunately, it can be calculated in a first approximation by the use of the results regarding UV light induced degradation of BP molecules (see chapter 4.3). The respective fit function obtained by the UV/vis measurements in is shown in Fig. 4.20.

Table 4.5 summarizes the results of the network parameter investigation. Although the methods to estimate the concentration of benzophenone units in the polymer volume return results that lie more or less in the same magnitude, only the spectroscopic method is taken into account. The effective cross-linking density ν_e is expected to differ in magnitude from ν_t, as first measurements with bones in the swollen state have shown. However, the measurement has shown to be very error prone with the swollen hydrogel samples. The differences between the three samples are marginal and the handling of the samples gives very unpredictable results. Most likely, this can be traced to the lack of proper sample arresting of swollen hydrogel samples and the prevention of water loss

during the stress-strain measurements. This makes any estimation of ν_e with the current measurement setup a very vague matter, for the calculations rely heavily on data aquired by stress strain measurements as shown by Tobolsky et al.: the effective cross-linking density ν_e can be estimated by using measured stress-strain data in accord with equation 4.8 [150]. R and T carry its normal meaning, σ is the applied stress, ϕ the polymer gel fraction and λ is the ratio of the deformed length l to the undeformed length l_o of the hydrogel.

$$\sigma = RT\nu_\epsilon\phi_p^{1/3}(\lambda - \lambda^{-2}) \tag{4.8}$$

4.9 Evaluation of porosigens for macroporous hydrogel films

The hydrogel materials characterized in the previous sections exhibit a high polymer volume fraction in the swollen state. As such, they are very close to non-porous gels in which diffusion is only possible through free volume. One possibility to increase the area that is available for adsorptive processes and simultaneously accelerate the diffusion speed of analytes into the hydrogel film would be the introduction of additional cavities into the film. The incorporation of such sacrificial materials - porosigens - into the deposition or synthesis of the hydrogel and their subsequent removal gives the possibility to create a interconnected set of cavities. A variety of porosigen concepts have been used in literature: they use solvent mixtures [152], supercritical carbon dioxide [153], ice crystals [154], gas bubbles [155, 156], short polymer chains [157], inorganic/organic nanoparticles [158] and salts [159]. However, there are strong incompatibilities between the synthetic concepts in literature and the strategy of depositing photocrosslinkable hydrogel precursors as used in this work.

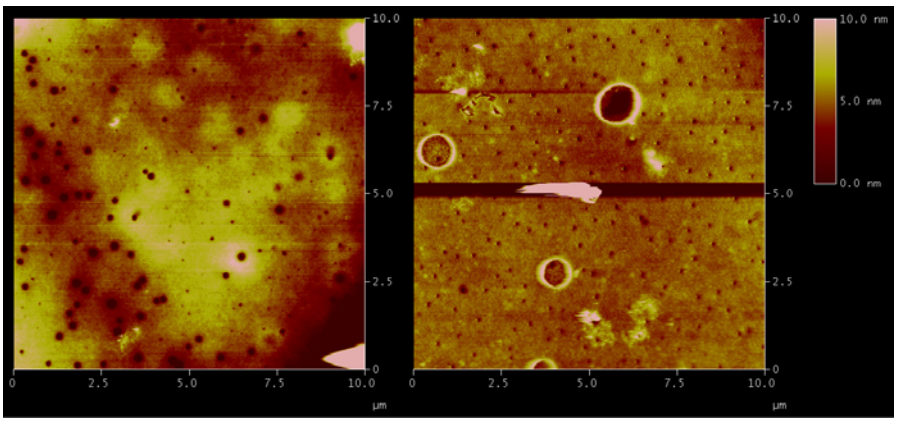

Fig. 4.21 AFM measurements of slides after the dissolving the porosigens. The incubation of the film in a solution of HCl in water left a film surface covered with holes. In comparison to a film without porosigens that has been fabricated with spincoating the structured film shows considerable surface roughness.

At a closer look, the remaining possibilities are materials that could be incorporated into the hydrogel precursor mixture prior to the deposition process e.g inorganic/organic polymer spheres synthesized by emulsion polymerization or inorganic salts like NaCl or $NHCO_3$. SiO_2 particles are problematic due to the remains of dissolved particles in the hydrogel and the difficulty of handling of hydrofluoric acid. In contrast, inorganic salts can be easily removed with water. However, achieving a homogeneous dispersion of the porosigens in the film is very challenging.

It was attempted to increase the porosity of the pHEMA-co-pMABP films with the use of $NaHCO_3$ porosigens. The hydrogel precursor salt mixture was produced by mixing polymer solutions with $NaHCO_3$ that was grinded with a electrical fine grinding mashine. After spin coating the mixture on a glass substrate functionalized with benzophenonesilane crosslinker, the films were crosslinked for one hour at a wavelength 365 nm. The materials were swollen in water with acidic (aqueous HCl) and neutral pH in order to remove any residual salt.

After deposition, mixtures with lower amounts of salt show a very strong radial distribution of the porosigens on the substrate. The amount of porosigens and the high porosigen

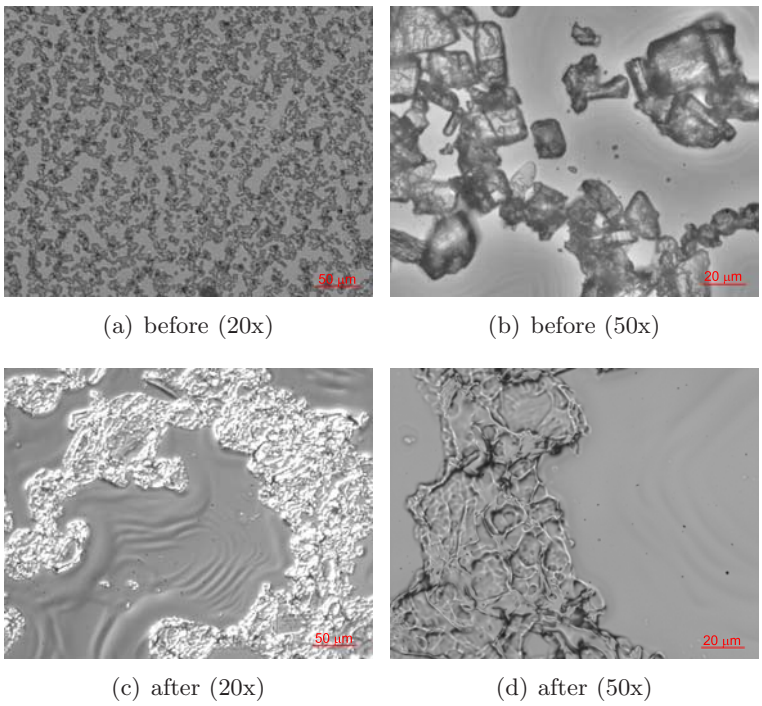

(a) before (20x) (b) before (50x)

(c) after (20x) (d) after (50x)

Fig. 4.22 DIC microscopy images (x-fold magnification) of pHEMA-co-pMABP films with $NaHCO_3$ before and after dissolving the porosigen with a solution of HCl in water.

grain size poses a problem to the overall film formation during the spin coating process. Upon exposure of the prepared polymer films to a acidic water a strong generation of CO_2 gas can be observed during the dissolving process of the porosigens. The best results regarding film quality and porosigen distribution are obtained with 2 g of a 10% polymer solution in DMF with 500 mg of finely pestled $NaHCO_3$. Optical microscopy images of a film deposited from this hydrogel - $NaHCO_3$ mix are shown in figures 4.22(a) to 4.22(d). While the microscopic images show larger craters on the sample surface after removal of porosigen material, an investigation of the dry film with atomic force microscopy (Fig. 4.21) shows smaller holes in the surface that possibly could belong to channels formed through the escaping CO_2.

All in all, while a thorough optimization process can improve the distribution of porosigens in the sample, the use of porosigens as template material brings strong problems of inhomogeneity and instability in regard to surface attachment that can not be eliminated. It is not possible to use the hydrogel films in any SPR/OW spectroscopy characterizations due to the strong light scattering that comes with the formation of cavities in the materials. At last, it remains doubtful that a interconnected set of pores can be produced with this method, as it would require an excellent control over the distribution of the inorganic particles and high stability of the deposited film.

4.10 Evaluation of 2D interference lithography for increase of hydrogel surface

Another approach in increase the amount of adsorbed molecules on the hydrogel material would be the use of photolithography to introduce micropatterns to the film surface. The principle of photolithography is the transport of a geometric pattern from a photomask

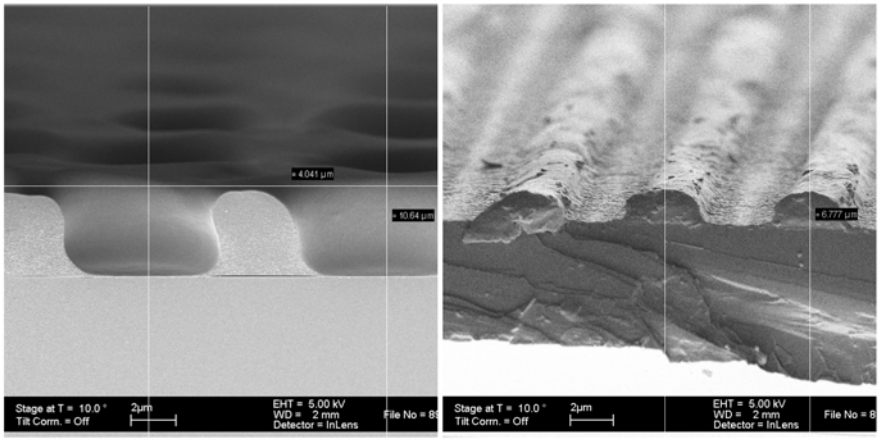

Fig. 4.23 Different pattern examples for microstructuring of HEMA based hydrogel precursor films with 1% BP content by 2D laser interference lithography, as measured by SEM. Original film thickness prior to crosslinking was 10 μm. **(left)** 4 μm residual amplitude of the pattern. **(right)** 2,2 μm residual film height.

to a light sensitive material. The light sensitive material undergoes a photochemical reaction, and consecutive chemical treatment removes unreacted light sensitive material and exposes the microstructure. In cooperation of Jens Wuesten from the IMM, the photomask is replaced with a stable 2D laser interference pattern: constructive interference generates maxima of UV/light light exposure in the irradiated film, while destructive interference does not have any effect on the hydrogel precursor film. As such, a variety of different theoretical interference patterns can be projected onto the photosensitive material [160].

Practically, the pHEMA-co-pMABP film is deposited on a quartz substrate functionalized with BP silane, exposed to the UV light laser interference field and developed by ultrasonic cleaning in water. The application of 2D interference lithography comes with the necessity to variate many different parameters in order to achieve a good surface pattern e.g. BP content in the polymer film, irradiation time, UV light wavelength and hydrogel precursor thickness and grating constant. Parallel experiments were reported

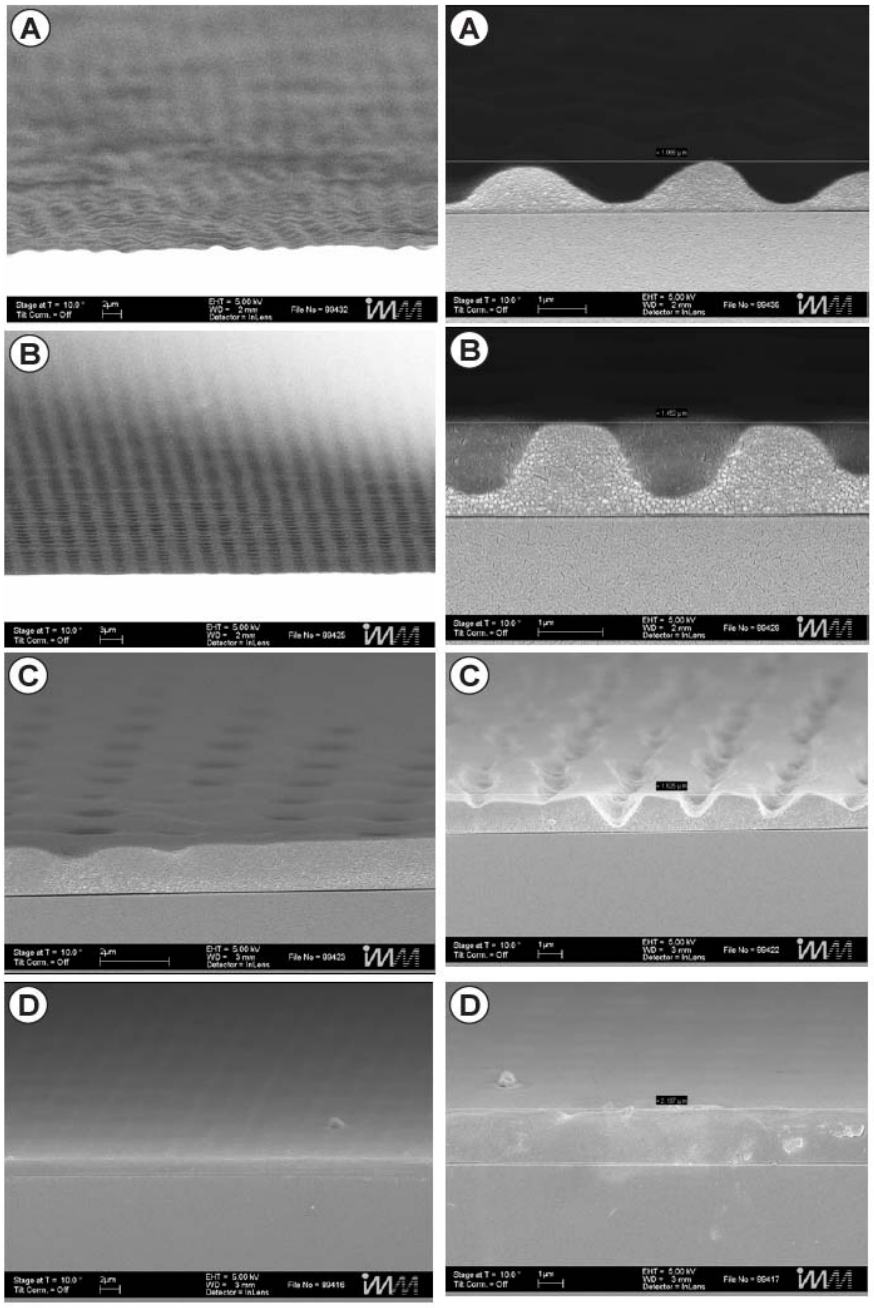

Fig. 4.24 SEM images of 2,5 μm thick pHEMA-co-pMABP films crosslinked at different irradiation times t_x by 2D laser interference lithography. **(A)** t_x = 2 s, remaining height = 1 μm, **(B)** t_x = 6 s, remaining height = 1,5 μm, **(C)** t_x = 12 s, remaining height = 1,45 μm and **(C)** t_x = 18 s, remaining height = 2 μm.

not to reach the desired micropattern quality on thinner NIPAAm hydrogel, resulting in very low amplitudes of around 1 μm [161]. However, the procedure was optimized to work with HEMA based hydrogel precursors with 1% BP content by Andre Radke and in the master thesis of Abderrazzek Toufali [162]: It was found that especially the grating constant needs be adjusted to the film thickness to observe good results - a further increase of the parameter to an optimum produces better defined surface patterns with the minima reaching to the glass substrate. However, it was not possible to introduce the interference pattern to the full height of the 10 μm thick hydrogel precursor film. The best results that could be achieved were 4 μm residual film height, as shown in Fig. 4.23. The formation of the surface micropatterns in dependence of irradiation time can seen in Fig. 4.24.

While the produced films showed a surface increase, no SPR/OW experiments in regard surface adsorption could be realized due to disturbing surface interference. Furthermore, as mentioned in chapter 6, the optical technique to generate hydrogel with surface micropattern can not be transferred to the threedimensional geometry of a PCR tube.

4.11 Conclusion

Photocrosslinkable hydrogels on pHEMA basis were deposited by spin coating and covalently attached to gold and glass surfaces with the help of UV light absorbing benzophenone based adhesion promotors. The films showed a good mechanical stability in the dry state and remain connected to the substrate after swelling.
The investigation of the kinetic of the crosslinking process shows an exponential decay of benzophenone groups during the irradiation. Furthermore, a weak dependence of the benzophenone decay rate on film thickness could be found.

Through depositing the precursor material from DMF films of excellent opticial quality can be produced: when measured with OW spectroscopy, films of 1,5 μm to 3,5 μm thickness could be fitted with the one-box model. Furthermore, it can be shown that the swelling of the films is complete after 20 hours.

The rather low swelling ratio of the pHEMA-co-pMABP films of 3%-4% can be enhanced significantly by the addition of additional charged groups into the polymer structure e.g. through the incorporation of the methacrylic acid groups. A reduction of crosslinking time increases the swelling degree further.

With the attachment of biotin anchor groups to the films, first proof of principle adsorption and diffusion experiments show that large biomolecules such as SA and IgG can be bound specifically to the hydrogel surface. Also, the used hydrogel materials do no exhibit permanent non specific adsorption processes with the components of blood plasma. It could be shown that streptavidin does not diffuse into the swollen pHEMA based hydrogel material. Instead, it is bound on the film surfaces in a stable manner. As such it can be safely said that there is no diffusion of biomolecules into the hydrogel due to the high gel fraction of the materials.

The incorporation of microchannels into the film with the use of porosigens proves to be difficult in regard to film stability and optical quality. As such, the diffusion of large bioanalytes such as DNA into the hydrogel film is not achievable with the used hydrogel system. However, surface adsorption is still a very good choice for a suitable function of the material in an application, as shown by the experiments with biotin-streptavidin. While 2D laser interference lithography showed interesting results in terms of an increase of accessible surface area, the transfer of the method to PCR tubes can not be realised.

4.12 Experimental

4.12.1 Preparation of quartz glass SiO_2 substrates

The benzophenonsilane is chemisorbed on the SiOx surface at room temperature from THF solution (20 mL of a 0.025 M solution). A drop of diluted HCl solution is added as a catalyst. The substrates are left to stand in the silane solution overnight. The samples are cleaned by rinsing with THF and ethanol. After each rinsing step, the sample was blown dry with nitrogen.

4.12.2 Preparation of LASFN9 substrates for SPR/OW spectroscopy

For the SPR and OW measurements LASFN9 glass slides (Hellma Optik GmbH Jena) are sputtered with a 2 nm chromium and a 50 nm gold film, deposited by evaporation with a Edwards Auto 306 evaporator. Subsequently, the freshly sputtered substrates are incubated in a 5 mM ethanolic solution of S-3-(4-benzoylphenoxy)propyl ethanthiol solution for 24 h at room temperature. After chemisorption the slides are cleaned by extensive rinsing with ethanol and blown dry with air.

4.12.3 Measurement procedure for SPR/OW spectroscopy experiments

Surface plasmon resonance (SPR) spectroscopy and optical waveguide (OW) spectroscopy was performed in the Kretschmann configuration. The measurement setup is described in chapter 2.8.3 and literature [136]. Only a short overview of the experimental technique is given in this chapter.

The sample $LASFN_9$ glass slide (refractive index $n = 1.8449$, corresponding to $\epsilon = 1.3583$) is optically matched to the base of a glass prism (refractive index $n = 1.8449$, corresponding to $\epsilon = 1.3583$) with the use of a paste. Monochromatic light (He/Ne laser, Uniphase, $\lambda = 632.8nm$) with linear, transverse-magnetic polarization (Glan-Thompson polarizer, Owis) is directed through the prism. Variation of the external angle of incidence Θ (two-cycle goniometer with a resolution of 0.005 degrees, Huber) and collecting the light with a photodiode (BPW 34B silicon photodiode, Siemens) yield angle-dependent intensities $I(\Theta)$.

The angle-dependent reflectivity of the prism base is modelled by solving Fresnel's equations by a transfer matrix algorithm [163] for a planar multilayer system consisting of glass (ϵ_{glass}), chromium ($d_{chromium}$, $\epsilon_{chromium}$), gold (d_{gold}, ϵ_{gold}), an adhesion promotor ($d_{promotor}$, $\epsilon_{promotor}$), a hydrogel ($d_{hydrogel}$, $\epsilon_{hydrogel}$) , and water (ϵ_{water}) with ϵ and d being the dielectric constants and thickness of the layers, respectively. For every ϵ, the real part ϵ' and the imaginary part ϵ'' have to be provided. Reflection losses at the prism-air interfaces as well as refraction are included to produce in the simulated $I(\Theta)$ values.

The layer parameters of the substrate are obtained by minimizing the difference between experimental and modelled $I(\Theta)$. In order to achieve this one parameter is changed while all other are kept constant. In practise, the measurements are done with multiple samples from the same batch e.g. one sample to characterize the sputtered LaSFN9 substrate, one sample to measure the SAM after incubation, and a hydrogel covered substrate to measure the film thickness in dry and swollen state. The measurement protocol is as follows:

Before deposition of the adhesion promotor and polymer film, a reference scan is performed that allows the determination of the substrate parameters ($d_{chromium}$, $\epsilon_{chromium}$, d_{gold}, ϵ_{gold}, and ϵ_{water}). A second $I(\Theta)$ scan after deposition of the adhesion promotor is used to determine $d_{promotor}$ and $\epsilon_{promotor}$. This is done under the assumption that all

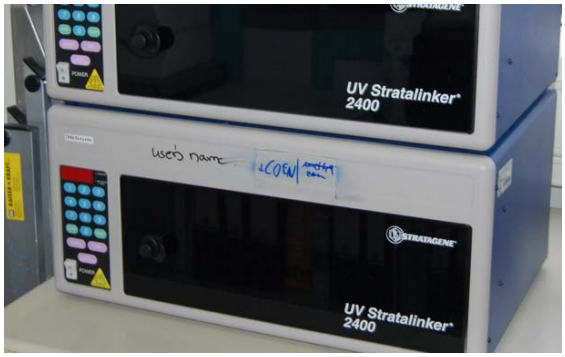

Fig. 4.25 Stratalinker UV crosslinking instrument.

other ϵ and d values are fixed.

A third $I(\Theta)$ scan after deposition and cross-linking of the polymer layer is used to determine $d_{hydrogel}$ and $\epsilon_{hydrogel}$ in the dry state. This is done under the assumption that all other ϵ and d values are fixed.

Optical waveguide (OW) spectroscopy measurements can be conducted if the polymer film is sufficiently thick ($\sim$ 1000 nm for pHEMA based gels). In this case, additional minima are observed as a result of the coupling of the laser beam into waveguide modes. As with the surface plasmon resonance mode, these optical waveguide modes directly depend on the thickness and refractive index of the hydrogel layer. This allows for a detailed characterization of these layers.

4.12.4 Deposition and crosslinking of the polymer films

Thin polymer films are deposited on the substrates by spincoating from polymer solutions in DMF onto the adhesion promotor layers. In example, if the polymer content of the solutions is kept at 8 wt %, it yields a film thickness of approximately 1 μm at 4000 rpm. The SPR samples are dried *in vacuo* at 50 °C and irradiated with a Stratagene UV Stratalinker 2400 operating at 75 W. With a peak wavelength of 365 nm for 1 h, the corresponding energy dose is $6,28\ J/cm^2$.

4.12.5 Sample preparation for mechanical measurements

In order to produce films of a defined thickness, the hydrogel precursor material is solved in DMF and cast into templates made from teflon. The amount of polymer solution for a specific film thickness could be approximated by the use of the density of the dry hydrogel material and the known area and volume inside the teflon template. The bulk of the solvent is removed by drying at room temperature and removed for good under high vacuum. After this, the films are removed mechanically from the samples and cut into bone shape prior wetting and mechanical measurements. The samples were kept in the dark during the entire process.

4.12.6 4-allyloxybenzophenone

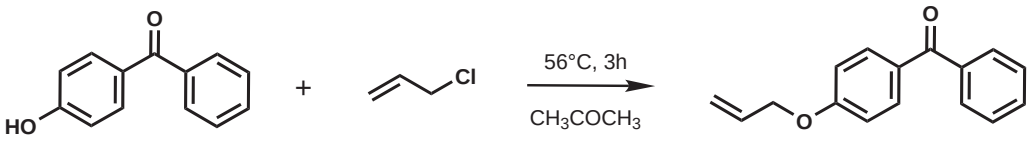

19,8 g 4-hydroxybenzophenone (100 mmol) and 14,31 g allylbromide (111 mmol) are solved in 30 ml dry acetone. 14 g potassium carbonate are added. After boiling for 3 hours under reflux the mixture is allowed to cool down to room temperature. 50 ml water are poured into the reaction mixture and the reaction mixture is extracted two times with 100 ml diethylether. The ether phases are washed two times with diluted sodium hydroxide solution (10%) and dried with $MgSO_4$. The crude product is purified through recrystalization in methanol.

Yield: 17,5 g $\sim$ 73 %

^{1}H-NMR (250 MHz, CDCl3): δ / ppm = 7, 26 (d, 2H, C-H), 7, 26 (d, 2H, C-H), 7, 26 (q, 2H, C-H), 7, 26 (q, 1H, C-H), 6, 97 (d, 2H, C-H), 6, 10 (m, 1H, C=C(H)-), 5, 42 (d, 1H, C=C-H), 5, 25 (d, 1H, C=C-H), 4, 70 (d, 3H, -CH_3).

4.12.7 S-3-(4-Benzoylphenoxy)propylethanthioate

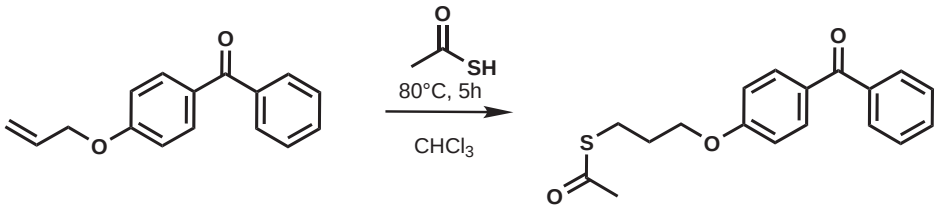

10 g (39, 8 mmol) of 4-allyloxybenzophenone, 0, 274 g (1, 690 mmol), AIBN and 3, 6 mL (50, 78 mmol) of ethanethioic S-acid are dissolved in 180 mL of chloroform. The mixture is heated to reflux for 5 h at 80 ℃ and then cooled to room temperature. The solution is extracted thrice with 200 mL of aqueous $NaHCO_3$. The aqueous phase is washed thrice with 90 mL of petroleum ether and the organic phase was extracted thrice with 90 mL of brine. The combined organic phases are dried over Na_2SO_4, and the solvent is evaporated. The crude product is purified by column chromatography with a mixture of cyclohexane/ethyl acetate (10:1) as the solvent.

Yield: 8,3 g $\sim$ 67 %

^{1}H-NMR (250 MHz, $CDCl_3$): δ / ppm = 7, 84 (d, 2H, C-H arom.), 7, 77 (d, 2H, C-H arom.), 7, 57 (q, 2H, C-H arom.), 7, 50 (q, 1H, C-H arom.), 6, 97 (d, 2H, C-H arom.), 4, 11 (t, 2H, O-CH_2), 3, 09 (t, 2H, S-CH_2), 2, 37 (s, 3H, Me), 2, 12 (quin, 2H, CH_2).

FD-MS [m/z]: 314 [M]+

4.12.8 Benzophenonthiole

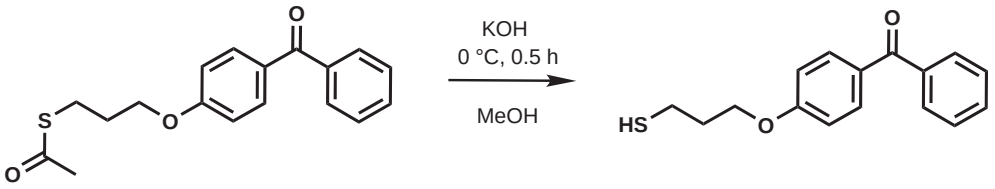

A solution of 1 g S-3-(4-benzoylphenoxy)propylethanthioate (31,84 mmol) in 10 ml methanol is degased with Argon and cooled down to 0 ℃. 300 mg potassiumhydroxide are added and the reaction is monitored by TLC. After the completion of the reaction, the reaction mixture is extracted with 100 ml ethylacetate. The ethylacetate layer is washed three times with 100 ml water, dried with $MgSO_4$ and evaporated under high vacuum.

Yield: 0,76 g $\sim$ 89 %

^{1}H-NMR (250 MHz, $CDCl_3$): δ / ppm = 7,75 (d, 2H, C-H arom.), 7,82 (d, 2H, C-H arom.), 7,55 (q, 2H, C-H arom.), 6,96 (dd, 2H, C-H arom.), 7,48 (q, 1H, C-H arom.), 4,16 (t, 2H, O-CH_2), 2,80 (t, 2H, S-CH_2), 2,11 (quin, 2H, CH_2, 1,41 (t, 1H, -SH).

FD-MS: m/z = 1084 [M]2+ (disulfide), 542 [M]+ (disulfide), 272 [M]+.

4.12.9 Benzophenonesilane

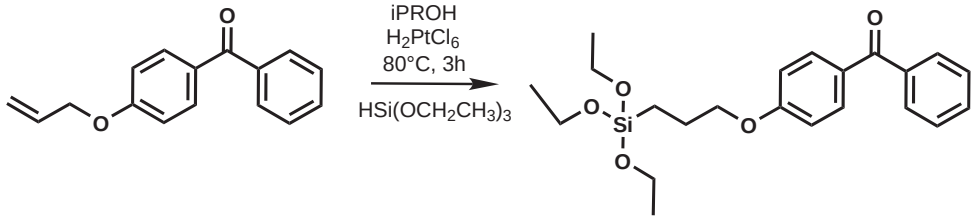

4-Allyloxybenzophenone (2 g, 8.4 mmol) and triethoxysilylhydride (20 g, 0.1 mmol) are added to a reaction flask and degased with argon. 3 ml of a 1.6 wt% solution of the catalyst in isopropanol are added. The mixture is stirred at 82 ℃ for 3 hours. After the reaction mixture is allowed to cool to room temperature the remaining triethoxysilylhydride is removed under high vacuum. The remaining crude product is purified by column chromatography (petrolether/ethylacetate = 7/1) with column packing material being previously passivated with HDMS.

Yield: 2,5 g $\sim$ 71 %

^{1}H-NMR (250 MHz, $CDCl_3$): δ/ppm = 7.81 (d, 2H, 2,6-phenone), 7.75 (d, 2H, 2,6-benzyl), 7.57 (t, 1H, 4-benzyl), 7.47 (t, 2H, 3,5-benzyl), 6.95 (d, 2H, 3,5-phenone); 4.03 (t, 2H, 1-propoxy), 3.84 (q, 6H, CH_2 ethoxy); 1.94 (td, 2H, 2-propoxy); 1.24 (t, 9H, CH_3 ethoxy), 0.78 (t, 2H, 3-propoxy).

FD-MS: m/z = 402.3 [M]+, 804.7 [2M]+.

4.12.10 pHEMA-co-pMABP-co-pBEMA with DIC

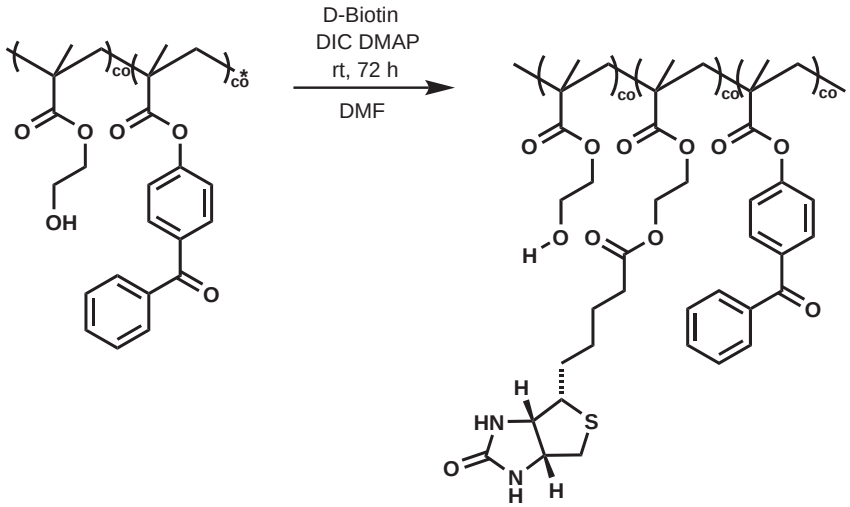

20 ml dry dimethylformamide are added to a mixture 4 g pHEMA-co-pMABP copolymer and DMAP (0,427 g, 3,495 mmol). The mixture is degased for 30 minutes and stirred at room temperature.

In a second flask D-biotin (1,15 g, 4,70 mmol) is degased and solved in 25 ml dry DMF. DIC (1,89 g, 14,9 mmol) is added, and the mixture is allowed to stir for 30 minutes. While keeping the argon atmosphere, the biotin - DMAP mixture is transferred to the solution containing the polymer and stirred for three days.

The polymer is purified by diffusion for six days in dimethylformamide using a 15000 KD cut off membrane. The purified polymer is precipitated in 800 ml diethylether and dried under high vacuum.

Yield: 3,2 g $\sim$ 62 %

^{1}H-NMR (250 MHz, d-MEOH): $\delta/ppm = 6,40$ (band, N-H); 4,50 (band, C-H); 4,30 (band, C-H); 4,20 (band, terminal CH_2 of biotinated pHEMA); $4,15$ (band, 2H, -CH_2-); $3,80$ (band, 2H, terminal -CH_2- of unmodified pHEMA); 3,3 (C-H, Biotin); 2,0 (band, CH_2 in backbone); 1,70-1,45 (band, CH_2 in biotin); $1,30-1,00$ (band, CH_3 backbone).

5 Film surface structuring strategy with photoactive blockcopolymers

5.1 Introduction

Large biomolecules such as DNA fragments do not diffuse into the pHEMA-co-pMABP hydrogel films - as shown in a proof of principle experiment with streptavidin (chapter 4). However, unpublished work by xxxx xxxxxxx from the xxxxxxx group in the MPIP indicates that an increase of the adsorptive surface in a PCR tube coming from surface bound PP polymer artifacts is responsible for an improvement in the amount of surface adsorbed DNA fragments. This indicates that an increase of the polymer surface area might be a good way to improve the DNA adsorption properties of the film.

Four approaches towards the mesostructuring of surface bound pHEMA hydrogel films have been tested in experiments. However, only one concept was chosen as a suitable way to increase the absorptive properties for films bound on complicated substrates.
The first strategy was photopatterning with 2D laser interference lithography, which was successfully employed in the case of thin hydrogel films [161]. In cooperation with Jens Wuesten from the IMM (Institute for Microsystem Technology Mainz) the method was optimized for HEMA based materials to work thicker films of 10 μm. A second

approach pursued by the IMM was the molding of mesostructures on the film surface prior to crosslinking with the hopes to enlarge the surface roughness of the hydrogel film in a mechanical way. Both concepts, however, failed due to the problematic transfer of the structuring technique to the parabolic shape of the PCR tube. —Also, in the case of 2D laser interference photostructuring a very low aspect ratio resulted in a surface area increase that was too small to justify the efforts. Chemical approaches known in literature using inorganic salts or Stoeber particles based porosigens made a homogeneous film deposition inside the PCR tube - as discussed in chapter 4 - too difficult to achieve. Another disturbance proved to be the fact that the resulting films proved to be unstable in lysis and PCR conditions. Also, in the case of inorganic porosigens based on SiO_2, the removal of the sacrificial materials involves the problematic handling of HF. Since the simple chemical concepts discussed above gave unsatisfactory results when it comes to the surface enlargement of bent planar films, a more sophisticated chemical approach based on blockcopolymer phase separation was chosen to be explored.

In this chapter, a strategy towards mesopatterning of hydrogel films deposited on bent planar surfaces is explored. This is supposed to be achieved by simultaneous photocleavage of a sacrificial polymer block and "freezing" of a second block through photocrosslinking. As such, a possible synthetic route towards such materials is explored.

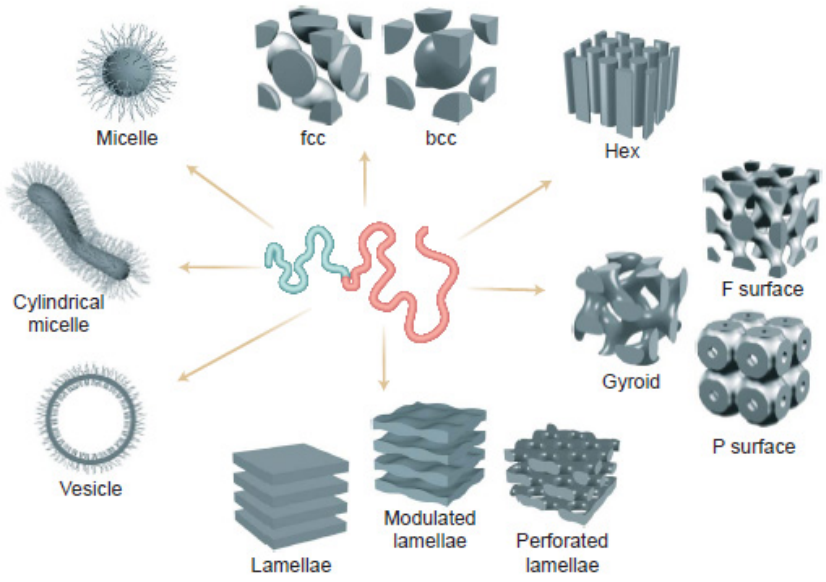

Fig. 5.1 Diblock copolymers are composed of two chemically distinct polymers joined together at one end. The immiscibility of the two blocks results in the microphase separation of the blockcopolymer into ordered nanoscopic domains. The phase separation of these blockcopolymers depends on polymer block volume and its chemical nature [164].

5.2 Strategy towards photoinduced mesostructuring of diblockcopolymer films

5.2.1 General concept

In contrast to polymer mixtures which macroscopically phase-separate into domains of many microns in size, block copolymers microphase-separate into ordered domains that are tens of nanometers in size. The microphase-separation of block copolymers is usually dominated by the enthalpic interactions between the different segments of the block copolymer (Fig. 5.1). The difference in the surface energies of the components forces the orientation of these domains, orienting the block with lower surface energy to the film surface [110].

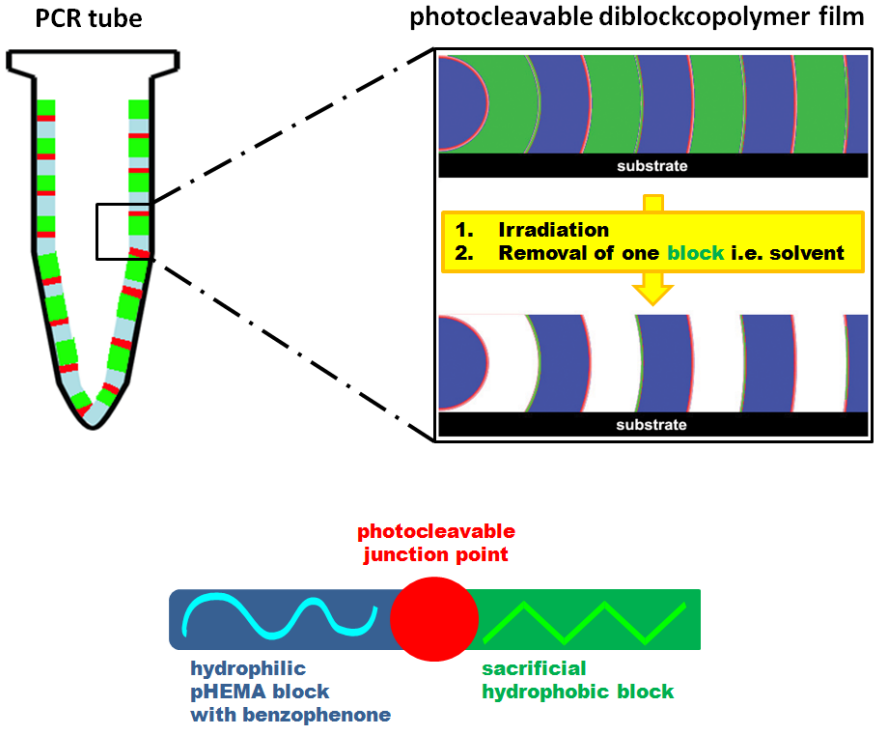

Fig. 5.2 Concept of photoinduced structuring of a hydrogel film on non planar geometries: A material consisting of a symmetric diblock copolymer with a photocleavable junction point is deposited on the inside of the PCR tube. The diblock copolymer microphase-separates into microdomains with dimensions on the scale of tens of nanometers. Upon exposure to UV light a simultaneous cleavage of the junction point and the crosslinking of the hydrophilic block occurs. The hydrophobic block can now be washed away with a suitable solvent, leaving a microscopically fine structured hydrogel surface.

With the usage of diblockcopolymer hydrogel precursors comes the opportunity to introduce these nanoscopic structures to the hydrogel surface. A new method has to be developed in order to deposit material on the problematic geometry of the PCR tube. Fig. 5.2 outlines the deposition of polymer material with the *stamp method* on the example of the PCR tube, as described in greater detail in chapter 6.5.

The desired hydrogel precursor material consists of two blocks - a hydrophobic block

and a hydrophilic photocrosslinkable block - which are connected to each other by a photocleavable group. The material is deposited on the inner surface of the PCR tube (2-10 μm film thickness) and left for phase separation to occur. Upon irradiation with UV light, the elements of the hydrophilic block crosslink into each other and into the substrate material. At the same time, the non-crosslinkable hydrophobic block is cleaved with the excitation of the photocleavable moiety and can be washed out with the use of an appropriate solvent.

The basic repeating unit of the sacrificial hydrophobic block was chosen to be polystyrene (pS). It should not participate in the crosslinking reaction due to its lack of crosslinking elements, phase separate from the hydrophilic pHEMA block, and is supposed to be mostly inert to the photocrosslinking processes of benzophenone at 365 nm irradiation wavelength [165, 166]. Another possibility would be the crosslinking of the polymer at a wavelength of 254 nm with the excitation of acrylic groups in the polymer backbone [167]. However, this route is not pursued in this study.

The main challenges in the synthesis of the phase separating precursor material are a) the incorporation of a photocleavable group in between the polymer blocks while b) maintaining a desired block length ratio for the polymer batch, and c) the simultaneous crosslinking of the hydrophilic block and cleavage of the two blocks. While the last point can be solved with appropriate choice of a photocleavable group with dual anchor positions, the first two points require a synthetic route with high regioselectivity and control of conversion. Also, only a reasonably low polydispersity index (PDI $\lesssim 1.15$) would allow to get a more or less defined phase separation of the material [168]. Hence it is decided to make use of atom-transfer radical polymerization (ATRP). In order to achieve such a high control over the reaction the target polymerization degree is chosen to be around 50 to 70 monomer units per polymer strand. In the following sections the choice of reactions and functional molecules that are suitable for our problem will be discussed.

5.2.2 Photodegradable polymer junction points

In addition of being the primary degradation route for lithographic applications, polymer photodegradation [169] has been extensively studied with hopes of preventing it, thereby increasing the mechanical lifetime of the parent material [170, 171] and controlling it for the development of designer degradable plastics [172]. Although much has been accomplished regarding the synthetic and theoretical aspects of photodegradable polymers, many opportunities for the development of novel photodegradable materials remain. According to literature, all known photodegradable polymers cleave at random sites along the polymerization backbone. Such reactions depend on the existence of chromophores - usually ketones, aromatic groups, or lightabsorbing impurities resulting from oxidation [171] in the polymer chain [173, 172, 174], the addition of small molecule radical initiators which act as chromophores [169, 175], or the existence of cleavable metal-metal bonds on the polymer backbone [175, 176]. In contrast, relatively little attention has been paid to polymers containing photocleavable sites at precisely defined locations within the polymer chain. Such polymers could potentially yield degradation products of defined structure and size.

The cleavage of two connected blockcopolymers has already been reported with ps-b-pMMA (polystyrene -block - polymethylmethacrylate) containing an anthracene dimer photocleavable junction point [177]. The anthracene dimer is reported to cleave at a wavelength of $\lambda \lesssim 300$ nm. A major drawback of the system is the fact that in order to get a dimeric species, two anthracene terminated polymer chains ends have to meet in the solution. Not only is this not very likely scenario, but the dimer is also known to revert thermally to anthracene.

A better choice of a photocleavable functionality is deemed to be the 6-nitroveratroyloxycarbonyl compound (NVoc) and its derivatives with two reactive termini. These groups have been

widely studied in the context of protecting groups for organic synthesis and linkers for solid-phase peptide synthesis [178, 179, 180]. However, they have also found application in the synthesis of polymerization materials [181, 182]. Especially the methylated derivative of NVoc is known for its improved cleavage efficiency regarding quantum yield and irradiation time [183]. The absorption of the NVoc functionality around 350 nm should allow simultaneous activation of benzophenone and o-nitrobenzyl groups while other functionalities in the blockcopolymer should not absorb significantly at this wavelength [184].

5.2.3 Synthesis of monodisperse polymer blocks by controlled polymerization (ATRP)

The unique compatibility of atom transfer radical polymerization (ATRP) [185] with recently emerged copper(I)-catalyzed azide-alkyne cycloaddition (CuAAC) [186, 187], also termed a '*click*' [188] reaction, has been employed for the synthesis of a range of novel materials [189, 190, 191, 192, 193, 194]. In addition, ATRP has been used for the preparation of a number of photoactive polymers and photodegradable materials, making it the tool of choice for the synthesis of diblockcopolymers [195, 196, 197, 198, 199, 184]. Since the controlled polymerization of styrene is much better known and less problematic than the polymerization of HEMA, it was decided to start with the synthesis of the hydrophobic block. The resulting pS polymer could then be used as macroinitiator for the attachment of the hydrophilic pHEMA block.

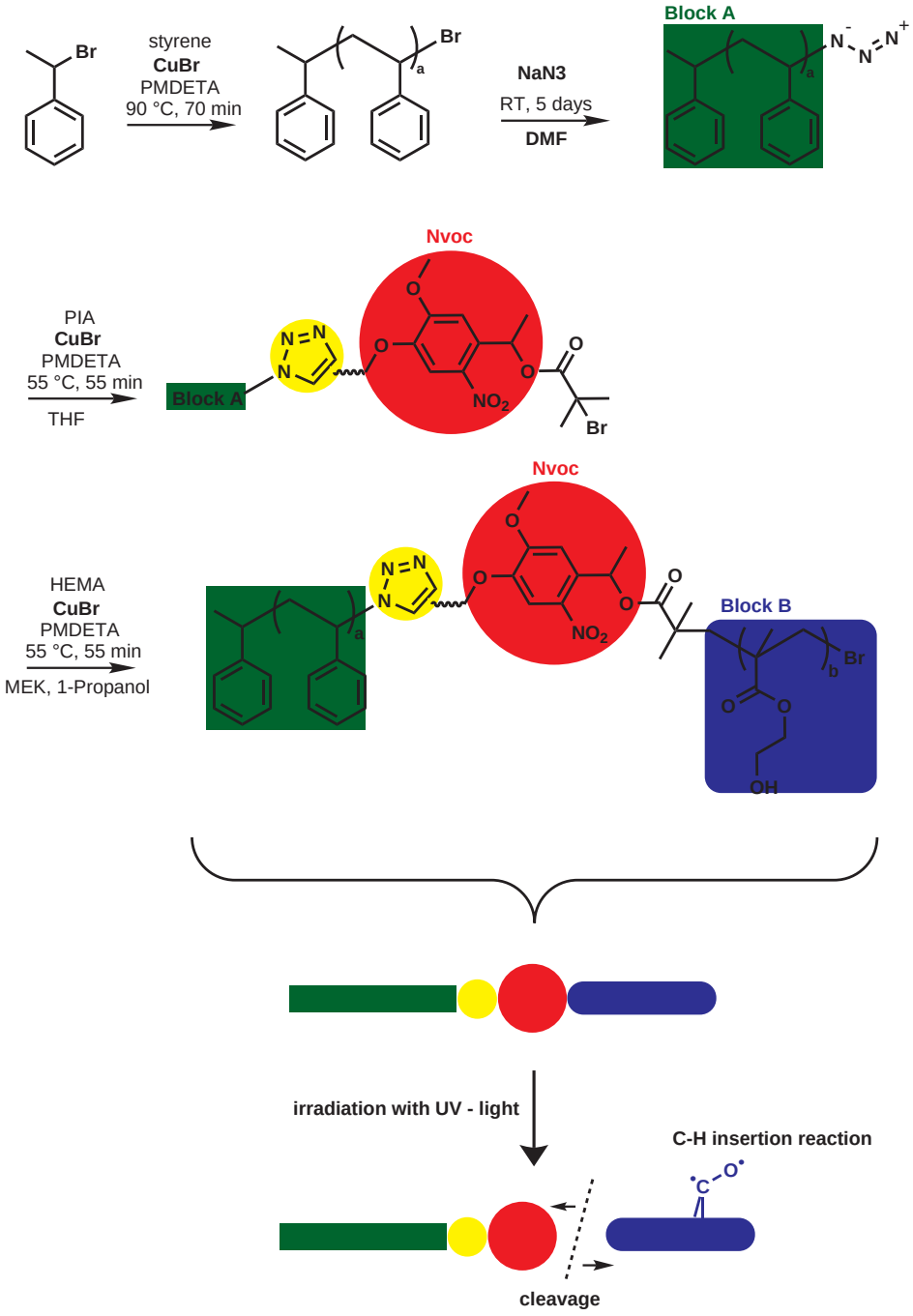

Block A: Polystyrene, very difficult to photocrosslink by UV light irradiation
Block B: pHEMA, photocrosslinkable at 254 nm wavelenght due to acrylic aldehyde group or at 365 nm wavelenght with incorporated benzophenone groups
Nvoc Group: Photocleavable at 365 nm wavelenght
Triazole linker

Fig. 5.3 Synthesis concept of photoactive hydrogel precursors based on blockcopolymers.

5.2.4 Incorporation of NVoc group through combining of ATRP and 'click'-chemistry

The incorporation of a photocleavable junction point in between two polymer block requires a reaction yield with very high chemical yield and regioselectivity. Naturally, the usage of *click* chemistry is a tempting approach for such an problem. The most pronounced example of a such a *click* reaction is the copper(I)-catalyzed Huisgen 1,3-dipolar cycloaddition between azides and terminal acetylenes, which leads to the formation of 1,4-disubstituted 1,2,3-triazole rings [186]. Over the last years, *click* chemistry has taken a tremendous flight in polymer chemistry to prepare main-chain triazole polymers [200, 201], dendrimers [202, 203, 204, 205], dendronized linear polymers [206, 207], hydrogels [208, 209], block copolymers [189], graft copolymers [210, 211], star polymers [191, 212, 213, 214] and new classes of functionalized monomers [215]. It has also been used to functionalize end groups [216, 217, 218] and side chains [219, 190, 220, 221] of polymers.

In this work the regioselectivity and high yield of the copper(I)-catalyzed Huisgen 1,3-dipolar cycloaddition is used to synthesize diblock copolymers [189, 222]. By making use of this strategy it is possible to insert the NVoc functionality between the two blockcopolymer chains: Fig. 5.3 shows the synthesis concept of the photoactive blockcopolymer hydrogel precursor. Following the controlled polymerization of the hydrophobic polymer block by ATRP, the bromo - terminated end group of the polymer chain is substituted by an azide group. The addition of a bifunctional, photocleavable linker molecule to the azide chain end with the use of copper catalyzed Huisgen 1,3-dipolar cycloaddition reaction yields a ATRP macroinitiator with a photolabile chain end. This macroinitiator is then subjected to another ATRP reaction with HEMA or a suitable derivative, yielding the desired photoactive material. The chosen synthetic route gives the possibility to use the same catalyst-ligand combination for both the ATRP and 'click' reaction, and -

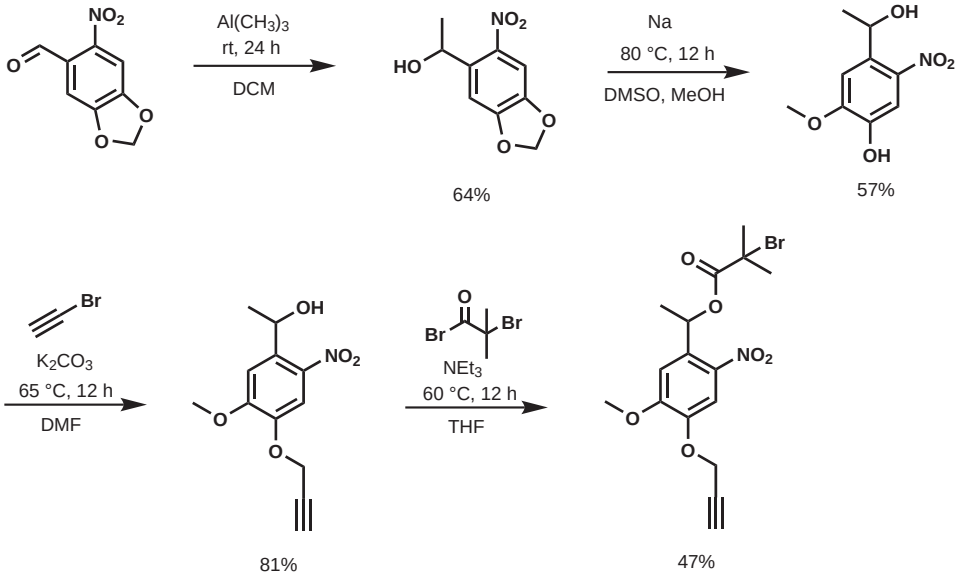

Fig. 5.4 Synthesis scheme of photocleavable ATRP initiator.

with exception of the separation from unreacted macroinitiator PS-PIA from the target blockcopolymer pS-PIA-b-pHEMA - makes the isolation of the different products after each reaction step achievable without too many complications.

5.3 Synthesis and characterization of photocleavable initiator for ATRP (PIA)

The synthesis scheme for the photocleavable initiator for ATRP reactions (PIA), containing an NVoc at its center, is shown in Fig. 5.4. A route in order to obtain a bifunctional NVoc linker group with high yield has been reported by Teague et al. [223], although most of the actual experimental procedure has been left out. As such, the first step of the synthesis featuring the nucleophilic methylation of the aldehyde group with trimethylaluminium was successfully adopted from a reaction procedure in literature [224]. The synthesis of the NVoc molecule is completed by a regioselective aromatic nucleophilic

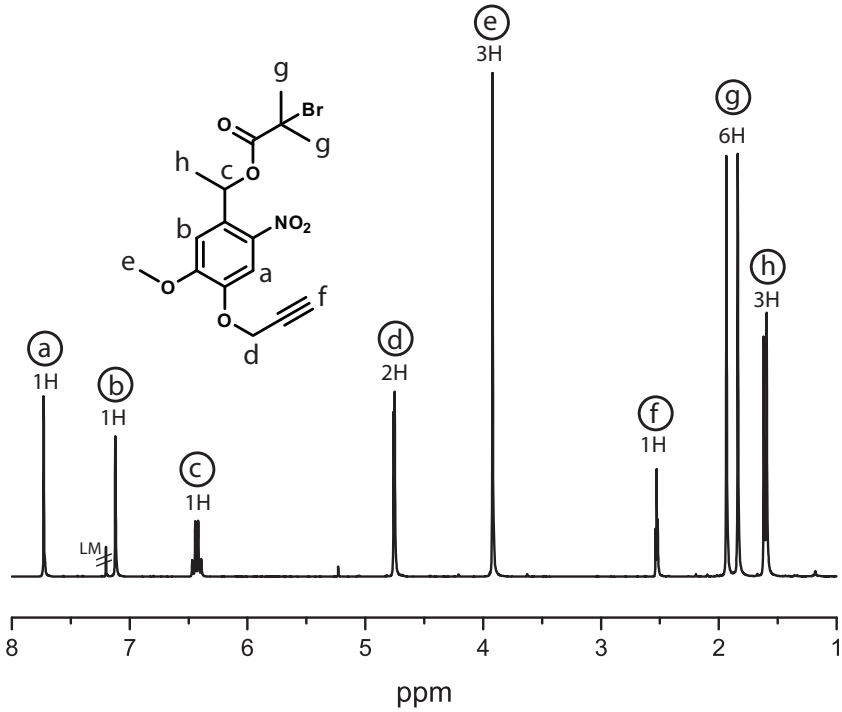

Fig. 5.5 250 MHz ^{1}H-NMR spectrum of a photocleavable initiator for ATRP (PIA) in $CDCl_3$.

displacement of the methoxide at 5-position. The secondary alcohol that is present in the starting material does not compete with the hydroxyle group bound to the aromatic ring, presumably because of a combination of steric effects and its lower pKa. This is followed by a regioselective alkylation of the diol [225], yielding a prop-2-yn-1-ol adduct on the more reactive, ringbound phenylic oxygen atom. In a last step, the moiety responsible for starting the ATRP reaction is introduced by reacting the remaining aliphatic hydroxyle group with 2-bromo-2-methylpropanoyl bromide (EBrP).

Fig. 5.5 shows the ^{1}H-NMR spectrum of the photocleavable initiator: The two aromatic protons show as singlets at 7,7 and 7,2 ppm. They are followed by the highly shifted hydrogen atom at 6,5 ppm that can be allocated to the carbon atom connected to the aromatic ring and to the electron withdrawing ester group. The two singlets at 4,6 ppm and 3,8 ppm correspond to the hydrogen atoms on the methoxy- and the prop-2-ynyloxy

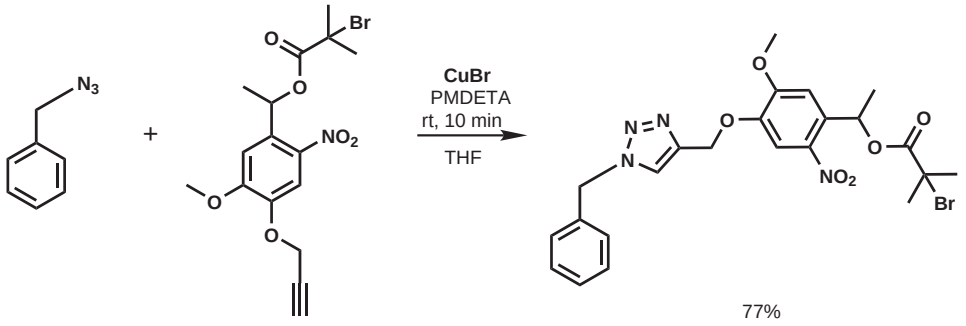

Fig. 5.6 Testing the "click" reaction of the photocleavable ATRP initiator PIA by reacting it to benzylazide.

moieties, while the acetylinic proton shows at 2,6 ppm. The six hydrogen atoms of methylpropanoate group can be found in a doublet signal at 1,8 ppm of the aliphatic region of the spectrum. The doublet signal at 1,6 ppm belongs to the remaining methyl group of the carbon atom at position 15.

5.4 Click reaction with photocleavable ATRP initiator

Finding a proof of the chemical attachment of the photocleavable ATRP initiator to the azide terminated polystyrene with ^{1}H-NMR spectroscopy is not a trivial task because of the low ratio of PIA molecules to the phenyl rings of polystyrene. Also, a second problem arises due to the overlapping of proton signals both in the aromatic and aliphatic regions of the spectrum. These broadened signal groups make the determination of product formation nearly impossible. As such, a more simple system that allows a much easier characterization and consequently an optimization of yield regarding reaction conditions is chosen. Such a system would be the reaction of benzylazide and PIA, as shown in Fig. 5.6.

THF and DMF are excellent solvents for all components of the reaction: polystyrene, HEMA monomer, pHEMA, PMDETA and the PIA molecule can be solved very well in

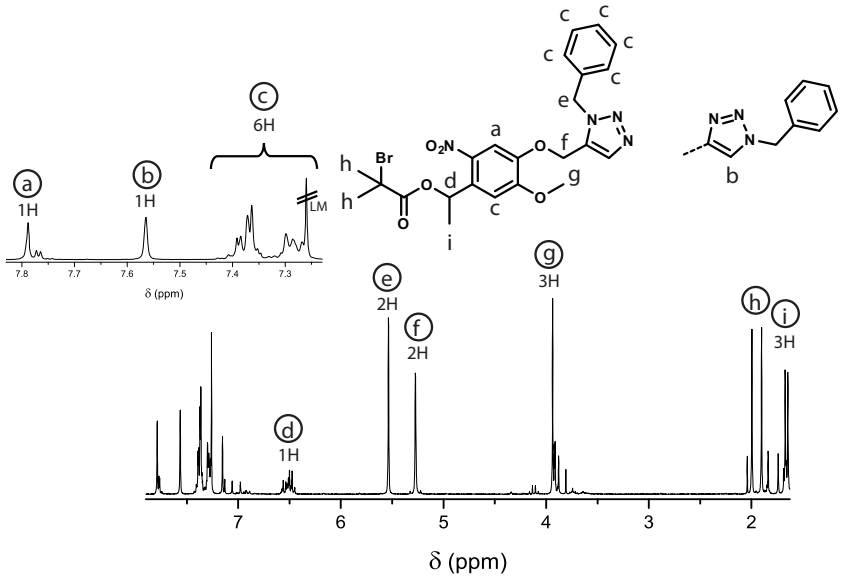

Fig. 5.7 250 MHz ^{1}H-NMR spectrum of the 'click' reaction product of benzylazide and PIA in $CDCl_3$. The exclusive appearance of the b band at 7,5 ppm indicates that the reaction yielded almost exclusively the anti-1,4 adduct.

these solvents. As such, the *click* reaction was both carried out in both THF and DMF at room temperature. The reaction was carried out in a small scale under protective gas atmosphere, with the products being purified by preparative TLC chromatography. While the reactions showed a very high reaction rate and a completion of the reaction after five to ten minutes in both solvents, the reaction in DMF showed more side products, making THF the preferred solvent for the reaction. It has to be noted that because of unavoidable light exposure - daylight and UV light from the TLC detector lamp - during the workup process a partial cleavage reaction is supposed to have taken place, as can be observed on the TLC plates.

The ^{1}H-NMR spectrum of the product obtained by the click reaction is shown in Fig. 5.5: The disappearance of the acetylenic proton at 2,6 ppm indicates the completion of the reaction of the triple bond. More interestingly, the singlet signal with an integral corres-

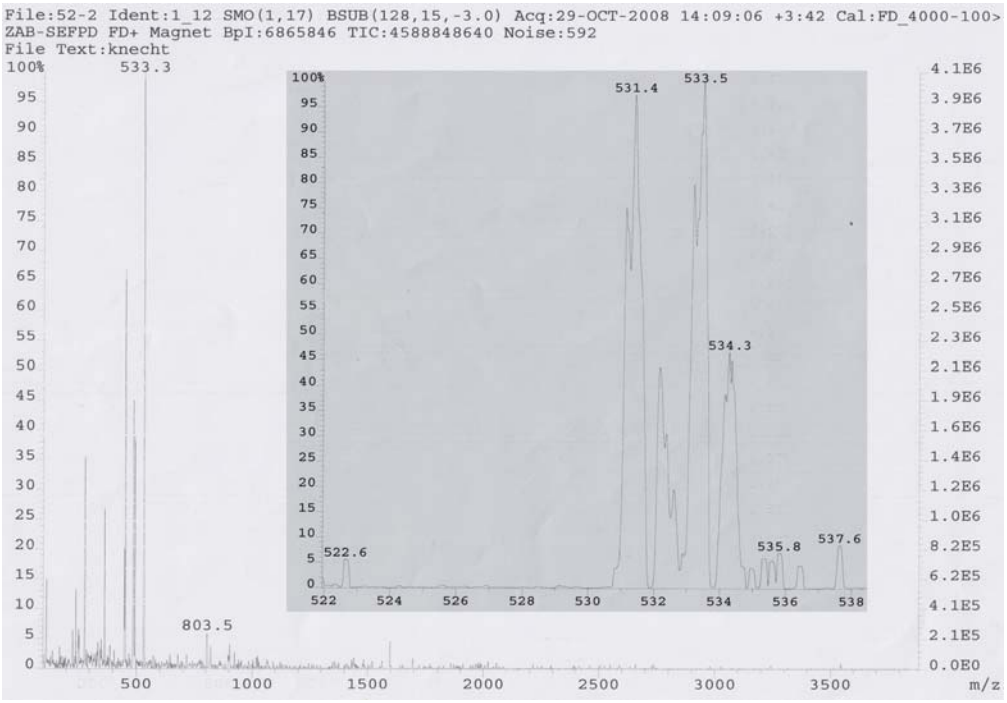

Fig. 5.8 FD mass spectroscopy measurement of the benzylazide - PIA aduct.

ponding to one hydrogen atom shows at 7,5 ppm and can be allocated to the hydrogen atom at 5 position of the 1,4-triazole ring. In addition, the relative value of the integral in the spectrum also indicates that the copper(I) catalyzed cycloaddition reaction has - as expected - mostly yielded the (anti-) 1,4 adduct. This is supported by the distribution of signal intensity in the aromatic region: a mixture with syn-product is expected to show at slightly lower chemical shift of around 7,3 ppm and would lead to uneven integral values - this, however, is not the case. With the exception of the aromatic hydrogen atom next to the nitro group, all other aromatic protons show in a multiplet in the region around 7,2 ppm to 7,3 ppm. The multiplet at 6,5 ppm can be allocated to the proton at the carbon atom that is connected to the aromatic ring and to the electron withdrawing ester group. The proton signals of the carbon atoms next to the triazole ring can be found at 5,1 ppm and 5,5 ppm, with the carbon atom that is close to the aromatic ring being exposed to a higher electron withdrawing effects. The methoxy

group shows at 3,8 ppm in the spectrum, while the hydrogen atoms of methylpropanoate group can be found in a doublet signal at 1,8 ppm of the aliphatic region. The doublet signal at 1,6 ppm belongs to the remaining methyl group of the carbon atom at position 15. Unfortunatly, the spectrum comes with a fair deal of impurities that either can be attributed to the photolysis of the molecule during purification - which is supported by the lower signal intensity of the h signal group than expected by theory - and reaction side products.

The FD mass spectrum in Fig. 5.8 brings further evidence towards the formation of the adduct: The adduct shows at 533.3 m/z units. Moreover, the typical isotope distribution for bromides (^{79}Br and ^{81}Br in roughly 1:1 ratio) can been seen as M+2 peaks in the enlargement of the product area.

5.5 Photocleavage of the PIA - benzylazide adduct

The cleavage of the PIA molecule was monitored by TLC and characterized both by mass spectroscopy and UV/vis spectroscopy. In the case of TLC chromatography, the disappearance of the product spot during irradiation and the appearance of multiple side products was a strong indication of photodegradation of the linker molecule. For monitoring the photodegradation behaviour, a solution of the molecule was irradiated at 365 nm wavelength at different time intervals and subsequently measured with UV/vis spectroscopy. The photodegradation behaviour as measured by UV/vis spectroscopy is shown in Fig. 5.9: Before any irradiation the NVoc group shows two strong absorption maxima at $\sim$ 300 nm and $\sim$ 350 nm. The result of the irradiation at 365 nm was a strong reduction of the band at 300 nm wavelength. At the same time a broadened band with a maximum at 375 nm appeared in the spectrum. This redshift indicates the release of benzyl ketone photoproduct and further supports the photocleavage of the

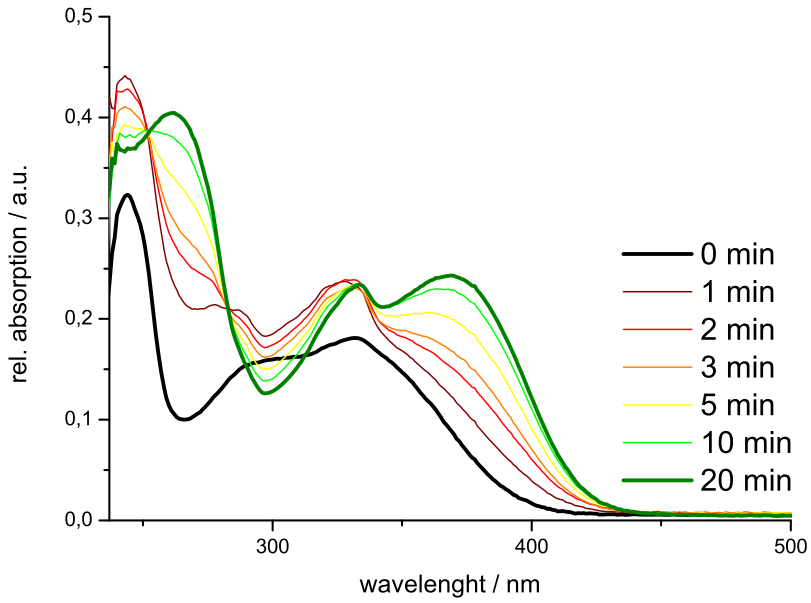

Fig. 5.9 Characterization of photocleavage of Benzyl-PIA derivative with UV/vis spectroscopy. The photo induced cleavage of PIA is reflected in the change of UV absorption bands at different irradiation times.

linker [226]. After further irradiation up to 2 hours no further change in the spectrum can be seen. This can be taken as an indication of a complete cleavage of the PIA - benzylazide adducts after 20 minutes.

5.6 Synthesis of photocleavable blockcopolymer and cleavage of block segments

Synthesis of the macroinitiator

Following reported procedure in literature [227], the polystyrene block was synthesized using Cu(I)Br/PMDETA as active catalyst pair and 1-phenylethylbromide as initiator.

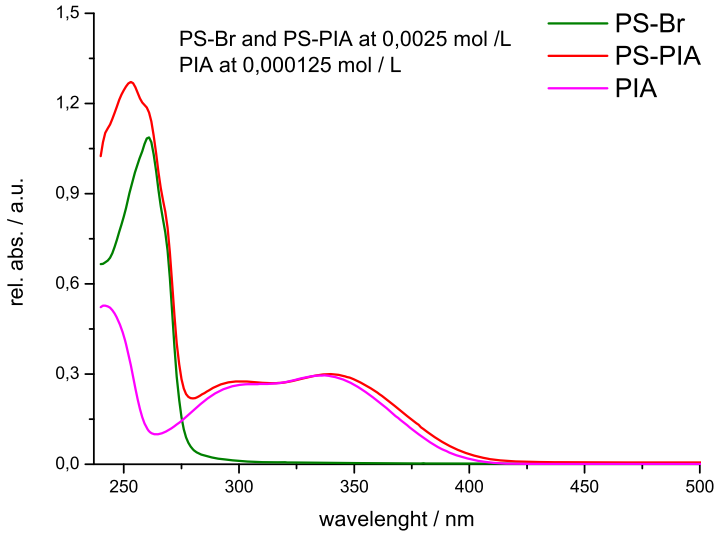

Fig. 5.10 UV/vis measurement of purified pS-Br, PIA and pS-PIA material in DMF. Added up, the first two curves yield the pS-PIA spectrum. The concentration of the the pS-Br curver is twenty times larger than the PIA curve, which is an indication that a fraction of pS polymer chains have an attached PIA molecule.

Due to the large batch of 20 g styrene monomer a very good polydispersity was reached. The freeze-thaw technique was not used, as a much simpler method gave satisfactory results. Instead, the reaction mixture was degased vigorously with Argon for a longer period of time. The obtained polystyrene was purified by precipitation in methanol, which also removed all but traces of the used copper catalyst. GPC in DMF with pS as standard showed the polymer to have M_n of 6113 g/mol and a M_w of 7068 g/mol. This indicates that the polymerization target has been well met. The ^{1}H-NMR spectrum of the polymer is shown in Fig. 5.11.

As described by the general synthetic route that was layed out in Fig. 5.3, the bromo end groups of the polystyrene polymer were transformed to azide groups using a procedure from literature [184]. The polymer was purified by fourfold precipitation into methanol.

This was followed by a reacting the azide end group of the polymer with the acetylene group of the PIA initiator, resulting in the photocleavable macroinitiator (pS-PIA). The macroinitiator was purified from unreacted PIA molecules by repeated precipitation in methanol. Due to the low amount of PIA molecules to styrene repeating units in macroinitiator it was not possible to characterize the product with ^{1}H-NMR. However, measurements with UV/vis spectroscopy - as shown in Fig. 5.10 - give an indication towards product formation. Thus, it had to be assumed that a part of the pS-polymers were functionalized. The purified macroinitiator was used in the subsequent ATRP reactions, which are summarized in Table 5.1.

Polymerizations with ATRP

The ATRP reactions were run in a 7 : 3 MEK/1-propanol solvent mixture at 50 °C. Typically, a 100 : 1 : 1 : 1 monomer/initiator/catalyst/ligand ratio was found to be the best reaction composition. The polymerization reactions were stopped at roughly 50% conversion to avoid complications.

In order to check whether the pS-PIA macroinitiator was in useful state it was compared to other initiators: ethyl 2-bromo-2-methylpropanoate (EBrP), PIA, and pS-Br and pS-PIA have been used in polymerizations. Also, both Cu(I)Cl and Cu(I)Br were used as catalyst.

Polymerizations with PIA and EBrP as intiator resulted in very similar conversion rates, as shown in Fig. 5.12. This leads to the conclusion that the PIA molecule is very well usable as an ATRP initiator for HEMA.

Table 5.1 summarizes the ATRP of HEMA that used PIA, EBrP, pS-Br and pS-PIA as initiator. The resulting PDIs were mostly in the range of 1,8 when using Cu(I)Br

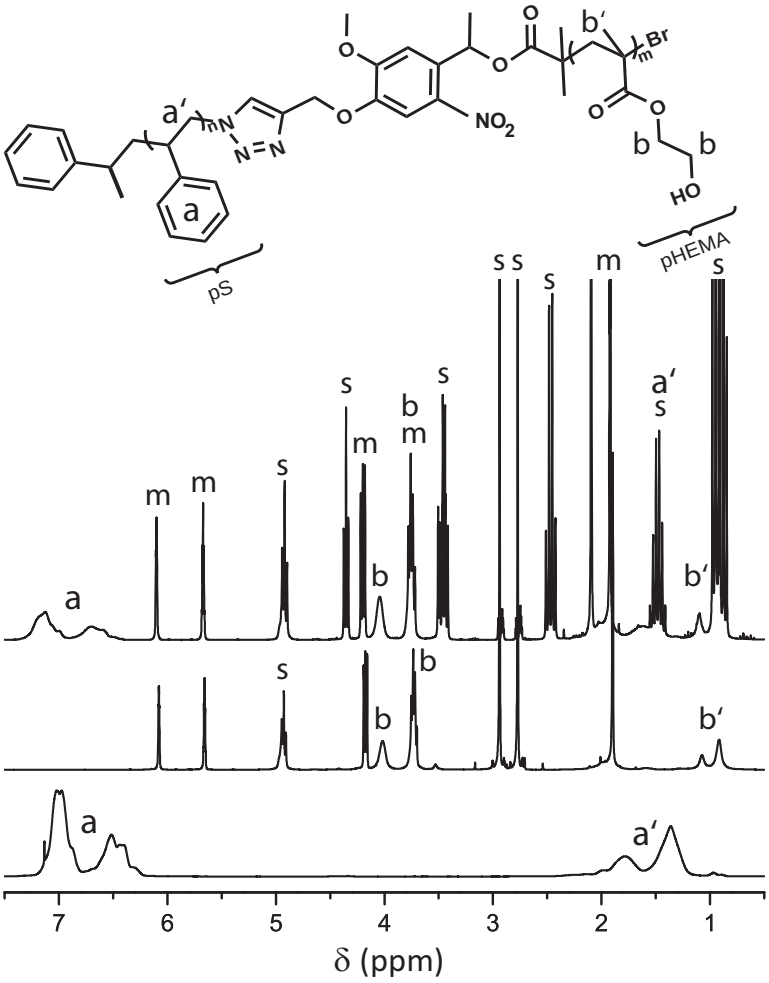

Fig. 5.11 Polymer ^{1}H-NMR spectra recorded in d-DMF. All reactions were run using ATRP. **Bottom**: pS-PIA macroinitiator with its aromatic (a) and aliphatic (a') signals . **Middle**: pHEMA polymer spectrum, as taken from reaction mixture. While NMR solvent and reaction solvent (MEK, 1-propanol) signals (s) and monomer signals (m) partially overlap with the polymer spectrum, the characteristic bands for pHEMA - (b) and (b') - can still be found **Top**: pS-PIA-pHEMA blockcopolymer, as taken from reaction mixture. Characteristic polymer bands for pS (a, a') and pHEMA (b, b') can be found in the spectrum. While the NMR of the reaction mixture is not enough evidence to prove the synthesis of the blockcopolymer, the GPC analytics underline its existance.

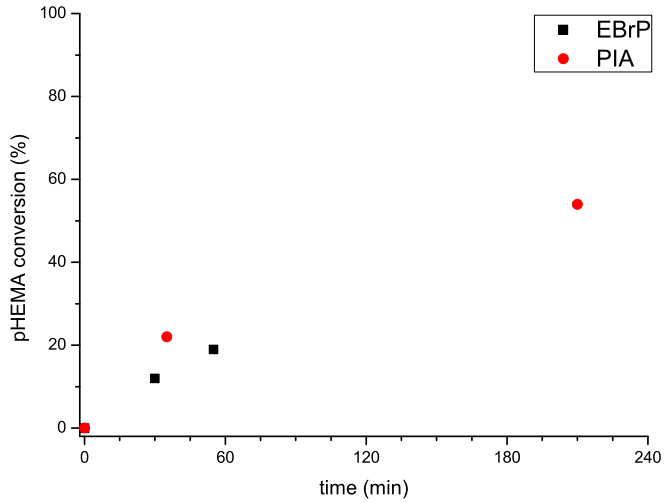

Fig. 5.12 Conversion of ATRP polymerizations of HEMA using PIA and EBrP as initiator and a HEMA/Cu(I)Br/PMDETA/initiator ratio of 100 : 1 : 1 : 1. 0,5 ml anisole per 3 g HEMA were added to the mixture as an internal standard for ^{1}H-NMR kinetic measurements.

as catalyst, and around 1,4 when choosing Cu(I)Cl. Moreover, GPC analysis of the blockcopolymers shows a bimodal distribution, indicating that a fraction of macroinitiator molecules have not reacted in the polymerization. Whether this was caused by the degeneration of the initiator prior to the reaction, residual free PIA molecules, or general lack of control of reaction conditions could not be determined. However, the resulting PDI of around 2 for the blockcopolymer is far from the values that are required to get defined phase separation in blockcopolymers [168, 164]. In addition to this, it was not possible to isolate the synthesised blockcopolymers through precipitation in organic solvents, making an analysis of the composition of the polymer impossible.

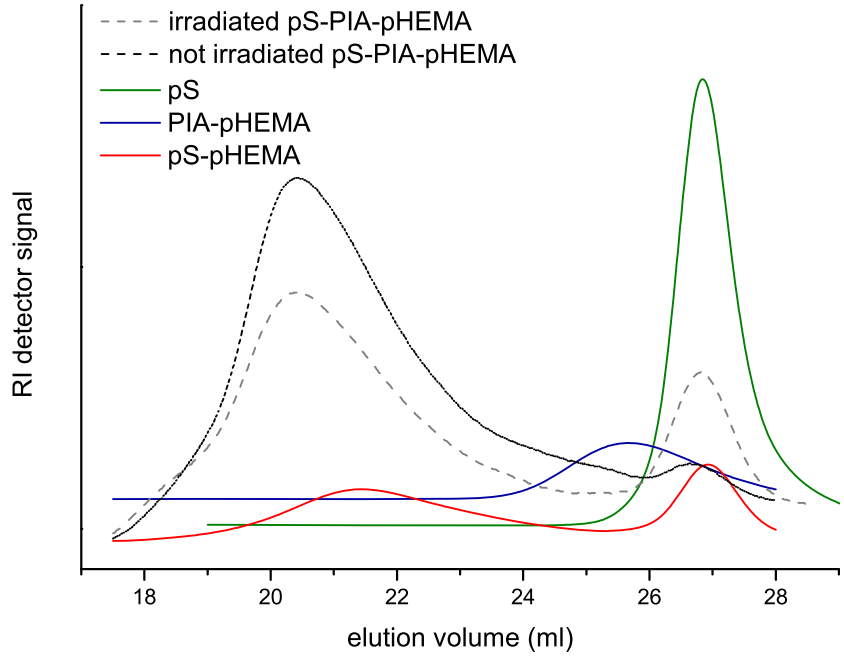

Fig. 5.13 Overlay of GPC measurements of synthesized blockcopolymers. All reactions were run up to a conversion of about 50%. As can been seen by the bimodal mass distribution of the GPC curve, the resulting pS-PIA-pHEMA blockcopolymer is not clean. The ratio of the signal bands changes when irradiating the blockcopolymer with UV - light: The signal band around 27 ml increases, while the broad band from 18 ml to 24 ml decreases. This indicates a separation of the polymer blocks due to a photoinduced cleavage reaction of the NVoc linker moiety.

Table 5.1 ATRP polymerizations stopped at roughly 50% conversion with a 100 : 1 : 1 : 1 monomer/initiator/catalyst/ligand ratio.

product	starter	monomer	ligand	catalyst	solvent	PDI
pS-Br	1-PEBr	styrene	PMDETA	Cu(I)Br	anisole	1,16
EP-PHEMA	EBrP	HEMA	Bpy	Cu(I)Br	MEK/iProp	1,70
EP-PHEMA	EBrP	HEMA	Bpy	Cu(I)Cl	MEK/iProp	1,44
PIA-pHEMA	PIA	HEMA	Bpy	Cu(I)Br	MEK/iProp	1,78
PIA-pHEMA	PIA	HEMA	Bpy	Cu(I)Cl	MEK/iProp	1,44
PIA-pHEMA	PIA	HEMA	Bpy	Cu(I)Cl	MEK/iProp	1,38
pS-pHEMA	pS-Br	HEMA	Bpy	Cu(I)Br	MEK/iProp	1,80
pS-PIA-pHEMA	pS-PIA	HEMA-TMS	Bpy	Cu(I)Br	MEK/iProp	~ 2

Cleavage of polymer blocks through UV irradiation

While it is difficult to prove the photocleavage of the blockcopolymer without being able to isolate it, a strong indication of a successful dissociation of the pHEMA and pS blocks in the blockcopolymer by irradiation with 365 nm light is given by a signal shift in the GPC plots shown in Fig. 5.13. A crude mixture of pS-PIA-pHEMA and unreacted macroinitiator are subjected to UV light irradiation for two hours. The exposure of the material to UV light results in an a) overall decrease of the blockcopolymer signal with a PDI of roughly 2 at 22 ml elution volume, and b) an increase of the known signal at 27 ml elution volume with a PDI of roughly 1,18 that can be attributed to the pS polymer. This leads to the assumption that a cleavage of blockcopolymer has taken place.

5.7 Conclusion

A chemical approach towards the structurering of hydrogel surface with the help of blockcopolymers and photochemistry has been investigated. For this, a NVoc based photolabile linker with ATRP initiator and *click* functionality has been synthesized. ATRP

and 'Click' conditions have been optimized for the linker, and its cleavage has been monitored by TLC and UV/vis spectroscopy. A photocleavable and photocrosslinkable blockcopolymer has been synthesized by polymerizing a pS block with ATRP, substituting its chain end group with an azide group, 'clicking' it to the acetylene group of the photocrosslinkable initiator for ATRP (PIA) linker and finally polymerizing it with HEMA monomer. The cleavage of the blockcopolymer was tested with a model molecule: a benzylazide PIA adduct. Unfortunatly, the obtained material could not be purified properly and was found to be strongly mixed with leftovers of unreacted macroinitiator. The blockcopolymer samples exhibit much slower cleavage behaviour than in the model studies. This rendered the material useless for further phase separation studies.

5.8 Experimental

5.8.1 Methyl-6-nitropiperonal

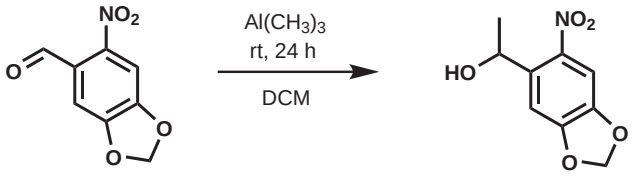

Important note: Trimethylaluminium is easily ignited by air moisture. It is imperative that the entire procedure is taking place under protective gas atmosphere, and that even small amounts of residual TMA are neutralized.

9,543 g (48,9 mmol) 6-Nitropiperonal are solved in 150 ml dichloromethane and degased with Argon. The solution is cooled with an ice bath, and 7,95 g (55,1 mmol) trimethylalumnium are added slowly through a degased syringe. The reaction mixture is allowed to equilibrate to room temperature. After stirring overnight, the reaction mix-

ture is cooled with an ice bath and 12 ml of a solution of saturated $NaHCO_3$ are added dropwise. The organic layer is is separated, filtrated and dried with $MgSO_4$. The crude product is purified by column chromatography (EtAc:Hex 1:1; product Rf=0,65).

Yield: 6,58 g $\sim$ 64 %

^{1}H-NMR (250 MHz, DCM): δ/ppm = 7,52 (s, 1H, arom. -H), 7,48 (s, 1H, arom. -H), 6, 25 (s, 2H, -O-CH_2-O-), 5,5 (m, 1H, (HO-)(H_3C-)C-), 1, 5 (d, 3H, -CH_3).

5.8.2 4-(1-Hydroxyethyl)-2-methoxy-5-nitrophenol

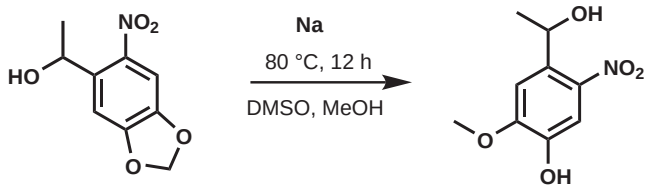

To a degased solution of 5,3 g (25,1 mmol) methyl-6-nitropiperonal in 35 ml DMSO and 18 ml methanol is added in small portions 0,651 g (28,3 mmol) sodium under counter-current flow. The reaction mixture is heated at 80 ℃ overnight. The reaction mixture is poured into 600 ml 2M HCl and extracted 4 times with 300 ml ethyl acetate. The organic phase is dried with magnesium sulfate and removed under vacuum. The crude product is purified by column chromatography.

Yield: 3,06 g $\sim$ 57 %

^{1}H-NMR (250 MHz, DCM): δ/ppm = 7,60 (s, 1H, arom. -H), 7,44 (s, 1H, arom. -H), 5, 80 (s, 1H, arom. -OH), 5, 50 (m, 1H, aliph. -H), 4, 00 (s, 3H, -OCH_3), 2, 80 (s, 1H, aliph. -OH), 2, 80 (s, 3H, -CH_3).

5.8.3 1-(5-Methoxy-2-nitro-4-(prop-2-ynyloxy)phenyl)ethanol

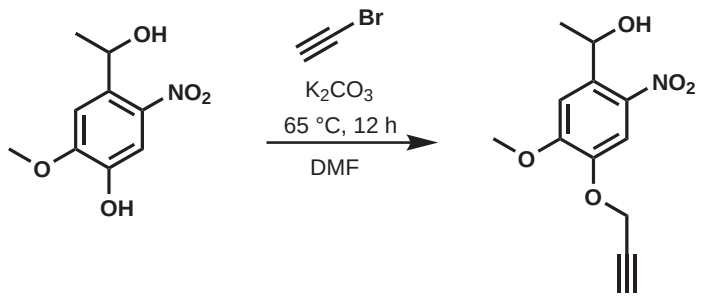

To a solution of 499 mg (2,34 mmol) 4-(1-hydroxyethyl)-2-methoxy-5-nitrophenol in 22 ml dry DMF is added 400 mg K_2CO_3. The mixture is degased with Argon and 330 mg (3,11 mmol) bromoethyne are added through a syringe. The reaction is stirred 65 °C overnight. 150 ml water are added to the reaction mixture for the workup procedure. The aqueous layers is extracted four times with 150 ml ether. The unified organic fractions are washed with 300 ml water and dried with $MgSO_4$. The solvent is removed under reduced pressure. Purification is done by column chromatography.

Yield: 0,5 g $\sim$ 81 %

^{1}H-NMR (250 MHz, DCM): $\delta/ppm = 7,6$ (s, 1H, arom. -H), $7,2$ (s, 1H, arom. -H), $5,4$ (s, 1H, aliph. -H), $4,7$ (s, 2H, -O-CH_2-), $3,8$ (s, 3H, -O-CH_3), $2,5$ (s, 1H, propynyl), $2,3$ (s, 1H, -OH), $1,4$ (d, 3H, -CH_3).

5.8.4 1-(5-Methoxy-2-nitro-4-(prop-2-ynyloxy)phenyl) ethyl 2-bromo-2-methylpropanoate (PIA)

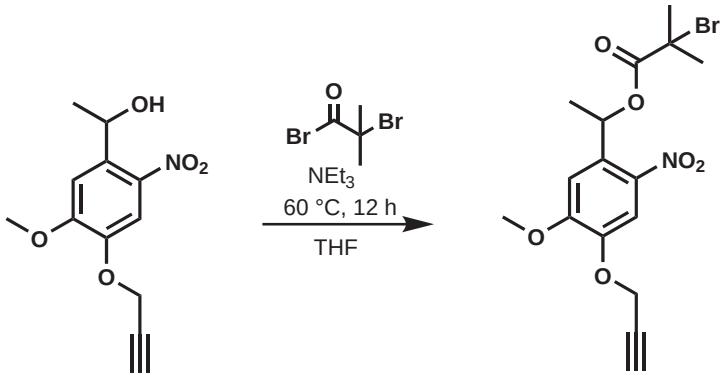

1,305 g (5,19 mmol) 1-(5-methoxy-2-nitro-4-(prop-2-ynyloxy)phenyl)ethanol are solved in a solution of 5 ml dry NEt_3 in 60 ml dry THF. After stirring for 15 minutes, 3,5 g (15,41 mmol) 2-bromo-2-methylpropanoyl bromide are added to the solution through a syringe and the reaction mixture is stirred overnight at 60 °C. The solvent is removed under reduced pressure, and 130 ml ethyl acetate are added to the crude mixture. The organic phase is washed with 200 ml deionized water, 300 ml 1M aqueous HCl solution, 300 ml 1M aqueous NaOH solution, and two times with 100 ml saturated ammoniumchloride solution. The solvent is removed under reduced pressure, and the crude product is purified by column chromatography (R_f 0,5 with EtAc/hexane = 1:1)

Yield: 0,98 g $\sim$ 47 %

^{1}H-NMR (250 MHz, DCM): $\delta/ppm = 8,73$ (s, 1H, (3) arom. -H), $7,1$ (s, 1H, (4) arom. -H), $6,45$ (m, 1H, -C(OO)C-H(-CH_3)(-Ph)), $3,85$ (s, 3H, methoxy), $2,5$ (s, 1H, propynyl), $1,70 - 1,95$ (d, 6H, -CH_3).

5.8.5 ATRP of Styrene

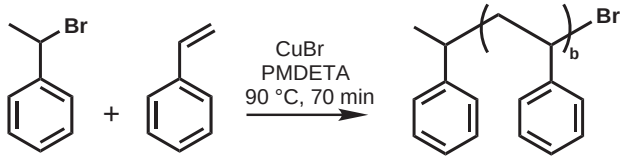

20,835 g styrene and 2 ml dry anisole are degased in a schlenk tube for 30 minutes. 0,4792 g of freshly distilled PMDETA are added and the mixture is degased for further 10 minutes. 0,4818 g 1-phenylethylbromide are added and the mixture is degased for 60 more minutes. After stirring at 90 ℃ for 70 minutes, the polymerization is stopped by exposing the reaction mixture to air and immersing the reaction tube in liquid nitrogen. 20 ml diethylether are added, and the mixture is precipitated in 500 ml methanol. The crude polymer is purified by threefold solving in 100 ml ether and precipitation in 1,8 L methanol.

PDI: 1.15

Mw: 7.400 g/mol

m 11.1 g

^{1}H-NMR (250 MHz, DCM): $\delta/ppm = 6,1-7,1$ (band, 5H, arom. -H), $1,0-2,0$ (band, 3H, (aliph. -H).

5.8.6 Polystyrene with terminal azide group

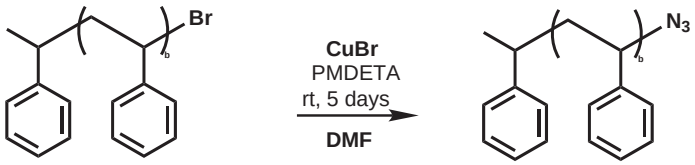

To a degased solution of 5,61 g bromo - terminated polystyrene (M_W 15500, PDI 1,15) in 80 ml dry DMF are added 700 mg of sodium azide. The reaction mixture is stirred at room temperature for 5 days. The crude polymer is precipitated in a mixture of 800 ml methanol and 1200 ml distilled water. The precipitated polymer is washed once with 400 ml water and twice with 400 ml methanol. This is followed by drying under high vacuum.

Yield: 4,25 g $\sim$ 75 %

^{1}H-NMR (250 MHz, DCM): $\delta/ppm = 6,1 - 7,1$ (band, 5H, arom. -H), $1,0 - 2,0$ (band, 3H, (aliph. -H).

5.8.7 Benzyl-PIA via Click

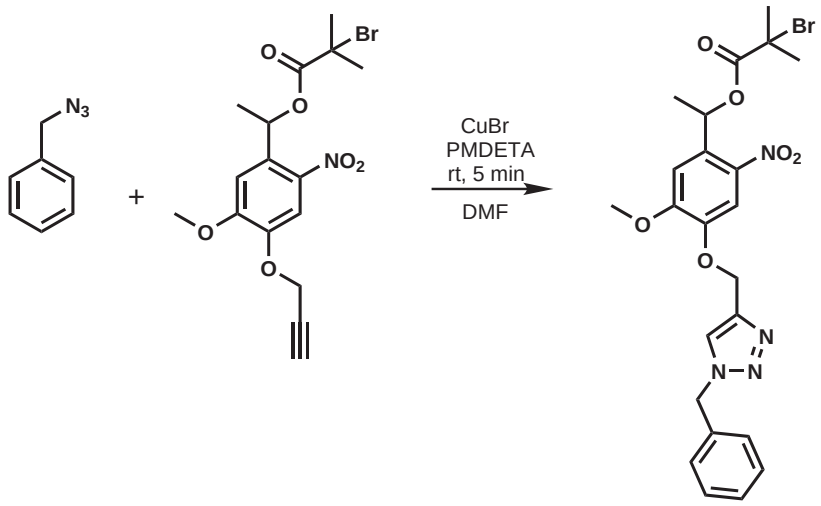

To a degased mixture of 0,041 g benzylazide and 0,029 g (0,073 mmol) PIA are added 3 ml dry tetrahydrofurane. To this mixture 1 ml of a catalyst stock solution (4,7 mg/ml cupper(I)bromide and 8,8 mg PMDETA/ml in oxygen free THF) are added. The reaction flask is covered with alumina foil and the reaction is monitored by TLC. After completion

of the reaction after 5 minutes the solvents are removed *in vacuo*. The crude product is solved and purified by preparative thin layer chromatography (ethylacetate/hexane 1:1, $R_f = 0{,}5$).

Yield: 0,03 g $\sim$ 77 %

^{1}H-NMR (250 MHz, DCM): $\delta/ppm = 7,8$ (s, 1H, arom. -H), $7,65$ (s, 1H, arom. -H), $7,3 - 7,5$ (m, 5H, benzyl), $6,5$ (m, 1H, aliph. -H), $5,6$ (s, 2H, Ph-CH_2-N_3-), $5,2$ (s, 2H, -N_3-CH_2-O-), $3,8$ (m, 3H, -O-CH_3), $2,0$ (d, 2H, -CH_3), $1,6$ (s, 6H, -CH_3).

5.8.8 Polystyrene-PIA via Click

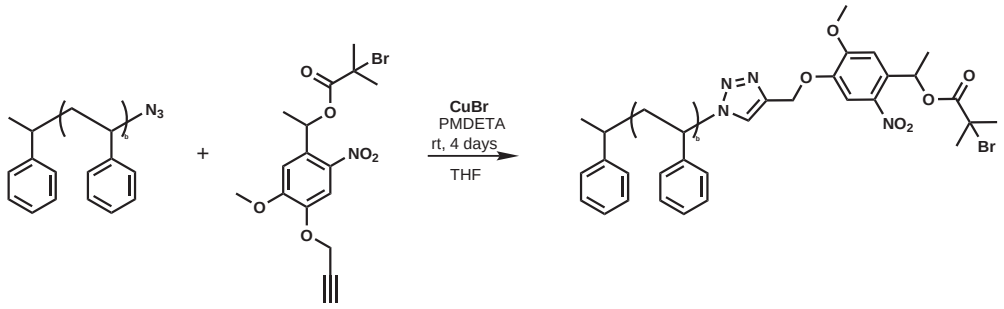

To a degased mixture of 5,126 g polystyrene azide (PS-N3, M_W 15,5 KD, PDI 1,2) and 0,302 g PIA (7,5 mmol) 10 ml dry THF are added. The mixture is degased for 15 minutes, and 25 ml of a stock solution (4,7 mg/ml cupper(I)bromide and 8,8 mg PMDETA/ml in oxygen free THF) are added. The reaction flask is sealed and covered with alumina foil. The reaction mixture is allowed to stir at room temperature for 4 days. For workup, the polymer is precipitated in 1,5 L methanol, dried under high vacuum, redissolved in 50 ml DMF, precipitated in 1,5 methanol and dried under vacuum again.

Yield: 3,9 g $\sim$ 78 %

^{1}H-NMR (250 MHz, DCM): $\delta/ppm = 6,1-7,1$ (band, 5H, arom. -H), $1,0-2,0$ (band, 3H, (aliph. -H).

5.8.9 PIA-pHEMA

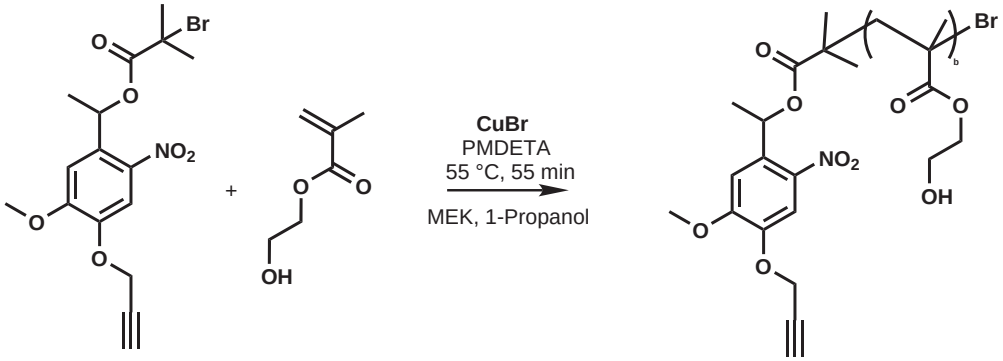

306 mg PIA (7,62 mmol) are degased in a schlenk flask. 0,5 ml anisole and HEMA are added. The reaction mixture is degased for 30 minutes, 6 g of the catalyst stock solution (preparation described below) are added and the reaction is stirred at 55 °C. After 55 minutes, the reaction is stopped by exposing the mixture to air and immersing schlenk tube in liquid nitrogen.

The catalyst stock solution is prepared as follows: to a degased amount of 16 ml dry anisole are added 380 mg PMDETA and 168 mg Cu(I)Br.

5.8.10 pS-PIA-b-pHEMA

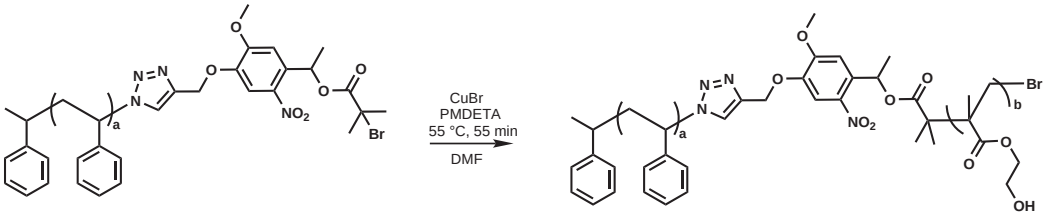

0,392 g pS-PIA macroinitiator are degased in a schlenk flask. 0,5 ml anisole and HEMA are added. The reaction mixture is degased for 30 minutes,6 g of the catalyst stock solution (preparation described in 5.8.9) are added and the reaction is stirred at 55 ℃. After 55 minutes, the reaction is stopped by exposing the mixture to air and immersing Schlenk tube in liquid nitrogen. Purification with column chromatography and precipitation in various solvents failed: The product could not be precipitated and was lost during the workup procedure. However, GPC measurements were done from samples of the reaction mixture.

6 Evaluation of pHEMA hydrogels for gDNA isolation from blood with QPCR

6.1 Introduction

In chapter 3 and chapter 4 it was reported that pHEMA based hydrogel films produced through photocrosslinking of previously synthesized copolymer precursors showed sufficient mechanical stability and adsorptive properties in order to be used as an analytical matrix for surface binding of biomolecules. Apart from the variation of crosslinking density, the investigated hydrogel could be chemically adjusted to the problem e.g. by attachment of specific functional groups which were capable to bind to streptavidin analytes. This chapter will evaluate the practical use of photocrosslinked pHEMA based hydrogel films for the isolation of genomic DNA from human whole blood by means of high-throughput quantitative polymeraze chain reaction (QPCR) and identify suitable functional groups and parameters for this process.

In order to be able to use the parallel processing of the QPCR instruments, the pHEMA hydrogel film that was deployed on planar surfaces has to be transferred to the geometry of commercially available 8-strip PCR containers made from polypropylene.

6.2 Strategies for the isolation of gDNA from human blood

6.2.1 Finding and testing of suitable pHEMA-based biomaterials

There are major obstacles to overcome when accessing segments of DNA for PCR amplification. The often formed view of DNA as a naked train track stretching out to infinity (on a molecular scale) is not realistic. In practice, DNA is wrapped up tightly like a ball of anionic knitting wool, at the very least being surrounded by some cationic species to enable it to hold together. As shown in Fig. 6.1, much of this role in cell nuclei is provided by histone proteins. In addition, metal salts and other small molecules such as polyamines contribute significantly to this task [228]. Especially in the case of lysed whole blood these biological components are going to be present next to the DNA fragments. As such, the analyte in question comes with many other molecules of various sizes and charge, making specific DNA targeting prior to adsorption a difficult task.

The quantitative polymerase chain reaction (QPCR) - as introduced in chapter 2.9 - is one of the most powerful and sensitive DNA analysis techniques available. It is used extensively in industrial, academic and diagnostic labs. There is no need to run a gel [14], and the data is quantified by the instrument as the PCR reaction progresses [229]. The detection is more accurate because readings are taken during exponential phases of the PCR reaction. As such, there is no bias from limiting reagent concentrations. The closed format of the PCR tubes reduces the risk of contamination while giving the possibility to deploy and test larger quantities of samples. At last, it gives the possibility to optimize method parameters in a quick manner - e.g. the choice of lysis chemicals or pHEMA matrix modifications [229].

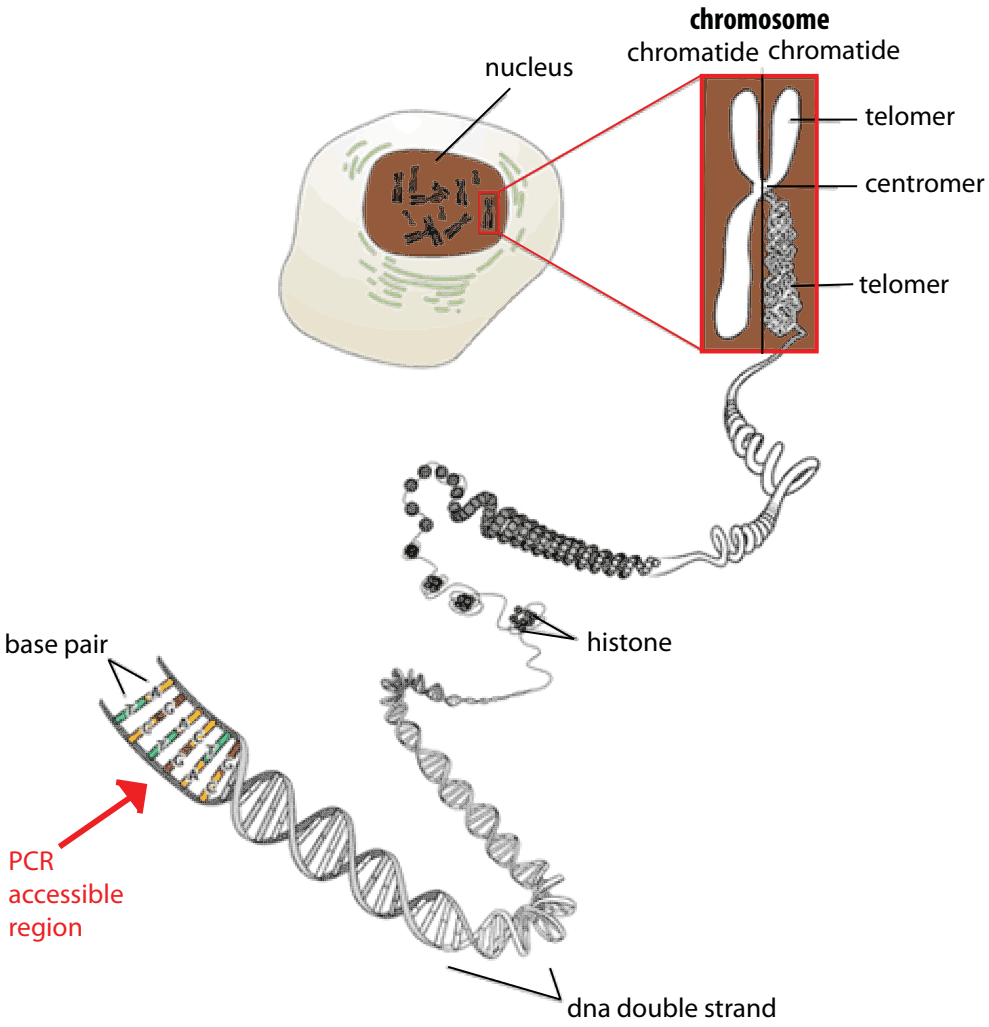

Fig. 6.1 Schematic overview of DNA storage in the human organism: Each cell with a nucleus contains all of the organism's genetic instructions stored in the form of DNA, which itself is tightly wound and packaged in a set of chromosomes. Chromosomes are a combination of DNA and proteins - e.g. histones - that make up the contents of the nucleus of a cell. As a result, the DNA is packaged into a structure that is strengthened to avoid damage. Also, it is smaller in volume and thus easier to be stored in the respective cell. In order to access the DNA with a PCR, the chromosome with its double helix needs to be converted into a much simpler, linear structure with minimal steric hindrances for the PCR enzymes [142, 229].

6.2.2 Selection of DNA-"fishing" groups

In order to obtain a DNA adsorptive surface, it is important to consider where and how the functional moieties on the polymer surface bind to DNA. The process of molecular recognition often involves conformational adjustments on the part of the interacting species. In that way, the DNA helix may end up considerably distorted. As shown in figures 6.2(a) and 6.2(b), three fundamentally different modes of DNA binding to external can be identified: non-specific external association with the negatively charged phosphate backbone, (major and minor) groove binding, and intercalation through interaction with the electron donor groups of the DNA bases [230].

There exist numerous organic and inorganic molecules that are capable of interact with DNA in a specific manner: So far immobilizing DNA has been attained, in the most cases, by chemical modification of DNA with a particular functional group such as thiol [231], amine [232], and biotin [233] to make the DNA surface more reactive. Even the recently reported methods, the use of electropolymerizable pyrrole-DNA conjugate [234] or the postpolymerization grafting method [235] also requires chemical derivatizations of DNA. Other publications report the binding of DNA to chemical agent like fucomarine derivatives [236] or platinum [237] based materials.

However, the adsorption process of the DNA to the hydrogel surface - and any chemical reactions connected to this process - have to be reversible in order for the PCR reaction to proceed smoothly. Another important matter is the fact that there is no way to selectively modify gDNA in human whole blood. This leaves the functionalization of the adsorptive polymer with DNA-"fishing" groups the remaining alternative. As such the following strategy for non-directed interactions of a modified polymer surface with DNA strands is deemed suitable: A pHEMA hydrogel bearing DNA binding side groups that are introduced through adding functional HEMA derivatives to the polymerization mix-

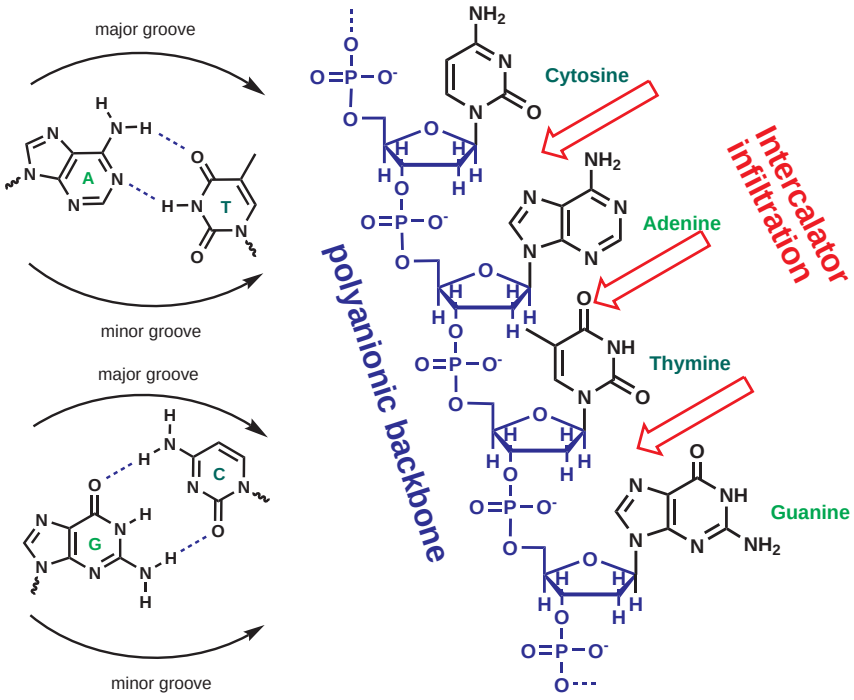

(a) DNA grooves (b) anionic/intercalation sites

Fig. 6.2 **(a)** Complementary adenine-thymine and guanine-cytosine base pairs showing the minor and major DNA grooves. The wiggly bonds indicate the links to the sugar backbone. **(b)** The four DNA bases showing their connectivity to the anionic phosphate-sugar backbone in DNA [230, 142]. While polymer bound DNA intercalators are thought to move in between the nucleobases, charge bearing functional groups are interacting with the polyanion backbone of DNA.

ture. The functional side groups are of hydrophobic/hydrophilic/charge bearing nature and are chosen from commercially available HEMA derivatives. Monomers bearing more complex side groups - such as DNA intercalators - are synthesized.

In order to be able to adjust hydrophilic properties of the polymer surface and it's surface charges, a variety of monomers - among them of derivatives of HEMA with functional side groups attached to the ethoxy moiety - have been obtained commercially. As such, methoxy terminated HEMA, 2-phenoxyethyl methacrylate, methacrylic acid, 2-(methacryloyloxy)-N,N,N-trimethylethanaminium, heptan-3-yl methacrylate, 2-(phosphonooxy)ethyl methacrylate, 2-(sulfooxy)ethyl methacrylate, diethyl vinyl phosphate, and derivatives of poly(ethylene glycol) methacrylates have been chosen to cover both negatively charged, positively charged, neutral hydrophobic chain ends. Since the olefinic moiety is very closely related to HEMA, homogeneous copolymerization behaviour can be expected, making it possible to adjust the copolymer ratios to a high degree.

6.3 Design, synthesis and characterization of monomers with DNA intercalating end groups

6.3.1 Introduction to DNA intercalators

DNA intercalation was defined by Mainwaring et al. as the sandwiching of a molecule between two adjacent pairs of bases in the DNA double helix [238]. Intercalating ligands are characterised by the possession of an extended electron deficient planar aromatic ring system. Upon binding, they extend and unwind the deoxyribose - phosphate backbone and are stabilised by π - π stacking interactions with the planar aromatic bases. A bound

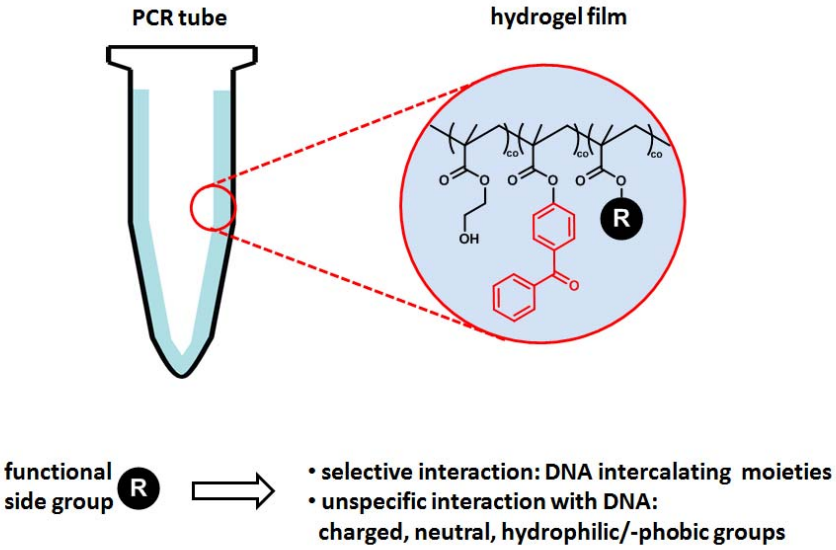

Fig. 6.3 PCR tubes coated with functionalized pHEMA based hydrogel films with a thickness of 2 to 10 μm. The functional side groups are incorporated into the hydrogel in the precursor polymerization with a relative amount of 10%.

intercalator lies in a plane perpendicular to the helix axis such that the perpendicularity of the base pairs to the helix is not significantly altered. Hence an intercalator molecule has to be either planar or have an extended planar component which can slide between DNA base pairs [239].

6.3.2 Design of the DNA intercalating monomer

There are three possibilities of integrating the intercalating agents into the the hydrogel: The first is the implementation of the moiety into the polymerization process, exposing the molecules to the conditions of free radical polymerization and photocrosslinking, the second features the postsynthetic functionalization of the hydrogel precursors and the third method is the modification of surface attached hydrogel films after their deposition and crosslinking. While the latter option avoids the irradiation of the introduced

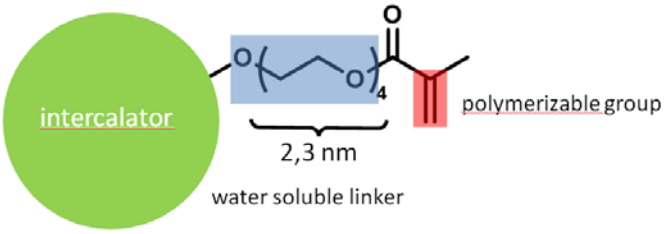

Fig. 6.4 Schematic picture of the DNA intercalating monomer with the polymerizable methacrylic acid ester derivative, the hydrophilic linker and the DNA binding polyaromatic moiety.

functional groups with UV light, it introduces new complications. First, it it requires a very high reaction yield regarding the attachment of the functionalizing species to the crosslinked polymer film. Secondly, statistical and steric factors and the hindrance of the tube geometry in respect to more complex reaction designs make this method less preferable. Since literature did not indicate any degradation of the intercalating end groups under free radical polymerization conditions, it was chosen to design a set of suitable monomers for copolymerization with HEMA and MABP. In view of the fact that the film formation features the irradiation of the hydrogel precursor with 365 nm UV light it is necessary to investigate possible occurrence of photobleaching processes that could render the intercalating moieties useless.

As shown in Fig. 6.4, the functionalized molecule is built from the following components: A polymerizable part, an intercalating group, and a linker chain that allows the intercalating group to move more freely from the hydrogel backbone. The effective double helix diameter grows rapidly with decreasing ionic strength and can be several times higher than the geometric one. This can be be attributed to the fact that DNA, unlike an uncharged polymer chain, is a highly charged polyelectrolyte capable of electrostatic repulsions that can make the effective diameter much greater than the geometrical diameter of 2 nm. Thus, literature reports the DNA diameter in a range from 2 to 5 nm, depending on solvent, ionic strength and temperature [240, 241, 242].

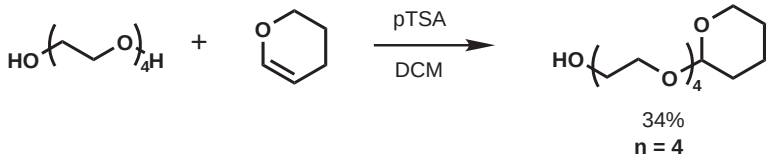

Fig. 6.5 Synthesis of protected ethyleneglycol linkers.

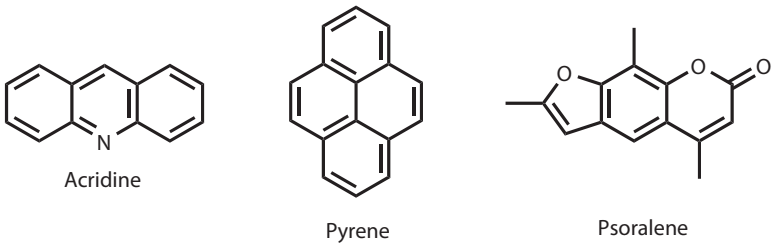

Fig. 6.6 Overview of molecules chosen to function as DNA intercalating moiety.

The first choice for the polymerizable group would be a methacrilic acid ester, resembling HEMA in polarizability and electron density. An aromatic molecule would serve as DNA intercalating fragment. A tetraethylene glycol (TEG) chain is considered to be the best choice from the perspective of hydrophilicity because it greatly enhances the solubility of uncharged polyaromatic compounds. The length of the TEG based linker is difficult to choose - it should be long enough to allow the intercalating moiety to intrude into the DNA helix and take a position with maximum π - π interactions while not being a hindrance to the infiltration by itself.

6.3.3 Choice of DNA intercalator

There is a vast number of DNA intercalating agents to choose from. Apart from the known properties in literature and ease of handling, other important factors are the spectrum of chemical reactions that could be performed on the molecule and the range of conditions the intercalator could handle without suffering from degeneration.

Acridine and ethidium bromide are primary choice of DNA intercalators because of their

well known DNA intercalating properties [243, 244]. Since ethidiumbromide is extremely cancerogenic and difficult to handle, pyrene [245, 246] is chosen as a comparative example instead.

Another well known class of molecules are the linear isomers of furocoumarin family, better known as psoralenes. After formation of a noncovalent complex with DNA through intercalation of the psoralene between adjacent base pairs, irradiation with UV light (320-400 nm) triggers psoralenes to undergo a photoaddition reaction to a pyrimidine base. This results in a covalently bonded monoadduct [247]. There are currently two psoralen derivatives in wide use in the scientific community. Out of these two, trioxsalene (4,5,8-trimethylpsoralene) is chosen as intercalating agent.

While the chosen DNA intercalators are well known in literature, methacrylic monomers with a TEG chain have not been reported at the time when the experiments were conducted. In order to prevent the creation of bisintercalators, one of the hydroxyle groups of the TEG linker has to be reacted with a protective group. Since the reaction is carried out under basic conditions, the THP ether protective group with its lability to acidic environments is being used. The protective group can be removed on the spot during the workup of the reaction exposure to acidic aquous solution e.g. in the separating funnel. Another approach would be the use of TEG in excess e.g. three times as much as the used reaction solvent. Both approaches require thorough purification with column chromatography and liquid-liquid extractions.

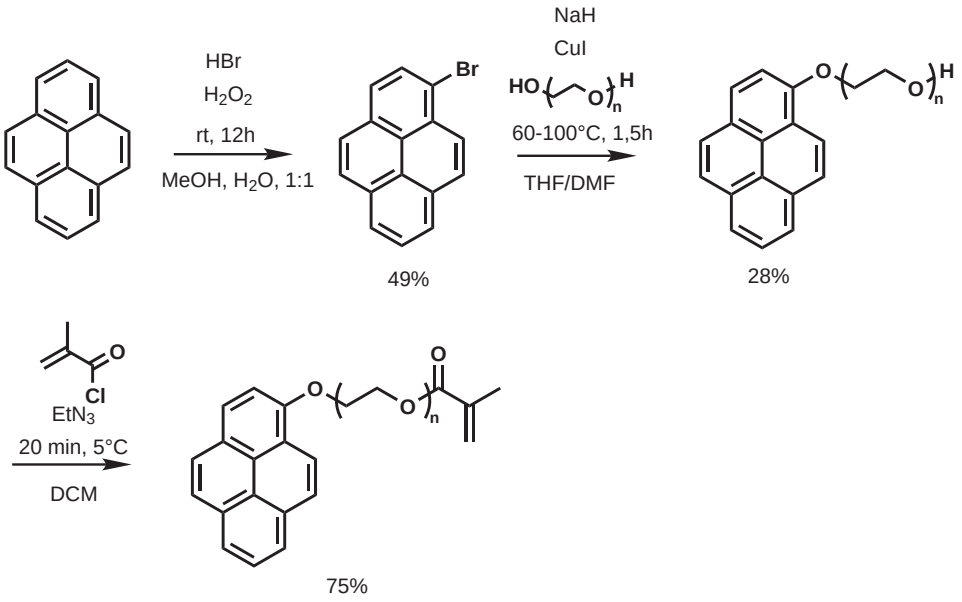

Fig. 6.7 Synthesis route for the pyrene monomer derivative with both TEG and EG linker chain.

6.3.4 Synthesis and characterization of DNA intercalating monomers

Pyrene

In a first step, the ethyleneglycol linker is attached to the 1-bromo-pyrene ring by a nucleophilic substitution reaction of brom with the deprotonated oxygen group of the linker chain [248, 249]. The deprotection of the THP protective group is done *in situ*. After thorough purification, the reactive methacrylic monomer group is attached to the hydroxy terminated linker chain through a transesterification reaction using methacrilic ester chloride as reactant.

The ^{1}H-NMR spectrum (Fig. 6.8) of the polymerizable intercalator on pyrene basis shows three signal groups in the aromatic region, two signals in the olefinic region, and 6 signal groups in the aliphatic region. The total signal intensity of the aromatic region is 9 protons, split into three distinct signal groups: the doublets at $8,4$ ppm and $7,5$

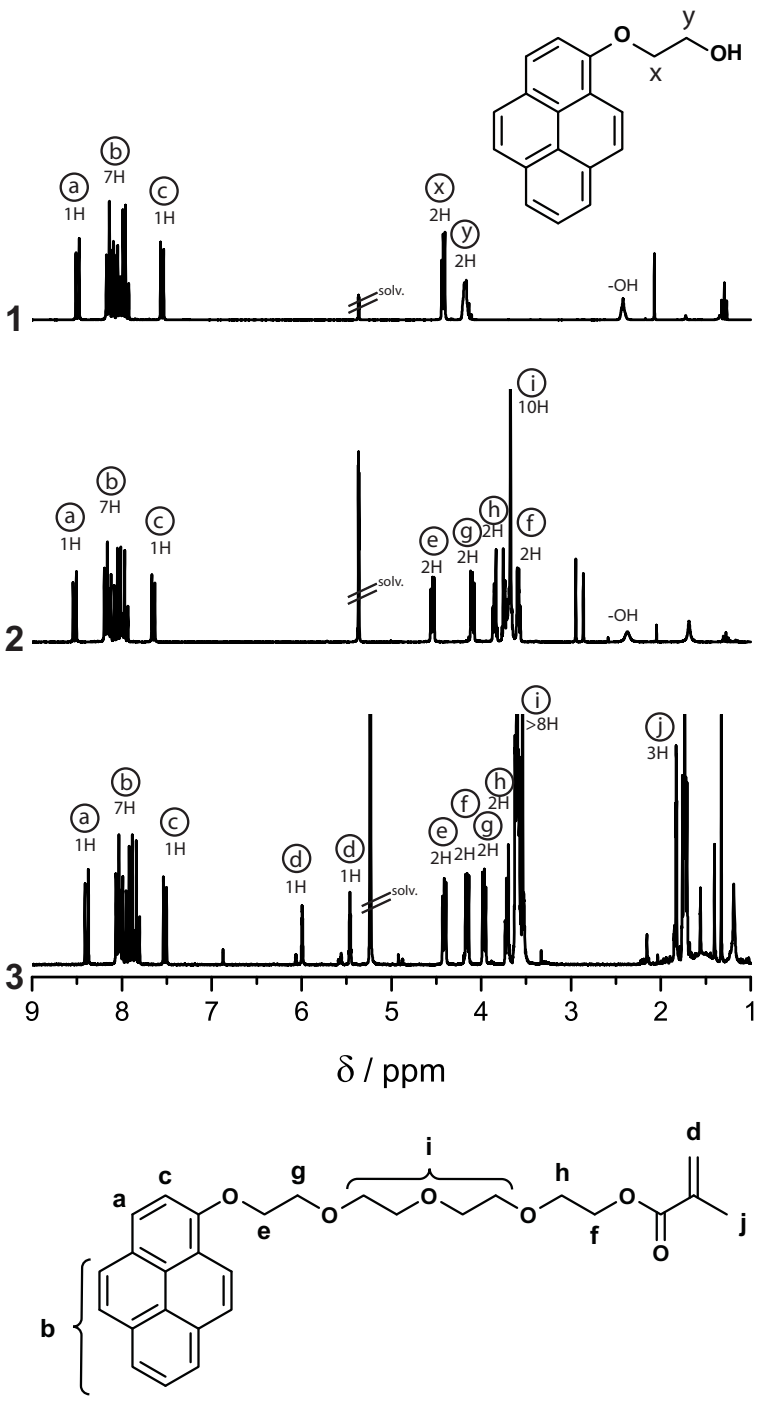

Fig. 6.8 250 MHz ^{1}H-NMR spectra in d-DCM: pyrene with **(1)** ethane-1, 2-diol linker, **(2)** TEG linker and **(3)** methacrylate terminated TEG linker attached to 1-position of the ring.

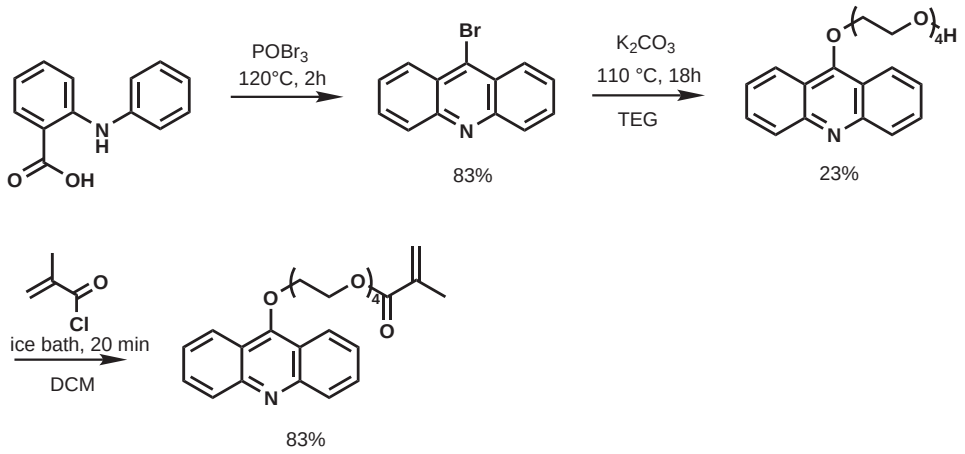

Fig. 6.9 Synthetic route for the acridine monomer derivative with TEG linker chain.

ppm belong to the protons in 3 and 2 position, while the remaining five protons are showing in multiple signals at 8 ppm. The two singlets with the intensity of one proton each at 6,0 and 5,4 ppm can be attributed to the polymerizable olefine group in the methacrylic ester. Eight of the sixteen hydrogen atoms of the TEG linker are split into triplet signals with the intensity of two protons each. The signals that originate from the carbon atoms next to the intercalator and polymerizable group are shifted to lower field at 4,4 and 4,25 ppm, while the second nearest carbon atoms from the intercalator and polymerizable group can be allocated at 3,9 and 3,7 ppm. The singlet signal at 1,8 ppm can be allocated to the methyl group in the methacrylic ester moiety. The remaining eight hydrogen atoms should be represented by a multiplet at 3,6 ppm - this multiplet, however, has a higher than expected integral which can be traced to impurities that could not be removed during the workup of the TAG linker and the polymerizable group attachment.

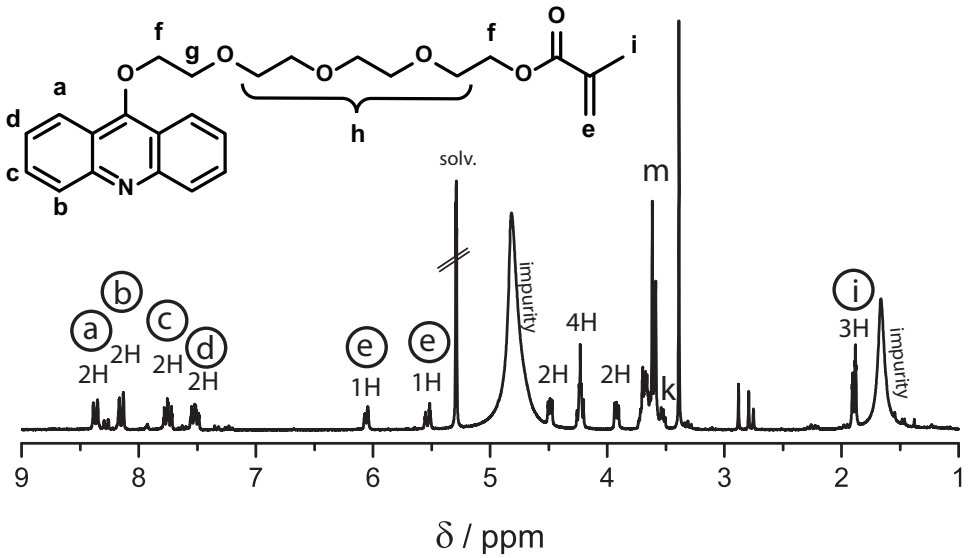

Fig. 6.10 250 MHz ^{1}H-NMR spectrum in deuterated DCM of polymerizable acridine intercalator group with TEG chain linker.

Acridine

N-phenylanthranilic acid is used as starting material for the synthesis of acridine terminated monomer. In a first step, 9-bromo-acridine is obtained through a cyclization reaction involving phosphortrioxybromide as solvent and reactant [250]. Next, the tetraethyleneglycol chain is attached to the aromatic ring through a nucleophilic substitution reaction using potassium carbonate as base. The TEG linker is used in large excess in order to prevent the creation of bisintercalators. After thorough purification with multiple chromatography columns with a solvent gradient, the polymerizable end group is then attached as previously described to the terminal hydroxyle group.

In the ^{1}H-NMR spectrum four signal groups of two protons each can be found in the aromatic region. The groups signal with the highest chemical shift at $8,7$ ppm and $8,4$ ppm are doublets which can be allocated to the chemical equivalent protons at positions 4 and 5 and 1 and 8 on the aromatic ring. The triplets at $7,75$ ppm and $7,5$ ppm can be assigned to the corresponding hydrogen atom at ring positions 2 and 7 and ring positions 3 and 6 respectively. The two olefinic protons of the methacrylate groups can be found as singlets at $6,2$ ppm and $5,6$ ppm. As with the pyrene intercalator monomner, most of the hydrogen atoms bound to the aliphatic linker chain are overlapping in a multiplet at $3,6$ ppm. Unfortunaly, residual impurities e.g. TEG make it very difficult to obtain a clear spectrum of the material. Simulations of ^{1}H-NMR spectra show that the integral corresponding to four protons could be connected to the carbon atoms f in the molecule. This remains, however, a very vague speculation. While the three aliphatic protons in the methacrylic group are responsible for the singlet at $1,8$ ppm, the signal k and m can not be clearly identified and show too large integrals. While FD mass spectroscopy measurement show the formation of product, it could not be purified sufficiently to characterize it with ^{1}H-NMR spectroscopy.

Trioxsalene

The trioxsalene monomer derivative is synthesized starting from 4,5,8-trimethylpsoralen [251, 252, 253]. In a first step, a bromomethyl group is added at 4-position of the trioxsalene ring with the addition of bromomethylmethylether in glacial acetic acid. The procedure in literature used chloromethylmethylether, which is a substance with high cancerogenic properties that is therefore replaced by its bromo derivative. The TEG linker is attached in a etherification reaction, which is done through heating the brominated psoralene derivative in TEG until all reactant is solved. Chloromethacrylicacid is reacted with the terminal hydroxyle group of the TEG chain in a final step.

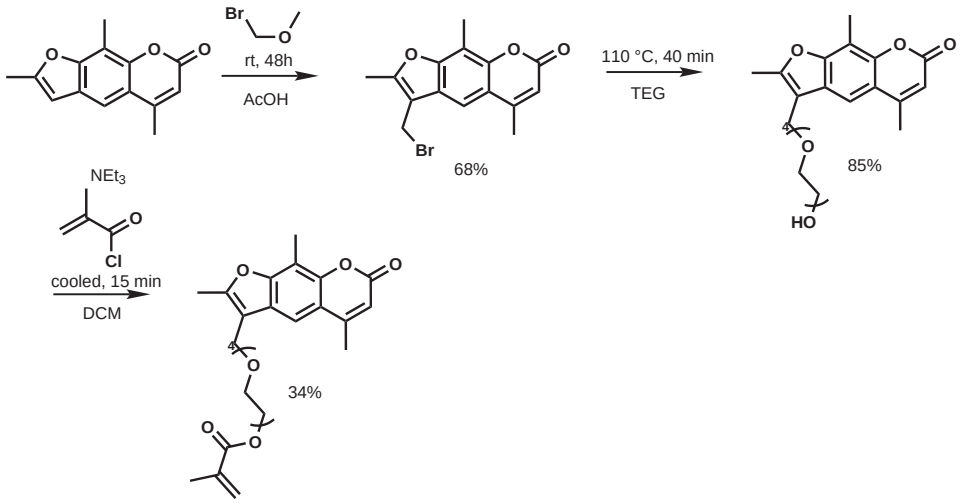

Fig. 6.11 Synthetic route for the trioxsalene monomer derivative with TEG linker chain.

The ^{1}H-NMR spectrum of the polymerizable trioxsalene derivative shows one singlet in the aromatic region at $7,65$ ppm that can be allocated to the proton at the 5-position of the coumarine ring. Three olefinic singlets can be found at $6,4$ ppm, $6,1$ ppm and $5,6$ ppm. The first represents the ethylene proton at 6 - position of the coumarine ring while the latter two can be attributes to the ethylene group in the methacrylic ester moiety. In the aliphatic region of the spectrum, the two protons of the oxymethyl group in 3 position of the trioxsalene structure show in a singlet at $4,65$ ppm. From the TEG chain, the hydrogens of the two carbon atoms next to the methacrylic ester group are allocated in triplet signals $4,3$ ppm and $3,7$ ppm with an intensity of 2 protons each, with the signal at lower field being attributed to the carbon atom next to the ester oxygen group. Unfortunatly, this signal shows a higher integral than expected in theory. This can be traced to residual impurities from the addition of the TEG and methacrylic moieties. The remaining 12 protons of the linker can be found in a multiplet at $3,6$ ppm.

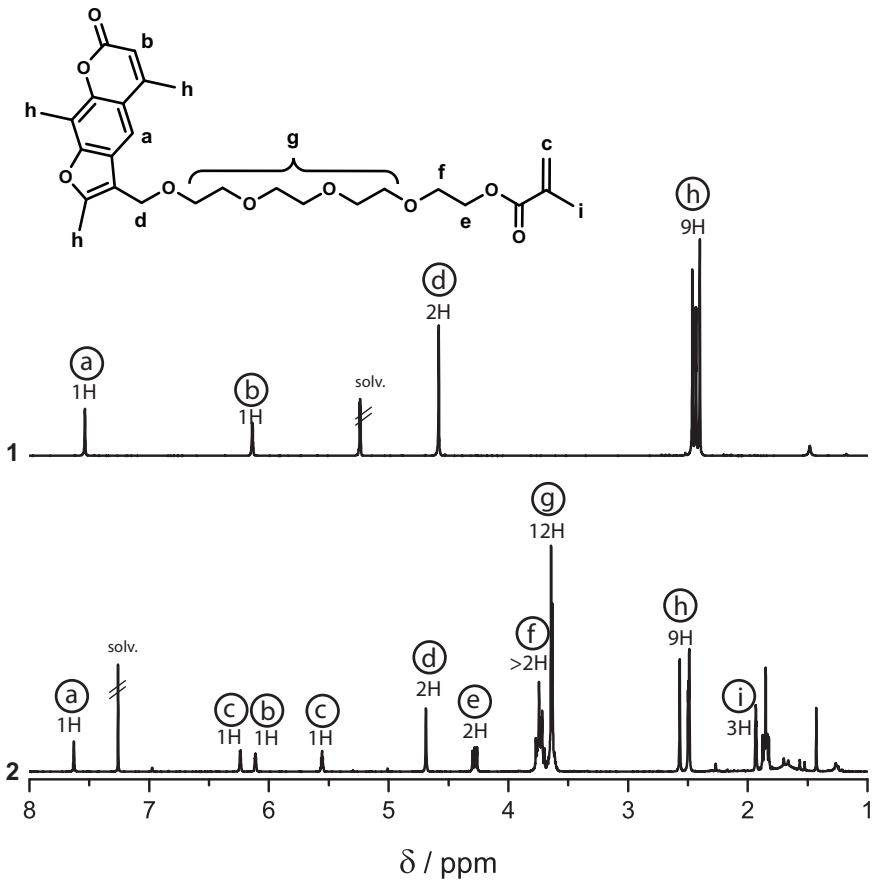

Fig. 6.12 250 MHz ^{1}H-NMR spectra of the **(1)** trioxsalene prior to TEG attachment in d-DCM and the **(2)** polymerizable trioxsalene intercalator group with TEG chain linker in $CDCl_3$.

6.3.5 Photodegradation behaviour of intercalator monomers

Figure 6.13(a) shows the UV/vis absorption spectra of the intercalators acridine, pyrene, trioxsalene and the used photocrosslinker MABP. Pyrene shows the characteristic absorption bands at 330 and 270 nm. Acridine shows a broad absorption from 300 to 405 nm, and a strong absorption band starting below 275 nm. Trioxsalene covers the entire range from 240 to 375 nm with a absorption band, making it the most likely candidate for photolysis.

Since all of the used intercalators show strong absorbance bands near the used photocrosslinking wavelength of 365 nm, it is important to check their photodegradation behaviour at this particular wavelength. Figure 6.13(b) shows a plot of the concentration dependence of intercalators at a relative absorption maximum. All three intercalators show a linear correlation between concentration in the range of 10^{-6} to 10^{-4} mol L^{-1}. When taking an intercalator modified hydrogel film with a thickness of 200 nm and a random distribution of intercalator groups in the film volume into account, the number of intercalator groups would fall in the range of linear absorption of the intercalators and thus could be used for comparative photolysis studies.

To examine the photodegradation process of the intercalator groups next to the hydrogel, the material is subjected to the conditions in the crosslinking process: UV light irradiation at a wavelength of 365 nm under oxygen atmosphere. The intercalators are covalently bound to the hydrogel and thus embedded into a matrix of photoactive benzophenone and aldehyde groups. This matrix produces its own signal regarding UV/vis absorption. In order to be able to evaluate the photodegeneration process in a comparative and quantitative manner, it is thus important to separate the underlying background signal from the intercalator absorption bands of the material. This can be done by making comparative measurements with a material but with nearly identical molecular

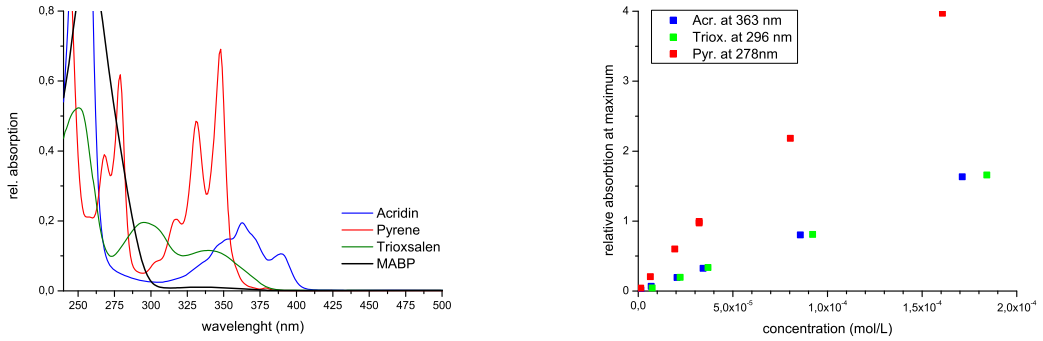

(a) UV/vis absorption spectra

(b) molar absorption coefficients

Fig. 6.13 **(a)** Intercalator and MABP monomer spectra. **(b)** Dependence of absorption maxima of the intercalators from their concentration in solution

composition, deposition process and film thickness but without intercalator groups. The only difference between the material used for the background measurements and the intercalator functionalized hydrogel would be the lack of intercalator groups. That way, a recorded background can be subtracted from the spectrum of the intercalator hydrogel in investigation, resulting in pure intercalator bands:

$$\Psi_{(pIntercal)} = \Psi_{(pHEMA-co-pMABP-co-pIntercal)} - \Psi_{(pHEMA-co-pMABP)} \tag{6.1}$$

The correction of the spectrum is displayed in figure 6.14(a) in the example of the pyrene containing hydrogel. The graph shows the absorption spectra of MABP containing hydrogel with and without intercalator before any irradiation with UV light. The absorption spectrum of the intercalator functionalized hydrogel features relatively stronger absorption bands in the region of 250-270 nm, while retaining the characteristic band structure seen in the measurement of pure intercalator in solution. After substracting the hydrogel spectrum containing the large absorption band at 254 nm from the original spectrum,

the intensity values of the bands around 330 and 350 nm are the same, while the correct proportions of the characteristic absorption bands of pyrene can be found around 270 nm.

The difference spectras of pyrene functionalized hydrogel after exposure of the material to UV light for a timespan of 20, 40 and 60 minutes are shown in figure 6.14(b). Comparing the absorption spectrum of material not exposed to UV irradiation to spectrum of the irradiated material, a loss in intensity of 5% to 10% can be found in all absorption bands after the exposure of 20 and 40 minutes. However, the band structure is conserved, leading to the conclusion that some of the intercalator groups should still be intact after irradiation.

In the case of acridine, displayed in figure 6.14(c), the major absorption band at 260 nm is much broader than in the solution measured in solution. After the irradiation with UV light for 20 minutes, a 10% decrease in intensity can be observed in the absorption spectrum. After 40 and 60 minutes of total exposure, the absorption band has lost 20% and 30% of its original intensity. Also, a slight shift of the band towards loner wavelength can be observed. This leads to the assumption that the acridine intercalator is exposed to strong photobleaching. In the time frame of a shortened photocrosslinking procedure it is questionable whether the bleaching process is of acceptable magnitude. Also, it might be noted that the intercalator groups bound to the film surface might be the first to undergo photodegradation processes.

The trioxsalene derivative intercalator shows much stronger lability towards 365 nm irradiation than pyrene or acridine. While the characteristic band structure of the molecule is very well defined in the measurement of uncrosslinked material, figure 6.14(d) shows an almost complete loss of band intensity after irradiation of 20 minutes. A shift of the band at 250 nm towards lower wavelengths can be observed that corresponds to the loss

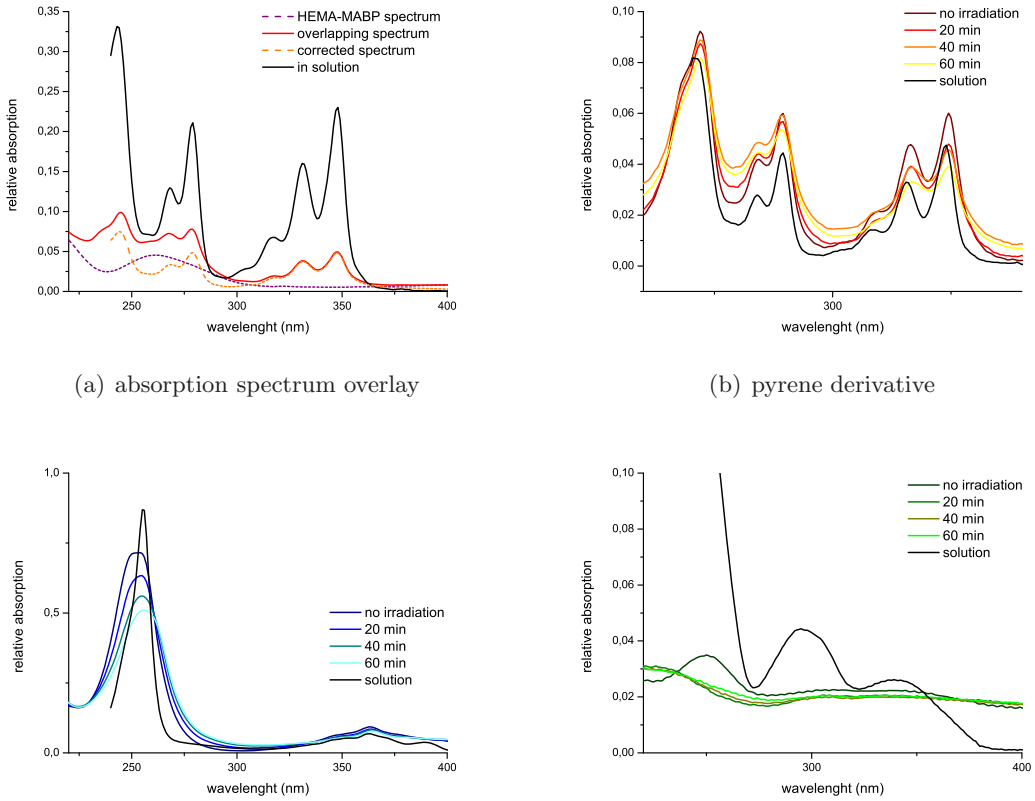

(a) absorption spectrum overlay

(b) pyrene derivative

(c) acridine derivative

(d) trioxsalene derivative

Fig. 6.14 **(a)** UV/vis spectrum with *polymer film background* correction on the example of pHEMA-co-MABP-co-PyrEMA. The black line shows the spectrum of pyrene is solution and the orange spectrum shows the absorption caused by the pyrene groups inside the hydrogel **(b),(c) and (d)** shows the photodegradation behaviour of pyrene, acridine and trioxsalene under irradiation with UV - light of 365 nm under oxygen atmosphere.

of absorption band intensity. The disappearance of the original band structure of the spectrum suggests a complete photolysis of all intercalator molecules.

In order to reduce the amount of destroyed intercalator groups during the crosslinking process several options should be discussed. Changing the wavelength out of the boundary of the intercalator absorption bands is not possible, since the only available other light source is 254 nm, a wavelength very well in the middle of the absorption maxima of all intercalators that goes along with much higher energy. This leaves only with two viable options: First, the increase of total number of intercalator groups, and second, the reduction of the irradiation time to a minimum. The amount of intercalators in the polymer can be easily increased to 20%, with the consequence of altering the surface properties of the hydrogel to a more hydrophobic nature. The crosslinking time, however, can only be reduced to a time frame of 5 to 15 minutes without the risk of losing film integrity and film attachment to the substrate. The fact that most of the photobleaching damage is expected to happen at first at the surface of the film where the exposure to DNA is supposed to take place makes the synthesized intercalators not very useful with the concept of film fabrication by photocrosslinking.

6.4 Synthesis of functionalized hydrogel precursors

The photocrosslinkable hydrogel precursors with side groups for DNA interaction were synthesized by free radical polymerization and purified by repeated precipitation in cold ether as described in chapter 3. Since most monomers are based on HEMA, it is expected that the proportions of the monomers in the feed in the polymerization will be matching the polymer composition. Table 6.1 shows the types of samples produced, including hydrophilic end groups with positive charges (c), negative charges (a,b,e), and neutral charge with hydrophilic and hydrophobic end groups (d,f,g,h), and lastly, end groups

Table 6.1 functional groups added to the pHEMA-co-pMABP polymers

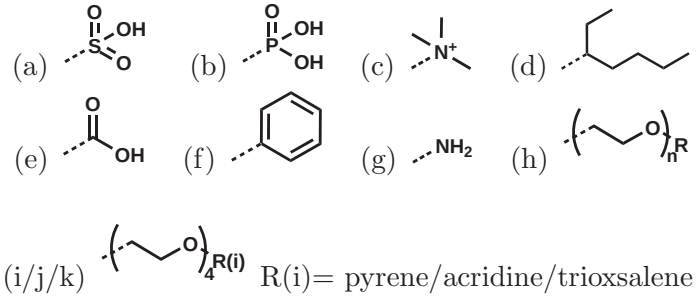

containing the DNA intercalators (i,j,k). Since phosphonic acid ester groups are expected to be cleaved at the conditions of the DNA isolation procedure they are written down in the form of phosphonic acid.

6.5 Deposition and characterization of hydrogel films on PCR tubes

Two methods for the deposition of hydrogel films on the non-planar PCR tube surface have been developed and tested under RT-PCR conditions: The *stamp method* yields thicker films that cover the entire interior of the PCR tube, while *adsorptive deposition* gives only partial coverage. Both methods give hydrogel films that are stable under PCR conditions.

6.5.1 Production of 10 μm thick films with the stamp method

A PDMS stamp created from imprinting of the PCR tube inside surface was dipped in a 10% solution of the hydrogel precursors and then used to cover the inside of the tubes wells (Fig. 6.16a). The protocol is described in detail in the experimental section.

(a) deposition technique

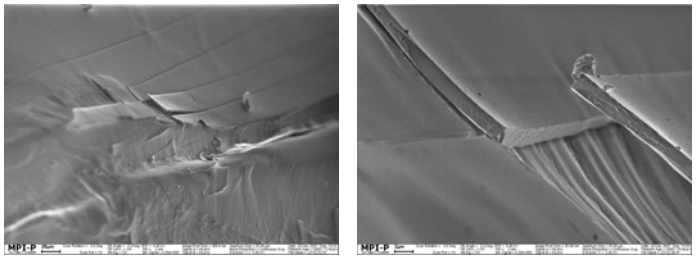

(b) after deposition (c) after deposition

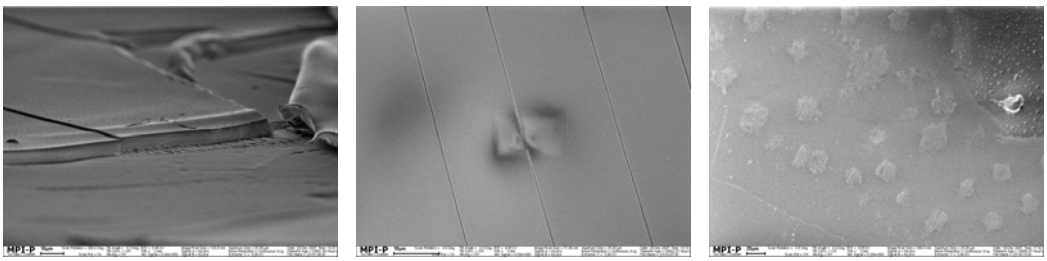

(d) lysis (e) washing (f) PCR

Fig. 6.15 **Top row:** Stamp for coating the interior of PP PCR tubes on a *8-strip* with hydrogel precursor materials. **Middle & bottom rows:** SEM pictures from PP PCR Tubes coated with crosslinked pHEMA hydrogel using the stamp method (see 6.8.13) after performing blood lysis, washing and PCR protocols with all the chemicals but blood. The cracks in the films are coming from the cutting of the PCR tube prior to SEM imaging. Note that all samples have been dried before the SEM measurement.

Fig. 6.16(b/c) shows SEM images of the films deposited on the PCR tubes. As can be shown with SEM and white light confocal microscopy, the entire inner tube surface is covered with hydrogel material with a film thickness ranging from 2 to 10 μm. The cracks in the film are coming from sample preparation prior to SEM imaging. In order to examine the film stability, the crosslinked hydrogel films in the PCR tube are exposed to the chemicals - with the exception of blood - and conditions used in the DNA amplification process. The SEM images recorded after the respective steps of the DNA amplification protocol, as shown in Fig. 6.16(d/e/f), indicate that the films remain intact and are still bound to the PCR tube surface. The decrease in image quality can be explained with the presence of salts and other residual species after exposure of the films to washing buffers and PCR chemicals.

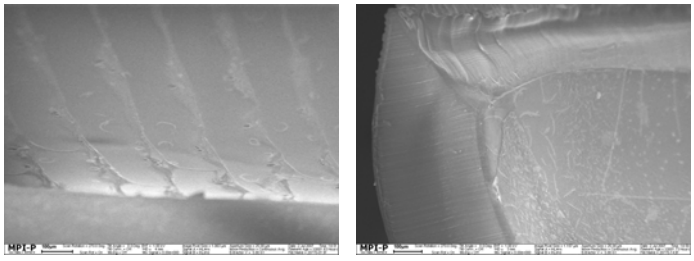

(a) after deposition (b) after deposition

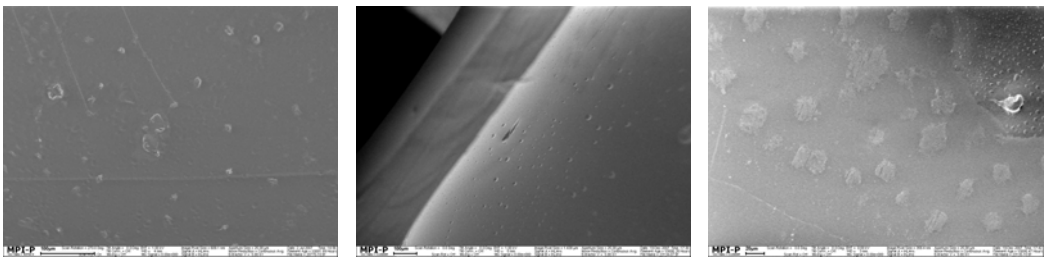

(c) lysis (d) washing (e) PCR

Fig. 6.16 SEM pictures show PP PCR Tubes with pHEMA hydrogel deposited material by the adsorption method (see 6.8.14) after performing blood lysis, washing and PCR protocols with all the chemicals but blood.

6.5.2 Production of thin irregular films by adsorptive deposition

A much more simple method to deposit hydrogel on the PCR tube surface is to expose it to a solution of precursor material for a limited amount of time. As can be seen on figures 6.16(a) and 6.16(b), drying and photocrosslinking of the residual material gives only a partial coverage of the PCR tube surface: while the bottom part of the PCR tube is covered by a film similar to the one obtained by the *stamp method*, the hydrogel material in higher segment of the PCR well forms lamellar structures. As with the films produced by the stamp method, SEM imaging indicates that most of the deposited material remains intact under PCR conditions and are still bound to the PCR tube surface. However, it can not be said for certain whether the thinner films may loose some material during the lysis and PCR steps.

6.6 Evaluation of hydrogel films regarding DNA adsorption from blood with high-throughput QPCR

In order to make a first screening regarding a suitable functional group for DNA isolation, a series of tests are carried out on materials with the composition of about 89 % HEMA backbone, 1% benzophenone groups and 10% functional groups. Suprisingly, the samples produced by *adsorptive deposition* of hydrogel material proved to be reliable in terms of analytic results, while the films made by the *stamp method* often showed disturbances of the PCR during the DNA amplification cycles. As optimization in regard to crosslinking time and deposition technique could not solve the problem, it is speculated that the nature of the disturbance can be traced to the detachment of small fragments from the hydrogel material and their subsequent role in the inhibition the PCR reaction. To avoid this problem materials were deposited by the adsorptive method in order to characterize

Table 6.2 Screening of functional groups

funtional group		nature	$\frac{m(DNA)}{m_{Ref}(DNA)}$	buffer
sulfonic acid	A	anionic	1,2	Ficoll
phosphonic acid	B	anionic	15,8	EL
			6,8	RLT-EtOH
			5,0	PEG-Tween
			2,8	LiCl-IpropOH
carboxyle	E	anionic	$\lesssim 1$	all
quart. amine	C	cationic	$\lesssim 1$	all
aliphatic	D	amphiphilic	$\lesssim 1$	all
phenyl	F	amphiphilic	$\lesssim 1$	all
amine	G	neutral	$\lesssim 1$	all
polyethyleneglycol	H	neutral	$\lesssim 1$	all
pHEMA-co-pMABP	H	neutral	$\lesssim 1$	all

them in regard to their DNA adsorption potential.

Of all the functional groups mentioned in Table 6.1, including the unfunctionalized pHEMA-co-MABP hydrogel, only one showed promising results in terms of DNA isolation. Table 6.2 shows the results of this screening, with the unmodified PP PCR tube being the reference material: All but the phosphonated materials yielded either no amplified DNA mass (m_{DNA}) due to possible inhibition of the PCR, or returned - like in the case of the unmodified hydrogel - DNA quantities that were in the range of those reached by the completely unmodified PP PCR tube. However, the phoshonated HEMA gels gave excellent results in EL (low salt), RLT (high salt), PEG-Tween and LiCl-Isopronol (high salt) buffers, with the first returning almost 16 times the amount of DNA than in the unmodified PP PCR tube.

Since the introduction of phoshonic acid groups showed promise, the phoshonated pHEMA material was subjected to more thorough investigation regarding the influence of the benzophenone groups and phosphonic acid groups on the DNA isolation. Figure 6.17(a) shows the cycle threshold (C_T) values phoshonated hydrogels with various phosphonic

acid content in dependence of the lysis buffer in use. While in some cases a larger amount of phoshonic acid yields a much smaller cycle threshold - and thus a comparatively larger amount of DNA - no general trend regarding the amount of phosphonic acid groups can be found. Also, 6.17(a) reveals that the choice of the lysis buffer has a greater influence on the cycle threshold than the magnitude and type functionalization of the hydrogel film.

One explanation of the strong influence of buffer choice on DNA isolation might be the accessibility of the DNA to both the PCR amplification reagents and the absorptive surface. A change in the chemical composition of the buffer gives a different outcome of the lysis in regard of size, number and state of agglomeration of the DNA containing material. This is supported by the inverse fluorescence images of blood that has been marked with picogreen dye prior to lysis has been recorded for each lysis buffer, as shown in Fig. 6.18. Especially the buffers EL and RLT, which show good results in regard to DNA isolation, are showing a high number of particles of both small and large sizes. Apart from the strong influence of the nature of the buffer on the adsorptive properties of DNA and its isolation, the parameters of blood donor, blood sample age also have a strong influence on the outcome of the experiments. This complex system makes it difficult to identify tendencies in the collected data.

6.7 Conclusion

The photocrosslinkable pHEMA based hydrogel matrix developed and characterized in previous chapters has been transferred to the 3D geometry of the PCR tube and proven to be stabile under QPCR conditions. The matrix has been functionalized with a variety of groups that were suspected to enhance its DNA adsorption properties. For this, new intercalator bearing HEMA derivatives have been synthesized and tested for their

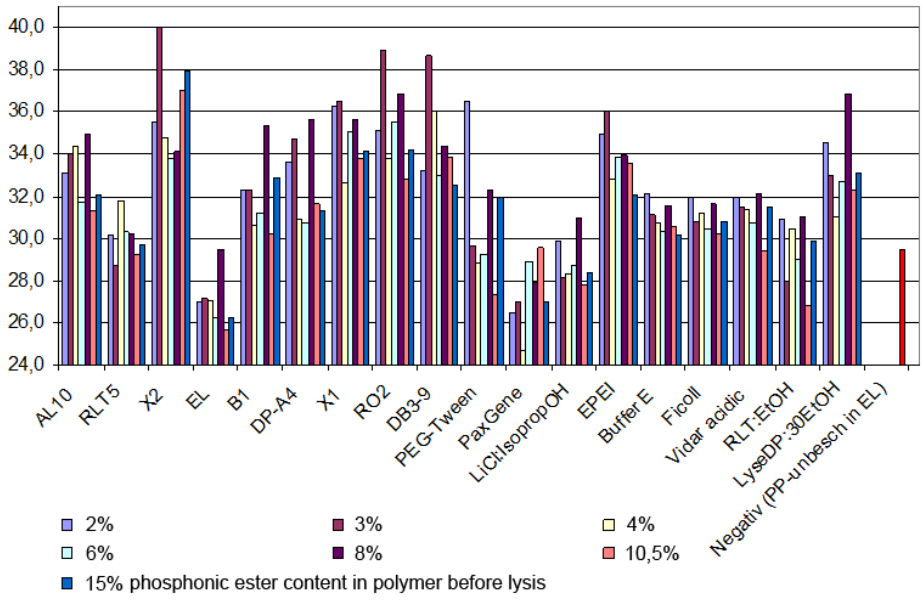

(a) Dependence of C_T on phosphonic acid amount in copolymer and buffer mixture.

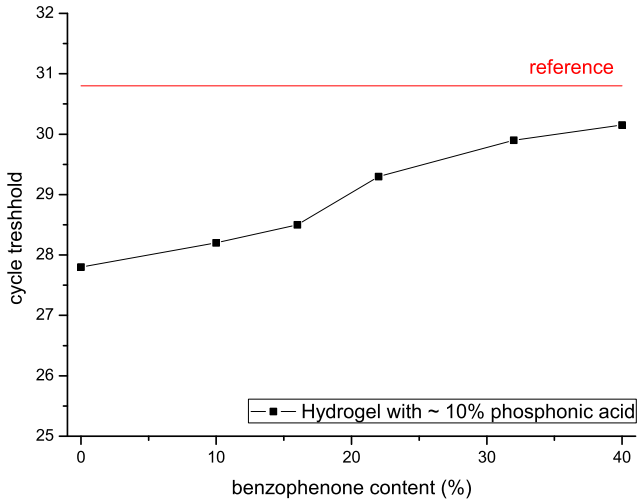

(b) Dependence of C_T on benzophenone content in the hydrogel.

Fig. 6.17 QPCR results for photocrosslinked HEMA hydrogel film with phosphonic acid ester functional groups. **(a)** shows the variation the phosphonic acid content in the material under a variety of buffers and **(b)** shows the influence of the BP amount on the QPCR under EL buffer conditions. The reference sample is the uncoated PP PCR tube.

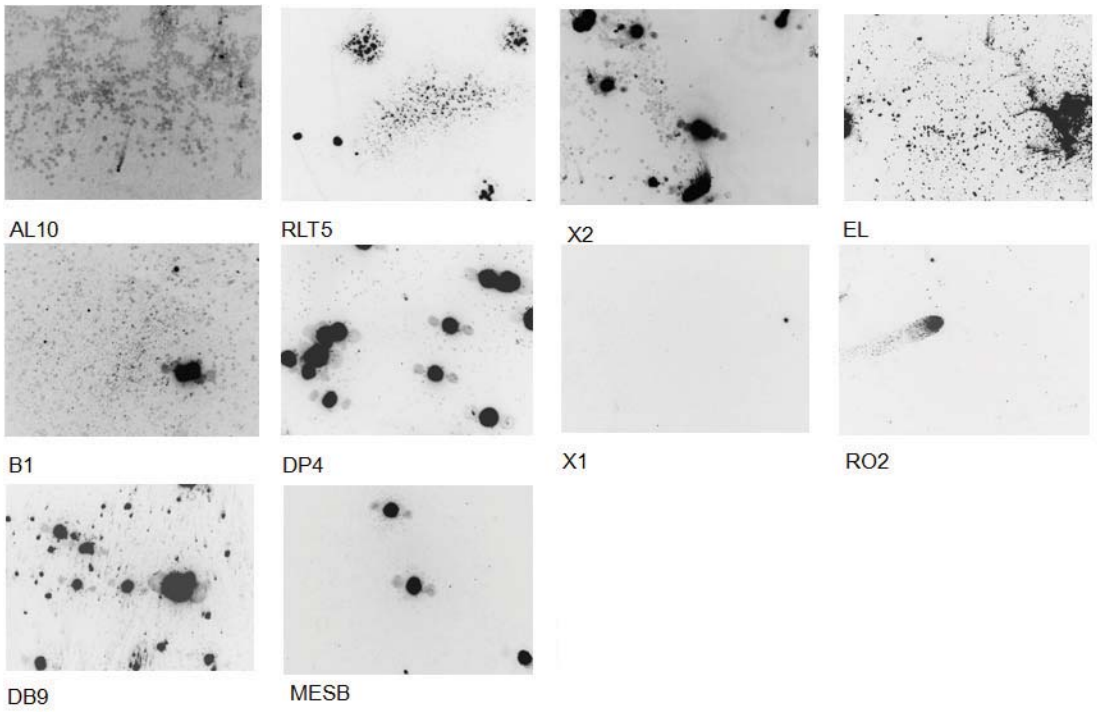

Fig. 6.18 Inverse fluorescence images with intercalated picogreen marker in the DNA of lysed blood cells showing the difference in the size and distribution of DNA fragments of a surface.

photobleaching behaviour under the conditions of 365 nm UV light irradiation. Apart from the intercalator monomers, a series of commercially available HEMA derivatives was copolymerized into the photocrosslinkable hydrogel precursor.
The materials were tested for the DNA adsorption properties with QPCR. With the exception of the hydrogel functionalized with phosponic acid, pHEMA materials - unmodified basic hydrogel and the materials obtained through functionalization with both small side groups - proved to be less effective in isolating gDNA from human blood than the unmodifed PCR tube.

Further experiments could not show a relation between phosponic acid content in the hydrogel and amount of isolated DNA. However, an increased amount of benzophenone crosslinker seemed to lower gDNA yield, leading to the assumption that a hydrophobization of the hydrogel could decrease the adsorption efficiency of gDNA.

6.8 Experimental

6.8.1 2-(Tetrahydro-2H-pyran-2-yloxy)ethanol

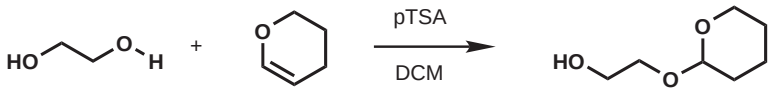

Ethyleneglycol (13 g,209,6 mmol) and p-toluensulfonicacid (2.7 g, 15,8 mmol) are added to 150 ml tetrahydrofuran. An ice bath is used to cool the mixture to 5 °C during the dropwise addition of 3,4-dihydro-2H-pyran (17.6 g, 202,2 mmol). The reaction mixture is stirred for two more hours at room temperature. The solvent is removed *in vacuo* and the product is purified by flash column chromatography using a gradient eluent (starting mixture ethylacetate/hexane = 3/1, ending mixture ethylacetate/hexane = 10).

Yield: 11 g $\sim$ 34 %

^{1}H-NMR (250 MHz, DCM): $\delta/ppm = 4,8$ (t, 1H, -H in THP), $4,0 - 3,4$ (m, 6H), $3,0$ (broad s, H, -OH), $2,0 - 1,4$ (m, 6H, -CH_2-).

6.8.2 (Tetrahydro-2H-pyran-2-yloxy)tetraethyleneglycol

Tetraethyleneglycol (59.37 g, 950 mmol) and p-toluensulfonicacid (2.7 g, 15,8 mmol) are added to 200 ml dichloromethane. An ice bath is used to cool the mixture to 5 ℃ during the dropwise addition of 3,4-dihydro-2H-pyran (11 g, 130 mmol). The reaction mixture is stirred for two more hours at room temperature. The solvent is removed *in vacuo*. The product is purified by flash column chromatography using a gradient eluent(starting mixture ethylacetate/hexane = 1/10, ending mixture ethylacetate/hexane = 1/3).

Yield: 12 g $\sim$ 32 %

^{1}H-NMR (250 MHz, DCM): $\delta/ppm = 4,8$ (t, 1H, -H in THP), $3,5 - 4,0$ (m, 18H), $2,8$ (broad s, H, -OH), $1,40 - 1,90$ (m, 6H, -CH_2-).

6.8.3 9-Bromo-acridine

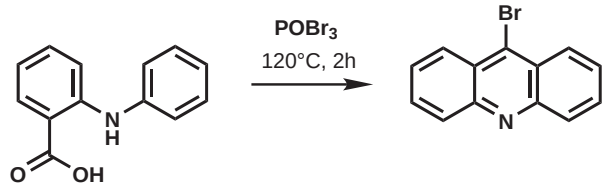

To a mixture of N-phenylanthranilic acid (3 g, 14.1 mmol) and $POBr_3$ (30.0 g, 100.4 mmol) was heated without solvent at 120 ℃. A violent fuming reaction occurred within 30 min. After heated for 2 h, the resulting solid was allowed to cool to room temperature. The mixture was carefully added to 300 ml of 25% aqueous ammonium hydroxide and dichloromethane. The dichloromethane phase was separated and the remaining aqueous phase extracted with dichloromethane. The organic phases were dried with $MgSO_4$ and purified with flash column chromatography. Evaporation of the solvent gave 9-bromoacridine as a yellow solid.

Yield: 2,9 g $\sim$ 83 %

M.p. (115 ℃, lit. 116 ℃);

^{1}H-NMR (250 MHz, CDCl3): δ/ppm = 8.42 (dd, J = 8.4, 1.2 Hz, 2H), 8.22 (d, J = 8.6 Hz, 2H), 7.80 (ddd, J = 8.4, 6.6, 1.2 Hz, 2H), 7.64 (ddd, J = 8.4, 6.6, 1.2 Hz, 2H).

6.8.4 (9-Acridinyloxy)tetraethyleneglycol

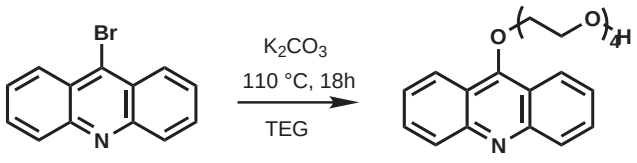

9-Bromo-acridine (2.9 g, 11.2 mmol) is added to a degased mixture of tetraethyleneglycole (61 g, 400 mmol) and K_2CO_3 (38 g, 275 mmol) in 100 ml dry DMF. The mixture is heated for 18 hours at 110 ℃. K_2CO_3 is filtered off and the solvent removed *in vacuo*. 500 ml water are added, and the mixture washed eight times with 100 ml dichlormethane. The organic phase is washed with 800 ml water, dried with $MgSO_4$. The solvent is then removed under vacuum, resulting in 2.5 g crude product. The product is purified with

flash column chromatography (I. hexane/THF = 3:2 II. ethylacetate).

Yield: 1,0 g $\sim$ 23 %

^{1}H-NMR (250 MHz, DCM): $\delta/ppm = 8,4$ (d, 2H, arom. -H), $8,2$ (d, 2H, arom-H), $7,75$ (m, 2H, arom. -H), $7,5$ (m, 2H, arom. -H), $4,25$ (m, 4H, -CH_2-), $3,83$ (t, 2H, -CH_2), $3,51 - 3,75$ (m, 10H+, -CH_2-). Impurities in spectrum at 3.8 ppm and below.

6.8.5 (9-Acridinyloxy)tetraethyleneglycolmethacrylate

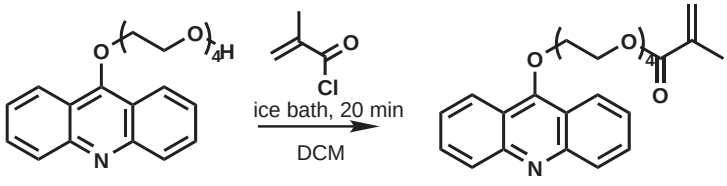

A degased solution of (9-acridinyloxy)tetraethyleneglycol (300 mg, 0.9 mmol) and triethylamine (1.1 g, 10.8 mmol) in 70 ml dry dichloromethane is cooled with an icebath. Chloromethacrylic acid (1.65 g, 15.8 mmol) is added in dropwise manner. The reaction mixture is then washed with 70 ml water. The aqueous phase is separated and washed three times with 50 ml dichloromethane. The organic phases are dried with $MgSO_4$ and the solvent is evaporated in vacuo. The pure product is obtained after purification with flash column chromatography (hexane/THF = 1:1).

Yield: 0,3 g $\sim$ 83 %

^{1}H-NMR (250 MHz, DCM): $\delta/ppm = 8,4$ (d, 2H, arom-H), $8,2$ (d, 2H, arom-H), $7,75$ (m, 2H, arom. -H), $7,5$ (m, 2H, arom. -H), $4,25$ (m, 4H, -CH_2-), $6,21$ (d, 1H, oleph. -H), $5,69$ (d, 1H, oleph. -H), $3,83$ (t, 2H, -CH_2), $3,49 - 3,77$ (m, 10H, -CH_2-), $1,81$ (s, 3H, methacrylate CH_3).

6.8.6 1-Brom-pyrene

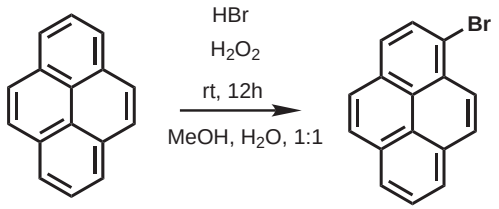

To a stirred solution of pyrene (7 g; 34,5 mmol) and hydrobromic acid (2,53 g; 5.19 mL of a 48% aq. solution; 36,1 mmol) in methyl alcohol water 1:1 mixture (80 mL) is slowly added hydrogen peroxide (1,05 g; 3.5 mL of a 30% aq. solution; 30 mmol) over a period of 15 min at 10-15 ℃. The reaction is left at room temperature for 20 h whilst monitoring its progress by TLC. After the completion of bromination, the solvent is removed under reduced pressure and the crude product is taken in ethyl acetate and washed with water, brine and dried over anhydrous sodium sulphate. The pure product is isolated by careful column chromatography on flash silica gel (ethyl acetate/hexane = 1:9) to give pure 1-bromo-pyrene as a light brown solid.

Yield: 4,79 g $\sim$ 49 %

^{1}H-NMR (250 MHz, DCM): $\delta/ppm = 7,5$ (d, 1H), $7,8-8,1$ (m, 7H), $8,4$ (d, 1H).

6.8.7 (Pyren-1-yloxy)tetraethyleneglycol

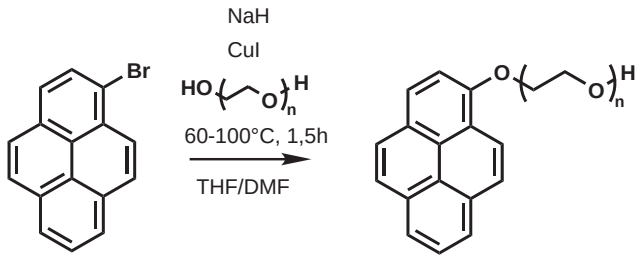

7 ml dry THF are added to a degased reaction flask containing sodiumhydride (170 mg, 7.1 mmol). The mixture is cooled with ice and stirred. This mixture is then slowly added to a degased solution of TEG (27 g, 133 mmol) (CAUTION! H_2 is generated in this reaction!). The mixture is stirred for 1 hour at room temperature. 10 ml dry DMF, cupper iodide (0.4 g, 2,1 mmol), and 1-brompyrene (3 g, 10.6 mmol) are added under protective gas atmosphere to the reaction mixture and stirred at 120 ℃ overnight. The reaction mixture is cooled down, the solvent is evaporated *in vacuo* and methanol is added. The mixture is extracted with the addition of 100 ml dichloromethane and washing the organic phase with 100 ml water. The organic phases are dried with $MgSO_4$ and the solvent is removed *in vacuo*. The crude product is purified using the a flash chromatography technique with short chromatography tube and solvent gradient (starting mixture: hexane/ethylacetate = 6/1; end mixture: hexane/ethylacetate = 1/6).

Yield: 0,4 g $\sim$ 28 %

^{1}H-NMR (250 MHz, DCM): $\delta/ppm = 7,5$ (d, 1H), $7,8 - 8,2$ (m, 7H), $8,4$ (d, 1H), 4,6 (m, 2H, -CH_2-), 4,1 (m, 2H, -CH_2-), $3,5 - 3,8$ (m, 12H, CH_2 on TEG), 2,4 (band, 1H, -OH).

6.8.8 (Pyren-1-yloxy)tetraethyleneglycolmethacrylate

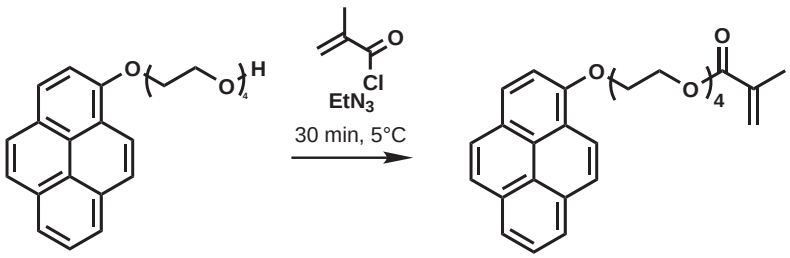

Triethylamine (0.370 g, 3.4 mmol) and (pyren-1-yloxy)tetraethyleneglycol (0.4 g, 10

mmol) are added under protective atmoshere to 25 ml of dry dichloromethane. The mixture is cooled with an ice bath. Under vigirous stirring, chloromethacrylic acid (1 g, 9.5 mmol) is added in dropwise manner. After 2 hours stirring, the reaction mixture is washed four times with 200 ml water. The aqueous phase is washed once with dichloromethane. The organic phases are dried with $MgSO_4$, and the solvent is removed *in vacuo*, yielding brown oil as crude product. The product is purified by flash chromatography (hexane/ethylacetate = 2/1).

Yield: 0,35 g $\sim$ 75 %

^{1}H-NMR (250 MHz, DCM): $\delta/ppm = 7,5$ (d, 1H), $7,8-8,2$ (m, 7H), $8,4$ (d, 1H), $4,6$ (m, 2H, -CH_2-), $6,0$ (s, 1H, olefinic H), $5,5$ (s, 1H, olefinic H), $4,4$ (m, 2H, -CH_2-), $4,2$ (m, 2H, -CH_2-), $4,0$ (m, 2H, -CH_2-), $3,5-3,8$ (m, 8H, CH_2 on TEG), $1,8$ (s, 3H, -CH_3).

6.8.9 4'-(4,5',8-Trimethylpsoralen)-methylbromide

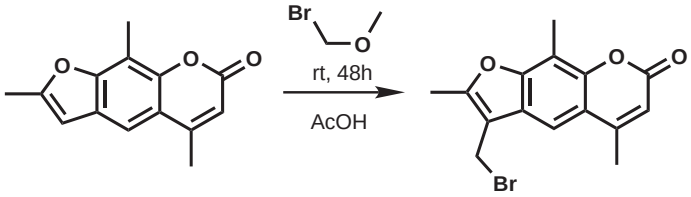

Trioxsalene (4.597 g, 20.1 mmol) is dissolved in 550 mL of glacial acetic acid by gentle heating and cooled to room temperature. 7,2 ml (7g, 56,1 mmol) of chloromethylmethyl-ether is then added, and the mixture is allowed to stand at room temperature for 48 h. The reaction flask is placed on ice and 12 h later an abundant white precipitate is collected. Another crop is isolated from the filtrate and the combined precipitates are purified by flash column chromatographyto using the eluent gradient technique (starting composition ethylacetate/hexane = 3/2; end composition ethylacetate/hexane 1/6).

Yield: 4,35 g $\sim$ 68 %

^{1}H-NMR (250 MHz, DCM): $\delta/ppm = 7,5$ (s, 1H, H_{arom}), 6,2 (s, 1H, -C=C(-H)-C=C-), 4,5 (s, 1H, CH_2Br), $2,2 - 2,5$ (m, 9H, -CH_3).

6.8.10 4'-(4,5',8-Trimethylpsoralen)methyltetraethyleneglycol

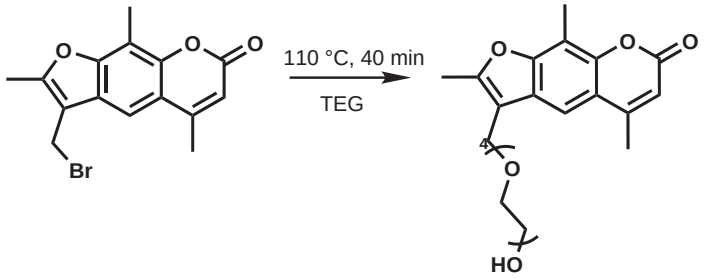

4'-(4,5',8-trimethylpsoralen)-methylbromide (1.25g, 3.8 mmol) are added into a degased reaction flask with freshly opened TEG (100 g, 515,1 mmol). The solid psoralene dissolves after heating the mixture at 110 °C for 20 minutes. After heating for further 20 minutes the mixture is cooled to room temperature. 500 ml water are added, and the mixture is extracted four times with 400 ml dichloromethane. The organic solvent is removed, and the remaining material poured into 70 ml water. The resulting mixture is extracted eight times with 50 ml dichloromethane. The organic phase are dried with $MgSO_4$ and evaporated *in vacuo*, and the remaining crude material purified with flash column chromatography using the eluent gradient technique and short chromatopgraphy columns (I. MeOH/EtAc = 1:8, II. THF/hexane = 6:1).

Yield: 1,44 g $\sim$ 85 %

^{1}H-NMR (250 MHz, DCM): $\delta/ppm = 7,4$ (s, 1H, H_{arom}), 6,2 (s, 1H, -C=C(-H)-C=C-), 5,8 (1s, 2H, -CH_2-O-TEG), $3,4 - 3,6$ (m, 14H, TEG CH_2), $2,3 - 2,5$ (m, 9H, -CH_3).

6.8.11 4'-(4,5',8-Trimethylpsoralen)methyltetraethyleneglycolmethacrylate

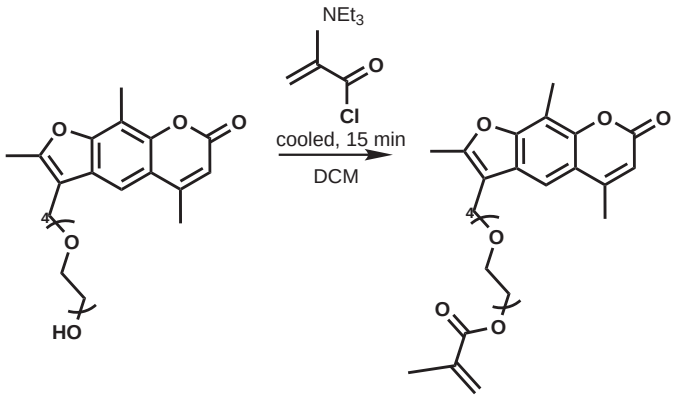

4'-(4,5',8-trimethylpsoralen)methyltetraethyleneglycol (1.25g, 2.88 mmol) and dry triethylamine (1g, 9.9 mmol) are added to 70 ml dry dichloromethane under protective gas atmosphere. After cooling the solution with an ice bath, chlormethacrylic acid (721 mg, 6.9 mmol) are added in a dropwise manner. The reaction is monitored by TLC. After 15 minutes, all educt is used up, and 70 ml water are added to the reaction mixture. The dichloromethane phase is separated, and the aqueous phase is washed three times with 70 ml dichloromethane. The combined organic layers are washed once with 100 ml water, dried with $MgSO_4$ and removed under vacuum. The crude product is purified by flash column chromatography (I. THF/Hexane = 6:1 II. THF/hexane = 3:1).

Yield: 0,5 g $\sim$ 34 %

^{1}H-NMR (250 MHz, DCM): $\delta/ppm = 7,6$ (s, 1H, H_{arom}), 6,15 (s, 1H, -C=C(-H)-C=C-), 6,05 (s, 1H, methacrylic oleph. H), 5,6 (s, 1H, methacrylic oleph. H), 4,8 (1s, 2H, -CH_2-O-TEG), 4,3 (m, 2H, TEG CH_2), $3,4 - 3,6$ (m, 14H, TEG CH_2), $2,3 - 2,5$ (m, 9H, -CH_3), 5,8 (1s, 2H, -CH_2-O-TEG), $3,4 - 3,6$ (m, 14H, TEG CH_2), $2,3 - 2,5$ (m, 9H, -CH_3), 2,1 (s, 3H, methacrylic CH_3).

6.8.12 Taqman Quantitative PCR (QPCR)

PCR tubes

0.2 ml LP Strip Tubes (8-Strip) and Optical Flat Cap Strips (natural color) were bought from the company Biozym Scientific GmbH.

PCR protocol

50 μl of Lyse-buffer is dispensed into each well of the hydrogel coated PCR tube strips. Next, 10 μl of blood is added to each well and mixed by pipetting up/down 10 times. The incubation of the tube strips at room temperature for 20 minutes is followed by the removal of the liquid by aspiration with the use of a pipette connected to a vacuum pump. After this, 120 μl of washing solution are dispensed into the appropriate wells. After repeated removal of all liquid with the vacuum pipette 25 μl of the PCR Mastermix are added and QPCR prodecure is initiated.

Buffer solutions for washing and cell lysis steps

All buffer solutions were obtained from the company Qiagen:
AL10 (Diluted Buffer AL 1:10, 560 mM GuHCl, 2% Tween-20, 5 mM Tris-Maleat pH 6.0), RLT5 (Diluted Buffer RLT 1:5, 0.7 M GITC, 5 mM NaCitrat pH 7.0), X2 (100 mM Ammonium-Acetat pH 4.0, 1% Tween-20, 1 mM EDTA), EL500 (NH_4Cl 500 mM, $KHCO_3$ 10 mM), B1 (50 mM EDTA, 50 mM TrisCl, pH 8.0, 0,5% Tween 20, 0,5% Triton X-100), DP-A4 (100 mM Tris pH 8.0, 2,5% Triton X-100, 5 mM EDTA, 5% Ethanol), X1 (10 mM NH_4HCO_3, 1% Tween-20, 1 mM EDTA), R02 (5% Tween-20, 155 mM NH4Cl, 10 mM KHCO3), DB3-9 (100 mM K-Hydrogenphthalate pH 4.5, 5% Triton X-100, 10

mM EDTA), MES-B (10% Tween, 1 mM EDTA, 25 mM MES pH 5). EL (Erethrocyte Lysis buffer).

6.8.13 Deposition of hydrogel precursors with the stamp method

Production of stamps

The PDMS stamps are produced with a commercially available PDMS mixture. Sylgard 184 Curing Agent and Sylgard 184 Base Silicon Elastomer are mixed in a mass 1 : 10 ratio. The mixture is left for 20 minutes in high vacuum and poured into the PCR tubes. A thick piece of wire is added to the mixture in order to function as handle. The material inside the PCR tubes is crosslinked overnight at 85 ℃. The finished stamps are removed from PCR tubes.

Plasma treatment of PCR tubes

In order to improve the quality of the surface coverage, the hydrophilicity of the PP surface is increased through a one minute exposure to gas plasma in a plasma reactor (TepPla 200-G Plasma System from Technics Plasma GmbH). The reaction conditions were as following: 0,3 mBar O_2 pressure, 280-290 W power.

Deposition of Hydrogel precursors

The PCR tubes are coated with a hydrogel precursor film with the help of the PDMS stamp: The stamp is dipped into a 13% ethanolic solution of the hydrogel precursor in order to cover it with polymer material. That is followed by putting and turning of the

the stamp covered with precursor material inside the PCR tube until a homogeneous surface distribution of the precursor material in the tube can be seen. In order to prevent a flow and deformation of the deposited film, the modified PCR tube 8-strips are stored for 2 minutes in a drying oven at 90 ℃ to 100 ℃. The PCR tubes are the left to dry at room temperature for 30 minutes.

Crosslinking

The deposited films are crosslinked for 15 minutes at a wavelength of 365 nm in the UV crosslinker.

6.8.14 Deposition of hydrogel precursors through adsorption

50 μL of a hydrogel precursor solution (2 mg / ml) are pipetted into the PCR wells. After 5 minutes, the solutions are removed with a vacuum tube. The residual polymer film is dried for 1 h at 50 ℃ and subsequently photocrosslinked for 1 h with a UV lamp at a wavelength of 365 nm.

7 Conclusion and outlook

This thesis presents the synthesis, characterization and optimization of pHEMA based hydrogels and their usage as DNA adsorbing films in the process of isolation of gDNA from human whole blood. Their properties, i.e. the degree of swelling, mechanical properties, thermal degradation, theoretic network parameters and interaction with biomolecules were investigated to understand the experimental results and to adjust the experimental procedures to reach the desired material properties.

A synthetic strategy for the hydrogels featuring the synthesis with free radical polymerization yielded photocrosslinkable hydrogel precursors with excellent properties for the production of high quality films on non-planar surfaces. The deposition of the precursor materials on a substrate of choice and subsequent crosslinking to a hydrogel with UV light irradiation produced hydrogel films with mechanical and thermal stability meeting the requirements for the DNA isolation process.

The basic gels with a composition of 99% HEMA and 1% MABP photocrosslinker showed very low equilibrium swelling ratios in aqueous solvent. While this prevented any diffusion of larger biomolecules such as streptavidin or DNA into the gel network, the functionalization of the hydrogel with specific groups such as biotin gave hydrogel adsorptive properties for specific molecules. The biotinated hydrogels still exhibited the anti-adsorptive properties known to HEMA based materials.

A chemical strategy towards the increase of the surface area of the hydrogel coating by introducing a mesostructure through the use of photosensitive phase separating block-copolymer hydrogel precursors has been explored. While photocrosslinkable and photocleavable blockopolymer hydrogel precursors on the basis of pS-b-pHEMA could be synthesized, the purification of the materials was found to be too difficult to achieve, making phase separation tests impossible.

Various implementations of the basic hydrogels composition with 89% HEMA, 1% MABP and 10% of a functionalized HEMA monomer derivative were screened with Taqman QPCR for an enhancement of DNA isolation performance from lysed blood. Of the many modifications introduced to the hydrogel, such as changes in hydrophilicity, positively and negatively charged polymer bound groups, the introduction of phosphonic acid groups to the pHEMA backbone showed great promise in the *one pot* gDNA isolation procedure. While the magnitude of backbone modification with phosphonic acid groups did not show a direct correlation with DNA absorption efficiency, a suitable set of PCR chemicals with very good performance was identified. With the use of lysis buffers like EL, RLT, LiCl-Isopronol and PEG-Tween, up to 5 ng of gDNA could be isolated from 10 μl of human blood - an amount large enough to perform PCR reactions and conduct further investigations. This makes it possible to conduct the isolation of gDNA in one single reaction container functionalized by a highly adsorptive hydrogel coating.

Bibliography

[1] Aristotle. *De Generatione Animalium*. approximatly fourth century B.C.

[2] G. Mendel. Versuche ueber pflanzenhybriden. *Verhandlungen des Naturforschenden Vereins Bruenn*, 4:3–47, 1866.

[3] Charles Darwin. *On the Origin of Species by Means of Natural Selection*. John Murray, 1859.

[4] Oswald T. Avery, Colin M. MacLeod, and Maclyn McCarty. Studies on the chemical nature of the substance inducing transformation of pneumococcal types: Induction of transformation by a desoxyribonucleic acid fraction isolated from pneumococcus type iii. *Journal of Experimental Medicine*, 79:137158, 1944.

[5] J.D. Watson and F.H.C. Crick. A structure for deoxyribose nucleic acid. *Nature*, 171:737–738, 1953.

[6] F. H. Crick, L. Barnett, S. Brenner, and R. J. Watts-Tobin. General nature of the genetic code for proteins. *Nature*, 192:1227–1232, 1961.

[7] H. J. Matthaei, O. W. Jones, R.G. Martin, and M.W. Nirenberg. Characteristics and composition of rna coding units. *Proceedings of the National Academy of Sciences of the United States of America*, 48:666–667, 1962.

[8] Bruce Alberts. *Molecular Biology of the Cell*. Garland Science, New York, 4 edition, 2002.

[9] Eric S. Lander. Initial impact of the sequencing of the human genome. *Nature*, 470:187–197, 2011.

[10] John Marshall Butler. *Forensic DNA typing: biology, technology, and genetics of STR markers*. Academic Press, 2005.

[11] Wolf Rogowski. Genetic screening by dna technology: A systematic review of health economic evidence. *International Journal of Technology Assessment in Health Care*, 22:327–337, 2006.

[12] J.P. Clewley. The polymerase chain reaction, a review of the practical limitations for human immunodeficiency virus diagnosis. *Journal of Virological Methods*, 25:179–187, 1989.

[13] A. T. Bowling. Historical development and application of molecular genetic tests for horse identification and parentage control. *Livestock Production Science*, 72:111–116, 2001.

[14] Qiagen GmbH. *Two-Step Affinity Purification System Handbook*. 2005.

[15] Ramiro Ramirez-Solis, Jaime Rivera-Perez, James D. Wallace, Marie Wims, Hui Zheng, and Allan Bradley. Genomic dna microextraction: A method to screen numerous samples. *Analytical Biochemistry*, 201:331–335, 992.

[16] Beverley C. Millara, Xu Jirua, John E. Moore, and John A. P. Earle. A simple and sensitive method to extract bacterial, yeast and fungal dna from blood culture material. *Journal of Microbiological Methods*, 42:139–147, 2000.

[17] Venture Planning Group VPG. U.s. molecular diagnostics markets. *Molecular Diagnostics Market Research Reports*, 2003.

[18] Venture Planning Group VPG. Global diagnostics market dynamics and trends. *Molecular Diagnostics Market Research Reports*, 2011.

[19] German Federal Ministry of Education and Research (BMBF). Combating diseases through genome research - the national genome research network. Germany, 2003.

[20] T.R. Hoare and D.S. Kohane. Hydrogels in drug delivery: Progress and challenges. *Polymer*, 49:1994–2007, 2008.

[21] Joshua S. Boateng, Kerr H. Matthews, Howard N.E. Stevens, and Gillian M. Eccleston. Wound healing dressings and drug delivery systems: a review. *Journal of Pharmaceutical Sciences*, 97:2892–2923, 2008.

[22] Joshua M.G. Swann and Anthony J. Ryan. Quantifying laser response using laser light pattern. *Soft Matter*, 58:285–289, 2009.

[23] B. Jeong and A. Gutowska. Lessons from nature: stimuli-responsive polymers and their biomedical applications. *Trends in Biotechnology*, 20:305–311, 2002.

[24] R. Landers, U. Hubner, R. Schmelzeisen, and R. Muelhaupt. Rapid prototyping of scaffolds derived from thermoreversible hydrogels and tailored for applications in tissue engineering. *Biomaterials*, 23:4437–4447, 2002.

[25] Thomas Zacher and Erik Wischerhoff. Real-time two-wavelength surface plasmon resonance as a tool for the vertical resolution of binding processes in biosensing hydrogels. *Langmuir*, 18:1748–1759, 2002.

[26] N. A Peppas, Y. Huang, M. Torres-Lugo, J.H. Ward, and J. Zhang. Physicochemical foundations and structural design of hydrogels in medicine and biology. *Annu. Rev. Biomed. Eng.*, 2:9–29, 2000.

[27] N. A Peppas, P. Bures, W. Leobandung, and H. Ichakawa. Hydrogels in pharmaceutical formulations. *European Journal of Pharmaceuticals and Biopharmaceuticals*, 50:27–46, 2000.

[28] N. A. Peppas, J. Z. Hilt, A. Khademhosseini, and R. Langer. Hydrogels in bio-

logy and medicine: From fundamentals to bionanotechnology. *Advanced Materials*, 18:1345–1360, 2006.

[29] Arvind M. Mathura, K. Shailender, K. Moorjaniaa, and Alec B. Scrantona. Methods for synthesis of hydrogel networks: A review. *Journal of Macromolecular Science, Part C: Polymer Reviews*, 36:405–430, 1996.

[30] M. A. Gauthier, M. I. Gibson, and H. A. Klok. Post-polymerization modification. *Angew. Chem. Int. Ed.*, 48:48–58, 2009.

[31] A.D. Fuchs and J.C. Tiller. Novel antimicrobial coatings and surfaces. *Angew. Chem. Int. Ed.*, 45:6759–6762, 2006.

[32] M. G. Zolotukhin, H. M. Colquhoun, L. G. Sestiaa, D. R. Rueda, and D. Flot. One-pot synthesis and characterization of soluble poly(aryl ether-ketone)s having pendant carboxyl groups. *Macromolecules*, 36:4766–4771, 2003.

[33] Robert Fokko Roskamp. *Functional Hydrogels*. PhD thesis, University of Mainz, 2009.

[34] C. Holm, K. T. Kremer, and A. Vilgis. Polyelektrolyte: Grundlegende probleme bei der beschreibung weitverbreiteter substanzen. *Physikalische Blaetter*, 54:1013–1016, 1998.

[35] D. Ratner, editor. *Biomaterials science: an introduction to materials in medicine*. Elsevier Academic Press, 2004.

[36] N. A. Peppas. *Hydrogels in Medicine and Pharmacy.* CRC Press, Boca Raton, FL., 1987.

[37] A.S. Hickey and N. A. Peppas. Mesh size and diffusive characteristics of semicrystalline poly(vinyl alcohol) membranes. *J. Membr. Sci.*, 107:229–237, 1995.

[38] A. A. O. Sarhan, M. S. Ibrahim, M. M. Kamal, K. Mitobe, and T. Izumi. Synthesis, cyclic voltammetry, and uvvis studies of ferrocene-dithiafulvalenes as anticipated electron-donor materials. *Monatshefte Chemie*, 140:315–323, 2009.

[39] E. J. Kupchick and R. J. Kiesel. Reactions of triphenyltin hydride with certain acid chlorides and carboxylic acids. *J. Org. Chem.*, 31:456–461, 1966.

[40] Bernward A.F. Mann. *The Swelling of Polyectrolyte Networks*. PhD thesis, Johannes Gutenberg University Mainz, 2005.

[41] Y. Li, N. Wang, X. He, S. Wang, H. Liu, Y. Li, X. Li, J. Zhuang, and D. Zhu. Synthesis and characterization of ferrocene-perylenetetracarboxylic diimidefullerene triad. *Tetrahedron*, 61:1563–1569, 2005.

[42] I. Tranchant, A.-C. Herve, S. Carlisle, P. Lowe, C. J. Slevin, C. Forssten, J. Dilleen, D. E. Williams, A. B. Tabor, and H. C. Hailes. Design and synthesis of ferrocene

probe molecules for detection by electrochemical methods. *Bioconjugate Chem.*, 17:1256–1264, 2006.

[43] E. Karadag, D. Saraydin, and O. Guven. Influence of some crosslinkers on the swelling of acrylamide-crotonic acid hydrogels. *Turkish Journal of Chemistry*, 21:151–161, 1997.

[44] Kossmehl. Herstellung und charakterisierung von hydrogelen als kontaktlinsenmaterialien. *Angewandte Makromolekulare Chemie*, 123:241–259, 1984.

[45] B. D. Ratner. *Hydrogels in Medicine and Pharmacy*, volume 1. Boca Raton, 1986.

[46] A. Halperin, M. Tirell, and T. P. Lodge. Tethered chains in polymer microstructures. *Advances in Polymer Science*, 100:31–71, 1992.

[47] Pawley. Low voltage scanning electron microscopy. *Journal of Microscopy-Oxford*, 136:45–68, 1984.

[48] J. Butler, D. Joy, G. Bradley, and S. Krause. Low-voltage scanning electron microscopy of polymers. *J. Polymer*, 36:1781–1790, 1995.

[49] D. Joy and C. Joy. Low-voltage scanning electron microscopy. *Micron*, 27:247–263, 1996.

[50] G. Binning, C. F. Quate, and C. Gerber. Atomic force microscopy. *Phys. Rev. Lett.*, 56:930–933, 1986.

[51] Y. Martin, C. C. Williams, and H. K. Wickramashinghe. Atomic force microscope - force mapping and profiling on a sub 100 a scale . *J. Appl. Phys*, 61:4723–4729, 1987.

[52] T. Albrecht, P. Grutter, D. Horne, and D. Rugar. Frequency modulation detection using high-q cantilevers for enhanced force microscope sensitivity. *J. Appl. Phy*, 69:668–673, 1991.

[53] H. Butt, R. Berger, Y. Chen E. Bonaccurso, and J. Wang. Impact of atomic force microscopy on interface and colloid science. *J. Adv. Colloid Interface Sci.*, 133:91–104, 2007.

[54] Hans-Juergen Butt, Karlheinz Graf, and Michael Kappl. *Physics and Chemistry of Interfaces*. Wiley-VCH Verlag and Co. KGaA, 2003.

[55] L.E. Nielsen and R.F. Landel. *Mechanical Properties of Polymers and Composites*. Marcel Dekker, New York, 2nd edition, 1994.

[56] H. Raether. *Surface Plasmons on Smooth and Rough Surfaces and on Gratings*. Springer-Verlag, 1988.

[57] E. Kretschmann. Die bestimmung optischer konstanten von metallen durch an-

regung von oberflaechenplasmaschwingungen. *Zeitschrift fuer Physik A Hadrons and Nuclei*, 241:313–324, 1971.

[58] Allan W. Snyder and William R. Young. Modes of optical waveguides. *J. Opt. Soc. Am.*, 68:297–309, 1978.

[59] A. Otto. Excitation of nonradiative surface plasma waves in silver by the method of frustrated total reflection. *Zeitschrift fuer Physik A: Hadrons and Nuclei*, 216:398–410, 1968.

[60] R. Higuchi, G.Dollinger, P.S. Walsh, and R. Griffith. Simultaneous amplification and detection of specific dna sequences. *Biotechnology*, 10:413–417, 1992.

[61] R. Higuchi, C. Fockler, G. Dollinger, and J. R. Watson. Kinetic pcr: Real time monitoring of dna amplification reactions. *Biotechnology*, 11:1026–1030, 1993.

[62] P.M. Holland, S. Agrawal, C. Flores, P.C. Zamecnik, and D.E. Wolf. Detection of specific polymerase chain reaction product by utilizing the 5' -¿ 3' exonuclease activity of theramus aquaticus dna polymerase. *Proc. Nat. Acad. Sci. USA*, 88:7276–7280, 1991.

[63] R.A. Cardullo, S. Agrawal, C. Flore, P.C. Zamecnik, and D.E. Wolf. Detection of nucleic acid hybridization by nonradiative fluorescence resonance energy transfer. *Proc. Nat. Acad. Sci. USA*, 85:8790–8794, 1988.

[64] S. Tyagi and F.R. Kramer. Molecular beacons: probes that fluoresce upon hybridization. *Nature Biotechnology*, 14:303–308, 1996.

[65] C.T. Wittwer, M.G. Herrmann, A.A. Moss, and R.P. Rasmussen. Continuous fluorescence monitoring of rapid cycle dna amplification. *Biotechniques*, 22:130–138, 1997.

[66] K.J. Livak, S.J.A. Flood, J. Marmaro, W. Giustu, and K. Deetz. Oligonucleotides with fluorescent dyes at opposite ends provide a quenched probe system useful for detecting pcr product and nucleic acid hybridization. *PCR Methods and Applications*, 4:357–362, 1995.

[67] O. Wichterle and D. Lim. Hydrophilic gels for biological use. *Nature*, 185:117–118, 1960.

[68] J.P. Montheard, M. Chatzopoulos, and D. Chappard. 2-hydroxyethyl methacrylate (hema): Chemical properties and applications in biomedical fields. *Journal of Macromolecular Science, Part C: Polymer Reviews*, 32:1–34, 1992.

[69] C.D. Young, J.R. Wu, and T.L. Tsou. Fabrication and characteristics of polyhema artificial skin with improved tensile properties. *Journal of Membrane Science*, 146:83–93, 1998.

[70] O. Garcia, M.D. Blanco, J.A. Martn, and J.M. Teijon. 5-fluorouracil trapping in

poly(2-hydroxyethyl methacrylate-co-acrylamide) hydrogels: in vitro drug delivery studies. *European Polymer Journal*, 36:111–122, 2000.

[71] O. Moradi, H. Modarress, and M. Noroozi. Experimental study of albumin and lysozyme adsorption onto acrylic acid (aa) and 2-hydroxyethyl methacrylate (hema) surfaces. *Journal of Colloid and Interface Science*, 271:16–19, 2004.

[72] P.D. Dalton, L. Flynn, and M.S. Shoichet. Manufacture of poly(2-hydroxyethyl methacrylate-co-methyl methacrylate) hydrogel tubes for use as nerve guidance channels. *Biomaterials*, 23:3843–3851, 2002.

[73] Rosa M. Trigo, M. Dolores Blanco, Paloma Huerta, Rosa Olmo, and Jose M. Teijon. l-ascorbic acid release from phema hydrogels. *Polymer Bulletin*, 31:577–584, 1993.

[74] A. Hirao, H. Kato, K. Yamaguchi, and S. Nakahama. Polymerization of monomers containing functional groups protected by trialkylsilyl groups. 5. synthesis of poly(2-hydroxyethyl methacrylate) with a narrow molecular weight distribution by means of anionic living polymerization. *Macromolecules*, 19:1294–1299, 1986.

[75] H. Chu and D. Fu. Preparation of poly(hydroxyethyl methacrylate) and poly(hydroxypropyl methacrylate) latices. *Macromolecular Rapid Communications*, 19:107–110, 1998.

[76] J. V. M Weaver, I. Bannister, K.L. Robinson, X. Bories-Azeau, S.P.Armes, M. Smallridge, and P. McKenna. Stimulus responsive water soluble polymers based on 2-hydroxyethyl methacrylate. *Macromolecules*, 37:2395–2403, 2004.

[77] T. Caykara, C. Ozyurek, O. Kantoglu, and O. Guven. Influence of gel composition on the solubility parameter of poly(2-hydroxyethyl methacrylate-itaconic acid) hydrogels. *Journal of Polymer Science: Part B: Polymer Physics*, 40:1995–2003, 2002.

[78] Atul R. Khare and Nikolaos A. Peppas. Swelling/deswelling of anionic copolymer gels. *Biomaterials*, 16:559–567, 1995.

[79] Oliver von Egen. *Synthese und Modifizierung von hochfunktionellen Monomeren auf Basis der 2-Hydroxymethacrylsaeure*. PhD thesis, Univesity of Wuppertal, 1998.

[80] Kinam Park Hossein Omidian and Umadevi Kandalam. Swelling and mechanical properties of modified hema-based superporous hydrogels. *Journal of Bioactive and Compatible Polymers*, 25:483–497, 2010.

[81] Megan S. Lord, Martina H. Stenzelb, Anne Simmonsa, and Bruce K. Milthorpea. The effect of charged groups on protein interactions with poly(hema) hydrogels. *Biomaterials*, 27:567–575, 2006.

[82] R. Sariri and V. Jafarian. The effect of itaconic acid on biocompatibility of hema. *European Cells and Materials*, 4:41, 2002.

[83] N.J. Turro. *Modern Molecular Photochemistry*. University Science Books, 1991.

[84] D. Kuckling, M.E. Harmon, and C.W. rank. Photo cross-linkable pnipaam copolymers 1: Synthesis and characterization of constrained temperature-responsive hydrogel layers. *Macromolecules*, 35:6377–6383, 2002.

[85] P. W. Beines, I. Klosterkamp, B. Menges U. Jonas, and W. Knoll. Responsive thin hydrogel layers from photo-cross-linkable poly(n-isopropylacrylamide) terpolymers. *Langmuir*, 23:2231–2238, 2007.

[86] O. Prucker, C.A. Naumann, J. Ruhe, W. Knoll, and C.W. Frank. Photochemical attachment of polymer films to solid surfaces via monolayers of benzophenone derivatives. *Journal of the American Chemical Society*, 121:8766–8770, 1999.

[87] L.K. Ista, S. Mendez, V.H. Perez-Luna, G.P., and Lopez. Synthesis of poly(n-isopropylacrylamide) on initiator-modified self-assembled monolayers. *Langmuir*, 17:2552–2555, 2001.

[88] M.A. Cole, M. Jasieniak, N.H. Voelcker, H. Thissen, R. Horn, and H.J. Griesser. Switchable surface coatings for control over protein adsorption. *Proceedings of the SPIE - The International Society for Optical Engineering*, 6416:641606–641616, 2006.

[89] D.L. Huber, Manginel R.P., M.A. Samara, B.I. Kim, and B.C. Bunker. Programmed adsorption and release of proteins in a microfluidic device. *Science*, 301:352–354, 2003.

[90] A. Mizutani, A. Kikuchi, M. Yamato, H.Kanazawa, and T. Okano. Biomaterials. *Preparation of thermoresponsive polymer brush surfaces and their interaction with cells*, 29:2073–2081, 2008.

[91] C. D. H Alarcon, T. Farhan, V. Osborne, W.T.S. Huck, and C. Alexander. Bioadhesion at micro-patterned stimuli-responsive polymer brushes. *Journal of Materials Chemistry*, 15:2089–2094, 2005.

[92] D. Cunliffe, C.D. Alarcon V. Peters, J.R. Smith, and C. Alexander. Thermoresponsive surface-grafted poly(n-isopropylacrylamide) copolymers: Effect of phase transitions on protein and bacterial attachment. *Langmuir*, 19:2888–2899, 2003.

[93] M. Yamat and T. Okano. Cell sheet engineering. *Materials Today*, 7:42–47, 2004.

[94] X. H. Cheng, Y. B. Wang, Y. Hanein, K.F. Bohringer, and B. D. Ratner. Novel cell patterning using microheater-controlled thermoresponsive plasma films. *Journal of Biomedical Materials Research Part A*, 70A:159–168, 2004.

[95] T. Okano, N. Yamada, H. Sakai, and Y. Sakurai. A novel recovery system for cultured cells using ... with poly(n-isopropylacrylamide). *Journal of Biomedical Materials Research*, 27:1244–1251, 1993.

[96] Jie Song, Viengkham Malathong, and Carolyn R. Bertozzi. Mineralization of syn-

thetic polymer scaffolds: A bottom-up approach for the development of artificial bone. *J. Am. Chem. Soc.*, 127:3366–3372, 2005.

[97] Rong Jin, Christine Hiemstra, Zhiyuan Zhong, and Jan Feijen. Study of dna condensation and buffer capacity on gene transfection. *Biomaterials*, 28:2791–2800, 2007.

[98] N. A. Peppas. *Comprehensive Polymer Science*, volume 6. Pergamon Press, New York, 1989.

[99] J. M Anderson, T. Koinis, and T. Nelson M. Horst D.S. Love. *Hydrogels for medical and related applications*, volume 31. American Chemical Society, Washington, DC, acs symposium series edition, 1976.

[100] S. Aiba, N. Minoura, K. Taguchi, and Y. Fujiwara. Covalent immobilization of chitosan derivatives onto polymeric film surfaces with the use of a photosensitive hetero-bifunctional crosslinking reagent. *Biomaterials*, 8:481–488, 1987.

[101] S. Sicsic, J. Leonil, J. Braun, and F. LeGoffic. *Chitin in nature and technology*. Plenum, New York, 1986.

[102] D. Kuckling C. D. Vo, H.-J. Adler, and M. Schnhoff. Preparation of thermosensitive nanogels by photocrosslinking. *Colloid Polym Sci*, 280:400–409, 2002.

[103] A. Aulasevich, R. F. Roskamp, U. Jonas, B. Menges, J. Dostalek, and W. Knoll. Optical waveguide spectroscopy for the investigation of protein-functionalized hydrogel films. *Macromolecular Rapid Communications*, 30:872–877, 2009.

[104] R. Toomey, D. Freidank, and J. Ruehe. Swelling behavior of thin, surface-attached polymer networks. *Macromolecules*, 37:882–887, 2004.

[105] K. Horie, H. Ando, and I. Mita. Photochemistry in polymer solids 8. mechanism of. photoreaction of benzophenone in poly(viny1 alcohol). *Macromolecules*, 20:54–58, 1987.

[106] M.K. Park, S. Deng, and R. C. Advincula. ph-sensitive bipolar ion-permselective ultrathin films. *J. Am. Chem. Soc.*, 126:13723–13731, 2004.

[107] K. Laenge, S. Grimm, and M. Rapp. Chemical modification of parylene c coatings for saw biosensors. *Sensors and Actuators B*, 125:441–446, 2007.

[108] H.G. Elias. *Makromolekuele, Band 1*. Wiley-VCH, 2001.

[109] P. Beines. *Synthese und Charakterisierung einer Hydrogelmatrix fuer die Multianalyt-Sensorik*. PhD thesis, University of Mainz, 2007.

[110] G. Odian. *Principles of Polymerization*. Wiley Interscience, 2004.

[111] Miroslaw Gibas and Anna Korytkowska-Walach. Polymerization of 2-hydroxyethyl

- acrylate and methacrylate via michael-type addition. *Polymer Bulletin*, 51:17–22, 2003.

[112] Z. S. Nurkeeva, G. A. Mun, and V.B. Golubev. On the activity of monomers and polymers on the basis of vinyl ethers of glycols in radical reactions. *Macromolecular Chemistry and Physics*, 193:1117–1122, 1992.

[113] G. M. Geurts, C.M. Gotttgens, M.A. Van Graefschepe, R.W. Welland J.J.G., Steven Van Es, and A.L. German. Syntheses of new amino-functionalized methacrylates and their use in free radical polymerizations. *Journal of Applied Polymer Science*, 80:1401–1415, 2001.

[114] D. A. Tirrell. *Copolymer Composition*, volume 3 of *Comprehensive Polymer Science*. Pergamon Press, Oxford, 1989.

[115] J. M. G. Cowie. *Chemie und Physik der synthetischen Polymeren*. Friedrich Vieweg und Sohn Verlagsgesellschaft mbH, 1997.

[116] F. R. Mayo and F. M. Lewis. Copolymerization. i. a basis for comparing the behavior of monomers in copolymerization; the copolymerization of styrene and methyl methacrylate. *J. Am. Chem. Soc.*, 6:1594–1601, 1944.

[117] M. Finemann and S. D. Ross. Linear method for determining monomer reactivity ratios in copolymerization. *J. Polym. Sci.*, 5:259–262, 1950.

[118] T. Kelen and F. Tudos. Analysis of the linear methods for determining copolymerization reactivity ratios. i. a new improved linear graphic method. *Journal of Macromolecular Science, Part A*, 9:1–27, 1975.

[119] S. Nanjundan, C. Sreekuttan Unnithan, C.S. Jone Selvamalar, and A. Penlidis. Homopolymer of 4-benzoylphenyl methacrylate and its copolymers with glycidyl methacrylate: synthesis, characterization, monomer reactivity ratios and application as adhesives. *Reactive and Functional Polymers*, 62:11–24, 2005.

[120] P.S. Vijayanand, C. S. Unnithan, A. Penlidis, and S. Nanjundan. Copolymerization of benzoylphenyl methacrylate with methyl methacrylate: Synthesis, characterization and determination of monomer reactivity ratios. *Journal of Macromolecular Science Part A*, 42:555–569, 2005.

[121] T. Alfrey Jr. and C. C. Price. Relative reactivities in vinyl copolymerization. *Journal of Polymer Science*, 2:101–106, 1947.

[122] Charles C. Price. Some relative monomer reactivity factors. *Journal of Polymer Science*, 3:772–775, 1948.

[123] Greenley. Q and e values for free radical copolymerization of vinyl monomers and telogens. *Polymer handbook*, 1:267–274, 1989.

[124] J. Borchardt and E. Dwyann Dalrymple. Calculation of alfrey-price q-e values from 13c-nmr data. *Pol. Sci. Polymer Chemistry Edition*, 20:1745–1764, 1982.

[125] A. Y. Fadeev and T. J. McCarthy. Studies indicating that molecular topography contributes to contact angle hysteresis. *Langmuir*, 15:3759–3766, 1999.

[126] M. J. Tarlov, D. R. F. Burgess, and G. Gillen. Uv photopatterning of alkanethiolate monolayers self-assembled on gold and silver. *J. Am. Chem. Soc.*, 115:5305–5306, 1993.

[127] H. Li and G. McGall. Photoactivateable silane compounds and methods for their synthesis and use. *US Patent*, 0234788, 2004.

[128] Dirk W. Schubert and Thomas Dunkel. Spin coating from a molecular point of view: its concentration regimes, influence of molar mass and distribution. *Materials Research Innovations*, 7:314–321, 2003.

[129] R. J. Fort and T. M. Polyzoidis. Intrinsic viscosity-molecular weight relationships for poly(2-hydroxyethyl methacrylate). *Eur. Polym. J.*, 12:685–689, 1976.

[130] R. Yoshida, Okuyama, K. Sakai, T. Okano, and Y. Sakurai. Sigmoidal swelling profiles for temperature-responsive poly(n-isopropylacrylamide-co-butyl methacrylate) hydrogels. *J. Membr. Sci.*, 89:267–277, 1994.

[131] D.J. Enscore, H.B. Hopfenberg, and V.T. Stannett. Effect of particle size on the mechanism controlling n-hexane sorption in glassy polystyrene microspheres. *Polymer*, 18:793–800, 1977.

[132] X.Z. Zhang and R.X. Zhuo. Synthesis of temperature-sensitive poly(n-isopropylacrylamide) hydrogel with improved surface property. *J. Colloid Interface Sci.*, 223:311–313, 2000.

[133] X.Z. Zhang, D. Wu, and C.J. Chu. Effect of the crosslinking level on the properties of temperature-sensitive poly(n-isopropylacrylamide) hydrogels. *Journal of Polymer Science Part B: Polymer Physics*, 41:582–593, 2003.

[134] Malcolm B. Hugh, Mahmoud M. Rehab, and Mat B. Zakaria. Thermodynamic interactions in copolymeric hydrogels. *Macromolecules*, 19:2986–2991, 1986.

[135] B. Johnson, D.J. Beebea, and W.C. Crone. Effects of swelling on the mechanical properties of a ph-sensitive hydrogel for use in microfluidic devices. *Materials Science and Engineering C*, 24:575–581, 2004.

[136] W. Knoll. Interfaces and thin films as seen by bound electromagnetic waves. *Annu. Rev. Phys. Chem.*, 49:569–638, 1998.

[137] P. Englebienne, A. V. Hoonacker, and M. Verhas. Surface plasmon resonance: principles, methods and applications in biomedical sciences. *Spectroscopy*, 17:255–273, 2003.

[138] D. K. Kambhampati and W. Knoll. Surface-plasmon optical techniques . *Current opinion in Colloid and Interface Science*, 4:273–280, 1999.

[139] Anette Brunsen. *Functional Dextran-Based Hydrogels*. PhD thesis, University of Mainz, 2010.

[140] Pochi Yeh. *Optical Waves in layered media*. Wiley, 1988.

[141] W. Karthe and R. Mller. *Integrierte Optik*. Akademische Verlagsgesellschaft Geest und Portig, 2 edition, 1991.

[142] Lubert Stryer. *Biochemistry*. W.H. Freeman and Company, 5th edition, 2002.

[143] Robert J. McMahon, editor. *Methods and Applications Series: Methods in Molecular Biology*, volume 418. Springer-Verlag, 2008.

[144] Jakub Dostlek, Amal Kasry, and Wolfgang Knoll. Long range surface plasmons for observation of biomolecular binding events at metallic surfaces. *Plasmonics*, 2:97–106, 2007.

[145] Yi Wang, Annette Brunsen, Ulrich Jonas, Jakub Dostalek, and Wolfgang Knoll. Prostate specific antigen biosensor based on long range surface plasmon-enhanced fluorescence spectroscopy and dextran hydrogel binding matrix. *Anal. Chem.*, 81:9625–9632, 2009.

[146] Haifeng Gao and Krzysztof Matyjaszewski. Synthesis of molecular brushes by grafting onto method: Combination of atrp and click reactions. *J. Am. Chem. Soc.*, 129:6633–6639, 2007.

[147] Wenbao Li, Anthony W. Czarnik, John Lillig, and Xiao-Yi Xiao. Kinetic study of organic reactions on polystyrene grafted microtubes. *J. Comb. Chem.*, 2:224–227, 2000.

[148] Chung-Daw Young andJing Ran Wu and Tai-Li Tsou. High-strength, ultra-thin and ber-reinforced phema articial skin. *Biomaterials*, 19:1745–1752, 1998.

[149] B. Barr-Howell and N. A. Peppas. Importance of junction functionality in highly crosslinked polymers. *Polymer Bulletin*, 13:91–96, 1985.

[150] A. V. Tobolsky, D.W. Carlson, and N. Indictor. Rubber elasticity and chain configuration. *Journal of Polymer Science*, 54:175–192, 1961.

[151] M. F. Refojo. *Kirk-Othmer Enzyclopedia of Chemical Technology*, volume 6. J. Wiley VCH, New York, 3 edition, 1979. Contact Lenses".

[152] M. Murat Ozmen and Oguz Okay. Formation of macroporous poly(acrylamide) hydrogels in dmso/water mixture: Transition from cryogelation to phase separation copolymerization. *Reactive and Functional Polymers*, 68:1467–1475, 2008.

[153] Sonia Partap, Andrew K. Hebb, Ihtesham ur Rehman, and Jawwad A. Darr. Formation of porous natural-synthetic polymer composites using emulsion templating and supercritical fluid assisted impregnation. *Polymer Bulletin*, 58:849–860, 2007.

[154] H.R. Oxleya, P.H. Corkhilla, J.H. Fittona, and B.J. Tighe. Macroporous hydrogels for biomedical applications:: Methodology and morphology. *Biomaterials*, 14:1064–1072, 1993.

[155] J. Chen, H. Park, and K. Park. Hydrogels with fast swelling and superabsorbent properties. *J. Biomed. Mater. Res.*, 44:53–62, 1999.

[156] R. Gemeinhart, H. Park, and K. Park. Pore structure of superporous hydrogels. *Polymers for Advanced Technoligies*, 11:617–625, 2000.

[157] M. Badiger, M. McNeill, and N. Graham. Porosigens in the preparation of microporous hydrogels based on poly(ethylene oxide). *Biomaterials*, 14:1059–1063, 1993.

[158] Y.-J. Lee and P.V. Braun. Tunable inverse opal hydrogel ph sensors. *Advanced Materials*, 15:563–566, 2003.

[159] Qing Liu, Elizabeth L. Hedberg, Zewen Liu, Raman Bahulekar, Rudolf K. Meszlenyi, and Antonios G. Mikos. Preparation of macroporous poly(2-hydroxyethyl methacrylate) hydrogels by enhanced phase separation. *Biomaterials*, 21:2163–2169, 2000.

[160] Karolin Mellert. Aufbau einer interferenzlithographie-anlage zur herstellung photonischer kristalle. Master's thesis, Rheinischen Friedrich-Wilhelms-Universitaet, 2002.

[161] Matthias Junk. Struktur und strukturierung von photovernetzbaren, thermoresponsiven hydrogelsystemen. Master's thesis, Johannes Gutenberg University of Mainz, 2007.

[162] Abderrazzek Toufali. Nanostrukturierung von oberflaechen mittels interferenzlithographie fuer anwendungen in der mikrofluidik. Master's thesis, Fachhochschule Wiesbaden / Institut fuer Microsystemtechnik Mainz, 2009.

[163] Max Born. *Principles of Optics*. Cambridge University Press: Cambridge, U.K, 7 edition, 1999.

[164] David G. Bucknall and Harry L. Anderson. Polymers get organized. *Science*, 302:1904–1905, 2003.

[165] Ayako Torikai, Tetsuya Takeuchi, and Kenji Fueki. Photodegradation of polystyrene and polystyrene containing benzophenone. *Polymer Photochemistry*, 3:307–320, 1983.

[166] Bengt Ranby. Photochemical modification of polymers - photocrosslinking, surface photografting, and lamination. *Polymer Engineering and Science*, 38:1229–1243, 1998.

[167] Georges J. Smets, Sabr Nal El Hamouly, and Tae J. Oh. Photochemical reactions on polymers. *Pure and Applied Chemistry*, 56:439–446, 1984.

[168] Du Yeol Ryu, Kyusoon Shin, Eric Drockenmuller, Craig J. Hawker, and Thomas P. Russell. A generalized approach to the modification of solid surfaces. *Science*, pages 236–239, 2005.

[169] N. C Billingham. *Photodegradation of Polymers - Physical Characteristics and Applications*, volume 62. Springer, 1998.

[170] N. S. McKellar and J.F. Allen. Photodegradation and stabilization of commercial polyolefins. *J. F. Chem. Soc. Rev.*, 4:533–547, 1975.

[171] G. Scott. Polymers with enhanced photodegradability. *J. Photochem. Photobiol. A*, 51:73–79, 1990.

[172] Y. Merle, L. Merle-Aubry, and J.E. Guillet. Summary tert-butyl peresters based on aromatic hydrocarbon and aryl ketone chromophores with lowest lying t-t* transitions. *Macromolecules*, 17:288–292, 1984.

[173] G.E. Sheldrick and O. Vogl. Induced photodegradation of styrene polymers: a survey. *Polym. Eng. Sci.*, 16:65–73, 1976.

[174] J.R. Hwu and K.Y. King. Design, synthesis, and photodegradation of silicon-containing polyureas. *Chemistry - A European Journal*, 11:3805–4039, 2005.

[175] D.R. Tyler. Photochemically degradable polymers containing metalmetal bonds along their backbones. *Coord. Chem. Rev.*, 246:291–303, 2003.

[176] R. Chen, J. Meloy, B.C. Daglen, and D.R. Tyler. Photochemically reactive polymers. identification of the products formed in the photochemical degradation of polyurethanes that contain (c5h4r)(co)3mo-mo(co)3(c5h4. *Organometallics*, 24:1495–1500, 2005.

[177] James T. Goldbach, Thomas P. Russell, and Jacques Penelle. Nano- to macro-sized heterogeneities using cleavable diblock copolymers. *Macromolecules*, 35:4271–4276, 2002.

[178] V. N. R. Pillai. Photoremovable protecting groups in organic synthesis. *Synthesis*, pages 1–26, 1980.

[179] C. G. Bochet. Photocleavable protecting groups and linkers. *J. Chem. Soc., Perkin Trans.*, 1:125–142, 2002.

[180] S.P.A. Fodor, J.L. Read, M.C. Pirrung, L. Stryer, A.T. Lu, and D. Solas. Light-directed, spatially addressable parallel chemical synthesis. *Science*, 251:767–773, 1991.

[181] D.A. Nivens and D.W. Conrad. Photoactive poly(ethylene glycol) organosilane films for site-specific protein immobilization. *Langmuir*, 18:499–504, 2002.

[182] W.Y. Chiang and M.L. Lee. Synthesis and characterization of novel copolymers of

carboxyphenylmaleimide and methacrylates with trimethylsiloxy groups for deep-uv photoresists. *J. Appl. Polym. Sci.*, 90:1032–1037, 2003.

[183] Jerzy Olejnik. Photocleavable peptide-dna conjugates: synthesis and applications to dna analysis using maldi-ms. *Nucleic Acids Research*, 27:4626–6631, 1999.

[184] Jeremiah A. Johnson, M. G. Finn, Jeffrey T. Koberstein, and Nicholas J. Turro. Synthesis of photocleavable linear macromonomers by atrp and star macromonomers by a tandem atrp-click reaction: Precursors to photodegradable model networks. *Macromolecules*, 40:3589–3598, 2007.

[185] K. Matyjaszewski and J. Xia. Atom transfer radical polymerization. *J. Chem. Rev.*, 101:2921–2990, 2001.

[186] Zachary P. Demko and K. Barry Sharpless. A click chemistry approach to tetrazoles by huisgen 1,3-dipolar cycloaddition: Synthesis of 5-acyltetrazoles from azides and acyl cyanides. *Angew. Chem. Int. Ed.*, 41:2596–2116, 2002.

[187] C.W. Tornoe, C. Christensen, and M.J. Meldal. Peptidotriazoles on solid phase: [1,2,3]-triazoles by regiospecific copper(i)-catalyzed 1,3-dipolar cycloadditions of terminal alkynes to azides. *J. Org. Chem.*, 67:3057–3064, 2002.

[188] H.C. Kolb, M.G. Finn, and K.B. Sharpless. Click chemistry: Diverse chemical function from a few good reactions. *Angew. Chem. Int. Ed.*, 40:2004–2021, 2001.

[189] J.A. Opsteen and J.C.M. van Hest. Modular synthesis of block copolymers via cycloaddition of terminal azide and alkyne functionalized polymers. *Chem. Commun.*, pages 57–59, 2005.

[190] Michael Malkoch, Raymond J. Thibault, Eric Drockenmuller, Martin Messerschmidt, Brigitte Voit, Thomas P. Russell, , and Craig J. Hawker. Orthogonal approaches to the simultaneous and cascade functionalization of macromolecules using click chemistry. *J. Am. Chem. Soc.*, 127:14942–14949, 2005.

[191] M. Tambasco, J. E. G. Lipson, and J. S. Higgins. Blend miscibility and the flory-huggins interaction parameter: A critical examination. *Macromolecules*, 39:4860–4868, 2006.

[192] D.D. Diaz, K. Rajagopal, E. Strablea, J. Schneider, and M.G. Finn. Click chemistry in a supramolecular environment: Stabilization of organogels by copper(i)-catalyzed azide-alkyne [3 + 2] cycloaddition. *J. Am. Chem. Soc.*, 128:6056–6057, 2006.

[193] J.A. Johnson, D.R. Lewis, D.D. Diaz, M.G. Finn, J.T. Koberstein, and N.J. Turro. Synthesis of degradable model networks via atrp and click chemistry. *J. Am. Chem. Soc.*, 128:6564–6565, 2006.

[194] H. Gao, G. Louche, B.S. Sumerlin, N. Jahed, P. Golas, and K. Matyjaszewski. Gradient polymer elution chromatographic analysis of α,ω – dihydroxypolystyrene synthesized via atrp and click chemistry. *Macromolecules*, 38:8979–8982, 2005.

[195] R.M. Johnson and C.L. Fraser. Metalloinitiation routes to biocompatible poly(lactic acid) and poly(acrylic acid) stars with luminescent ruthenium tris(bipyridine) cores. *Biomacromolecules*, 5:580–588, 2004.

[196] C. Boyer, B. Otazaghine, B. Boutevin, C. Joly-Duhamel, and J.J. Robin. Synthesis of maleimide-terminated n-butyl acrylate oligomers by atom transfer radical polymerization: Study of their copolymerization with vinyl ethers. *J. Polym. Sci., Part A: Polym. Chem.*, 43:4303–4322, 2005.

[197] M. Degirmenci. Synthesis and characterization of novel well defined end functional macrophotoinitiator of poly(mma) by atrp. *J. Macromol. Sci., Part A: Pure Appl. Chem.*, 42:21–30, 2005.

[198] Gladys de los Santos, L.E. Elizalde, B. Castro, A.E. Garcia, and D.I. Medellin. Preparacion de copolimeros fotoactivos por polimerization radicalica por transferencia de atomo. *Rev. Soc. Quim. Mexico*, 48:332–337, 2004.

[199] Nicolay V. Tsarevsky, Brent S. Sumerlin, and Krzysztof Matyjaszewski. Step-growth click coupling of telechelic polymers prepared by atom transfer radical polymerization. *Macromolecules*, 38:3558–3561, 2005.

[200] D.D. Diaz, S. Punna, P. Holzer, A. McPherson, K. B. Sharpless, V.V. Fokin, and M.G. Finn. Click chemistry in materials synthesis. 1. adhesive polymers from copper-catalyzed azide-alkyne cycloaddition. *J Polym Sci Part A: Polym Chem*, 42:4392–4403, 2004.

[201] Dirk Jan V. C. van Steenis, Olivier R. P. David, Gino P. F. van Strijdonck, Jan H. van Maarseveen, and Joost N. H. Reek. Click-chemistry as an efficient synthetic tool for the preparation of novel conjugated polymers. *Chem. Commun.*, pages 4333–4335, 2005.

[202] P. Wu, A. K. Feldman, A.K. Nugen, C.J. Hawker, A. Scheel, B. Voit, J. Pyun, J.M.J. Frechet, K.B. Sharpless, and V.V. Fokin. Efficiency and fidelity in a click-chemistry route to triazole dendrimers by the copper(i)-catalyzed ligation of azides and alkynes. *Angew. Chem. Int. Ed.*, 43:3928–3932, 2004.

[203] Michael Malkoch, Kristin Schleicher, Eric Drockenmuller, Craig J. Hawker, Thomas P. Russell, Peng Wu, and Valery V. Fokin. Structurally diverse dendritic libraries: A highly efficient functionalization approach using click chemistry. *Macromolecules*, 38:3663–3678, 2005.

[204] Maisie J. Joralemon, Rachel K. O'Reilly, John B. Matson, Anne K. Nugen, Craig J. Hawker, and Karen L. Wooley. Dendrimers clicked together divergently. *Macromolecules*, 38:5436–5443, 2005.

[205] Peng Wu, Michael Malkoch, Jasmine N. Hunt, Robert Vestberg, Eiton Kaltgrad, M. G. Finn, Valery V. Fokin, K. Barry Sharpless, and Craig J. Hawker. Multivalent, bifunctional dendrimers prepared by click chemistry. *J. Chem Commun*, pages 5775–5777, 2005.

[206] B. Helms, J.L. Mynar, C.J. Hawker, and J.M.J Frechet. Dendronized linear polymers via click chemistry. *J. Am. Chem. Soc.*, 126:15020–15021, 2004.

[207] Justin L. Mynar, Tae-Lim Choi, Masaru Yoshida, Victor Kim, Craig J. Hawker, and Jean M. J. Frechet. Doubly-dendronized linear polymers. *J. Chem Commun*, pages 5169–5171, 2005.

[208] Michael Malkoch, Robert Vestberg, Nalini Gupta, Laetitia Mespouille, Philipe Dubois, Andrew F. Mason, James L. Hedrick, Qi Liao, Curtis W. Frank, Kevin Kingsbury, and Craig J. Hawker. Synthesis of well-defined hydrogel networks using click chemistry. *J. Chem. Commun.*, pages 2774–2776, 2006.

[209] Dmitri A. Ossipov and Joens Hilborn. Poly(vinyl alcohol)-based hydrogels formed by click chemistry. *Macromolecules*, 39:1709–1718, 2006.

[210] Bryan Parrish, Rebecca B. Breitenkamp, , and Todd Emrick. Peg- and peptide-grafted aliphatic polyesters by click chemistry. *J. Am. Chem. Soc.*, 127:7404–7410, 2005.

[211] Andrew P. Vogt and Brent S. Sumerlin. An efficient route to macromonomers via atrp and click chemistry. *Macromolecules*, 39:5286–5292, 2006.

[212] O. Altintas, G. Hizal, and U. Tunca. Abc type hetero arm star terpolymers through click chemistry. *J. Polym. Sci. Part A: Polym. Chem.*, 44:5699–5707, 2006.

[213] Richard Hoogenboom, Brian C. Moore, and Ulrich S. Schubert. Synthesis of star-shaped poly(ϵ–caprolactone) via click chemistry and supramolecular click chemistry. *Chem. Commun.*, pages 4010–4012, 2006.

[214] O. Altintas, B. Yankul, G. Hizal, and U. Tunca. A(3)-type star polymers via click chemistry. *J. Polym. Sci. Part A: Polym. Chem.*, 44:6458–6465, 2006.

[215] R.J. Thibault, K. Takizawa, P. Lowenheilm, B. Helms, J.L. Mynar, J.M Frechet, and C.J. Hawker. A versatile new monomer family: functionalized vinyltriazoles via click chemistry. *J. Am. Chem. Soc.*, 128:12084–12085, 2006.

[216] H.M. Li, F.O. Cheng, and A.M. Duft A. Adronov. Functionalization of single-walled carbon nanotubes with well-defined polystyrene by click coupling. *J. Am. Chem. Soc.*, 127:14518–14524, 2005.

[217] Giuseppe Mantovani, Vincent Ladmiral, Lei Tao, and David M. Haddleton. One-pot tandem living radical polymerisationhuisgens cycloaddition process (click) catalysed by n-alkyl-2-pyridylmethanimine/cu(i)br complexes. *Chem. Commun.*, pages 2089–2091, 2005.

[218] J.F. Lutz, H.G. Borner, and K. Weichenhan. Combining atrp and click chemistry: an universal method for preparing end-functional polymers. *Macromol. Rapid. Commun.*, 26:514–518, 2006.

[219] W.H. Binder and C. Kluger. Combining ring-opening metathesis polymerization

(romp) with sharpless-type click reactions: An easy method for the preparation of side chain functionalized poly(oxynorbornenes). *Macromolecules*, 37:9321–9330, 2004.

[220] B.S. Sumerlin, N.V. Tsarevsky, G. Louche, R.Y. Lee, and K. Matyjaszewski. Highly efficient click functionalization of poly(3-azidopropyl methacrylate) prepared by atrp. *Macromolecules*, 38:7540–7545, 2005.

[221] Robert Luxenhofer and Rainer Jordan. Click chemistry with poly(2-oxazoline)s. *Macromolecules*, 39:3509–3516, 2006.

[222] J.A. Opsteen and J.C. van Hest. Modular synthesis of abc type block copolymers by click chemistry. *Journal of Polymer Science Part A*, 45:2913–2924, 2007.

[223] Simon J. Teague. Facile synthesis of a o-nitrobenzyl photolabile linker for combinatorial chemistry. *Tetrahedron Lett.*, 32,:5751–5754, 1996.

[224] Kallolmay Biswas, Oscar Prieto, Paul J. Goldsmith, and Simon Woodward. Remarkably stable (me3al)2-dabco and stereoselective nickel-catalyzed alr3 (r=me, et) additions to aldehydes. *Angew. Chem. Int. Ed.*, 44:2232–2234, 2005.

[225] Y. Imakura, K. Okimoto, T. Konishi, M. Hisazumi, J. Yamazaki, S. Kobayashi, and S. Yamashita. Regioselective cleavage reaction of the aromatic methylenedioxy ring. v. cleavage with sodium alkoxides-alcohols, potassium tert-butoxide-alcohols, dimsyl anion-methyl alcohol, metallic sodium-alcohols, and sodium cyanide in dipolar aprotic solvents. *Chem. Pharm. Bull.*, 40:1691–1696, 1992.

[226] Renate Foerch, Holger Schoenherra, and A. Tobias A. Jenkins. *Surface design: applications in bioscience and nanotechnology*. WILEY VCH, 2009.

[227] Kyle B. Guice and Yueh-Lin Loo. Azeotropic atom transfer radical polymerization of hydroxyethyl methacrylate (hema) and dimethylaminoethyl methacrylate (dmaema) statistical copolymers and block copolymers with polystyrene. *Macromolecules*, 39:2474–2480, 2006.

[228] Bruce Alberts. *Molecular Biology of the Cell*. Garland Science, 2002.

[229] Cornel Muehlhardt. *Der Experimentator Molekularbiologie / Genomics*. Spektrum, 2009.

[230] G. Eichhorn and Y. Shin. The relative effect of various metal ions on dna helicity. *J. Am. Chem. Soc.*, 90:7323–7328, 1968.

[231] M. Maeda, Y. Mitsuhashi, K. Nakano, and M. Takagi . Dna-immobilized gold electrode for dna-binding drug sensor. *Anal. Sci.*, 8:83–84, 1992.

[232] M. Boncheva, L. Scheibler, P. Lincoln, H. Vogel, and B. A kerman. Design of oligonucleotide arrays at interfaces. *Langmuir*, 15:4317–4320, 1999.

[233] R.C. Ebersole, J.A. Miller, J.R. Moran, and M.D.Ward. Monolayers on metal surfaces: A strategy for immobilizing biological reagents and design of. piezoelectric biosensors. *J. Am. Chem. Soc.*, 112:3239–3241, 1990.

[234] N. Lassalle, A. Roget, T. Livache, P. Mailley, and E. Vieil . Electropolymerisable pyrrole-oligonucleotide: synthesis and analysis of odn hybridisation by fluorescence and qcm. *Talanta*, 55:993–1004, 2001.

[235] H. Korri-Youssoufi and A. Yassari. Electrochemical probing of dna based on oligonucleotide-functionalized polypyrrole. *Biomacromolecules*, 2:58–64, 2001.

[236] Stu Borman. Putting dna in a bind. *Chemical and Engineering News: Science and Technology*, 88:50–53, 2010.

[237] Trevor W. Hambley. Platinum binding to dna: structural controls and consequences. *J. Chem. Soc. Dalton Trans.*, 19:2711–2718, 2001.

[238] J. D. Pickering Mainwaring, J. H. Parish and N. H. Mann. *Nucleic Acid Biochemistry and Molecular Biology.* W. I. P. Blackwell Scientific Publications Oxford, 1982.

[239] V. Luzzati, F. Masson, and L.S. Lerman. Interaction of dna and proflavine: a small-angle x-ray scattering study. *J. Mol. Biol.*, 3:634–639, 1961.

[240] V. Rybenkov and A. Vologodskii. Effective diameter of dna. *Molek. Biol. (Russia)*, 26:1433–1439, 1992.

[241] Valentin V. Rybenkov, Nicholas R. Cozzarelli, and Alexander V. Vologodskii. Probability of dna knotting and the effective diameter of the dna double helix. *Proc. Natl. Acad. Sci.*, 90:5307–5311, 1993.

[242] A. A. Brian, H. L. Frisch, and L. S. Lerman. Thermodynamics and equilibrium sedimentation analysis of the close approach of dna molecules and a molecular ordering transition. *Biopolymers*, 20:1305–1328, 1981.

[243] J. Le Pecq and M. Le Bret. Dna polyintercalating drugs: Dna binding of diacridine derivatives. *Proc. Nat. Acad. Sci.*, 72:2915–2920, 1975.

[244] J. Le Pecq. *Biochemical Fluorescence: Concepts*, volume 11. M. Dekker, New York, 1976.

[245] Stephan Laib, Alexander Krieg, Pascal Hfliger, and Nikos Agorastos. Dna-intercalation on pyrene modified surface coatings. *Chem. Commun.*, 44:5566–5568, 2005.

[246] Hyun Seok Jeong, Myeongkee Park, Jeong Wu Yi, Taiha Jooa, and Byeang Hyean Kim. Structural diversity induced by pyreneintercalators in homogeneous oligodeoxyguanylates. *Mol. BioSyst.*, 6:951–953, 2010.

[247] P.S. Song M. L. Harter, I. C. Felkner. Near uv effects of 5,7-dimethoxycoumarin in bacillus subtilis. *Photochemistry and Photobiology*, 24:491–493, 1976.

[248] Pierre Demerseman, Jacques Einhorn, Jean Francois Gourvest, and Rene Royer. Synthese d'analogues furanniques du benzo[α]pyrene. *J. Heterocyclic Chem.*, 22:39–43, 1985.

[249] Pratibha Asthana and Shri Rastogi. Synthesis of 9-aryl/pyrimidyl/alkyl substituted (oxy/amino/carbonyl)-acridines and 1,3-bis(9-acridinyl)propan-2-ols as potential anti-cancer agents. *Indian Journal of Chemistry*, 30:853–858, 1991.

[250] Hidetoshi Kawai, Takashi Takeda, Kenshu Fujiwara, , and Takanori Suzuki. Isolation and low-temperature x-ray analysis of intramolecular triarylmethane-triarylmethylium complex: Preference for a c-h-bridged unsymmetric structure exhibiting a facile 1,5-hydride shift and charge-transfer interaction. *Journal of the American Chemical Society*, 127:12172–12173, 2005.

[251] Alicia J. Hager, Sheryl P. Evans, and Tetsuo Otsuki. Novel furucoumarin derivatives as a model related to dna-intercalating molecules. synthesis and photochemical reactivity. *Chemistry Letters*, pages 409–412, 1990.

[252] Andrea L. Koenig, Alicia J. Hager, and Tetsuo Otsuki. 4'-halomethyl-4,5'8-trimethylfurocoumarin. it's unusual substitution reaction. *Chemistry Express*, 8:463–466, 1993.

[253] Kwonil Kim, Kouzou Masumoto, Kazunori Matsuura, , and Nobuo Kimizuka. In situ observation of spherical dna assembly nucleo-cages in water and their stabilization by photo-crosslinking. *Chem. Lett.*, 35:supporting information (S1–S6), 2006.

List of acronyms

AFM	atomic force microscopy
AIBN	azobisisobutyronitrile
ATR	attenuated total reflectance
BP	benzophenone
CCD	charge coupled device
DCM	dichloromethane
d-DMF	deuterated dimethylformamide
DIC	differential interference contrast
DMF	dimethylformamide
DMSO	dimethylsulfoxide
DNA	deoxyribonucleic acid
DP	degree of polymeriation
DSC	differential scanning calorimetry
EBrP	ethyl 2-bromo-2-methylpropanoate
EtAc	ethyl acetate
EtOH	ethanol
FRET	fluorescence resonance energy transfer
FTIR	Fourier transformation infrared
gDNA	genomic deoxyribonucleic acid
GPC	gel permeation chromatography
HDMS	hexamethyldisilazane

HEMA 2-hydroxyethyl methacrylate

HF hydrofluoric acid

HOMO highest occupied molecular orbital

IMM Institut fuer Microsystemtechnik Mainz

IR infrared

IgG Immunoglobulin G

KD Kilo Dalton

LUMO lowest unoccupied molecular orbital

MAA methacrylic acid

MABP 4-benzoylphenyl methacrylate

MEK methylether ketone

MeOH methanol

MHz Mega Hertz

MPIP Max Planck Institute for Polymer Chemistry

NMR nuclear magnetic resonance

OW optical wave guide

PCR polymerase chain reaction

PDI polydispersity index

PEBP S-3-(4-Benzoylphenoxy)propylethanthioate

1-PEBr 1-phenyl ethylbromide

PIA photocleavable initiator for ATRP

pHEMA poly(2-hydroxyethyl methacrylate)

PMDETA N,N,N',N",N" pentamethyldiethylenetriamine

pNIPAAm poly(N-isopropylacrylamide)

PP	polypropylene
ppm	parts per million
pS	polystyrene
QPCR	quantitative polymeraze chain reaction
rt	room temperature
RTD	real time detection
SA	streptavidin
SEM	scanning electron microscopy
SI	systeme international
SPR	surface plasmon resonance
TE	transverse electric
TEG	tetraethyleneglycole
TGA	thermogravimetric analysis
THF	tetrahydrofurane
THP	tetrahydrolpyranole
TIR	total internal reflection
TLC	thin layer chromatography
TM	transverse magnetic
TMOS	tetramethoxysilane
UV	ultra violet
UV/vis	ultra violet/visible
wt%	weight percent

Acknowledgements

First, I would like to express my gratitude to all those who gave me the possibility to complete this thesis. I would like to thank my project leader Dr. xxxxx and my group director Prof. Dr. xxxxx for giving me the opportunity to do my PhD in his group at the Max Planck Institute for Polymer Research in Mainz. I also thank them for giving me freedom in all my scientific ideas and for their words of advice. All in all, it truly was the most frustrating, thrilling, challenging, educating and rewarding experience in my life. A time I shall never forget.

Second, I would like to thank Prof. xxxxxx from the Johannes Gutenberg University of Mainz that he kindly agreed to be the supervisor from the side of the university and spent his time for my thesis. Thank You for Your patience.

Third, thanks are due to my colleagues - cast together from many a country of the world and greatly different in background - in the research group. It was great to learn from each other, inspire each other by long discussion or debate, laugh together, and know that there are reliable hands when help is needed.

In this context I also would like to say that I am very grateful to my cooperation partners: For their help, I thank Dr. xxxxxxxx (SPR/OWS measurements), and Dr. xxxxx (PCR), Dr. xxxxxx (photolithography).
Moreover, I thank the project leaders and staff of the research group for all their helpful discussions, and the helpful staff in the mechanical and the electrical workshop, and all the supportive people that were in charge of the various measurements instruments of our group.

At last, many thanks Dr. xxxxxxxxxx, Dr. xxxxxxxxxxxxx, Dr. xxxxxxxxx and xxxxxxxxxxxx, who were so kind to proof read this thesis, and xxxxxxxxxx for her patience.